AFIT/GE/EN/91D-44

APPLICATION OF NONLINEAR QFT TO FLIGHT CONTROL DESIGN FOR HIGH ANGLE OF ATTACK MANEUVERS WITH THRUST VECTORING

THESIS

Steven J Rasmussen
Captain, USAF

AFIT/GE/EN/91D-44

December 1991 Master's Thesis

APPLICATION OF NONLINEAR QFT TO FLIGHT CONTROL DESIGN FOR HIGH ANGLE OF ATTACK MANEUVERS WITH THRUST VECTORING

Steven J Rasmussen
Captain, USAF

Air Force Institute of Technology
WPAFB OH 45433-6583

AFIT/GE/ENG/91D-44

Finley Barfield
WL/FIGX
Wright-Patterson AFB, OH 45433

Approved for Public Release; Distribution Unlimited.

Nonlinear Quantitative Feedback Theory (QFT) is applied to the design of an flight Control system (FCS) to control maneuvers of an agile aircraft. To do this, maneuvers are chosen that are desirable during within visual range combat. Plant transfer functions are developed through the use of system identification, using the input/output time histories of the maneuvers. During the system identification process the $q_{ij(0)}$ are found directly and are constrained to be minimum phase. After identifying the plants, the cascaded multiple-input multiple-output QFT technique is used to design the FCS. During the design of the FCS, stability boundaries are generated through the use of a Matrix$_x$ program. To prevent the formation of large RHP poles, Γ-boundries are developed. Before shaping the loops it is found that FCS scheduling is needed because of large uncertainty in the magnitude and phase of the plants. Because the orders of the designed controllers are too large for the YF-16 simulation program, reduced order controllers are developed through the use of straight line approximations on the Bode plot. After implementing the reduced order controllers in the nonlinear simulation program, problems developed in the modeling process are encountered that prevent the simulation of the FCS's.

Quantitative Feedback Technique, QFT, Nonlinear QFT, System Identification, Agile Maneuvers 178

Unclassified Unclassified Unclassified UL

GENERAL INSTRUCTIONS FOR COMPLETING SF 298

The Report Documentation Page (RDP) is used in announcing and cataloging reports. It is important that this information be consistent with the rest of the report, particularly the cover and title page. Instructions for filling in each block of the form follow. It is important to **stay within the lines to meet optical scanning requirements.**

Block 1. Agency Use Only (Leave Blank)

Block 2. Report Date. Full publication date including day, month, and year, if available (e.g. 1 Jan 88). Must cite at least the year.

Block 3. Type of Report and Dates Covered. State whether report is interim, final, etc. If applicable, enter inclusive report dates (e.g. 10 Jun 87 - 30 Jun 88).

Block 4. Title and Subtitle. A title is taken from the part of the report that provides the most meaningful and complete information. When a report is prepared in more than one volume, repeat the primary title, add volume number, and include subtitle for the specific volume. On classified documents enter the title classification in parentheses.

Block 5. Funding Numbers. To include contract and grant numbers; may include program element number(s), project number(s), task number(s), and work unit number(s). Use the following labels:

C	- Contract	**PR**	- Project
G	- Grant	**TA**	- Task
PE	- Program Element	**WU**	- Work Unit Accession No.

Block 6. Author(s). Name(s) of person(s) responsible for writing the report, performing the research, or credited with the content of the report. If editor or compiler, this should follow the name(s).

Block 7. Performing Organization Name(s) and Address(es). Self-explanatory.

Block 8. Performing Organization Report Number. Enter the unique alphanumeric report number(s) assigned by the organization performing the report.

Block 9. Sponsoring/Monitoring Agency Names(s) and Address(es). Self-explanatory.

Block 10. Sponsoring/Monitoring Agency. Report Number. (If known)

Block 11. Supplementary Notes. Enter information not included elsewhere such as: Prepared in cooperation with...; Trans. of ..., To be published in .... When a report is revised, include a statement whether the new report supersedes or supplements the older report.

Block 12a. Distribution/Availablity Statement. Denote public availability or limitation. Cite any availability to the public. Enter additional limitations or special markings in all capitals (e.g. NOFORN, REL, ITAR)

DOD - See DoDD 5230.24, "Distribution Statements on Technical Documents."
DOE - See authorities
NASA - See Handbook NHB 2200.2.
NTIS - Leave blank.

Block 12b. Distribution Code.

DOD - DOD - Leave blank
DOE - DOE - Enter DOE distribution categories from the Standard Distribution for Unclassified Scientific and Technical Reports
NASA - NASA - Leave blank
NTIS - NTIS - Leave blank.

Block 13. Abstract. Include a brief (Maximum 200 words) factual summary of the most significant information contained in the report.

Block 14. Subject Terms. Keywords or phrases identifying major subjects in the report.

Block 15. Number of Pages. Enter the total number of pages.

Block 16. Price Code. Enter appropriate price code (NTIS only).

Blocks 17. - 19. Security Classifications. Self-explanatory. Enter U.S. Security Classification in accordance with U.S. Security Regulations (i.e., UNCLASSIFIED). If form contains classified information, stamp classification on the top and bottom of the page.

Block 20. Limitation of Abstract. This block must be completed to assign a limitation to the abstract. Enter either UL (unlimited) or SAR (same as report). An entry in this block is necessary if the abstract is to be limited. If blank, the abstract is assumed to be unlimited.

AFIT/GE/EN/91D-44

APPLICATION OF NONLINEAR QFT TO FLIGHT CONTROL DESIGN FOR HIGH ANGLE OF ATTACK MANEUVERS WITH THRUST VECTORING

THESIS

Presented to the Faculty of the School of Engineering
of the Air Force Institute of Technology
Air University
In Partial Fulfillment of the
Requirements for the Degree of
Master of Science in Electrical Engineering

Steven J Rasmussen, B.S.E.E.
Captain, USAF

December, 1991

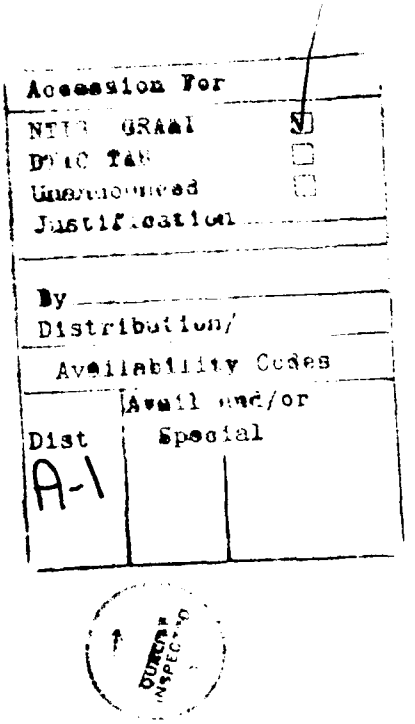

Acknowledgments

I send thanks to my father, Evan J. Rasmussen, for shaping me into an independent thinking person.

Thank you, fellow control students, for allowing me to be part of the team.

Prof Houpis and Prof Horowitz, thank you for allowing me to enter the wonderful world of nonlinear QFT.

Ryan, I'm proud of you for handling many of the small crises that I couldn't.

Carol, thank you for being there, maybe now you'll let me mow the yard.

I dedicate this work to my wife, Brenda who is my inspiration and my source of direction.

Steven J Rasmussen

Table of Contents

List of Figures

List of Tables

List of Symbols

Abstract

Nonlinear Quantitative Feedback Theory (QFT) is applied to the design of an flight Control system (FCS) to control maneuvers of an agile aircraft. To do this, maneuvers are chosen that are desirable during within visual range combat. Plant transfer functions are developed through the use of system identification, using the input/output time histories of the maneuvers. During the system identification process the $q_{ij(0)}$ are found directly and are constrained to be minimum phase. After identifying the plants, the cascaded multiple-input multiple-output QFT technique is used to design the FCS. During the design of the FCS, stability boundaries are generated through the use of a Matrix_x program. To prevent the formation of large RHP poles, Γ-boundries are developed. Before shaping the loops it is found that FCS scheduling is needed because of large uncertainty in the magnitude and phase of the plants. Because the orders of the designed controllers are too large for the YF-16 simulation program, reduced order controllers are developed through the use of straight line approximations on the Bode plot. After implementing the reduced order controllers in the nonlinear simulation program, problems developed in the modeling process are encountered that prevent the simulation of the FCS's.

APPLICATION OF NONLINEAR QFT TO FLIGHT CONTROL DESIGN FOR HIGH ANGLE OF ATTACK MANEUVERS WITH THRUST VECTORING

I. Introduction

1.1 Background

The United States Air Force is interested in weapon systems and tactics that will give its pilots an advantage over the enemy. Because of relatively new weapons systems such as the all-aspect missile, tactics can be developed for aircraft that will add to this advantage. If aircraft can be made more agile, this advantage over the enemy can be improved. Since agile aircraft will operate in highly nonlinear regions of the flight envelope, and since controlling aircraft in these regions of flight will depend on very fast responses, sophisticated flight control systems (FCS) must be developed to aid the pilot in controlling these aircraft. This thesis is part of a continuing effort to improve the design of FCS through the use of nonlinear Quantitative Feedback Theory (QFT) technique. QFT is a control system design method developed by Dr. Isaac Horowitz that quantifies the amount of uncertainty in the plant and uses this information to reduce the negative effects of using feedback in the controller. Nonlinear QFT uses the idea of quantifying uncertainty in the plant and extends it to quantifying the nonlinear behavior. By quantifying the nonlinear behavior and the uncertainty, the nonlinear plant can be rigorously represented in this design technique. Nonlinear QFT was used in previous theses by Kobylarz [12] and Miller [18]. Kobylarz applied nonlinear QFT with pilot compensation to the design of a FCS for a single-input single-output (SISO) model of the YF-16 aircraft. Miller applied the design techniques to the design of a FCS for a multiple-input multiple-output (MIMO) model of the YF-16, where there were two inputs and two outputs.This thesis applies nonlinear QFT to design a FCS for a three-input three-output model of the YF-16, with thrust vectoring, as it is flown through highly nonlinear maneuvers.

1.2 Problem Statement

Since agile aircraft will be able to maneuver in highly nonlinear regions of flight, a method of flight control design is needed to give an acceptable first-cut design of a FCS that enables the pilot to control the aircraft through these maneuvers. In the past a FCS design has been a matter of cut and try. By using a method such as nonlinear QFT, the amount of cut and try can be reduced significantly [9].

1.3 Assumptions

The following assumptions are made for this thesis.

- Only the desired outputs are of interest for final performance.
- The robustness of Matrix_x transfer function algorithms is adequate for the design process.

The first one is the basic assumption required in applying nonlinear QFT. The second is made because Matrix_x has limits to the robustness of its transfer function algorithms.

1.4 Scope

This thesis applies nonlinear QFT technique to the design of a FCS for the roll (p), pitch (q), and yaw (r) channels of a YF-16 simulation program. The YF-16 simulation is a full six-degrees-of-freedom nonlinear FORTRAN simulation. This simulation includes thrust vectoring in the pitch and yaw channels. The FCS is designed to control the aircraft through two specified maneuvers. The maneuvers are based on theoretical maneuvers for agile aircraft. A system identification methodology is discussed that constrains the plants to be minimum-phase (MP). QFT stability boundaries and other boundaries are computer generated to aid in the FCS design. The FCS is designed to have the time responses to p, q, and r commands specified in MIL–STD–1707A [17]. Order reduction on the controllers is accomplished. The reduced order controllers are coded in FORTRAN, and installed in the YF-16 simulation program. Finally, problems with model, that become evident during the nonlinear simulation, that prevent a successful simulation are discussed.

1.5 Standards

The thesis sponsor has provided specifications on the response to control inputs based on guidelines presented in MIL–STD–1797A [17]. The specifications on the particular maneuvers were developed by the sponsor [2] [4].

1.6 Approach

Maneuvers are developed by trial and error, for a six degree of freedom nonlinear YF-16 simulation. Input/output time histories are collected that adequately describe the maneuvers. System Identification is used to find linear-time-invariant (LTI) plants based on these time histories. Nonlinear QFT is used to design multiple unity feedback FCSs that are to be used to control the simulation through the prescribed maneuvers. Reduced order FCSs are coded in FORTRAN and scheduled based on the maneuver. The actual nonlinear simulations are not accomplished due to problems that arise due to mismodeling.

1.7 Summary

This thesis consists of eight chapters. The first chapter introduces the thesis problem. The second chapter gives a basic overview of the cascaded nonlinear MIMO QFT method. Chapter 3 explains how the maneuvers are developed and also describes the YF-16 simulation. Chapter four presents the manner with which LTI plants are derived from input/output time histories. The fifth chapter describes the method used in obtaining boundaries on the forward loop transmission, l. Described in Chapter 6 are loop shaping and the design of the prefilters. The seventh chapter covers the problems that appear during the nonlinear simulations. The final chapter, Chapter 8, contains a summary, conclusions, and recommendations.

II. Cascaded MIMO Nonlinear QFT

2.1 Introduction

The essence of the robustness of QFT is the method's ability to quantify uncertainty [10]. This chapter outlines the QFT method and how nonlinear plants can be modeled as LTI plants with uncertainty. First the QFT method is reviewed. Next, the cascaded MIMO QFT method of obtaining MISO effective loops is explained. Finally, the manner in which uncertain LTI plants are used to represent nonlinear plants is presented.

2.2 QFT Method

QFT is a design method that gives the designer a very good first cut at the final control system [9]. Through the use of QFT, one can design a fixed parameter controller based on a range of operating conditions. Included in QFT is the ability to design the controller to cause the system to produce outputs that meet required specifications based on particular inputs. The overall QFT design process is based on the diagram presented in Figure 2.1, where the elements in the figure can be either SISO or MIMO [5] [11]. U_{cmd} represents the commanded input and d_1 , d_2 are disturbance inputs. G(s) is a cascade compensator and F(s) is a prefilter. In QFT the plant, $\mathcal{P}$(s) , is represented by a set of J LTI transfer functions, representing the plant at different operating conditions. The individual transfer functions, $P_j(s) \in \mathcal{P}$(s), where j=1,2,...,J, are chosen by the designer so that the entire operational envelope of the plant is adequately described. The QFT technique determines boundaries, that must be satisfied by a nominal loop transmission function, which is plotted on a Nichols chart (NC). The boundaries are based on stability, tracking, and disturbance rejection performance specifications. In this thesis only stability bounds are specified so they are the only bounds described here. The nominal loop transmission (l_o) is the forward loop transmission expressed by:

$$l_o = GP_o \tag{2.1}$$

where P_o represents the nominal plant. The choice of P_o is arbitrary, but a particular P_o is chosen based on the designer's preference on the placement and shape of the

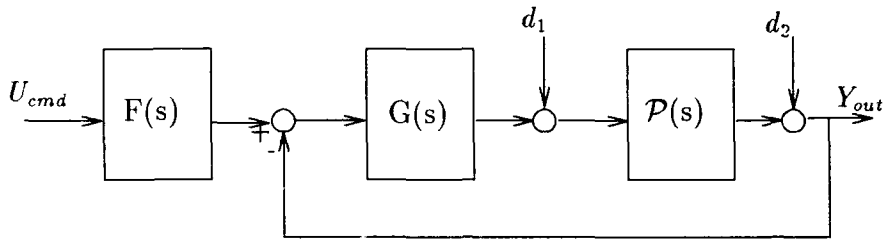

Figure 2.1. QFT Controller Design

boundaries. To form the stability bounds, templates are derived based on $\mathcal{P}$. These templates are plots of the magnitude versus phase, for a given frequency ω_i for each P_j contained within $\mathcal{P} = \{P_j\}$. For each ω_i a stability boundary $\mathcal{B}_s(j\omega)$ can be obtained by moving the template around the M-contour that corresponds to the required phase margin angle γ , and plotting the locus of points described by P_o. Once boundaries are obtained for a set of specified values of ω_i, l_o can be formed on the NC, with the restraint that at each ω_i, $l_o(j\omega_i)$ must lie on or above $\mathcal{B}_s(j\omega)$. After l_o is formed, G(s) can be derived from Equation (2.1). Once the feedback loop is formed, F(s) can be designed. A modified method is used to design F(s). This method involves the following steps:

1. A control ratio $T_{L_j}(s) = \frac{L_j(s)}{[1+L_j(s)]}$ is obtained for each $L_j(s) = G(s)P_j(s)$.
2. The frequency response is obtained for each $T_{L_j}(s)$
3. The Bode plots of all T_{L_J}, and the frequency responses of the tracking bounds, $T_{R_{U_i}}$ and $T_{R_{L_i}}$, are plotted on the same bode plot.
4. $F(s)_J$ is designed so that all Lm$[F(s)_J T_{L_J}]$ lie within the bounds given by Lm$[T_{U_J}]$ and Lm$[T_{L_J}]$

2.3 Cascaded MIMO QFT

In general, the MIMO QFT design method involves transforming the system of Figure 2.1, with no external disturbances, into equivalent multiple-input single-output (MISO) loops as shown in Figure 2.2 for the 3X3 case. This transformation is justified through the use of the fixed point theorem [11]. These MISO loops are represented by equations of the form of Equation (2.2), where t_{ij} is the control ratio

relating the i^{th} output to the j^{th} input, f_i is the prefilter, l_i is the forward loop transmission, and d_{ij} represents a disturbance input.

$$t_{ij} = \frac{f_{ij} l_i + d_{ij} q_{ij}}{1 + l_i} \tag{2.2}$$

The q_{ij} in these equations are the reciprocal of the terms contained in the inverse

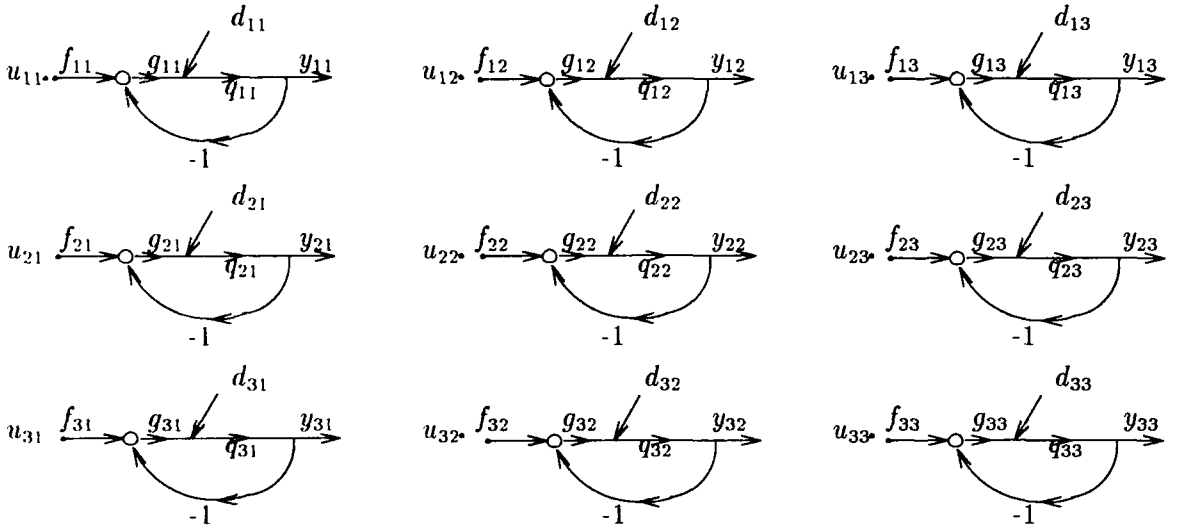

Figure 2.2. 3X3 MISO Equivalent Loops

of the square plant matrix **P**= $[p_{ij}]$. That is $P^*=[p^*_{ij}]=P^{-1}$ where $[p^*_{ij}] = \left[\frac{1}{q_{ij}}\right]$ and **Q** $=[q_{ij}]$. The disturbances in these MISO loops represent the cross-coupling between loops. To simplify the controller, the G(s) and F(s) matrices used in this thesis are diagonal, but non-diagonal G(s) and F(s) can be used. The design of the first loop is accomplished using the method described for the MISO case. After the first loop is designed, the set of effective plants, $\mathcal{Q}_{ij(1)}$ that accounts for the effect of the first loop on the succeeding loops is derived using Equations (2.3) through (2.6) [8].

$$t_{ij} = \frac{f_{ij} l_{i(k)} + d_{ij(k)} q_{ij(k)}}{1 + l_{i(k)}} \tag{2.3}$$

$$l_{i(k)} = g_i q_{ij(k)} \tag{2.4}$$

$$q_{ij(k)} = \frac{q_{ij(k-1)}(1 + l_{i(k-1)})}{1 - \gamma_{ij(k)} + l_{i(k-1)}} \tag{2.5}$$

$$\gamma_{ij(k)} = \frac{q_{ik(k-1)} q_{kj(k-1)}}{q_{ij(k-1)} q_{kk(k-1)}} \tag{2.6}$$

Where k in these equations indicates the kth loop that is previously designed. These are the same effective plants described by Houpis, [11] and Horowitz, [7], but these equations lend themselves to a recursive approach to finding effective plants. This approach is used here because the number of functions used in the computer algorithm is reduced allowing a simpler implementation. For the second loop only $q_{22(1)}$ needs to be calculated, but for the third loop $q_{33(1)}$, $q_{22(1)}$, $q_{32(1)}$, and $q_{23(1)}$ all need to be calculated. With $q_{22(1)}$, the second loop can be designed in a similar manner as the first loop. Once the second loop is determined, the set of effective plants for the third loop $\mathcal{Q}_{33(2)}$ is calculated based on Equations (2.3) through (2.6) with j=3, i=3, and k=2. Finally the third loop is designed in the manner of the previous loops. After the three loops are determined, the diagonal prefilters are designed.

2.4 Nonlinear QFT

The nonlinear behavior of a plant is quantified using the same method that quantifies the uncertainty of a plant. That is, a set of LTI transfer functions ($\mathcal{P}_i$), is found that represents a nonlinear plant W_i over a set of acceptable outputs $\mathcal{O}$ where $W_i \in \mathcal{W}$, Figure 2.3. A new $\mathcal{P}_i$ must be found for every $W_j \in \mathcal{W}$. It has been proven, using the fixed point theorem, that an acceptable design based on $\mathcal{P}_i$ will satisfy the design requirements of $\mathcal{W}$, $\mathcal{O}_i$ [9]. The design process involves first finding $\mathcal{P}$, where $\mathcal{P}_i \in \mathcal{P}$. To find a particular $\mathcal{P}_i$ an envelope of desired responses must be specified for the particular operating condition. These are all the possible responses that are required from the plant at that operating condition. A set of outputs $\mathcal{O}_i$ are chosen to adequately describe $\mathcal{W}_i$, within this envelope. The number of outputs needed will depend on the particular $\mathcal{W}_i$. The set of inputs $\mathcal{I}_i$ that are required to produce $\mathcal{O}_i$, are used to find the set of LTI transfer functions, $\mathcal{P}_i$. Finding $\mathcal{P}_i$ can be accomplished by either analytical means or as in the case of this thesis system identification. Next a set of templates is generated, based on $\mathcal{P}$, as in the SISO case. From this point the design method is the same as the LTI design method.

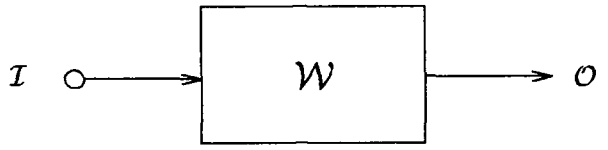

Figure 2.3. Nonlinear Diagram

2.5 Conclusion

This chapter reviews the basic techniques of the QFT method. A basic outline of MIMO QFT is given and the cascaded method of effective plant computation is explained. Finally, the difference between nonlinear QFT and linear QFT is explained. In the next chapter the desired maneuvers and the agile aircraft used in this thesis are described.

III. Desired Maneuvers and Agile Aircraft

3.1 Introduction

'Simply stated, fighter agility is that characteristic of a fighter aircraft which enables it to outmaneuver its adversary for a favorable position from which to launch its weapons [21].' Agility is an important part of air-to-air combat that occurs within visual range. Combat will be conducted within visual range for many reasons such as large enemy numbers, stealth aircraft, faulty missiles, and visual identification [21] [6]. Since an agile fighter is desirable, considerable interest exists in techniques that will improve agility. As Nguyen and Gilbert said, 'high agility requires the ability to generate substantial controllable angular rates over an expanded angle of attack (AOA) range [19].' An aircraft capable of maneuvering at high AOA can change its attitude very quickly and therefore point its nose at a target very quickly [21]. This chapter describes the development of the maneuvers that the FCS is designed to control and the aircraft model used in this thesis.

3.2 Maneuvers

Since increasing the AOA of an aircraft increases drag, maneuvers at high AOA cause a large loss of speed. This loss of speed translates into a loss of energy for combat maneuvering. Loss of energy can put an attacking aircraft at a distinct disadvantage if the first shot misses or if there are multiple targets [21]. Tamrat suggests that the most important use of high AOA maneuvers is in a defensive roll. One of the maneuvers is to pitch up to a certain angle and then point the nose at the target using the aircraft's yaw axis. Another maneuver is to increase the AOA quickly, which causes a rapid decrease in the aircraft's forward airspeed, causing the pursuing aircraft to move in front of the defending aircraft [21]. To regain energy from these high AOA maneuvers, the method is to pull the aircraft's nose down quickly to unload the wings and rapidly increase airspeed [19]. Another maneuver that can be useful is a banked turn at a high AOA. This maneuver would give the aircraft the ability to turn toward the enemy quickly allowing a first shot [2] [21].

3.3 Thrust Vectoring

Thrust vectoring is an attractive control to use on a fighter aircraft because it 'provides control moments that are essentially uncoupled from airframe aerody-

namics [3].' At flight conditions where aerodynamic control surfaces have little or no effectiveness, thrust vectoring provides control power. Examples of these flight conditions are low airspeed and high AOA [3]. Nguyen and Gilbert state that thrust vectoring matches or exceeds the control effectiveness needed to control aircraft during low speed flight [19]. Aircraft designers must use larger control surfaces to compensate for low speed flight. Thrust vectoring allows the aircraft designer to make these surfaces smaller, thus reducing drag and weight [3]. At higher AOA's the control surfaces don't provide enough control authority to maneuver the aircraft. During these flight conditions control surfaces can be augmented or replaced by thrust vectoring. At AOA's above the stall AOA, thrust vectoring must be used to control the aircraft [21]. During their research on three different fighter configurations, Capone and Mason [3] found that the pitching moment coefficient and the lateral aerodynamic coefficients varied linearly with the amount of thrust vectoring. No cross-coupling of the thrust vectoring controls existed between the lateral and longitudinal forces and moments. Thrust vector control power, for their design, was a function of Mach number and nozzle pressure ratio . In his design for a thrust vectoring controller of the F-15, Anderson [1] connected the pitch thrust control input to the same command as the collective stabilators. The yaw thrust vectoring was controlled by use of a command proportional to the sideslip angle. Because the F-15 has two engines a roll thrust vectoring control was used and this was commanded by the differential stabilator command. His design was tested in a flight simulator with USAF F-15 pilots and with simulated pilot commands. Anderson's results indicate that his thrust vector augmented F-15 was superior for most tasks when compared to the unaugmented F-15 model. One major drawback cited was the loss of airspeed in extended maximum turns.

3.4 Aircraft Model

The aircraft model used in this thesis is a FORTRAN implemented simulator of the YF-16. This is a nonlinear simulation and represents the full six degrees of freedom equations of motion. The simulator is provided by Tom Cord of FDL [4]. The YF-16 is a prototype version of the F-16, but it has less internal avionics and therefore it is much lighter and more agile [2]. Included in this simulation is a mechanism to add thrust vectoring to the YF-16. Thrust vectoring is modeled as a controllable moment driven through an actuator, that is produced by multiplying a

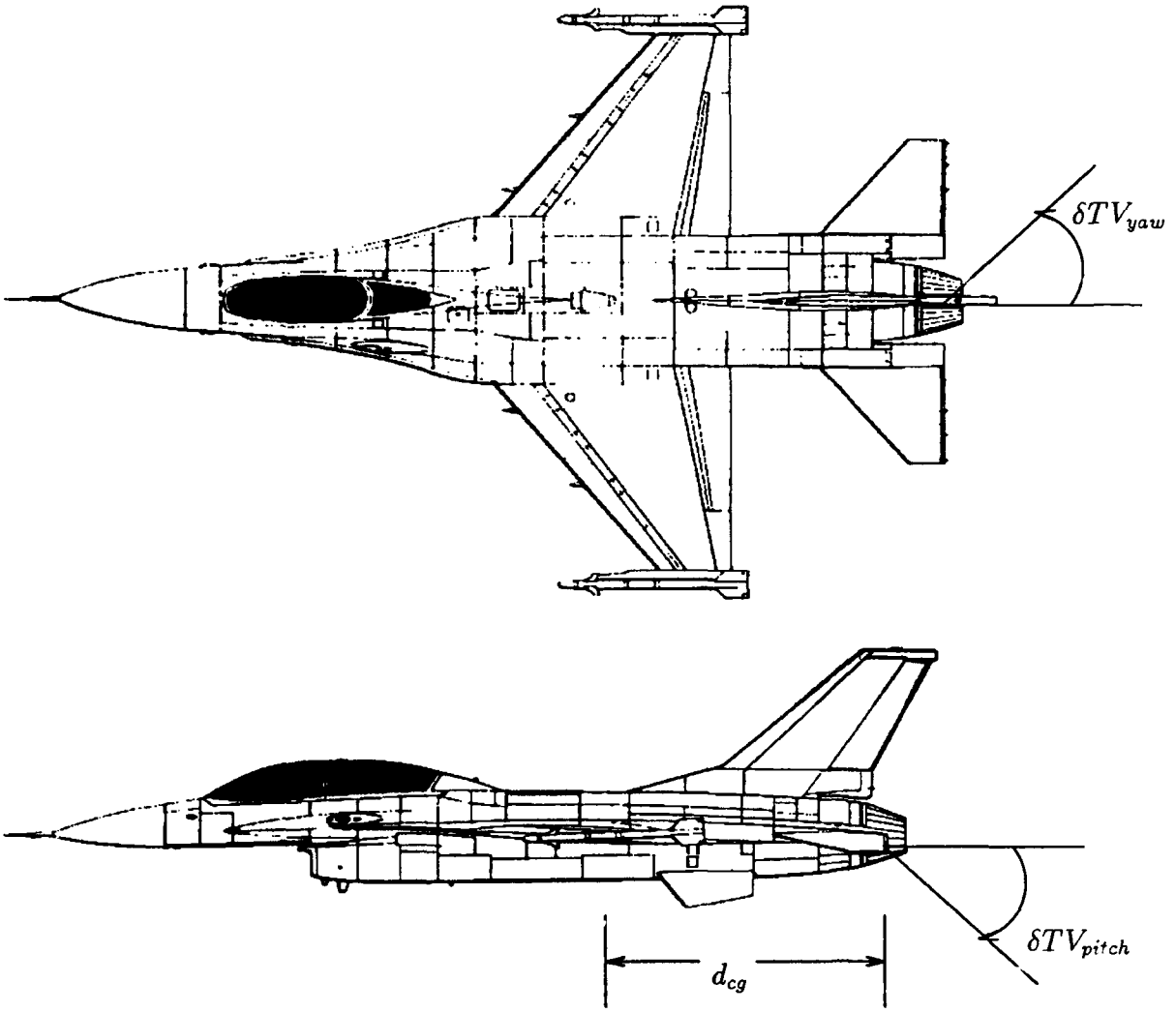

Figure 3.1. F-16

portion of the forward thrust by the distance from the center of gravity of the aircraft to the engine nozzle, in the pitch and yaw directions, see Equations (3.1) through (3.3) and Figure 3.1, where δTV_{pitch} and δTV_{yaw} are thrust deflection angles, T_x is the thrust along the x body axis, and M_y , M_z are moments produced by the thrust deflection about the y and z body axes.

$$T_x = \frac{T}{\sqrt{1 + tan^2(\delta TV_{pitch}) + tan^2(\delta TV_{yaw})}} \tag{3.1}$$

$$M_y = d_{cg} T_x tan(\delta TV_{pitch}) \tag{3.2}$$

$$M_z = d_{cg} T_x tan(\delta TV_{yaw}) \tag{3.3}$$

The effect of decreased forward thrust is also accounted for in Equation (3.1). Cord's simulation program contains a FCS which is denoted in this thesis as CFCS. The CFCS is modified to a version described in Chapter 4, shown in Figure 3.2, and denoted MFFCS . This modification is done in order to obtain the LTI models for the nonlinear plant as described in Chapter 4.

3.5 Maneuvers

The maneuvers are chosen to represent the types of maneuvers that Tamrat suggested. Three maneuvers are chosen but, due to time constraints only two maneuvers are modeled. The first maneuver is a quick pitch-up to a certain pitch angle, hold that angle and then pitch-down to unload the wings and regain energy. The second maneuver consists of a quick pitch-up and then a yaw/roll around the velocity vector. The third maneuver was to be a high alpha angle turn. To simulate the maneuvers the original control system is modified as shown in Figure 3.2. The pitch and roll channel FCSs are removed and replaced by simple feedbacks. The yaw channel FCS is left intact. These modifications are made to remove limiting devices in the original FCSs that restricted the AOA and angular rates of the aircraft simulation. There is further discussion of the control configuration in Chapter 4. Inputs to the modified FCS are in the form of vectors which are indexed in 0.05 sec increments. These vectors are developed using a Matrix_x program that facilitates trial and error input development. The simulation program is modified to read in the input vectors and write out Matrix_x programs that cause Matrix_x to plot the response verses time of several variables of interest. Before developing the specifications on the maneuvers, simulation runs are made to learn how to maneuver the simulated aircraft in a manner similar to the desired maneuvers. This is necessary to investigate how the aircraft reacts to different sets of inputs and controller gains. After each simulation run, angular rates, inputs to the plant, Euler angles, altitude, speed, AOA, sideslip angle, and control deflections are plotted versus the time of the simulation as shown in the example in Figures (3.3) through (3.5) and Appendix A. From these plots one can develop a good idea of what happens to the aircraft during the maneuvers. At this point, inputs are developed, by trial and error, to manipulate the simulated aircraft in order to fine tune the gains of the simplified FCS. One problem that arises is an excess β develops during some of the simulations. Because of stresses developed on the airframe due to β, this angle is to be kept below three degrees. This problem

is corrected by adjusting the thrust vector gains and increasing the engine thrust [2] [4]. The mechanisim used to increase the thrust from trim thrust level to maximum thrust, causes a step increase of the thrust at the start time of the simulation. This step increase in thrust is a control input to the plant that, because of an oversight, is not modeled in the development of the FCS and causes complications in latter stages of the design.

3.6 Specifications

Since there are no guidelines on the specifications on these types of maneuvers, specifications are developed that are based on maximum and minimum attainable rates and accelerations for the aircraft at certain attitudes and the experience of Barfield and Cord [2] [4]. For the pitch-up angular acceleration the specification is: the angular acceleration available from eighty percent of the difference between the maximum control power and the control power needed for stabilization. The pitch-down specification is given by the angular acceleration based on the stability derivative $C_{m_{\delta_{t_{min}}}}$=0.05. These two specifications on pitch rate acceleration $\dot{q}$ are calculated with Equations (3.4) through (3.9).

$$\dot{q}_{max} = 0.8(\dot{Q}_{total} - \dot{Q}_{stab}) \tag{3.4}$$

$$\dot{q}_{stab} = \frac{1}{I_{yy}} \left[C_{m_{\delta_e}} \delta_{e_{trim}}\right] \frac{1}{2}\rho v^2 s\bar{c} \tag{3.5}$$

$$\dot{q}_{total} = \dot{Q}_{aero} + \dot{Q}_{thrust} \tag{3.6}$$

$$\dot{q}_{aero} = \frac{1}{I_{yy}} \left[C_{m_{\delta_e}} \delta_{e_{max}}\right] \frac{1}{2}\rho v^2 s\bar{c} \tag{3.7}$$

$$\dot{q}_{thrust} = \frac{1}{I_{yy}} \left[C_{m_{\delta_t}} \delta_{t_{max}}\right] \frac{1}{2}\rho v^2 s\bar{c} \tag{3.8}$$

$$\dot{q}_{min} = \frac{1}{I_{yy}} \left[C_{m_{\delta_{t_{min}}}} \delta_{t_{max}}\right] \frac{1}{2}\rho v^2 s\bar{c} \tag{3.9}$$

The actual values for the variables are printed out from the simulation program. An additional specification is made to keep stresses on the airframe within acceptable limits, thus the sideslip angle β can not be more than 3 deg. The roll portion of the maneuvers is to accomplish a stability axis roll at three different rates. Equation (3.10) is used to convert the body axis rates to stability axis rates. The specifica-

tions for the maneuvers are contained in Table 3.1. Consolidated plots of all of the controlled variables and the velocity vector roll are shown in Figures (3.6) through (3.9).

$$p_{stab} = p\cos(\alpha) + \left[p\tan(\alpha) + \frac{g\cos(\theta)\sin(\phi)}{v_r}\right]\sin(\alpha) \tag{3.10}$$

Table 3.1. Specifications on Maneuvers

Variable	Minimum	Maximum
Positive q	15 deg/sec	50 deg/sec
Negative q	-15 deg/sec	-50 deg/sec
$\dot{q}$	15 deg/sec/sec	50 deg/sec/sec
Velocity Vector Roll	30 deg/sec	60 deg/sec

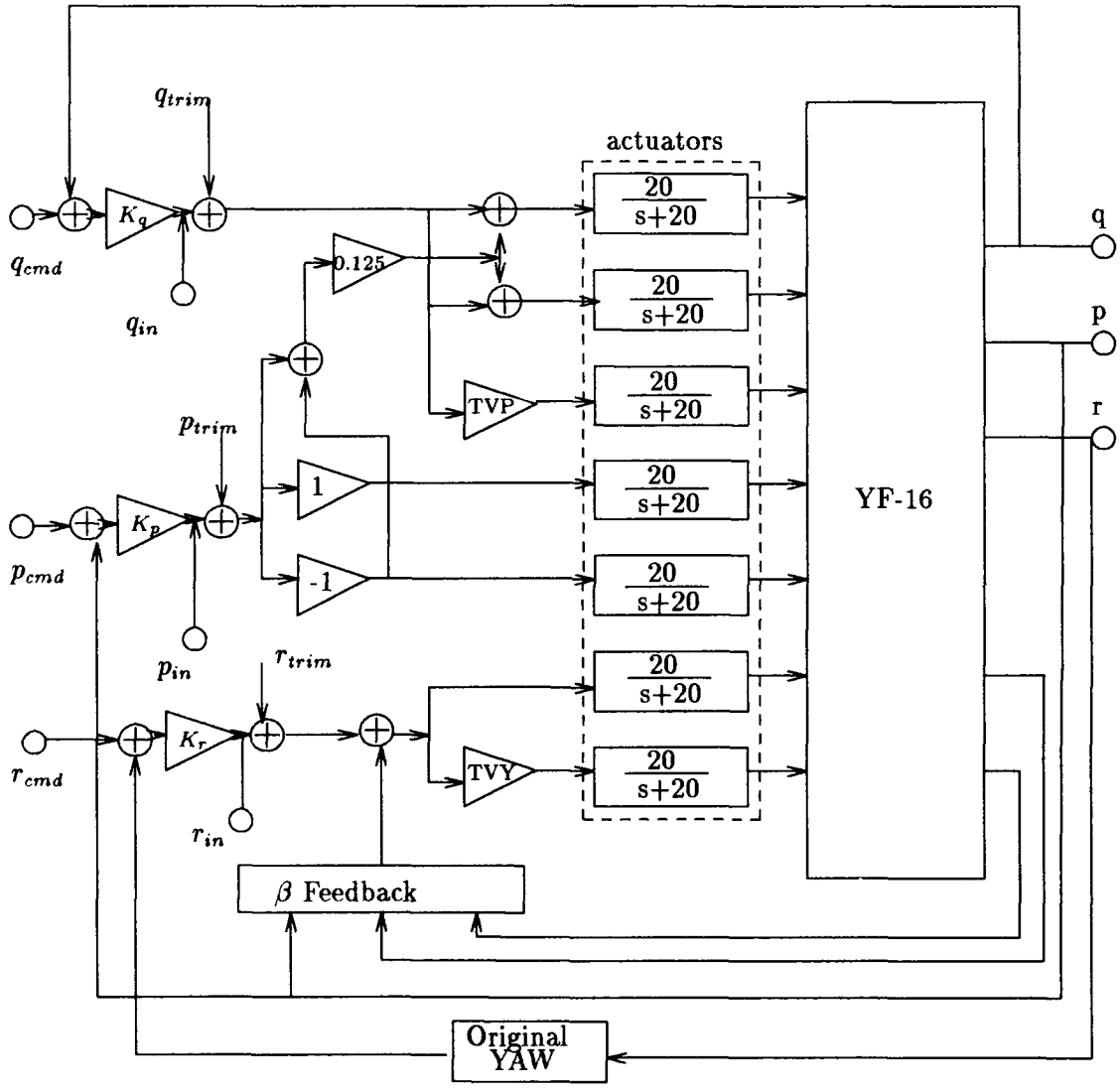

Figure 3.2. Simulation Configuration

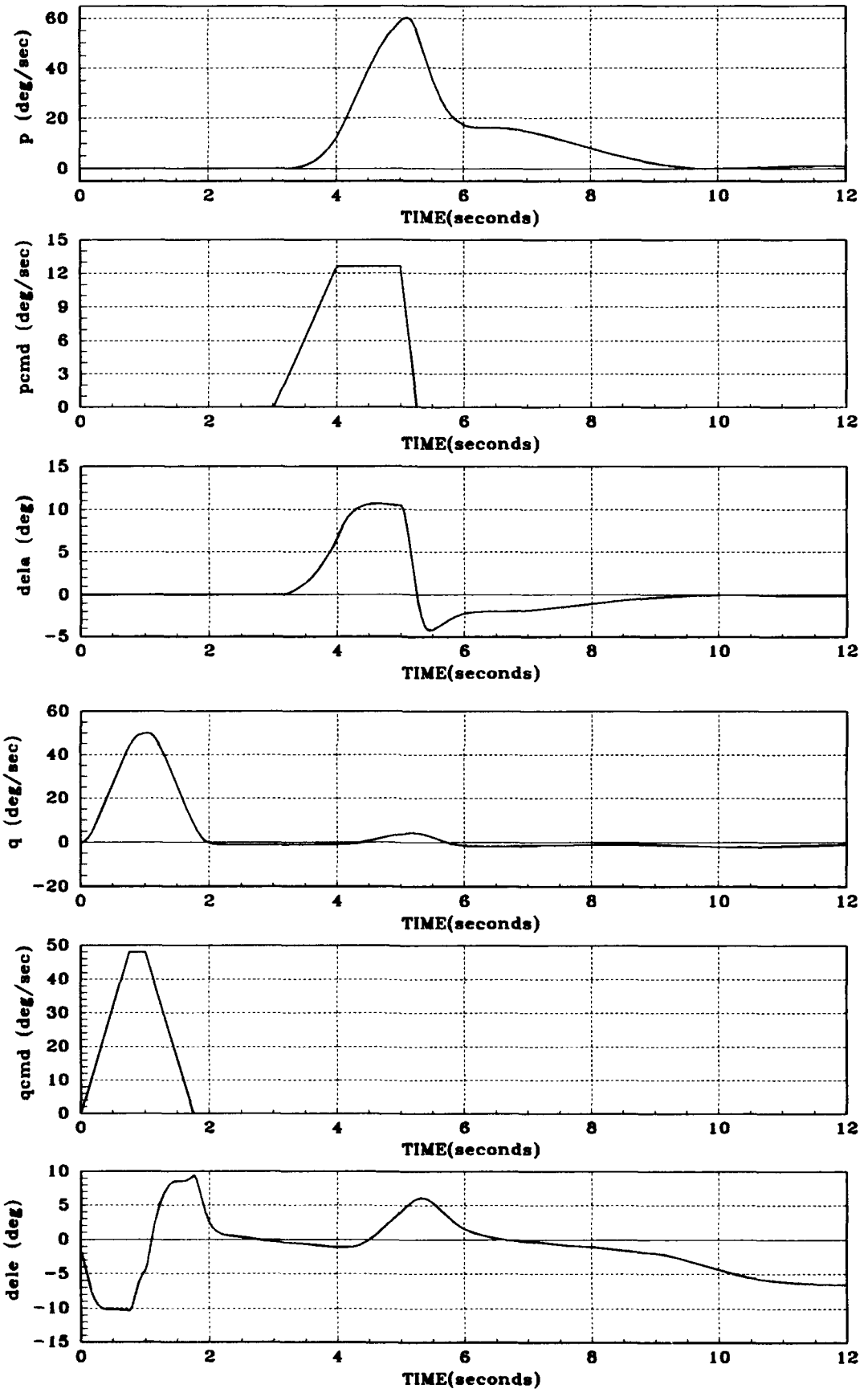

Figure 3.3. Example Maneuver #211

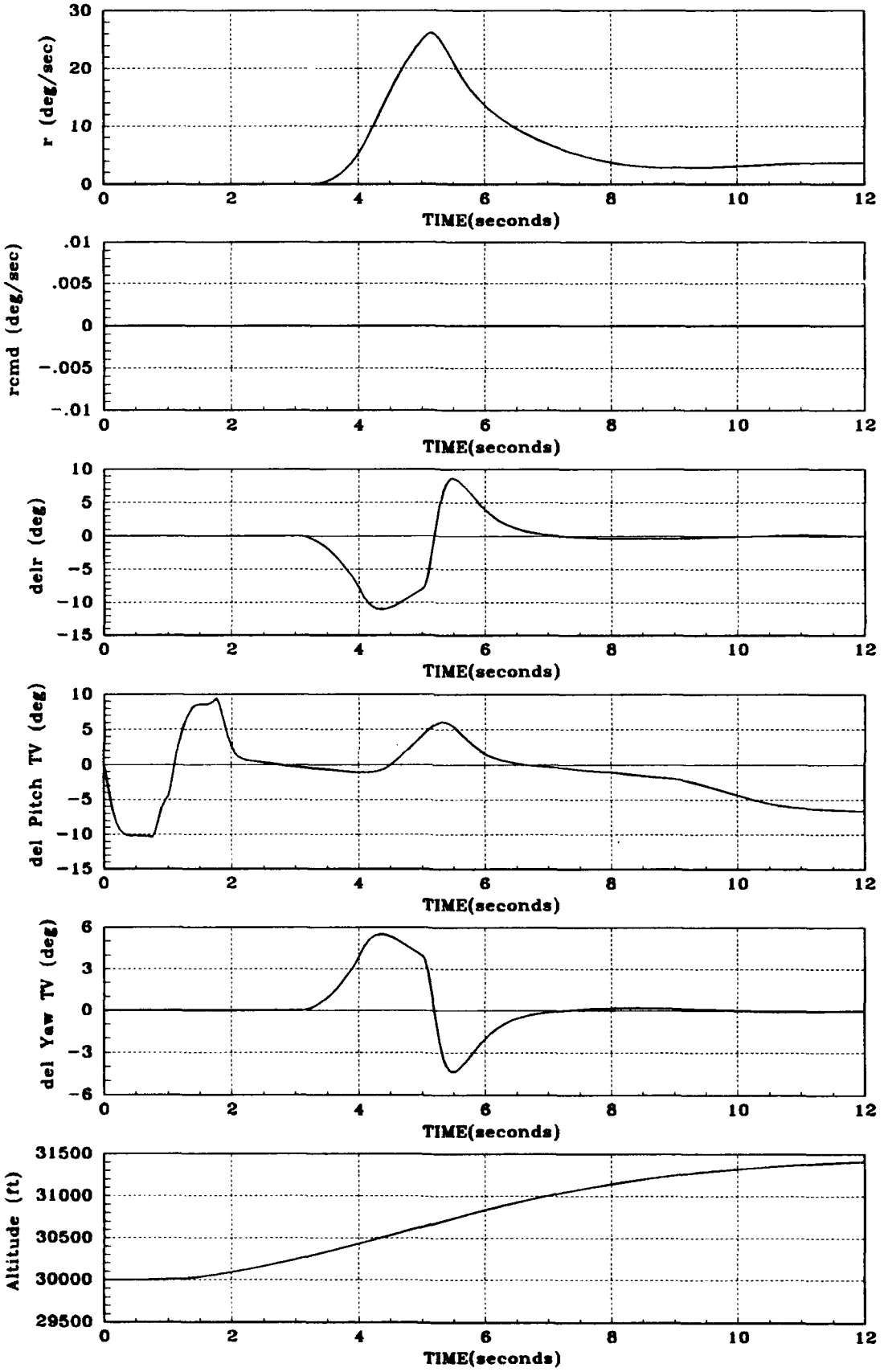

Figure 3.4. Example Maneuver #211, cont'd

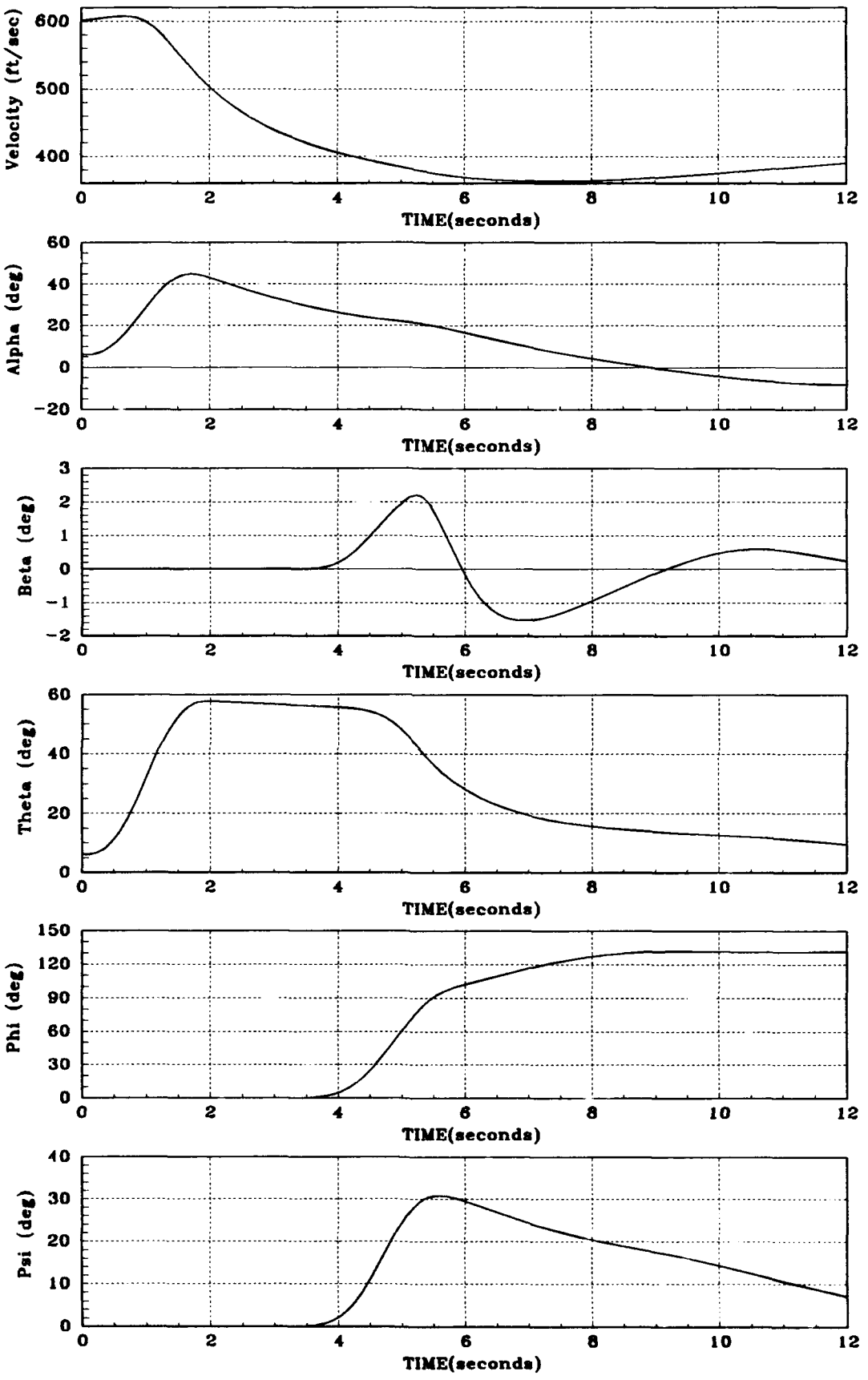

Figure 3.5. Example Maneuver #211, cont'd

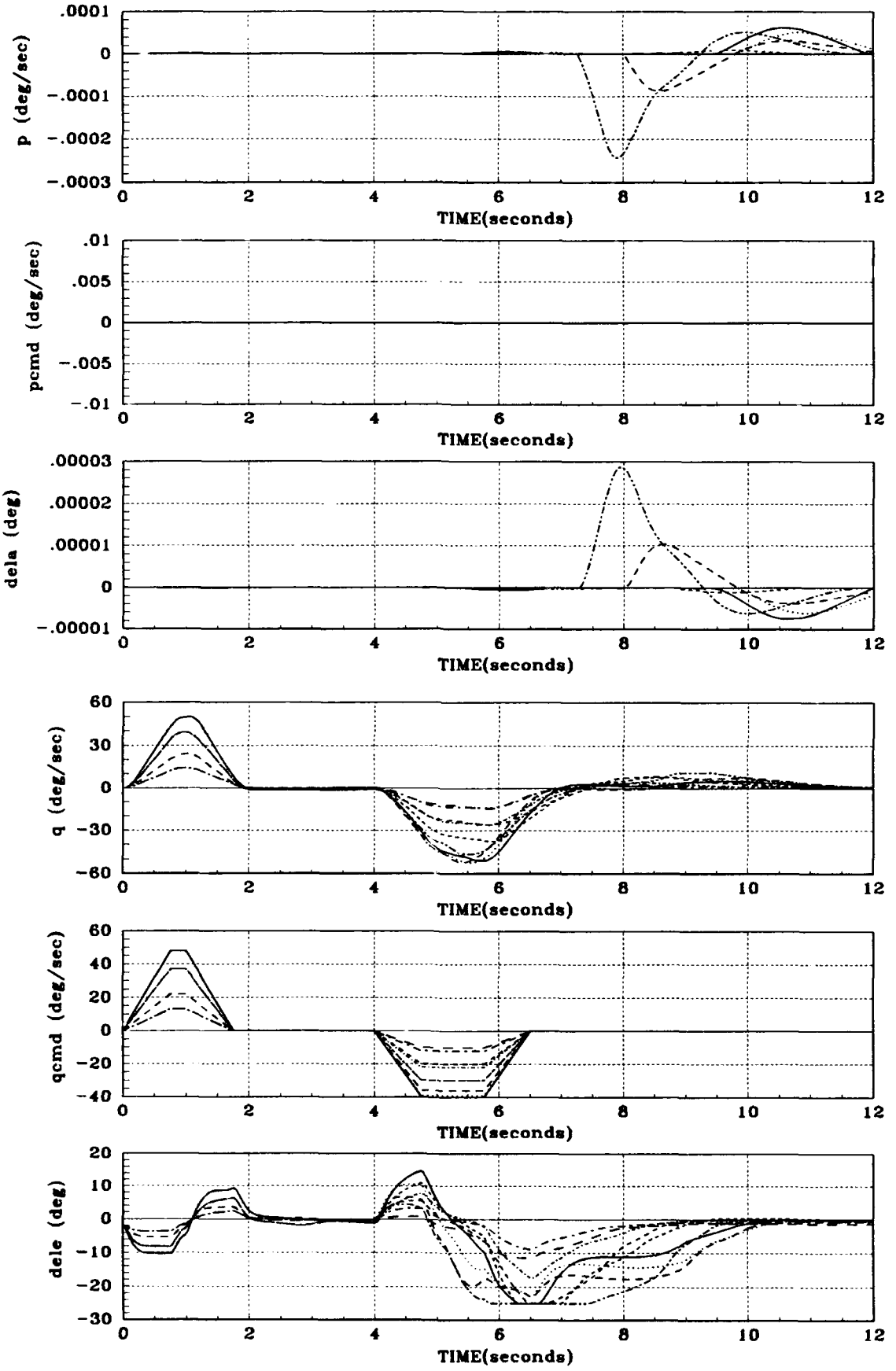

Figure 3.6. Consolidated Pitch-up/Pitch-down Maneuvers

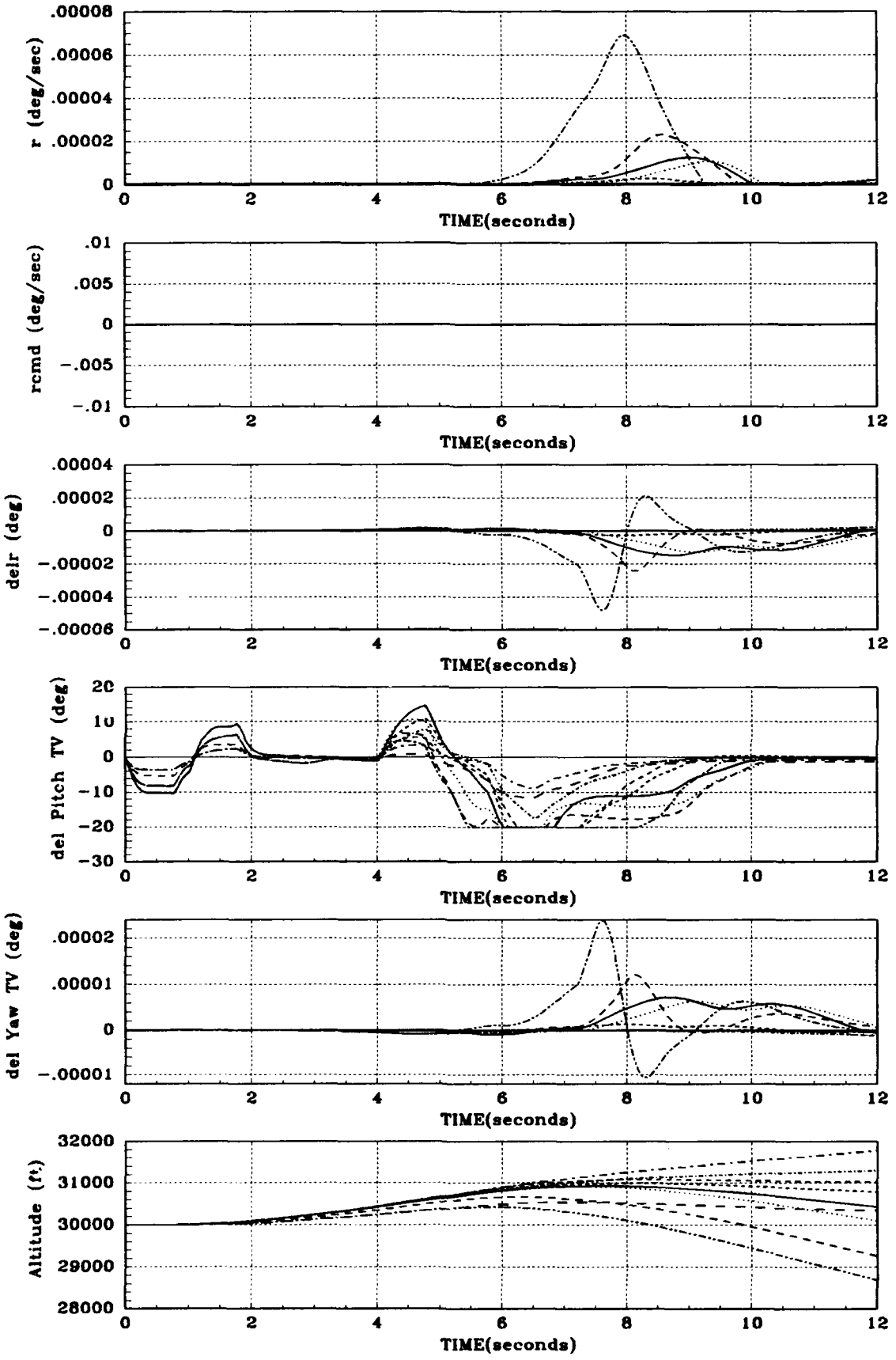

Figure 3.7. Consolidated Pitch-up/Pitch-down Maneuvers, cont'd

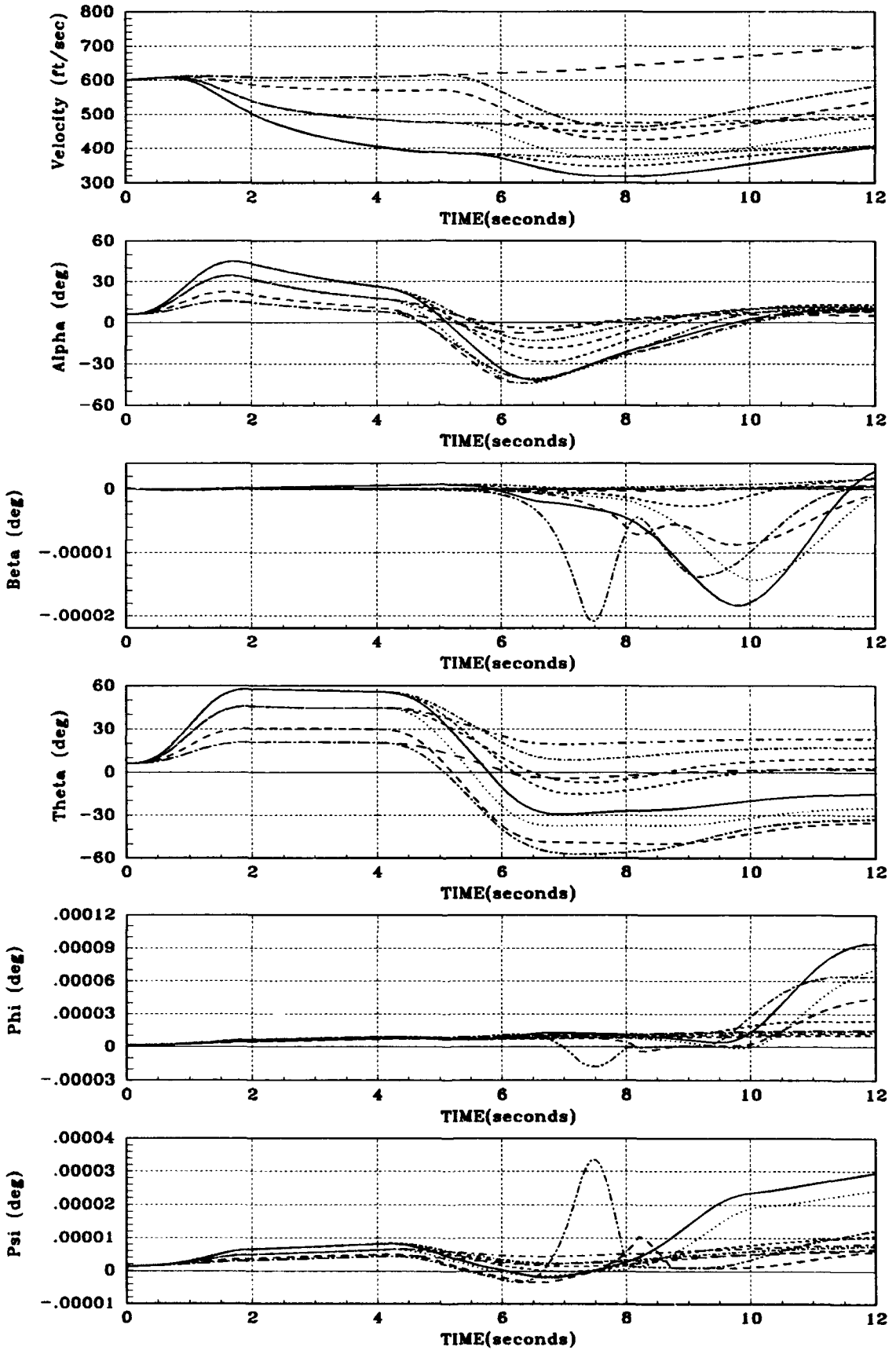

Figure 3.8. Consolidated Pitch-up/Pitch-down Maneuvers, cont'd

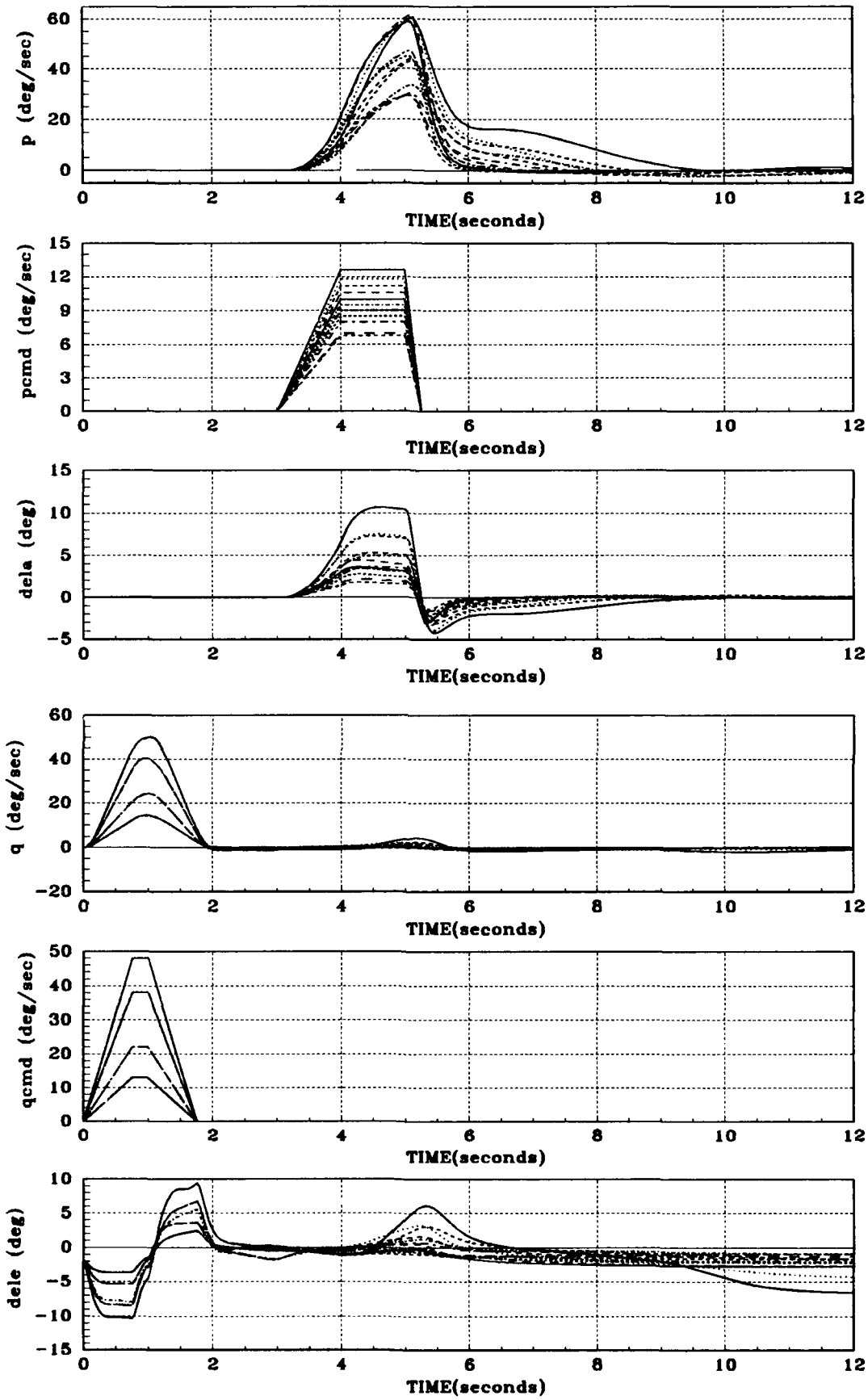

Figure 3.9. Consolidated Pitch-up/Roll Maneuvers

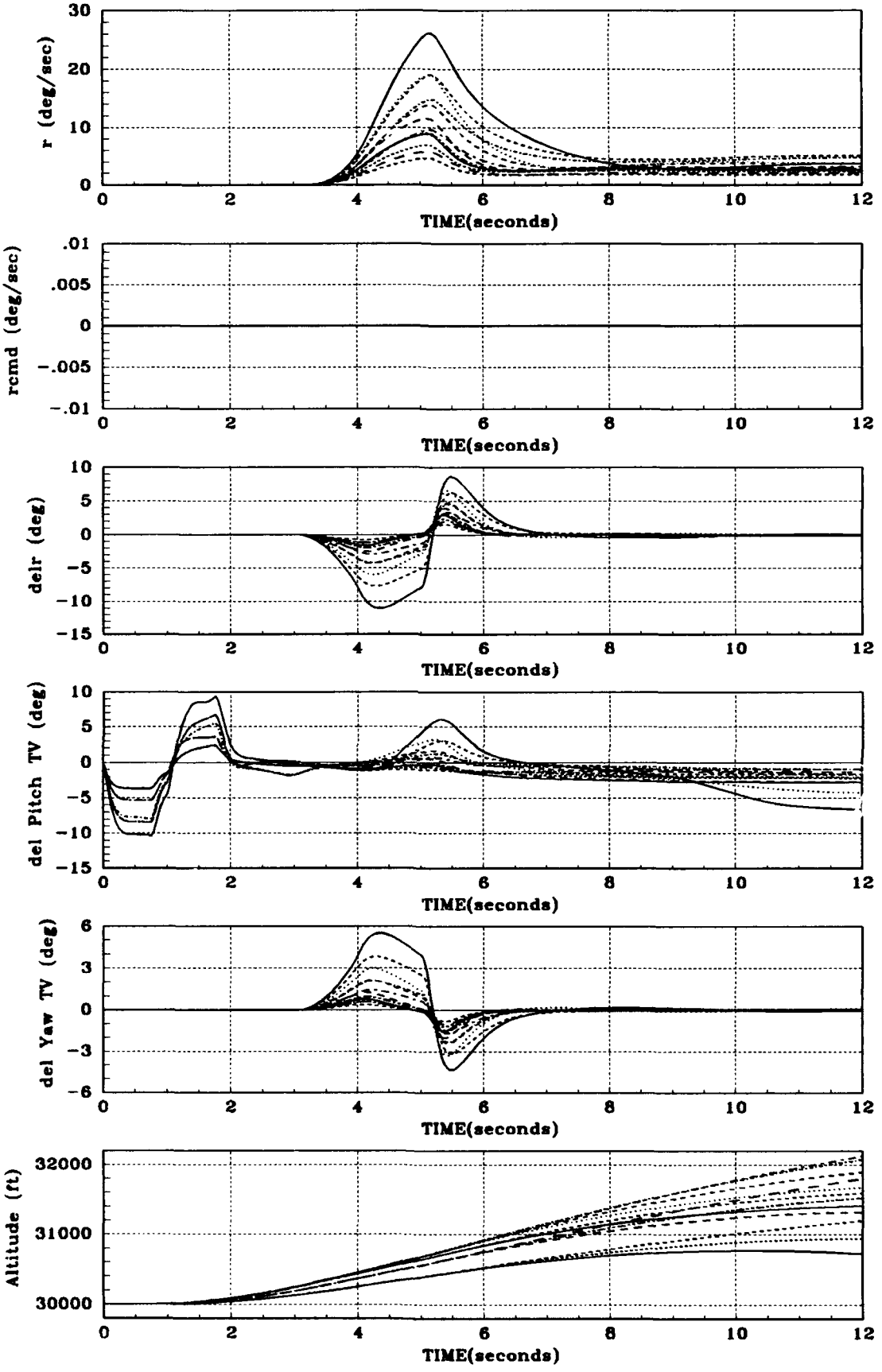

Figure 3.10. Consolidated Pitch-up/Roll Maneuvers, cont'd

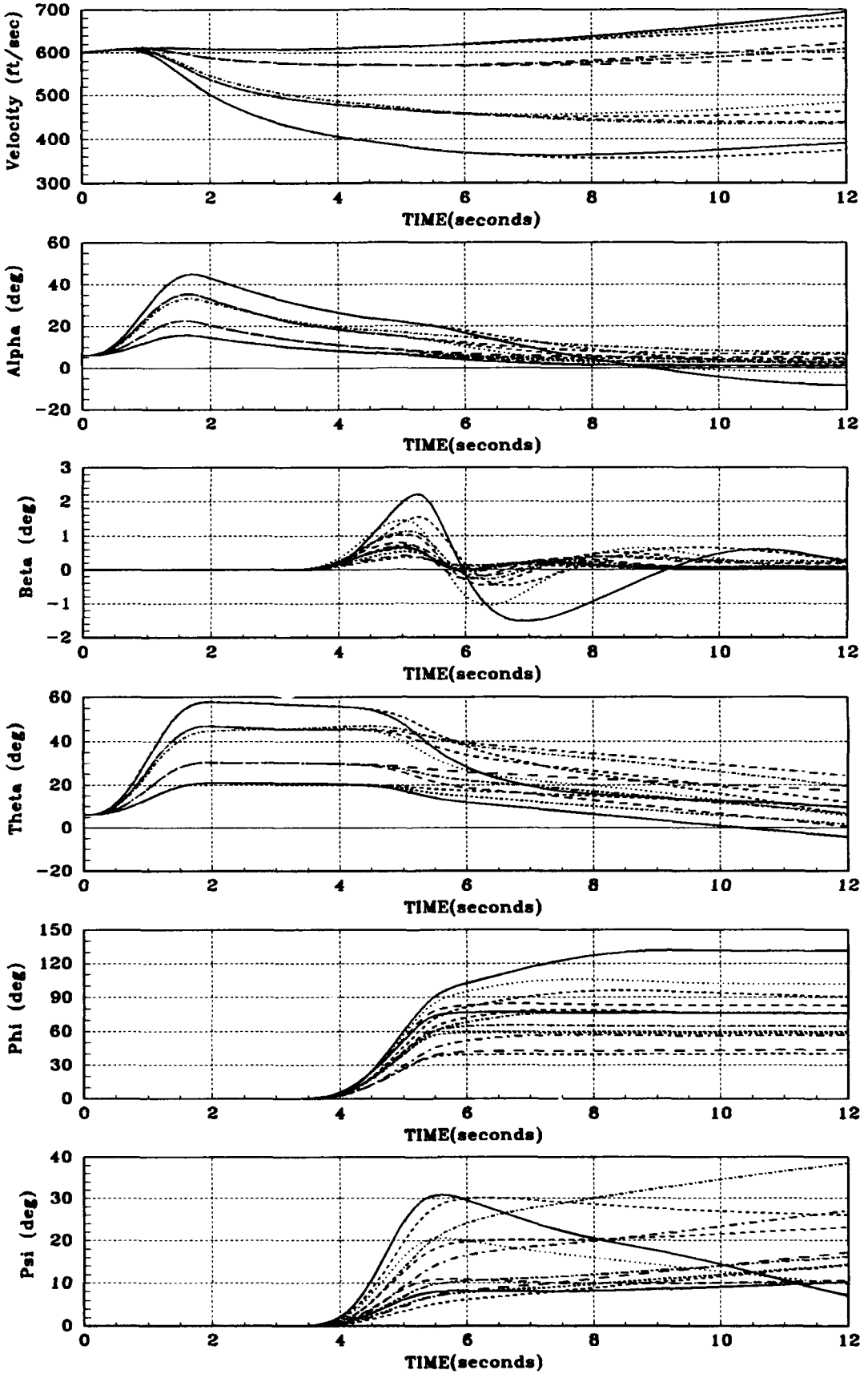

Figure 3.11. Consolidated Pitch-up/Roll Maneuvers, cont'd

3.7 Summary

This chapter presents the background for the choice of maneuvers and the aircraft. The maneuvers are chosen to emulate high AOA maneuvers that are theorized advantages for future aerial combat. The use of thrust vectoring with the YF-16 simulation produces a fighter aircraft model that can operate in an expanded flight envelope. This chapter also presents the specifications on the maneuvers and hence the FCS. Chapter 4 describes the model development based on system identification.

IV. Model Development

4.1 Introduction

This chapter describes the methods used and discusses some of the obstacles encountered during development of the mathematical models that are used to describe the aircraft in the nonlinear QFT design process. According to Ljung and Soderstrom developing a mathematical model of a physical system based on input/output time histories is called system identification [14]. There are two steps to this task: first is deciding on a family of candidate models and second is selecting the particular model from that set that adequately relates the input/output time histories. The adequacy of this model is an issue the developer must address based on the application intended for the model. There are two major classes of identification techniques, recursive and batch. Recursive techniques are predominantly used in on-line applications such as adaptive controllers. These techniques usually operate on one segment of the discrete time history per iteration. Batch identification techniques operate on the entire time history at one time and are used for identifying systems where the entire time histories are available. Because all of the time history is known, a batch identification technique finds an optimized model of the system, compared to models produced by recursive techniques. Since all of the time history is available for this thesis, a batch method is used.

4.2 Previous Research

Kobylarz and Miller, in their theses, used a batch technique for developing their mathematical models. This technique was based on a technique devised by Golubev [12][18]. Given a model for the transfer function or functions, this technique calculates the parameters of the model from the defining mathematical equations using a least squares approach. A good explanation of this technique can be found in Miller's thesis [18]. Kobylarz [12] used this technique on a SISO problem and Miller extended the technique for his MIMO design.

4.3 Other Techniques

Part of the goal of this thesis is to explore other methods of system identification. The majority of techniques used in batch identification are based on least

squares, extended Kalman Filter, and maximum likelihood. Techniques representing all three of these mathematical theories are implemented in Matrix$_x$ [16]. The least squares approach uses linear algebra to manipulate the time histories and then uses least squares to approximate the transfer function model parameters. By using an extended Kalman filter, the EKF function in Matrix$_x$ can estimate the states of the system. The state estimation can be used as is or transformed into a transfer function form. This thesis uses a Matrix$_x$ batch technique based on a maximum likelihood function called maxlike. There are two criteria used in the selection of the maxlike function. The identification technique has to be able to handle MIMO plant identification. Because of numerical accuracy limitations in Matrix$_x$, the function must be able to handle continuous transfer function matrices in the Laplace domain. The maxlike function meets both criteria.

4.4 Maximum Likelihood Function

Maxlike is a system identification function based on a maximum likelihood function. Essentially what maxlike does is iteratively execute a model, defined by the user, that relates the output time history data to the input time history data. This model can be any Matrix$_x$ executable program. During the iterations maxlike uses a maximum likelihood function to estimate parameters contained in the model to obtain a best fit of the model to the input/output time histories. An initial parameter vector is supplied by the user. The maxlike function iterates until it converges on a solution or until the user defined maximum number of iterations are exhausted. The maxlike function executes the model once for each parameter for each point in time so that the number of parameters, the complexity of the model and the number of time points all have an effect on the length of time required to find a solution.

4.5 Testing Maxlike

To become familiar with and test the maxlike function the F-16 simulation program Genesis is used to obtain linearized equations of motion for an F-16 traveling at 0.9 Mach at 30,000 ft. Using Matrix$_x$, step responses are produced for the equations and then using a state-space model, a system identification run is made. A state-space model is used because the linearized equations produced by Genesis are in state-space form. A step response for the resulting state-space system is calculated

and compared to the original step response. The two responses fit together very closely and therefore the new state space is a good candidate model of the first. There is a concern with cross-terms in the resulting equations being similar to those in the original equations, but according to Horowitz, in using the nonlinear QFT method, the equivalent system must reproduce the original output given the original input and no constraints are made as to the appearance of the equivalent plant [9]. During this testing, it is apparent that the quality of resulting equivalent systems is a function of the initial parameters, the form of the model, and the length of time of the data. Furthermore the length of time the identification process takes is a function of the computer system used. For one particular set of data and one particular model the identification process takes as long as 6 hours on a VAX to 30 minutes on a Sparc workstation. This time is a significant factor when ones considers that a large number of equivalent plants, 26 in this case, are necessary to model a relatively large flight envelope.

4.6 Simulator Compensator Configuration

After verifying that maxlike produces acceptable results for the test case, the next step is to set up the simulation program to be able to generate the necessary time histories. Cord's YF-16 simulator program is modified by removing the original compensator for the pitch and roll channels and modifying the compensator for the yaw channel. As shown in Figure 3.2, the original pitch and yaw compensators are replaced by simple feedback loops that consist of negative feedback of the variable of interest and the insertion of a gain in the forward loop. This type of compensation is used so that the commanded output of the aircraft is a signal similar to the desired output. Another reason to modify the existing pitch and roll compensation is the original compensation contained devices to limit the angle of attack.

4.7 Yaw Channel Configuration

Because the goal of a velocity vector roll is to keep the sideslip β at a minimum, some kind of feedback is required. This feedback can be made part of the plant as shown in Figure 3.2. In this figure the original yaw channel compensation is used and the feedback signals representing the yaw and β are separated. β feedback can also be accomplished after the inner loop compensator is designed. In this situation the original β feedback is used to obtain the desired output. Figure 4.1 shows how β

feedback is used for plant generation but is not part of the plant. As explained later in this chapter, there is a big difference in how each of these plants can be modeled with the maxlike function.

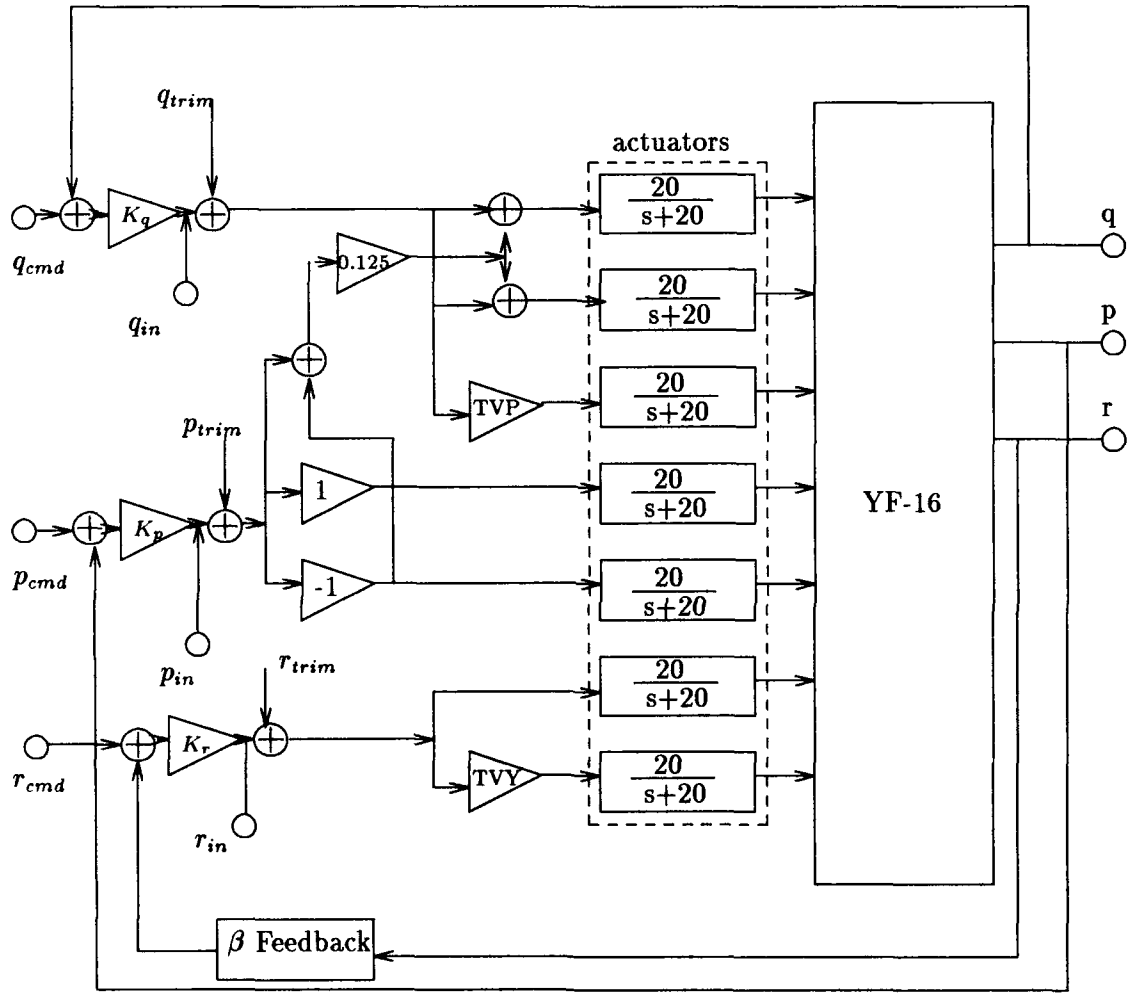

Figure 4.1. Simulation Configuration without β Feedback included in the Plant

4.8 Thrust Vectoring

In his simulation program, Cord designed a method to actuate a change in the direction of the thrust nozzle. For this simulation, based on Cords's experience [4], actuators similar to those of the control surfaces are used for the thrust vectoring.

The control signals to the pitch actuators and the yaw actuator are connected to the pitch and yaw thrust vectoring actuators through gain blocks as shown in Figure 4.1. By connecting the thrust vectoring this way a square plant matrix is achieved, thus, the task of developing a weighting matrix is eliminated. The gains in the thrust vectoring loops take the place of the weighting matrix and become part of the plant.

4.9 Simulations

After the simulation program is modified the input/output time histories are produced based on the specified maneuver envelopes. To produce the desired output from the simulation program, input command time history vectors are produced using Matrix_x . To find the desired response of the aircraft, the response to these input vectors, the variables of interest are plotted versus time. At first, simple step commands are applied to the inputs and the gains are adjusted to obtain the best response. The best response is one that follows the command as closely as possible without causing oscillations in the control surfaces. After many trials unity gain for pitch, roll, and yaw seem to give best results for all maneuvers. The thrust vectoring gains have the most effect on the response of the simulation. Any increase from unity resulted in oscillations in the related control surfaces. Since the maximum angles that the thrust actuators can move is 20 degrees and the maximum angle the control surface can move is 25 degrees, the thrust actuators vectoring saturate before the aerodynamic surfaces. Because of this, gains on thrust vectoring are lowered below the level that causes control surface oscillations to help prevent these saturations. Another indicator for the thrust gains is the amount of β. Note, as the gain on the yaw channel of thrust vectoring is reduced from unity the amount of β decreases until a particular gain is reached and then β increases.

4.10 Maneuvers

The maneuvers are produced by trial and error. An input vector that represents the command for the desired output is formulated using Matrix_x and then the simulation is executed using this input vector. The resulting output is plotted versus time and the input is adjusted until the desired output is produced. To represent the specifications on the pitch-up/pitch-down, four maneuvers are chosen and implemented as shown in Figure 3.6 through 3.8. To represent all of the conditions in this envelope, each pitch down rate must be accomplished after each specific pitch-up

maneuver. This gives sixteen responses. When the nose of the aircraft is not pitched up very high the fast pitch down causes problems with the system identification which is discussed later, and so these pitch down maneuvers are not implemented. Three roll maneuvers are chosen to represent the roll specifications as shown in Figure 3.9 through 3.11. Each of these roll maneuvers must be accomplished from the pitch attitude developed from one of the four pitch-up maneuvers so there are twelve maneuvers associated with roll. All together there are twenty-two maneuvers to represent the specifications. At this point the input/output vector time histories are stored in file to be used in the system identification process.

4.11 Initial System Identification

As stated before the equivalent plant is found through the use of maxlike in Matrix_x . The first model used to define the equivalent plant is shown in Equations (4.1) through (4.3).

$$P_k = \begin{bmatrix} \frac{p_{11}}{d_1} & \frac{p_{12}}{d_1} & \frac{p_{13}}{d_1} \\ \frac{p_{21}}{d_2} & \frac{p_{22}}{d_2} & \frac{p_{23}}{d_2} \\ \frac{p_{31}}{d_3} & \frac{p_{23}}{d_3} & \frac{p_{33}}{d_3} \end{bmatrix} \tag{4.1}$$

$$p_{ij} = P_{a_{ij}} s^4 + P_{b_{ij}} s^3 + P_{c_{ij}} s^2 + P_{d_{ij}} s + P_{e_{ij}} \tag{4.2}$$

$$d_i = P_{f_i} s^5 + P_{g_i} s^4 + P_{h_i} s^3 + P_{i_i} s^2 + P_{j_i} s + P_{k_i} \tag{4.3}$$

This model is a matrix of transfer functions each having fourth-order over fifth-order, numerator over denominator, with a common denominator for each row. This model proves to be unsatisfactory because of non-minimum-phase (NMP) plants, which is explained later in this chapter. From earlier testing the initial parameter vector is chosen to be a vector of zeros. Results from this setup are not good, the equivalent plant does not reproduce the original desired output with the corresponding input.

4.12 Time Segments

After trying different initial parameters, with no success, a smaller time segment is used to see if smaller individual features can be modeled and the resulting equivalent plant used as the initial parameter vector for a larger segment of time. The results are mixed, the smaller segment of time produces an acceptable model, one that follows the major features of the response, but when this plant is used as

an initial vector the equivalent plant is not acceptable. At this point it is decided that since there are intervals of time where the dynamics of the maneuvers are close to steady state which results in very small derivatives in these intervals, the maneuvers can be broken into time segments and used in the nonlinear QFT process as individual plants. This time division is made at the three second point in all maneuvers. The first three seconds of all of the maneuvers is a pitch up. For the nonlinear QFT process the four different pitch-up maneuvers result in four plants. The ten different pitch-down maneuvers are separate plants as are the twelve roll maneuvers. Subtracting the six plants not modeled due to the pitch-down problem gives a total of twenty equivalent plants to model.

4.13 Modeling Difficulties

The model chosen to represent the nonlinear aircraft equations is a matrix of transfer functions that are each fourth-order over fifth-order as shown in Equations (4.1) and (4.2). Modeling the remaining pitch-up/pitch-down maneuvers is accomplished with no difficulties. The roll maneuver presents some difficulty, probably because of the coupled nature of the maneuver. To try to get a good transfer function fit, different initial parameters are chosen. To choose the different parameters, knowledge of the physics of the aircraft and an insight in the operation of transfer functions are used to separate the transfer function matrix into three sub-matricies. The idea is to find the parameters for these sub-models and then combine the results into an initial parameter vector for the whole physical model. This approach produces acceptable transfer function fits.

4.14 Non-Minimum-Phase Plants

After the equivalent plants have been generated, they are examined by factoring the polynomials into roots. At this point the equivalent plants are found to be NMP. These zeros are in the range of 1 to 10, this means that the QFT design technique cannot be used for these transfer functions. According to Horowitz, the only control design method that has been shown capable of a design with this relative magnitude of right-half-plane (RHP) zeros is the singular-g method [9]. The singular-g method was used by Walke in his thesis and essentially uses matrix manipulation, a singular compensation matrix, and trial and error to design a compensator. To try to prevent NMP zeros, the initial parameters are manipulated to try to keep all of the zeros

negative, this does not work. After much work in manipulating the parameters, a new model is developed that constrains the equivalent plants to be MP. This model, shown in Equations (4.4) and (4.5) , uses Matrix_x functions such as the absolute value, abs, to insure no RHP zeros are allowed in the equivalent plants.

$$P_k = \begin{bmatrix} p_{11} & p_{12} & p_{13} \\ p_{21} & p_{22} & p_{23} \\ p_{31} & p_{23} & p_{33} \end{bmatrix} \tag{4.4}$$

$$p_{ij} = \frac{P_{a_{ij}}(s + |P_{b_{ij}}|)(s + |P_{c_{ij}}|)(s + |P_{d_{ij}}|)(s + |P_{e_{ij}}|)}{P_{f_{ij}}s^5 + P_{g_{ij}}s^4 + P_{h_{ij}}s^3 + P_{i_{ij}}s^2 + P_{j_{ij}}s + P_{k_{ij}}} \tag{4.5}$$

4.15 Non-Minimum-Phase Effects

There are parts of the maneuvers that can not be modeled under the constraint that a MP model be achieved. By removing the β inner loop feedback it is possible to model the roll maneuvers. It appears that the β feedback causes the plants to be strongly NMP. The β feedback is removed, as shown in Figure 4.1, and all of the maneuvers are simulated to collect the input/output time histories. Six of the maneuvers can not be modeled by this method. These maneuvers represent the fast pitch-down after a relatively slow pitch-up. It appears that these maneuvers can not be modeled as MP and the decision is made to exclude them from the flight envelope. This decision is justifiable because these maneuvers have the aircraft pitching down well past the attitude intended by the concept of the maneuvers.

4.16 Non-Minimum-Phase q's

After finding the equivalent MP plants for the maneuvers, it is necessary to invert the **P** matrices to obtain the **P*** matrices. Upon completion of this inversion, the individual $q_{ij(o)}$ transfer functions are found to be NMP. The solution to this problem is to bypass the direct development of the P matrices and use the system identification routines to directly identify the q_{ij}s under the constraint of achieving

MP q_{ij}s, see Equations (4.6) and (4.7).

$$\mathbf{p}^{-1} = \mathbf{p}^* = \left\{p_{ij}^*\right\} = \left\{\frac{1}{q_{ij}}\right\} = \begin{bmatrix} p_{11}^* & p_{12}^* & p_{13}^* \\ p_{21}^* & p_{22}^* & p_{23}^* \\ p_{31}^* & p_{23}^* & p_{33}^* \end{bmatrix} \tag{4.6}$$

where,

$$p_{ij}^* = \frac{1}{q_{ij}} = \frac{P_{a_{ij}} s^5 + P_{b_{ij}} s^4 + P_{c_{ij}} s^3 + P_{d_{ij}} s^2 + P_{e_{ij}} s + P_{f_{ij}}}{P_{g_{ij}}(s + \left|P_{h_{ij}}\right|)(s + \left|P_{i_{ij}}\right|)(s + \left|P_{j_{ij}}\right|)(s + \left|P_{k_{ij}}\right|)(s + 100)} \tag{4.7}$$

There are benefits derived from this solution. One is that no inversion of the three by three matrix of transfer functions is needed, easing the numerical burden on Matrix_x . Another is lifting the constraint that the rows in the transfer function matrices had to have a common denominator. Modeling the equivalent plant as a matrix of transfer functions with individual denominators produces better fits and the time required for system identification is reduced dramatically. Plots of the input, equivalent plant input, and outputs are shown in Appendix 2. All of the plants are modeled and the transfer functions are shown in Appendix 3.

4.17 Conclusion

This chapter covers the development of equivalent plants that are used in the nonlinear QFT method for FCS design. First system identification is discussed with a concentration on batch identification techniques. This is followed by by a discussion of the methods used to obtain the input/output time histories needed for system identification. Problems with identifying the plants is discussed including NMP plants, long time segments, and NMP q_is. In the next chapter, the method of finding the effective plants and Matrix_x generated boundaries are discussed.

V. QFT FCS Design

5.1 Introduction

This chapter details the development of $\mathcal{Q}_{ij(k)}$ and the design of boundaries that dictate the shape of $l_{o_{i(k)}}$. The first section of the chapter explains an experiment showing that Matrix$_x$ does not have a robust method of accommodating high order rational transfer functions, which has an observable impact on the development of $\mathcal{Q}_{ij(k)}$. Next is a discussion of $\mathcal{Q}_{ij(k)}$ and how, in some cases, boundaries can be developed to reduce the number of its large RHP poles. The final topic of this chapter is the development of the stability boundaries and the boundaries used to reduce large RHP poles which, in this thesis, are called Γ-boundaries .

5.2 Matrix$_x$ Algorithm Robustness

During the development of $\mathcal{Q}_{ij(k)}$, plants are developed that are as high as 54^{th} order. These high order transfer functions are probably due to inaccuracies which are a result of the Matrix$_x$ algorithms that are not robust enough to accommodate high order plants. A simple experiment is performed to show the limits of the Matrix$_x$ algorithm robustness [20]. Ten eigenvalues are taken whose values range from -1 to -10. These eigenvalues are used to form the polynomial B, as shown in Equations (5.1) and (5.1).

$$A = (\lambda+1)(\lambda+2)(\lambda+3)(\lambda+4)(\lambda+5)(\lambda+6)(\lambda+7)(\lambda+8)(\lambda+9)(\lambda+10) \quad (5.1)$$

$$B = poly(A) = \lambda^{10} + a_9\lambda^9 + a_8\lambda^8 + a_7\lambda^7 + a_6\lambda^6 + a_5\lambda^5 + a_4\lambda^4 + a_3\lambda^3 + a_2\lambda^2 + a_1\lambda^1 + a_0 \quad (5.2)$$

This is accomplished in Matrix$_x$ by entering the vector, A^t=[-1 -2 -3 -4 -5 -6 -7 -8 -9 -10], whose elements reresent the eigenvalues. The polynomial is then formed by using the Matrix$_x$ command, B=poly(a). The location of the roots of the resulting

polynomial are plotted in Figure 5.1. As seen in the figure, some warping has taken place, that is, the given real eigenvalues have migrated into the imaginary region. By changing the numbers of roots it is found that plants with 8^{th} order polynomials do not exhibit the warping associated with manipulations of higher order plants. As the order of plants increase the magnitude of the warping seems to increase, see Figure 5.2 for a 54^{th} order example. As in the first example, the second example starts with a 54^{th} order vector of all real eigenvalues, this time the λ_i's are arranged from -1 to -54 at increments of -1 along the real axis. When the eigenvalues are transformed

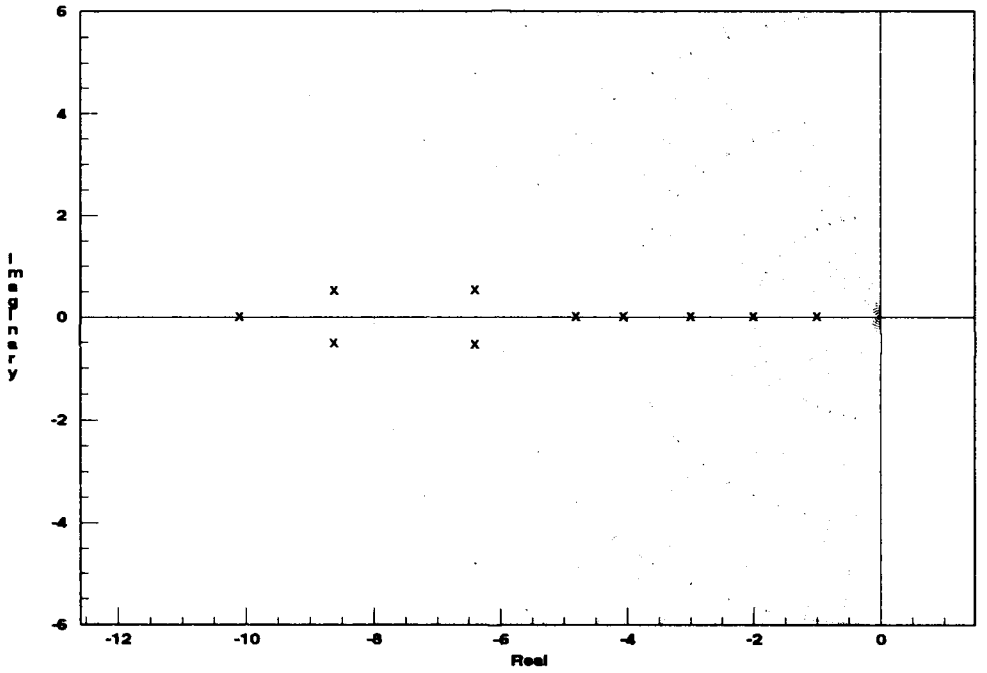

Figure 5.1. Matrix$_x$ Robustness 10^{th} Order Real Roots

into polynomial form as previously discussed, the roots of B, as shown in Figure 5.2, result. The implication of this experiment is: manipulations, such as convolution of transfer functions result in transfer functions where there are not many pole/zero cancellations due to warping, whereas in reality there can be common poles and zeros in these plants that should cancel. This compounds the problem because plant manipulations result in abnormally high order plants and any subsequent manipulations of these plants result in even more severe warping of poles and zeros. Matrix$_x$

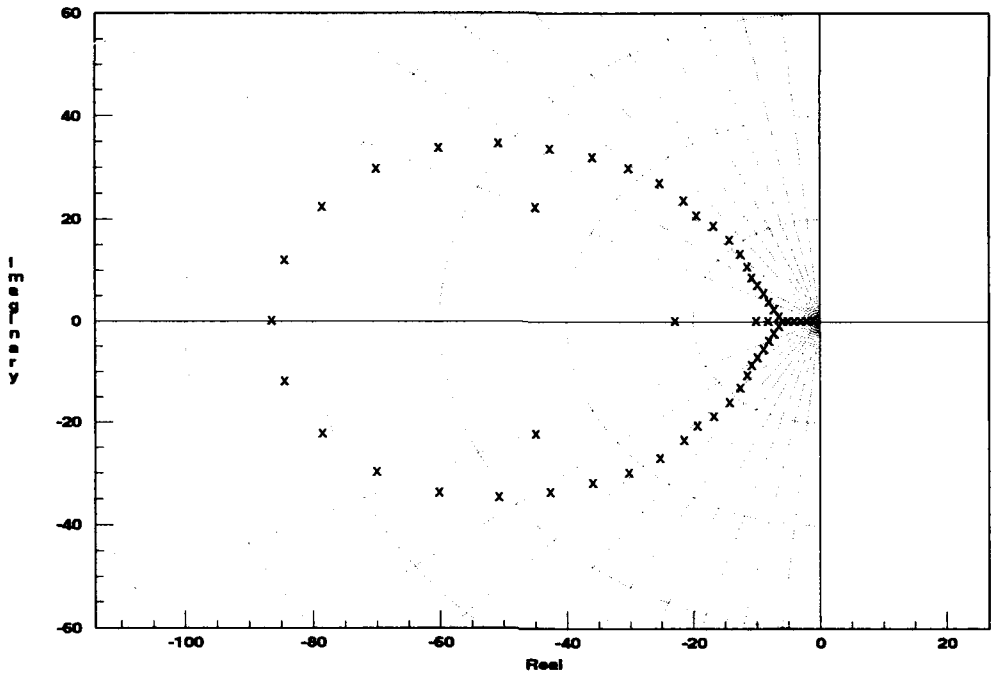

Figure 5.2. Matrix$_x$ Robustness 54^{th} Order Real Roots

is used for all the manipulations in this thesis because this problem did not show up until late in the design process. Subsequent theses will need to consider this problem early in the process.

5.3 $\mathcal{Q}_{ij(k)}$ Development

According to Horowitz, to ensure stability for the MIMO problem, $\mathcal{Q}_{ij(k)}$ must be developed [9].Since this thesis only uses stability bounds, cross-coupling in the plant matrix is not accounted for in disturbance boundaries, therefore the only factor that accounts for these cross-coupling terms is the use of $\mathcal{Q}_{ij(k)}$ in the design process. The equations used to develop $\mathcal{Q}_{ij(k)}$, repeated from Chapter 2, are Equations (5.3) and (5.4).

$$q_{ij(k)} = \frac{q_{ij(k-1)}(1 + l_{i(k-1)})}{1 - \gamma_{ij(k)} + l_{i(k-1)}} \tag{5.3}$$

$$\gamma_{ij(k)} = \frac{q_{ik(k-1)} q_{kj(k-1)}}{q_{ij(k-1)} q_{kk(k-1)}} \tag{5.4}$$

These equations are programmed in Matrix$_x$ to develop $\mathcal{Q}_{ij(k)}$. As explained in Chapter 6, the overall FCS is divided into FCSs that are scheduled in the nonlinear simulation. Each FCS is designed using the same method as the others, therefore this description concentrates on the design of the first loop and only give details of the design of the other loops when important. After l_{o_1} has been designed, Equations (5.3) and (5.4) are used to find $q_{22(1)}$ and $q_{33(1)}$ for each plant to be controlled by this FCS, these are the sets $\mathcal{Q}_{22(1)}$ and $\mathcal{Q}_{33(1)}$. To find $\mathcal{Q}_{33(2)}$, the sets of plants: $\mathcal{Q}_{32(1)}$, $\mathcal{Q}_{23(1)}$, and $\mathcal{Q}_{22(1)}$ also need to be calculated. With these plants calculated the set $\mathcal{Q}_{33(2)}$ is calculated. When a comparison is made of the Bode plots of $\mathcal{Q}_{22(1)}$ and $\mathcal{Q}_{33(2)}$ against $\mathcal{Q}_{22(0)}$ and $\mathcal{Q}_{33(0)}$, it is apparent that there are large RHP poles in $\mathcal{Q}_{33(2)}$ that do not appear in $\mathcal{Q}_{33(0)}$. This is a problem because these large RHP poles cause uncertainty, in phase angle of the frequency response of $\mathcal{Q}_{33(2)}$, to be greater than 300° until almost 10,000 $\frac{rad}{\text{sec}}$. This causes the phase margin frequency to be at least 10,000 $\frac{rad}{\text{sec}}$. This situation is also found in the second and third loops of the second FCS. If certain conditions are met, these large RHP poles, induced by the effective plant process, can be prevented. Since the third loop is modified by the two previous loops, if these loops can be shaped in a manner that make Equations (5.5) and (5.6) true, or if Equation (5.5) is true and Equation (5.7) is true for all of the plants, then the large RHP poles can be prevented [9]. In these equations β_p is some positive number.

$$\left|1 - \gamma_{ij(k+1)} + l_{i(k)}\right| \geq \beta_p \tag{5.5}$$

$$\mathcal{RE}\left\{\lim_{\omega\to\infty} 1 - \gamma_{ij(k+1)}(j\omega)\right\} \geq 0 \tag{5.6}$$

or

$$\mathcal{RE}\left\{\lim_{\omega\to\infty} 1 - \gamma_{ij(k+1)}(j\omega)\right\} < 0 \tag{5.7}$$

Equation (5.5) is used to prevent excursions across the $j\omega$ axis, which result in large RHP poles. Equation (5.6) is a condition that Equation (5.5) must satisfy unless all of the plants satisfy Equation (5.7). These are necessary conditions for even moderate

feedback benefit. These equations are implemented through the use of Γ-boundaries, which is discussed later. When the sets $\mathcal{Q}_{33(1)}$ and $\mathcal{Q}_{33(2)}$ are examined it is found that large RHP poles are induced by the set of $l_{1(0)}$s ($\mathcal{L}_{1(0)}$) in the denominator of Equation (5.3) and no large RHP are induced by $\mathcal{L}_{2(1)}$. For the second FCS, RHP poles are induced by both $\mathcal{L}_{1(0)}$ and $\mathcal{L}_{2(1)}$. When Equation (5.6) is evaluated based on $\mathcal{Q}_{33(1)}$ and ω=10^6 $\frac{rad}{sec}$ there are two $q_{33(1)}$ that fail the condition. The plants corresponding to these two $q_{33(1)}$ can either be eliminated or a separate FCS design can be made for them. The decision is made to eliminate these two plants and continue with the design process. This decision is made primarily based on the added time to design another FCS and that these plants are not plants on the boundaries of the maneuver envelopes. For the second FCS, it is found that 6 $q_{33(1)}$ out of 12 violate Equation (5.6). Based on the Bode plots of these plants, it is decided to split the third channel of the second FCS into three smaller FCSs, this is discussed further in Chapter 6. By reshaping the $l_{o_{1(0)}}$'s, based on boundaries developed from Equation (5.5) and trial and error, all of the large RHP poles induced in $\mathcal{Q}_{33(1)}$ are prevented. After shaping the necessary $l_{o_{i(k)}}$s, finding $\mathcal{Q}_{ij(k)}$ is a matter of running the Matrix$_x$ programs to do the calculations. Because of the problem of robustness of the Matrix$_x$ algorithms, two different methods of transfer function reduction are used, with very limited results. One of the methods is a pole-zero cancellations program written by Miller, [18], that uses Matrix$_x$ functions to separate the transfer function polynomials into roots and then compares the roots for cancellation. The second method is a Matrix$_x$ function called 'minimal' [16]. Neither method overcomes the warping problem and this results in very high order plants which are suspect.

5.4 l_o Boundaries

Because of the specification that the phase margin frequency be no more than 30 $\frac{rad}{sec}$, Horowitz points out that the stability boundaries will tend to be the dominate boundaries and it is decided to base the design on stability boundaries alone. To

develop the stability boundaries, templates representing the magnitude and phase uncertainty of the plants are developed using Matrix$_x$ and plotted on paper. The idea is to move these templates around the 3 dB M-contour on a Nichols chart, while tracking a nominal plant ($q_{oij(k)}$). The path that $q_{oij(k)}$ traces on the chart is the stability boundary. The 3dB M-contour is chosen because it represents a phase margin of 35 degrees. Instead of moving the template on the Nichols chart, Lacey developed a method in which the Nichols chart with the 3dB M-contour is plotted on clear acetate and the template is held stationary while the Nichols chart is moved [13]. After developing stability boundaries for the diagonal plants, the problem with large RHP poles is encountered. These RHP poles make it necessary to develop a Matrix$_x$ program that plots the Γ-boundaries and redetermines the stability boundaries.

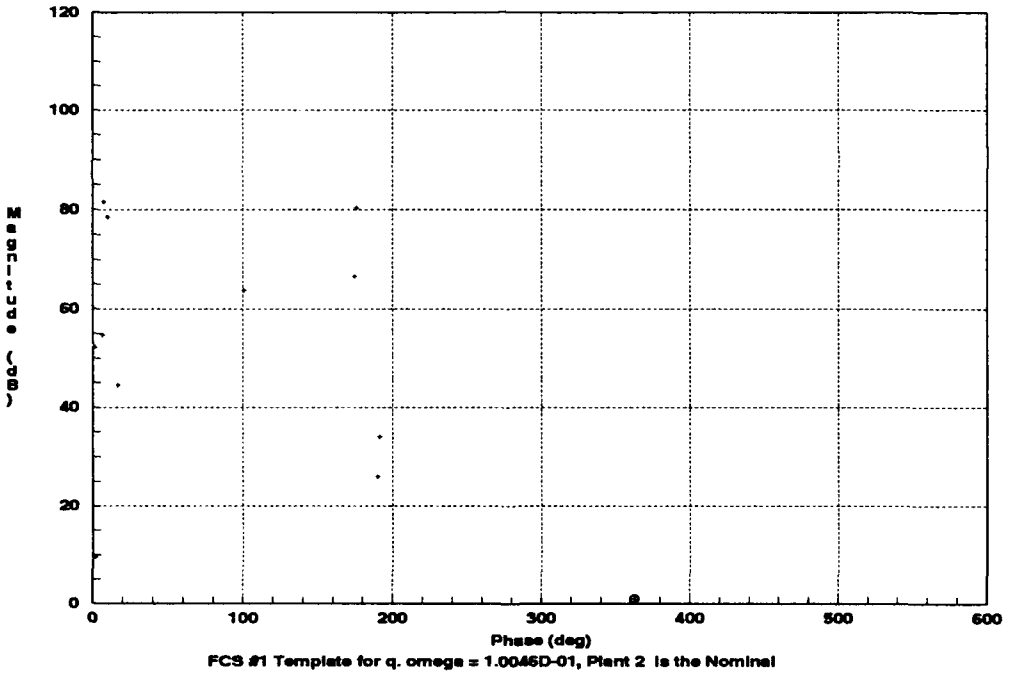

Figure 5.3. Example Template, ω=100 $\frac{rad}{sec}$

5.5 Matrix$_x$ Generated Stability Boundaries

Horowitz devised a method in which Equation (5.8) can be used in a computer program to develop stability boundaries, where M_m is the inverse log-magnitude of

the desired M-contour, in this case $M_m = 1.4125$, and $\mathcal{L}_{i(k)}$ is the set of loops to be shaped.

$$\frac{\left|\mathcal{L}_{i(k)}\right|}{\left|1+\mathcal{L}_{i(k)}\right|} \leq M_m \tag{5.8}$$

This method allows boundaries on the magnitude of the nominal loop ($l_{o_{i(k)}}$) to be found as a function of its phase. To develop this program, the following equation is formed that relates $\mathcal{L}$, $l_{o_{i(k)}}$, $\mathcal{Q}_{ij(k)}$, and the nominal plant ($q_{oij(k)}$):

$$\left|\mathcal{L}_{i(k)} = l_{oi(k)}\frac{\mathcal{Q}_{ij(k)}}{q_{o_{ij(k)}}}\right| \tag{5.9}$$

Equation (5.8) is rearranged resulting in Equation (5.10).

$$M_m\left|1+\mathcal{L}_{i(k)}\right| \geq \left|\mathcal{L}_{i(k)}\right| \tag{5.10}$$

Both sides of Equation (5.10) are squared, and Equations (5.11) and (5.12) are substituted in, where m is the magnitude of $l_{o_{i(k-1)}}$ and θ is the phase. This results in Equation (5.13), where A, B, and C are defined by Equations (5.14) through (5.16).

$$l_{o_{i(k-1)}} = m(\cos(\theta) + j\sin(\theta)) \tag{5.11}$$

$$\frac{\mathcal{Q}_{ij(k)}}{q_{o_{ij(k)}}} = \mu = \mu_2 + j\mu_2 \tag{5.12}$$

$$Am^2 + Bm + C \geq 0 \tag{5.13}$$

$$A = M_m^2\left(\mu_1^2 + \mu_2^2\right) \tag{5.14}$$

$$B = \left[2M_m^2\left(\mu_1\cos(\theta) - \mu_2\sin(\theta)\right) - \left(\mu_1^2 + \mu_2^2\right)\right] \tag{5.15}$$

$$C = M_m \tag{5.16}$$

By solving this quadratic equation in m for a specific θ, ω, $q_{ij(k)}$, and $q_{o_{ij(k)}}$, two roots are found that correspond to the magnitude of the boundaries on $l_{o_{i(k)}}$. This equation

must be solved for each $q_{ij(k)} \in \mathcal{Q}_{ij(k)}$, for each θ, for the boundaries at one value of ω. The upper stability boundary magnitude for that θ is the maximum value from the set of the maximum values of the two roots for all $\mathcal{Q}_{ij(k)}$. The lower boundary is the minimum value from the set of minimum values for all $\mathcal{Q}_{ij(k)}$. Example plots of boundaries are shown in Figures 5.4 through 5.4. Comparing the Matrix_x generated boundaries and the hand drawn boundaries shows good correlation. A good test of these boundaries is the plot of the set, $\mathcal{L}_{i(k)}$, on a Nichols chart as in the example in Figure 5.8.

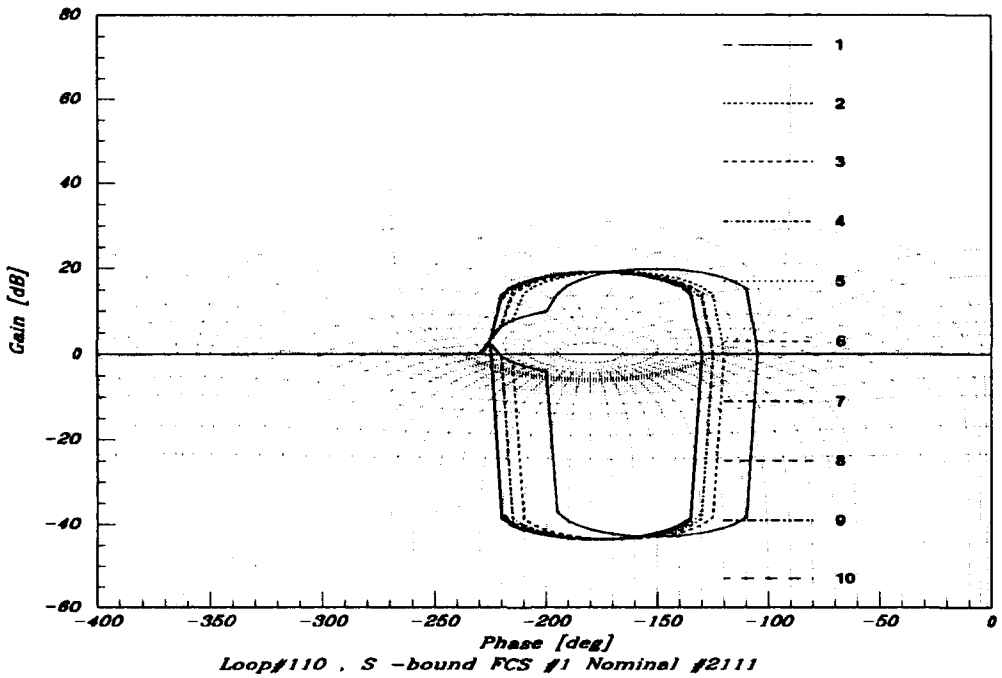

Figure 5.4. Example Stability Bound, for $\mathcal{L}_{o_{1(0)}}$ at ω=1 through 10 $\frac{rad}{sec}$

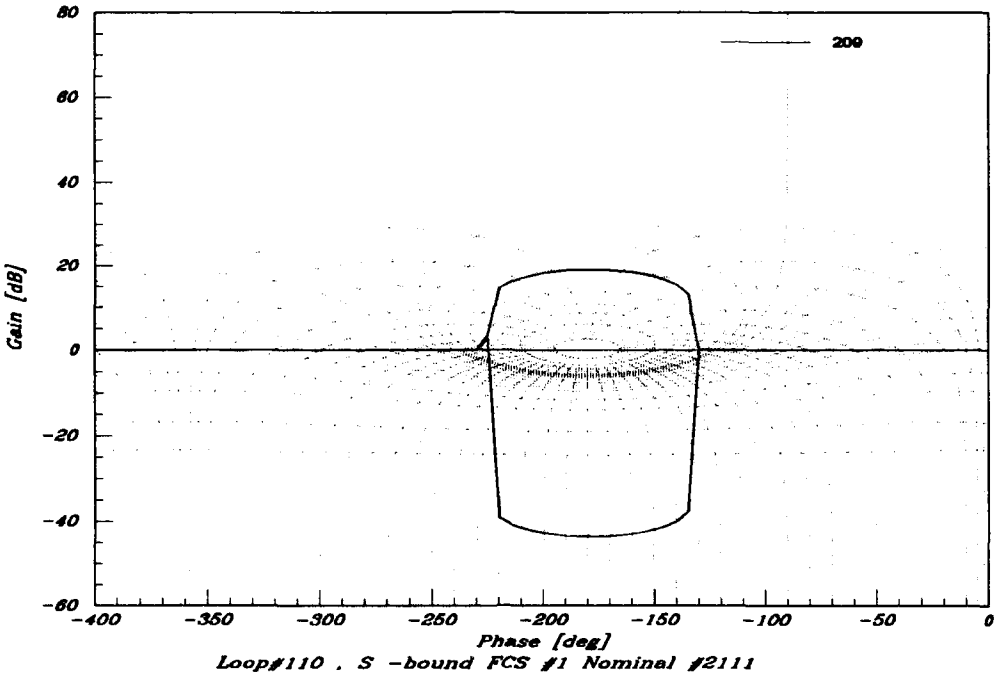

Figure 5.5. Example Stability Bound for $\mathcal{L}_{o_{1(0)}}$ at ω=20 $\frac{rad}{\text{sec}}$

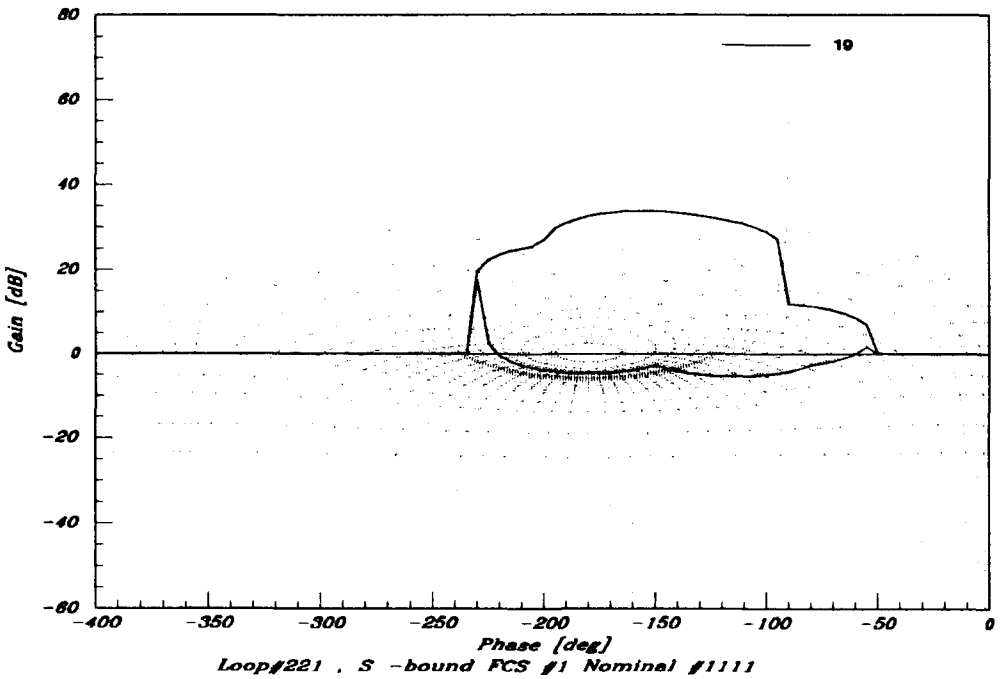

Figure 5.6. Example Stability Bound for $\mathcal{L}_{o_{2(1)}}$ at ω=1 $\frac{rad}{\text{sec}}$

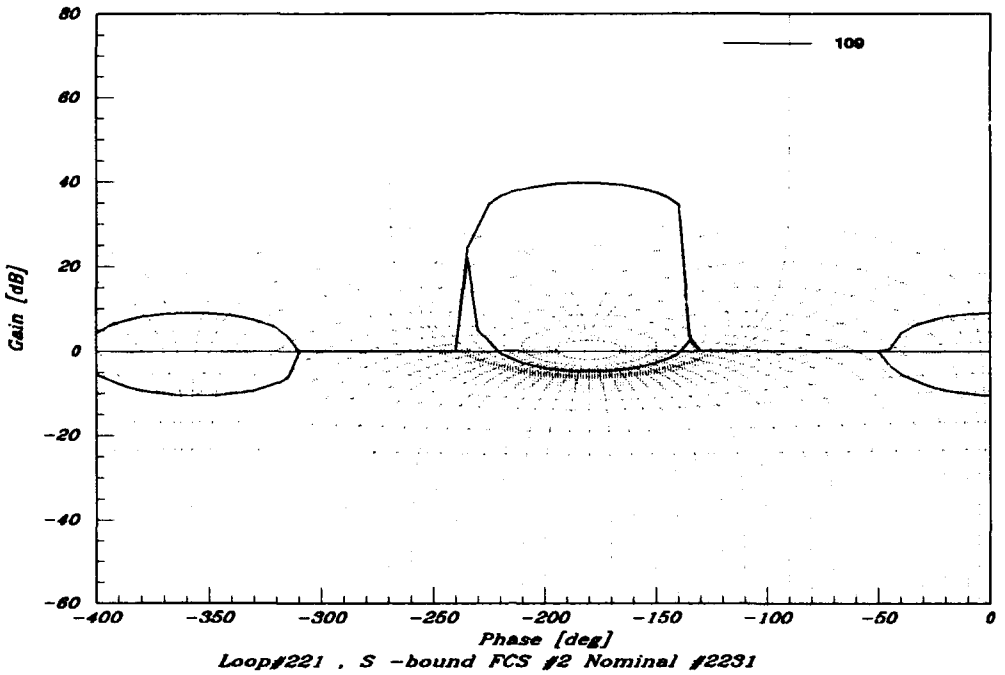

Figure 5.7. Example Stability Bound $\mathcal{L}_{o_{2(1)}}$ at ω=10 $\frac{rad}{\text{sec}}$

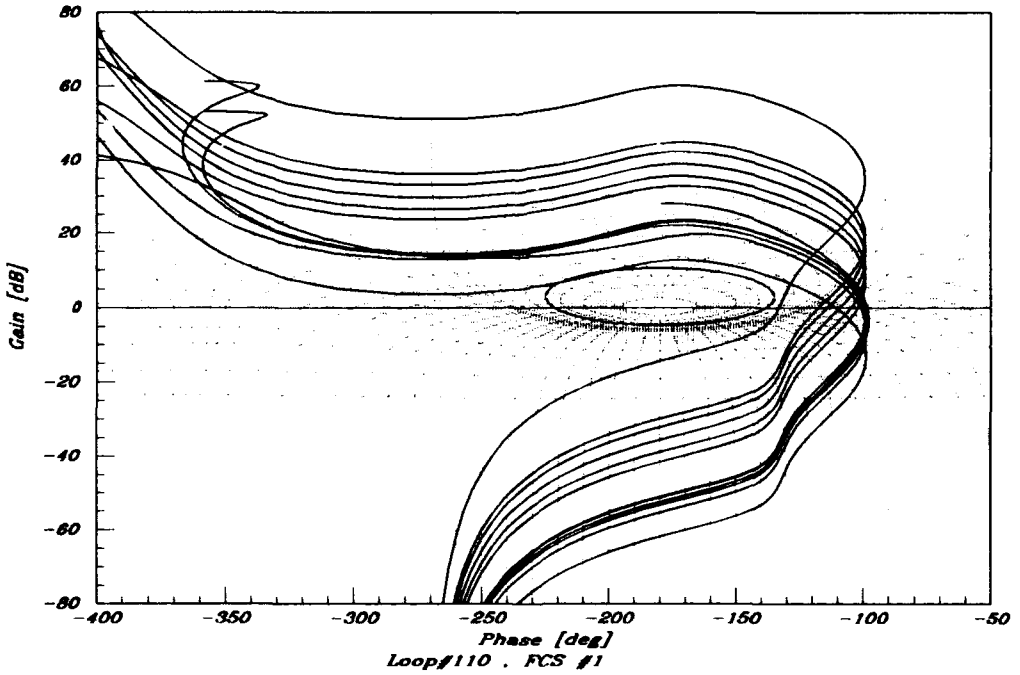

Figure 5.8. Example Plot of $\mathcal{L}_{1(0)}$ on Nichols Chart

5.6 Matrix$_x$ Generated Γ-Boundaries

Because of the necessity to prevent the development of large RHP poles in the effective plant process, Horowitz developed the following method to mechanize Γ-boundaries. The development is directly analogous to the development of the stability boundaries and is based on satisfying Equation (5.5), which is repeated in Equation (5.17), in this case, the choice of $\beta_p = 0.5$ is made.

$$\left|1 - \gamma_{ij(k+1)} + l_{i(k)}\right| \geq \beta_p \tag{5.17}$$

As in the case of the stability bounds, the object is to find boundaries on the magnitude of $l_{o_{i(k)}}$ as a function of its phase. Both sides of Equation (5.17) are squared and Equations (5.11), (5.12), and (5.18) are substituted in the resulting Equation (5.19) where A, B, and C are defined by Equations (5.20) through (5.22).

$$\gamma_{ij(k+1)} = \gamma_1 + j\gamma_2 \tag{5.18}$$

$$Am^2 + Bm + C \geq 0 \tag{5.19}$$

$$A = \left(\gamma_1^2 + \gamma_2^2\right) \tag{5.20}$$

$$B = 2\left[(1 - \gamma_1)\left(\mu_1 \cos(\theta) - \mu_2 \sin(\theta)\right) - \gamma_2\left(\mu_1 \sin(\theta) + \mu_2 \cos(\theta)\right)\right] \tag{5.21}$$

$$C = (1 - \gamma_1)^2 + \gamma_2^2 - \beta^2 \tag{5.22}$$

The Γ-boundaries are then generated in the same manner as the stability boundaries. Example plots of Γ-boundaries are shown in Figures 5.9 through 5.12. A test of these boundaries is if large RHP poles are generated after the use of Γ-boundaries. In most cases no large RHP poles are generated, but there are two cases where large RHP poles are generated. In these two cases the $l_{o_{i(k)}}$ are manipulated by trial and error until no large RHP poles are generated. It is unclear in both of these cases where the

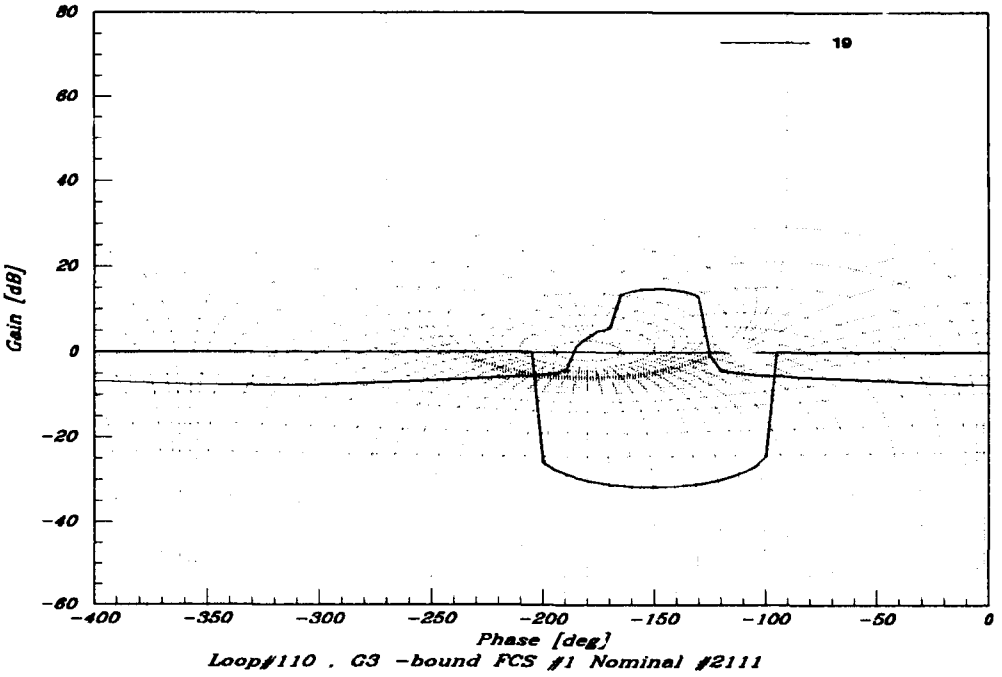

Figure 5.9. Example Γ-Boundaries for $\mathcal{L}_{o_{2(1)}}$ at ω=1 $\frac{rad}{sec}$, Based on $\mathcal{Q}_{33(0)}$

violations of the Γ-boundaries occurs, but in all the others cases where large RHP poles are generated, clear violations of the Γ-boundaries are present.

5.7 Matrix$_x$ Generated Boundaries: General Considerations

When using these algorithms to generate stability boundaries and Γ-boundaries, there are many factors to consider. In this Matrix$_x$ program the boundaries are constrained to start and stop at the 0 dB axis. This causes the boundaries to be exaggerated at the ends. When there are fast changes in the boundaries, the resolution along the phase axis is a major factor in how exaggerated the boundaries become. When there is large uncertainty in the phase of the $q_{ij(k)}$, see Figure 5.13, separate regions of boundaries are formed. In reality these regions should be connected with a continuous line, and care must be taken to identify the regions and shape $l_{o_{i(k)}}$ completely around the right side of the boundaries. Boundaries of plants that have large phase uncertainty can cause the width of the boundary to be masked by the repetitive nature of the Nichols chart. That is, for phase uncertainty more than 360°

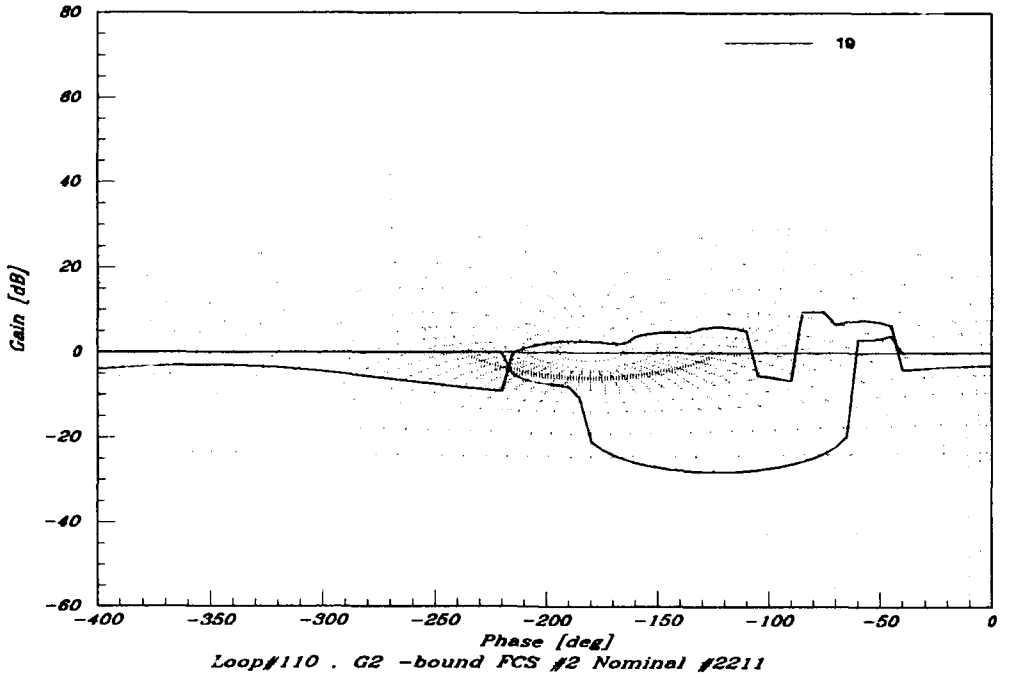

Figure 5.10. Example Γ-Boundariesfor $\mathcal{L}_{o_{2(1)}}$ at ω=1 $\frac{rad}{\text{sec}}$, Based on $\mathcal{Q}_{22(1)}$

the boundaries on the far right edge of the boundary overlap onto the region between -180° and -0°. These overlapped boundaries give a false indication of the right edge of the boundary. This matter is complicated when there are large separations between the phase of the plants. The area between the separations do not result in boundaries. This cause boundaries with numerous non-contiguous regions as shown in Figures 5.14 through, 5.21. The minimum frequency at which a loop can cross the 0 dB axis in these figures is 500 $\frac{rad}{\text{sec}}$. As shown, the complete right edge of the boundary emerges from the boundaries around the prohibited region that is 360° to the right of the original. This perception problem can be prevented by algorithmically drawing a closed contour around the mathematical template, as suggested by Sating [20].

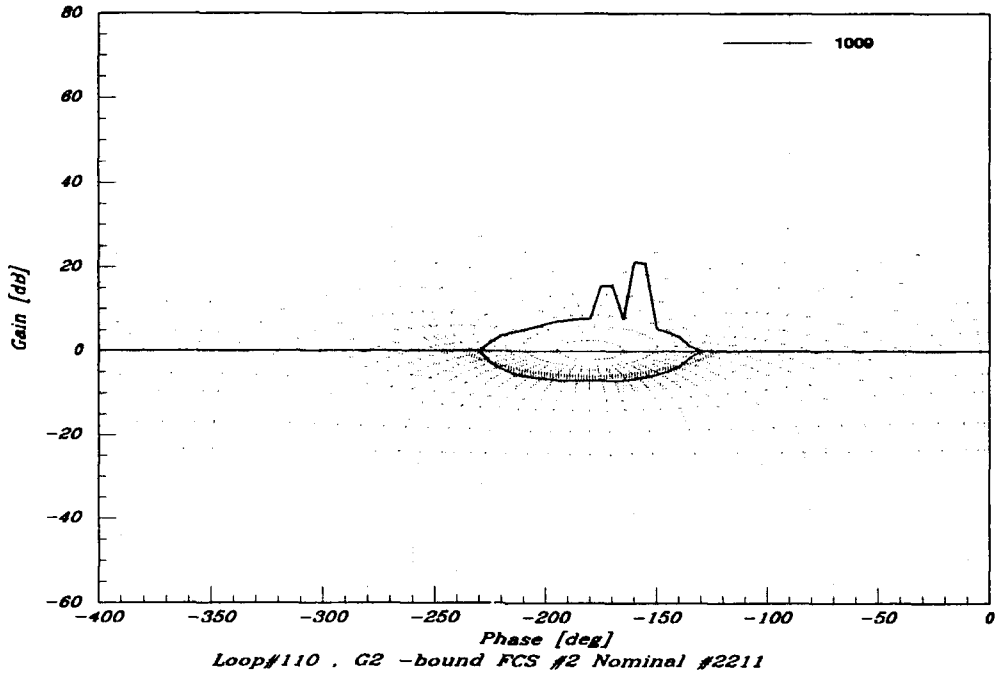

Figure 5.11. Example Γ-Boundaries for $\mathcal{L}_{o_{2(1)}}$ at ω=100 $\frac{rad}{\text{sec}}$, Based on $\mathcal{Q}_{22(1)}$

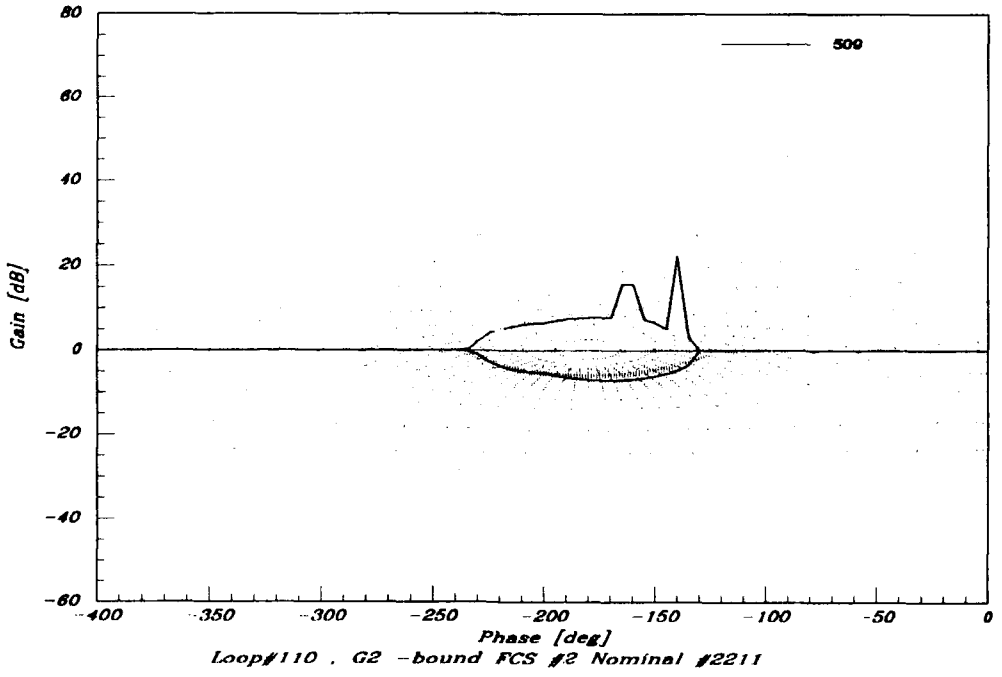

Figure 5.12. Example Γ-Boundaries for $\mathcal{L}_{o_{2(1)}}$ at ω=50 $\frac{rad}{\text{sec}}$, Based on $\mathcal{Q}_{22(1)}$

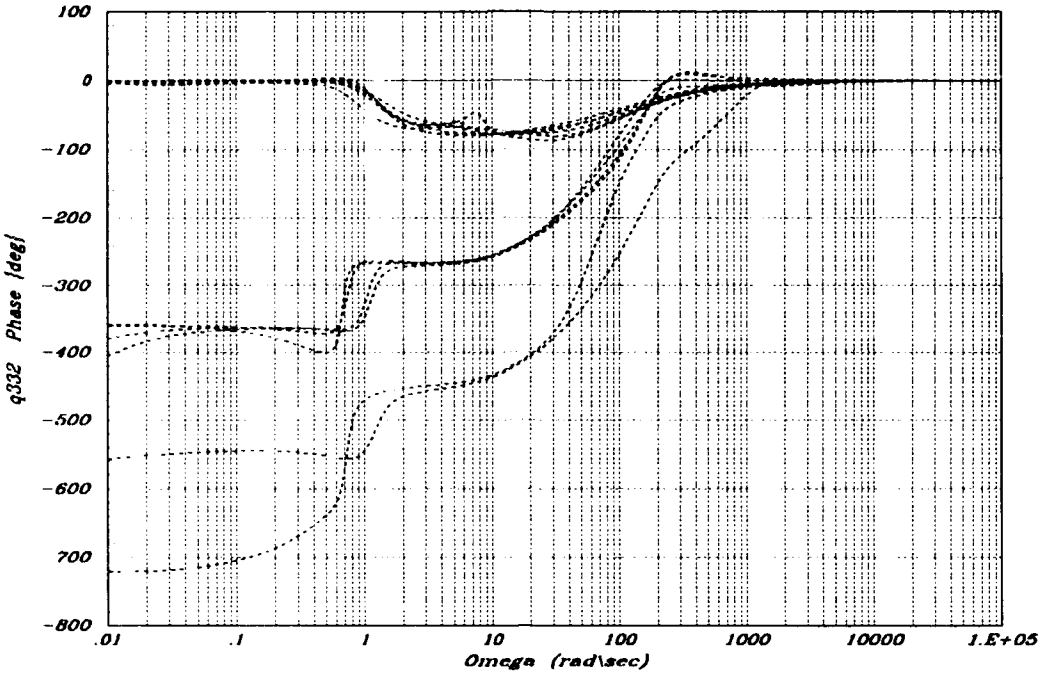

Figure 5.13. Large Uncertainty Example, Phase Plot for FCS#2 $\mathcal{Q}_{33(2)}$

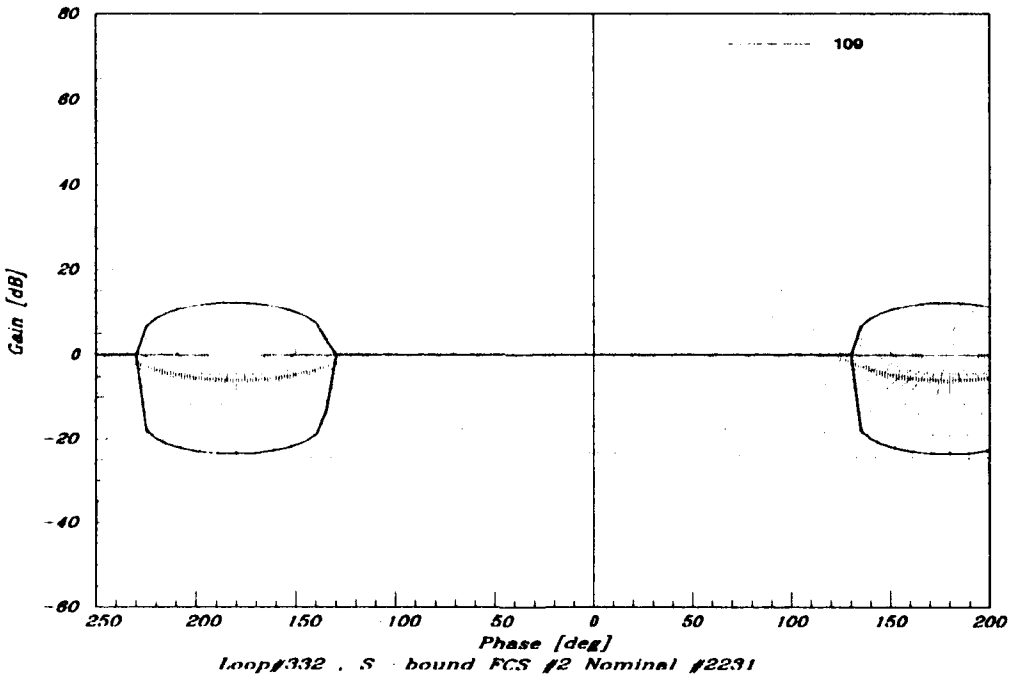

Figure 5.14. Large θ Uncertainty Example, Stability Boundaries for $\mathcal{L}_{o_{3(2)}}$ at ω=10 $\frac{rad}{sec}$

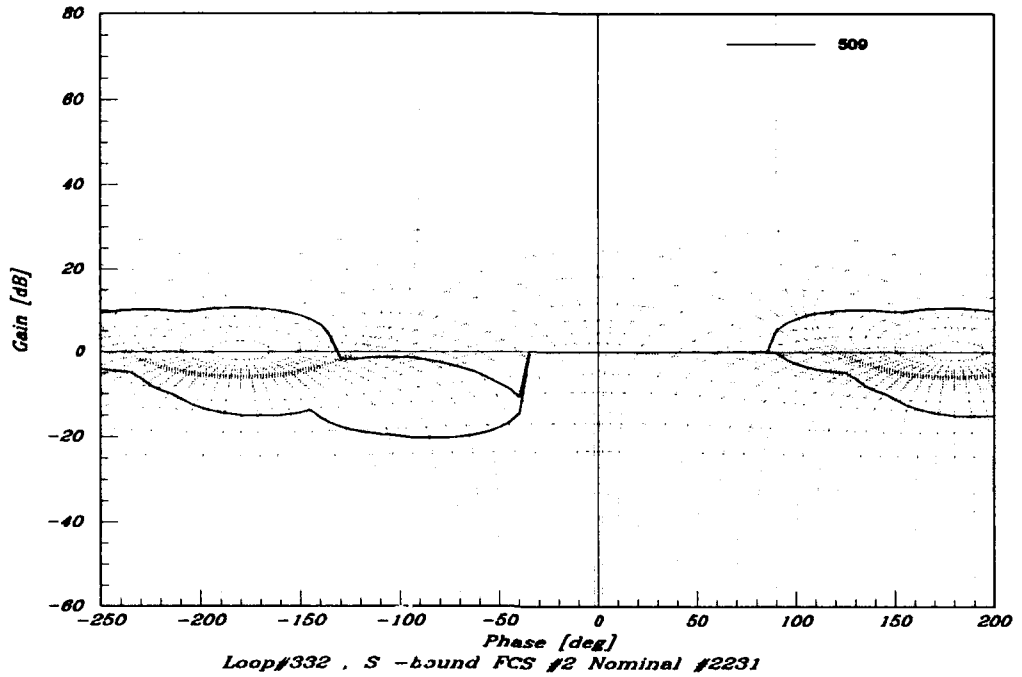

Figure 5.15. Large θ Uncertainty Example cont'd, Stability Boundaries for $\mathcal{L}_{o_{3(2)}}$ at ω=50 $\frac{rad}{\text{sec}}$

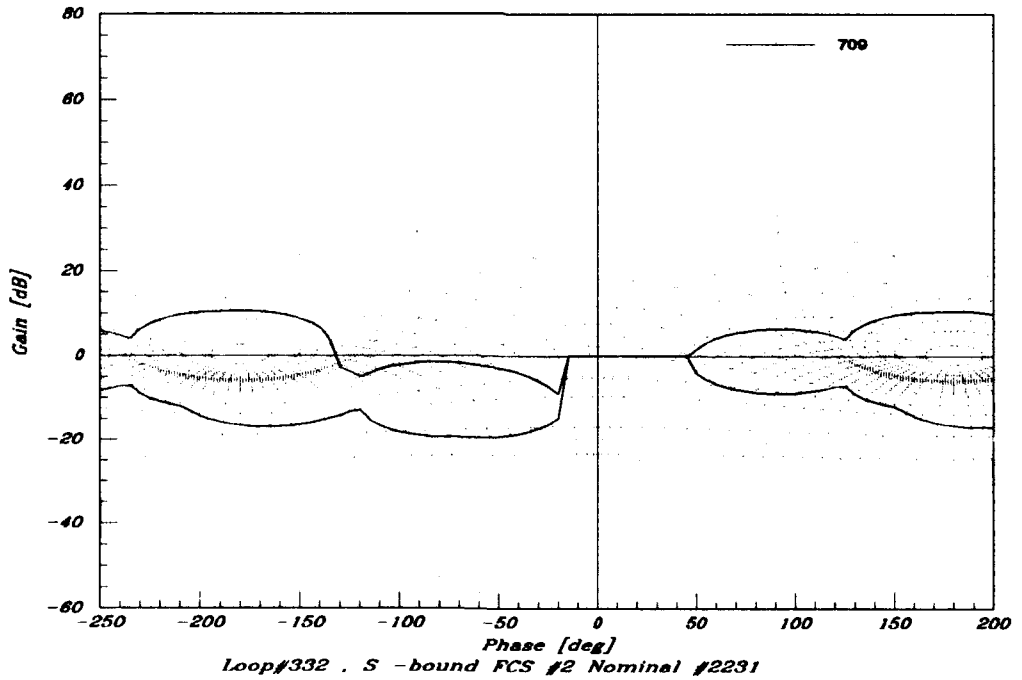

Figure 5.16. Large θ Uncertainty Example cont'd, Stability Boundaries for $\mathcal{L}_{o_{3(2)}}$ at ω=70 $\frac{rad}{\text{sec}}$

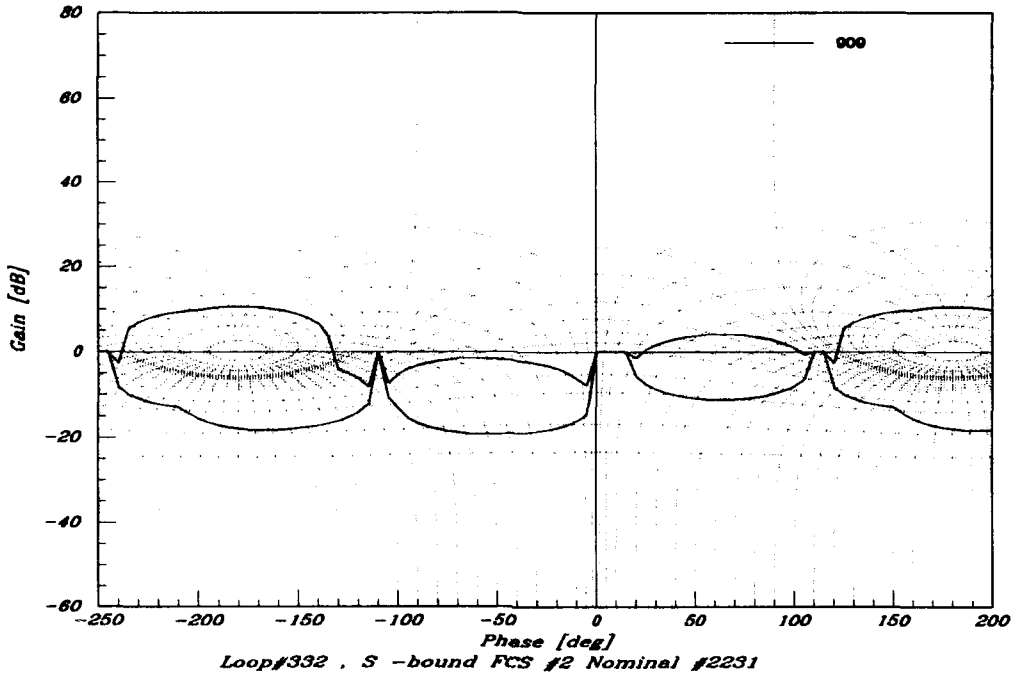

Figure 5.17. Large θ Uncertainty Example cont'd, Stability Boundaries for $\mathcal{L}_{o_{3(2)}}$ at ω=90 $\frac{rad}{\text{sec}}$

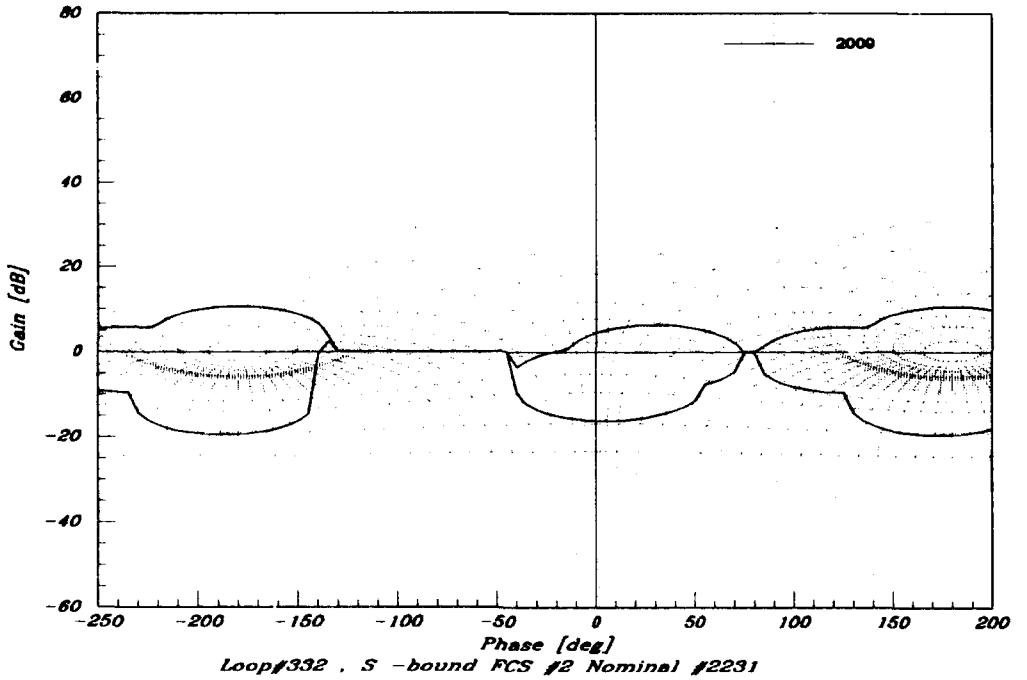

Figure 5.18. Large θ Uncertainty Example cont'd, Stability Boundaries for $\mathcal{L}_{o_{3(2)}}$ at ω=200 $\frac{rad}{\text{sec}}$

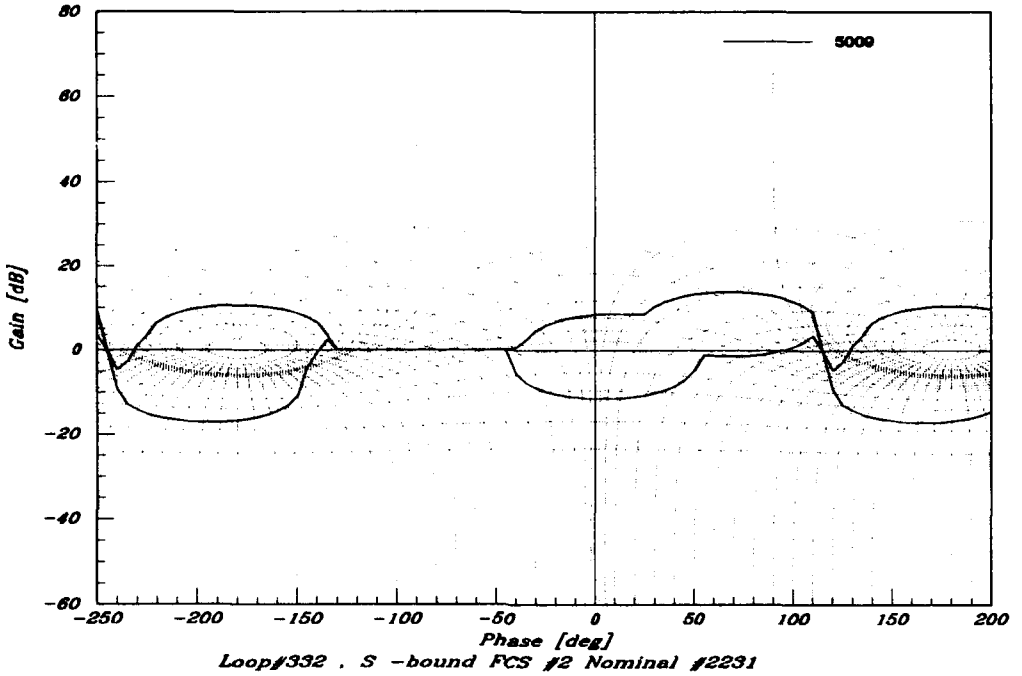

Figure 5.19. Large θ Uncertainty Example cont'd, Stability Boundaries for $\mathcal{L}_{o_{3(2)}}$ at ω=500 $\frac{rad}{\text{sec}}$

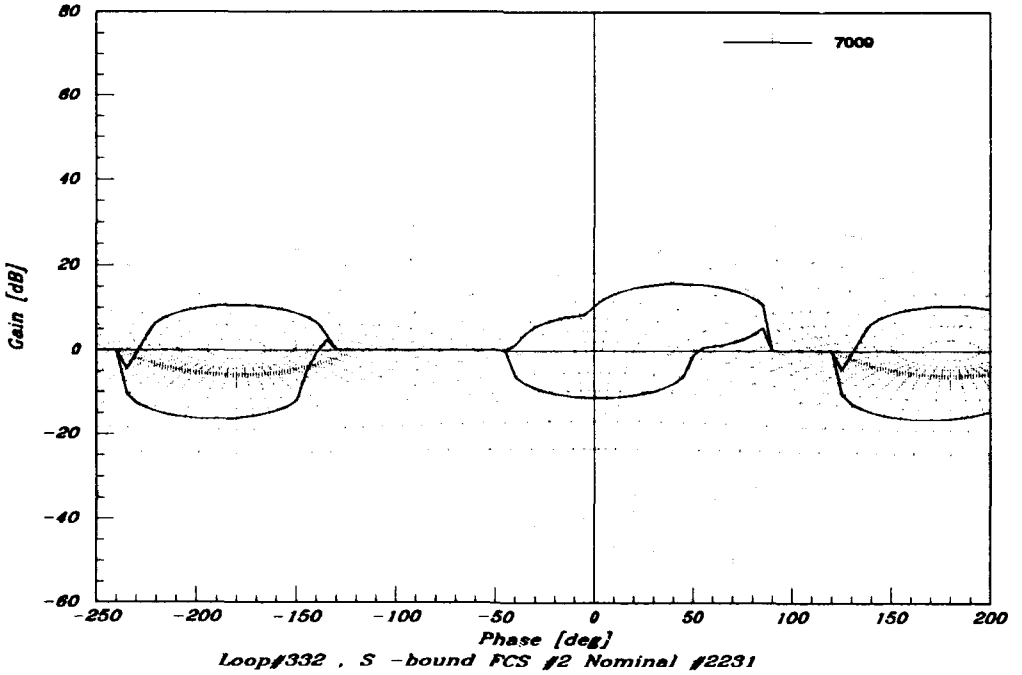

Figure 5.20. Large θ Uncertainty Example cont'd, Stability Boundaries for $\mathcal{L}_{o_{3(2)}}$ at ω=700 $\frac{rad}{\text{sec}}$

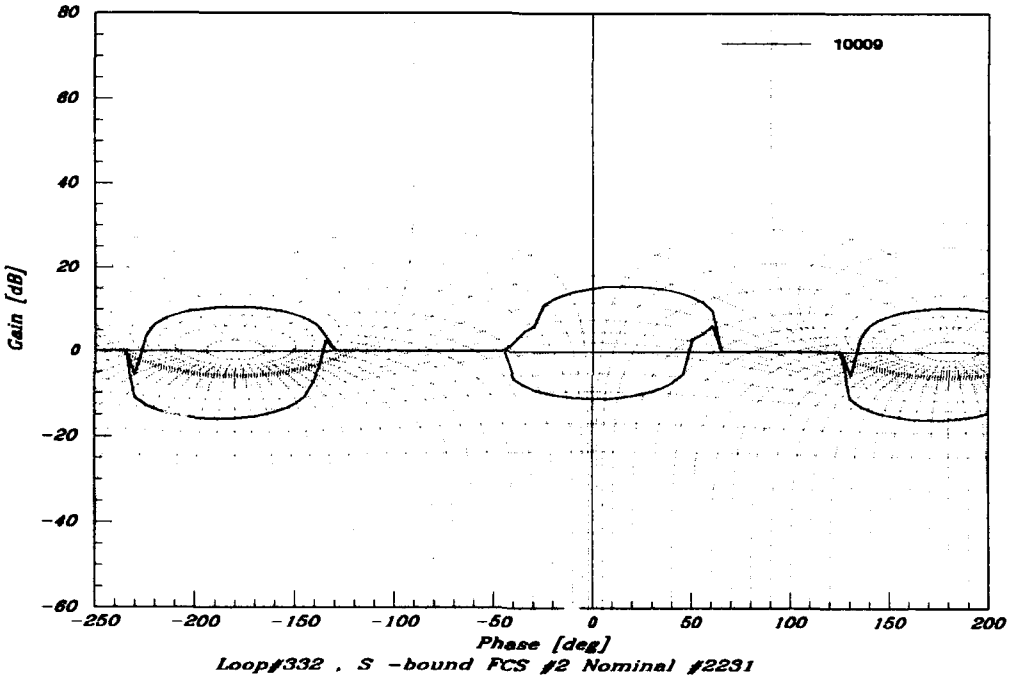

Figure 5.21. Large θ Uncertainty Example cont'd, Stability Boundaries for $\mathcal{L}_{o_{3(2)}}$ at ω=1000 $\frac{rad}{\text{sec}}$

5.8 Conclusion

This chapter covers development of the effective plants and generation of boundaries on $l_{0_{i(k)}}$. First, limitations of the Matrix$_x$ algorithms for manipulating plants are discussed and a basic experiment to show this is detailed. The development of $\mathcal{Q}_{ij(k)}$ and some of the problem encountered is discussed. These problems include the development of large RHP poles by the effective plant process, which is solved, in most cases, by Γ-boundaries. Finally, a discussion of Matrix$_x$ generated boundaries is presented. Horowitz's method for generating stability bounds is discussed first followed by his method for generating Γ-boundaries. The last sections outline some of the cautions in using the Matrix$_x$ generated boundaries. In Chapter 6 loop shaping and filter design are discussed.

VI. Loop Shaping and Filter Design

6.1 Introduction

This chapter details the design of the loop transmission and the prefilter. First, general considerations and the reason for controller scheduling are presented. Next, design of the loop transmissions for all FCSs is described, including many problems with RHP poles. Finally there is a description of the prefilters designed to cause the aircraft to respond in a specified manner to specified control inputs.

6.2 General Considerations

After developing the $\mathcal{Q}_{ij(0)}$, from the system identification algorithms, a Bode plot is obtained for all $q_{ii(0)} \in \mathcal{Q}_{ii(0)}$ i=1,2,3, Figures 6.1 through 6.3. On inspection

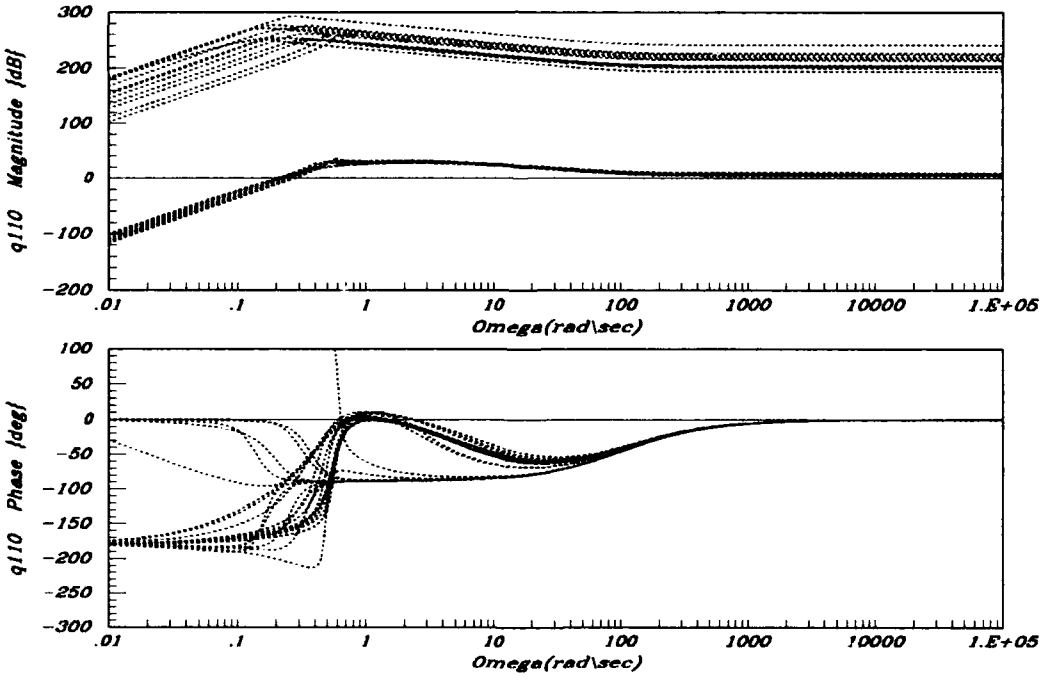

Figure 6.1. Bode Plots for All $q_{11(0)}$

the Bode plots reveal that the magnitudes have an extreme amount of uncertainty, but the $q_{ii(0)}$ are grouped in two groups. This indicates that scheduling of gain is

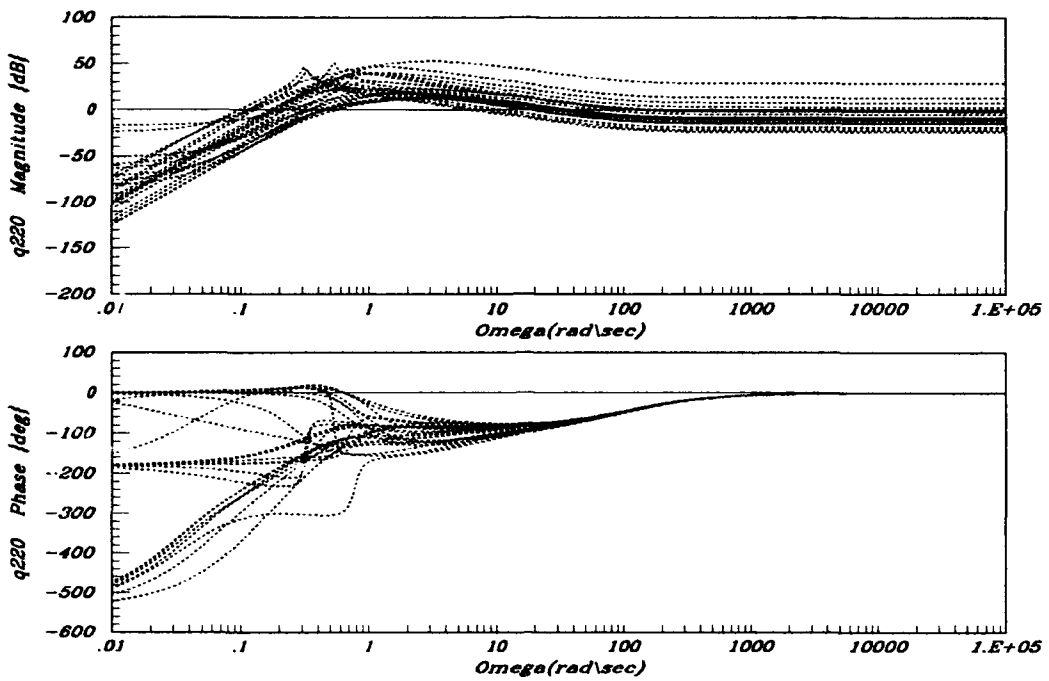

Figure 6.2. Bode Plots for All $q_{22(0)}$

needed for the FCS design. When the two groups are separated and plotted on Bode plots, Figures 6.4 through 6.9, it is evident that the uncertainty in phase is too large for just gain scheduling and separate controllers must be designed for the two groups. The decision is made to develop two FCS's and schedule the FCS based on the maneuver. Upon inspection it is found that the maneuvers associated with pitch- up/pitch-down can be grouped together and the maneuvers representing the velocity vector roll can be grouped together.

6.3 Loop Shaping

The first forward loop is shaped using hand generated stability boundaries. A Matrix$_x$ program is used to ease the task of loop shaping. Matrix$_x$ has an interactive Nichols chart, which means an ω of interest on $l_{o_{ij(k)}}$ can be identified by a cursor that moves on $l_{o_{ij(k)}}$. Because of this, one effective method of loop shaping is to use a Matrix$_x$ program to build a $l_{o_{ij(k)}}$ based on poles and zeros and then plot it on the Nichols chart. In this manner $l_{o_{ij(k)}}$ can be formed by adding, deleting, or moving

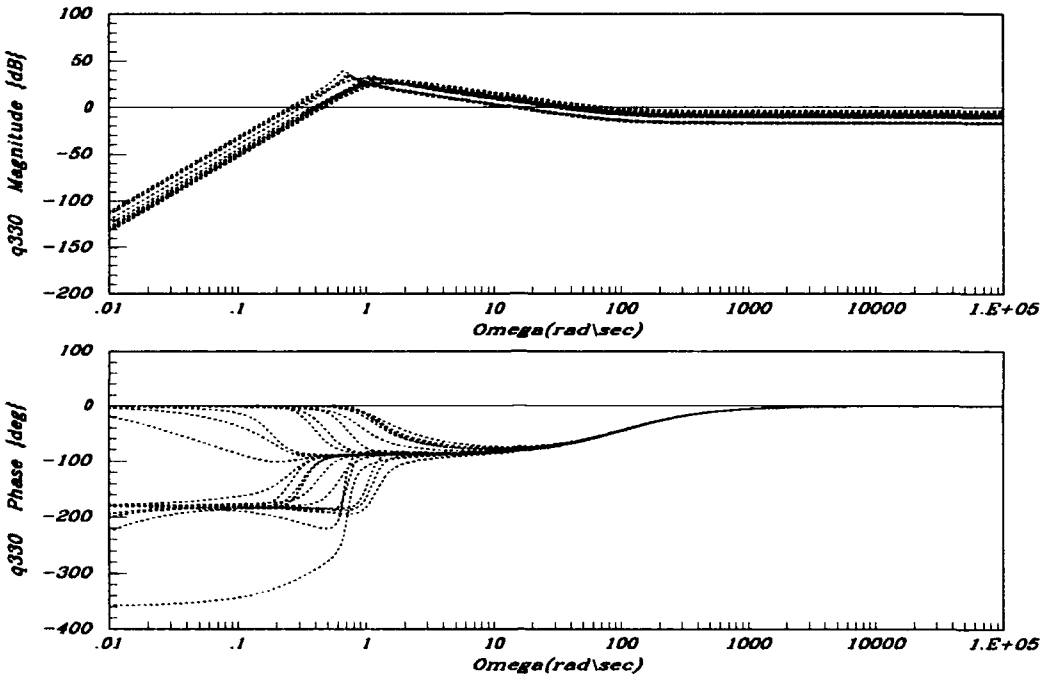

Figure 6.3. Bode Plots for All $q_{33(0)}$

poles and zeros and then checking the results on the Nichols chart. To do this loop shaping, using the Nichols chart, basic pole/zero relationships must be used. Some of the more important relationships are:

- adding a pole will pull $l_{o_{ij(k)}}$ to the left and causes the magnitude to decrease.
- adding a zero will pull $l_{o_{ij(k)}}$ to the right and causes the magnitude to increase.
- by adding a pole/zero pair $l_{o_{ij(k)}}$ can be moved to the right or to the left without changing the magnitude at the ω of interest. This can be accomplished by picking the position of the pole/zero and then placing the zero/pole an equal distance, on a log scale, from the ω of interest. The direction that the loop is moved, is left or right depending on whether the pole or the zero is of lesser magnitude
- A complex pair of zeros or poles can be used where a large change in phase is needed quickly without a corresponding quick change in magnitude. The change in phase and magnitude both depend on the damping factor thus the

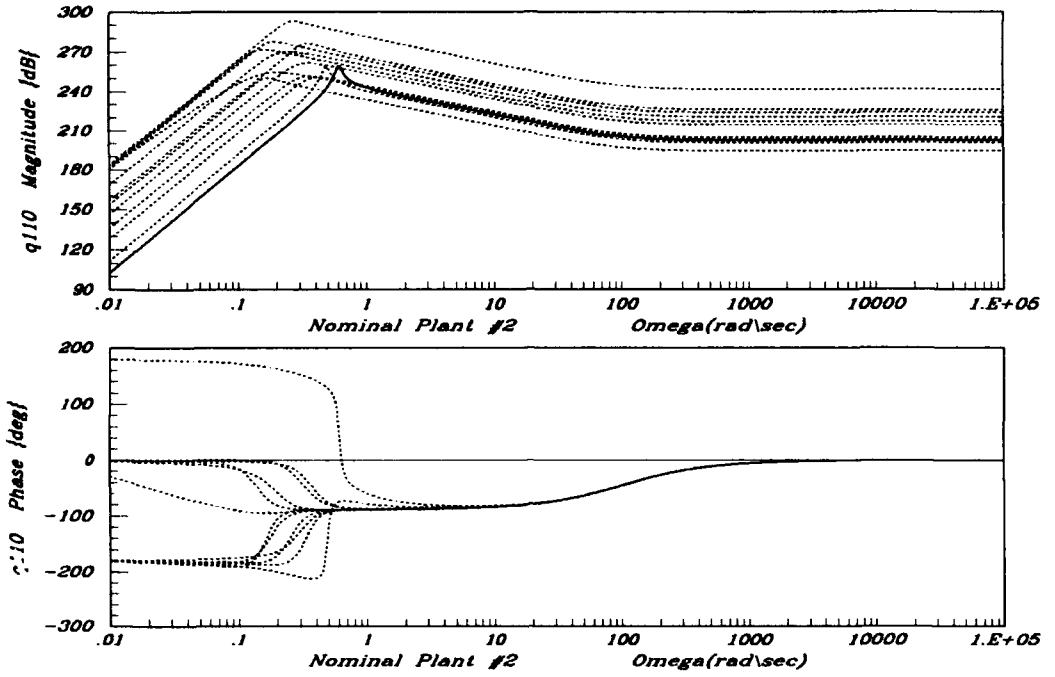

Figure 6.4. Bode Plots for FCS#1 $q_{11(0)}$

use of a chart, where complex roots are plotted with changes in damping factor, is helpful.

- When using a complex pair of poles to swing $l_{o_{(j\omega)}}$ around the bottom of the stability boundaries, the damping ratio has a major effect on the shape of the corner. A large damping ratio causes the corner to be smooth and displaced to the left when compared to the corner produced by a low damping factor. If the corner needs to be moved right a very low damping factor can be used. A small damping factor (.4–.6) is useful in turning the loop below the stability bound.

These are only the more important relationships that are helpful in loop shaping using the Nichols chart. In addition to these relationships one must know when these effects should take effect. These relationships can be derived from Bode plot rules. [5] There is a problem when using the frequency response algorithms of Matrix_x , and other CAD packages, for functions that contain RHP poles and/or zeros. When RHP factors are present Matrix_x shifts the phase plots by some value of phase. The

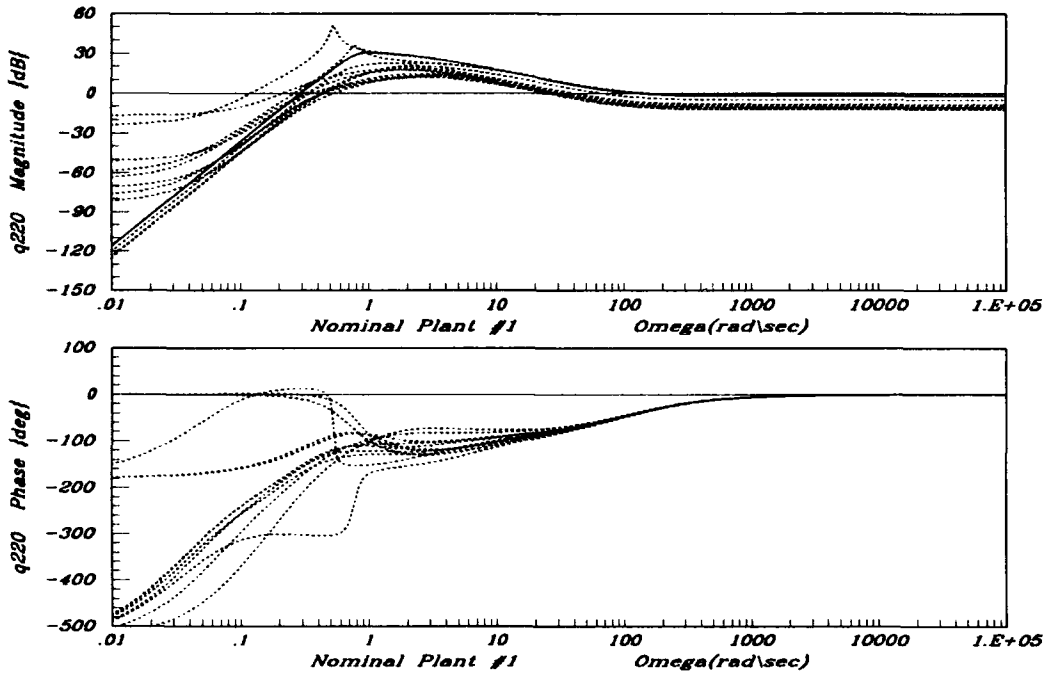

Figure 6.5. Bode Plots for FCS#1 $q_{22(0)}$

phase can be corrected by shifting the frequency data, in phase, by a factor obtained by computing the difference between the number of poles and zeros, multiplying this number by 90°, and subtracting the final phase of the frequency data from this number. The result is a phase correction factor that must be added to the phase plot.

6.4 FCS#1 Loop Design

For $l_{o_{1(0)}}$ of the first FCS, a $q_{o_{11(0)}}$ is chosen to be the lowest magnitude for most of the frequencies of interest. This choice is made to cause the boundaries to be below the 3 dB M-contour. The drawback of this choice is it makes it necessary that $l_{o_{1(0)}}$ be well below the 30 $\frac{rad}{\text{sec}}$ specification for phase margin frequency(ω_ϕ) so that all the other $l_{1(0)} \in \mathcal{L}_1$ satisfy the $\omega_\phi \leq 30\frac{rad}{\text{sec}}$ specification. With this choice, the stability boundaries are formed by the method of templates. Since $q_{o_{11(0)}}$ contains two RHP poles, they are included in $l_{o_{1(0)}}$. From this point, poles and zeros are added to shape the loop. After $l_{o_{1(0)}}$ has been designed, the $\mathcal{Q}_{ij(1)}$ needed for succeeding loops are

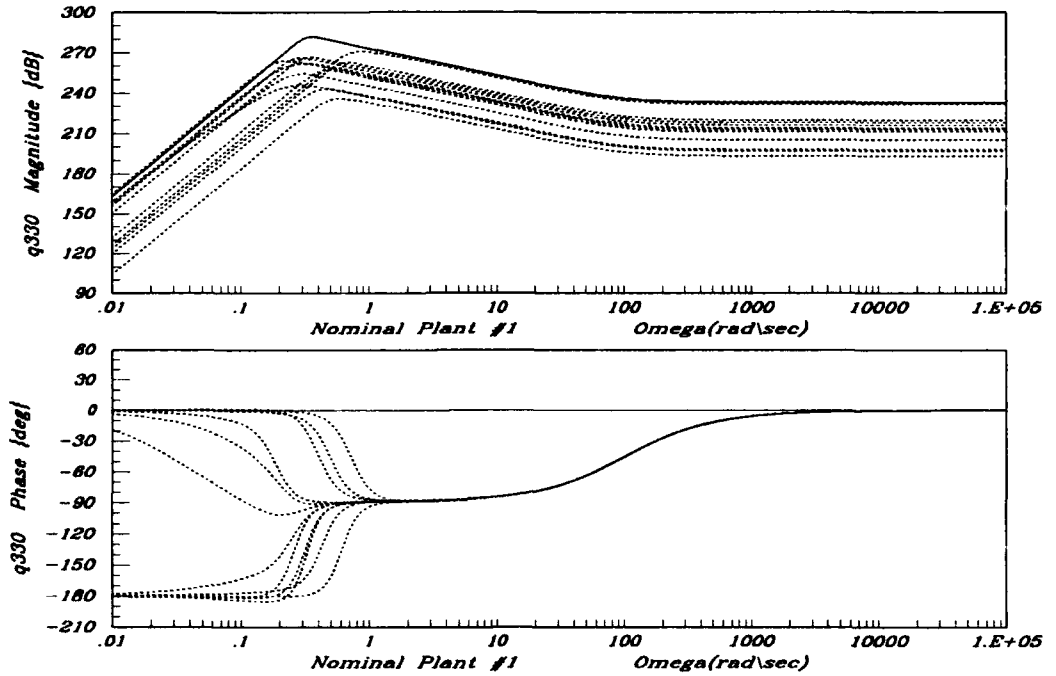

Figure 6.6. Bode Plots for FCS#1 $q_{33(0)}$

calculated. After shaping $l_{o_{2(0)}}$ and calculating $\mathcal{Q}_{33(2)}$ it is apparent that large RHP poles have been added to $\mathcal{Q}_{33(2)}$ and it is decided to use the method described in Chapter 6 to prevent the formation of large RHP poles. By examining $\mathcal{Q}_{33(1)}$ and $\mathcal{Q}_{33(2)}$, its is apparent that the large poles are a result of $l_{1(0)}$. Because two $q_{33(1)}$ violate the conditions on the Γ-boundaries, they are removed from the design. Since two $q_{33(1)}$ represent pitch-down manevers from a low magnitude pitch-up maneuver, their removal from the design changes the specified boundaries. A better method in handeling this situation is to design a separate FCS for these two $q_{33(1)}$ as is done for the third channel of FCS#2. The first loop is reshaped using Matrix_x generated stability boundaries and Γ-boundaries. The results are shown in Figures 6.10 and 6.11. For this loop, the Γ-boundaries did not prevent the existence of all of the large RHP poles in $\mathcal{Q}_{33(2)}$ and it is necessary to shift $l_{o_{1(0)}}$ outward away from the boundaries until the large RHP poles do not appear. In this case the boundaries do not appear to be correct since there are phases where there is an upper boundary below zero and no apparent lower boundary. As explained later, the boundaries are

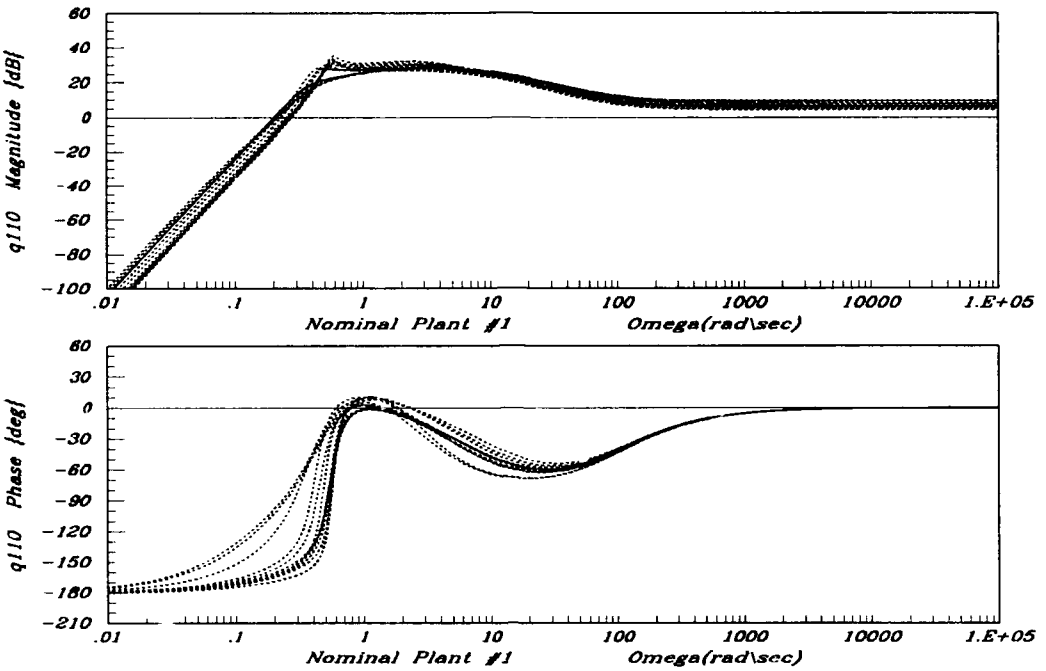

Figure 6.7. Bode Plots for FCS#2 $q_{11(0)}$

very effective in reducing the RHP poles in FCS #2. Once $l_{o_{1(0)}}$ is shaped, effective plants are calculated, $l_{o_{2(1)}}$ and $l_{o_{2(1)}}$ are shaped. It is not necessary to use the Γ-boundaries when shaping $\mathcal{Q}_{22(1)}$ because, in this case no large RHP poles are induced by $\mathcal{L}_2$ on $\mathcal{L}_3$. Figures 6.12 through 6.15 show $l_{o_{2(1)}}$ and $l_{o_{3(2)}}$. Appendix 4 contains all the G_1, G_2, and G_3 designed in this thesis. To check the validity of the $l_{o_{i(k)}}$, the sets, $\mathcal{L}_{i(k)}$ are plotted along with the 3 dB M-contor in Figures 6.16 through 6.18. Note: in Figure 6.18, 5 of the 12 $l_{3(2)}$ can not be plotted due to the high order of their corresponding $q_{33(2)}$s.

6.5 FCS#2 Loop Design

The second set of $\mathcal{L}_{i(k)}$'s is more difficult to design because of the large number of RHP poles generated by the effective plant process. After shaping $l_{o_{1(0)}}$ it is found that large RHP poles are generated in both $\mathcal{Q}_{22(1)}$ and $\mathcal{Q}_{33(1)}$. A check is made on

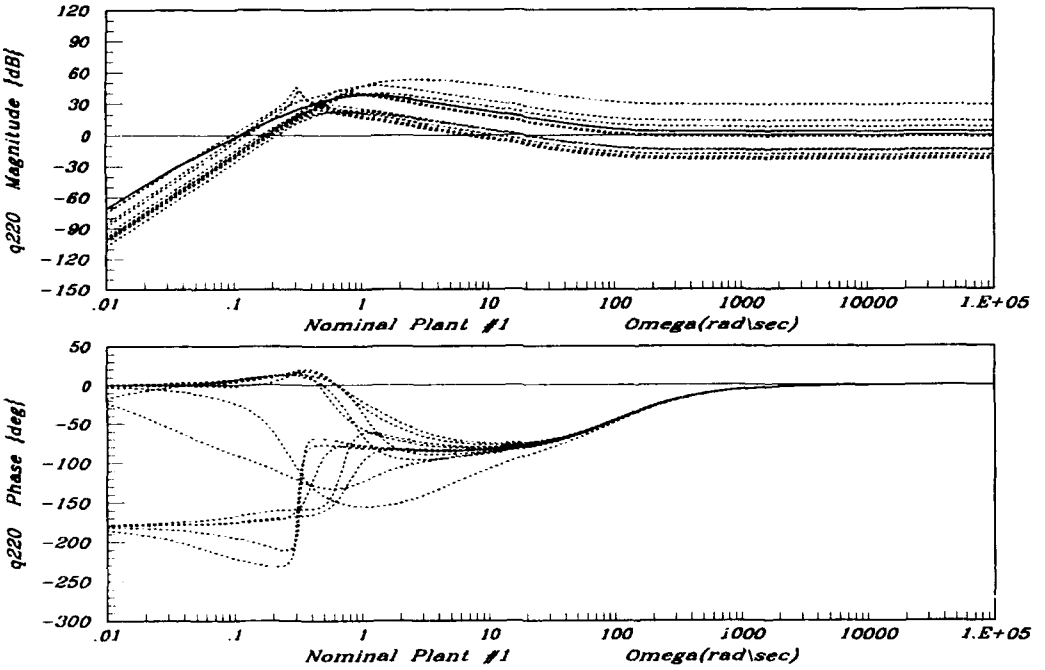

Figure 6.8. Bode Plots for FCS#2 $q_{22(0)}$

both for the condition of Equation (5.6), repeated here in Equation (6.1).

$$\lim_{\omega \to \infty} 1 - \gamma_{ij(k+1)}(j\omega) \geq 0 \tag{6.1}$$

The entire set $\mathcal{Q}_{22(1)}$ meets the condition, but only 6 of 12 of the set $\mathcal{Q}_{33(1)}$ meet this condition. It is decided to design 3 separate FCS for the third channel. $l_{o_{1(0)}}$ is shaped in the same manner as the loops in FCS#1. Because the Γ-boundaries for $l_{o_{1(0)}}$ based on $\mathcal{Q}_{22(1)}$ are complicated, $l_{o_{1(0)}}$ is re-shaped many times before it is discovered that the Γ-boundaries, that appear to have breaks, must be completely encircled by $l_{o_{1(0)}}$, see Figures 6.19 and 6.20. Once $l_{o_{1(0)}}$ is shaped to encircle the Γ-boundaries, $\mathcal{Q}_{22(1)}$ is calculated and $l_{o_{2(1)}}$ shaped, see Figures 6.21 and 6.22. The shaping of $l_{o_{2(1)}}$ is accomplished without the use of Γ-boundaries because large RHP poles are not generated in the $q_{33(2)}$ that do not violate the condition of Equation (6.1). As stated before, $\mathcal{Q}_{33(2)}$ is divided into three subsets. A separate FCS will is designed for each subset. The shaping of $l_{o_{3(1)}}$ for each of the subsets is accomplished

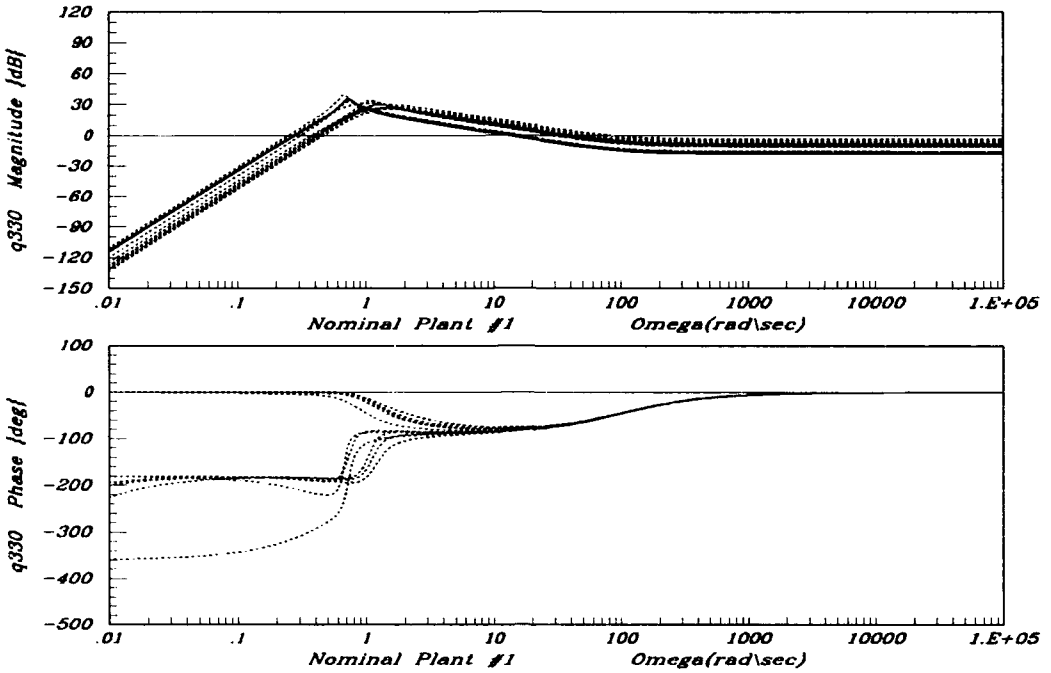

Figure 6.9. Bode Plots for FCS#2 $q_{33(0)}$

in the same manner as the previous loops, see Figures 6.23 through 6.25. The only problem with these loops is that one of them starts with 6 RHP poles which causes it to have a ω_ϕ of 3000 $\frac{rad}{\text{sec}}$. $\mathcal{L}_{i(k)}$ for FCS#2 are plotted in Figures 6.26 through 6.30.

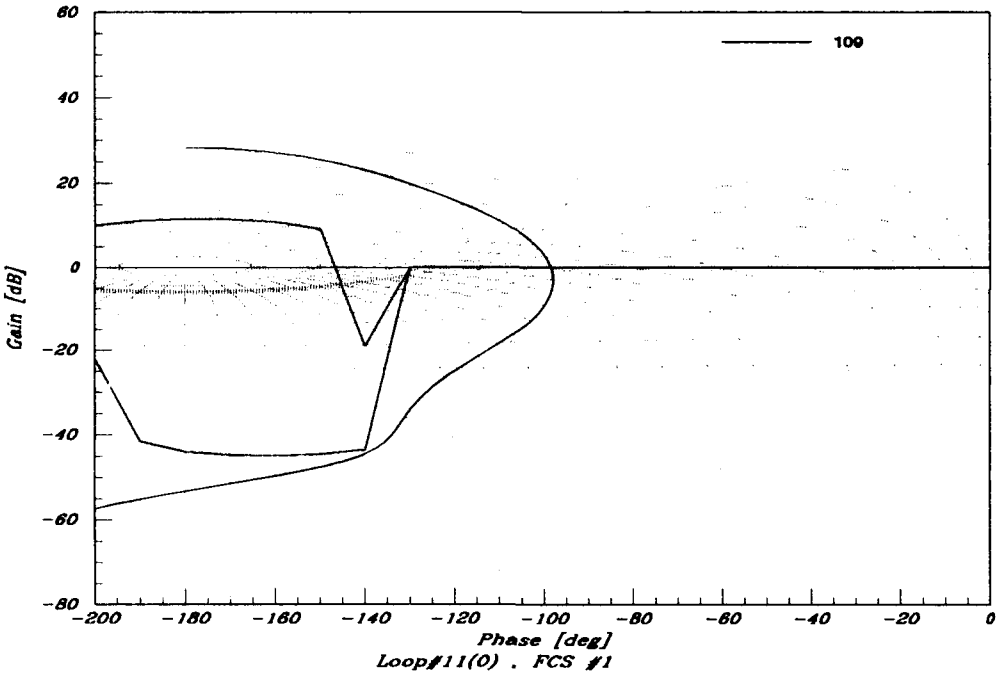

Figure 6.10. Loop Shape for FCS#1 $l_{1(0)}$ with Stability Boundareis

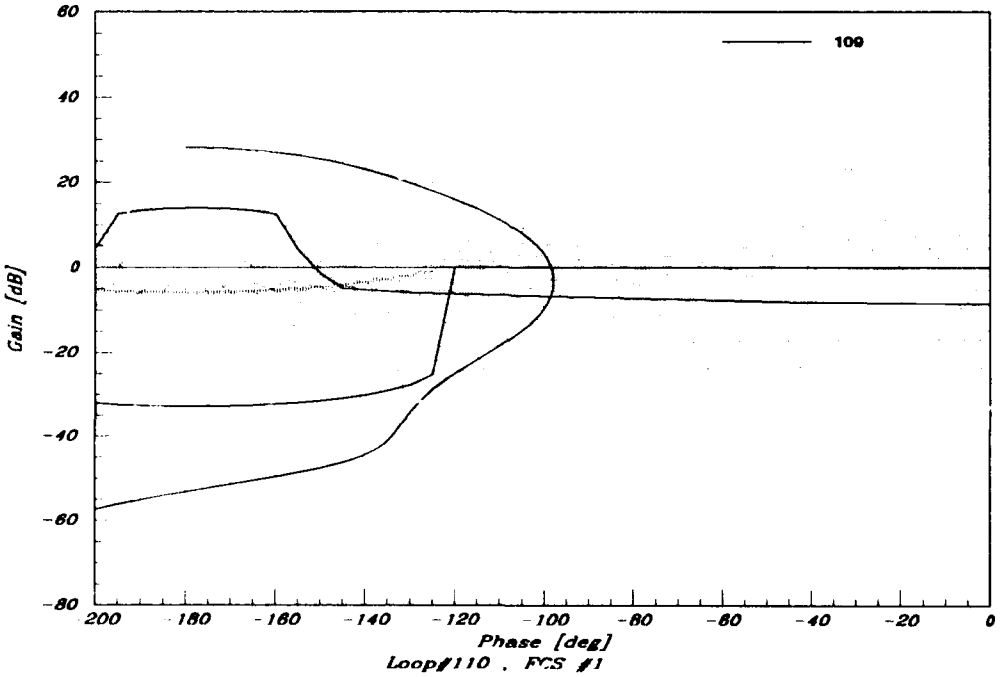

Figure 6.11. Loop Shape for FCS#1 $l_{1(0)}$ with Γ-Boundaries

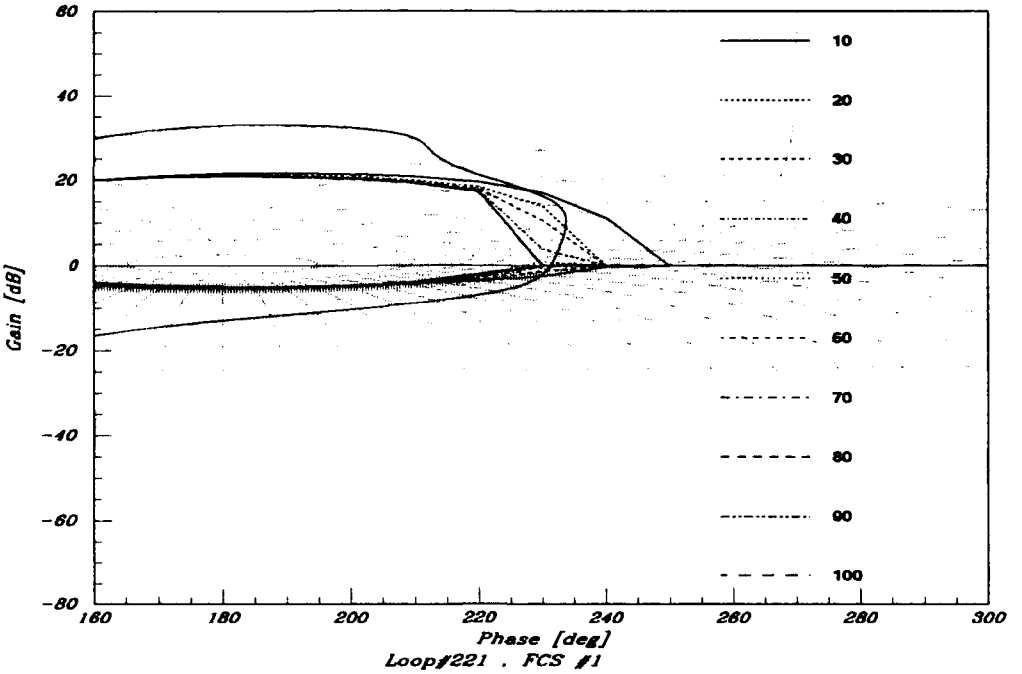

Figure 6.12. Loop Shape for FCS#1 $l_{2(1)}$ with Stability Boundaries

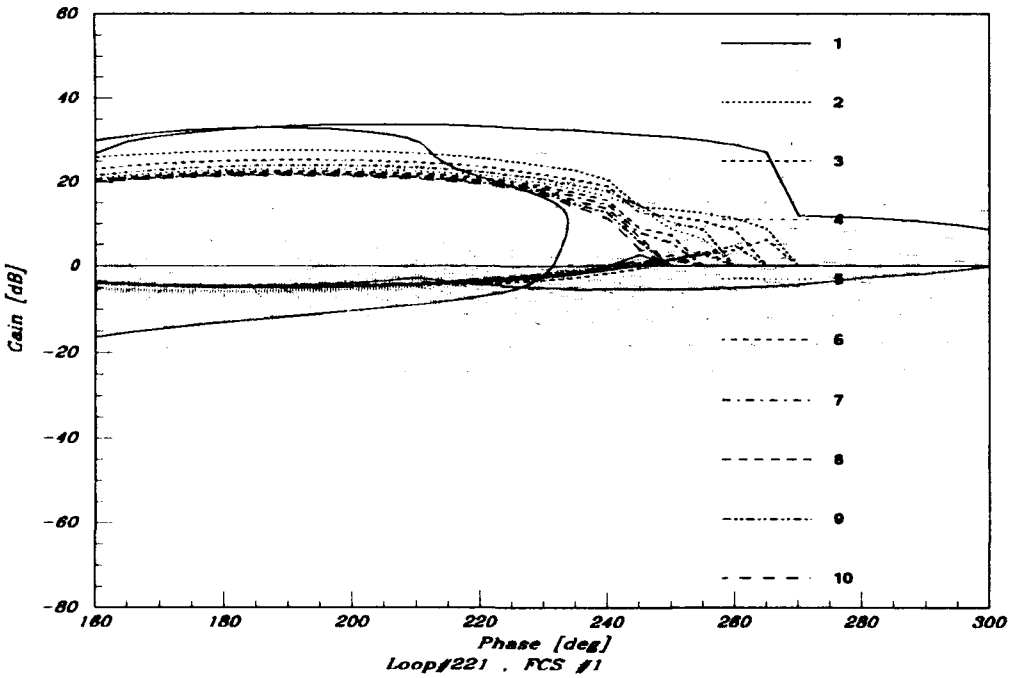

Figure 6.13. Loop Shape for FCS#1 $l_{2(1)}$ with Γ-Boundaries

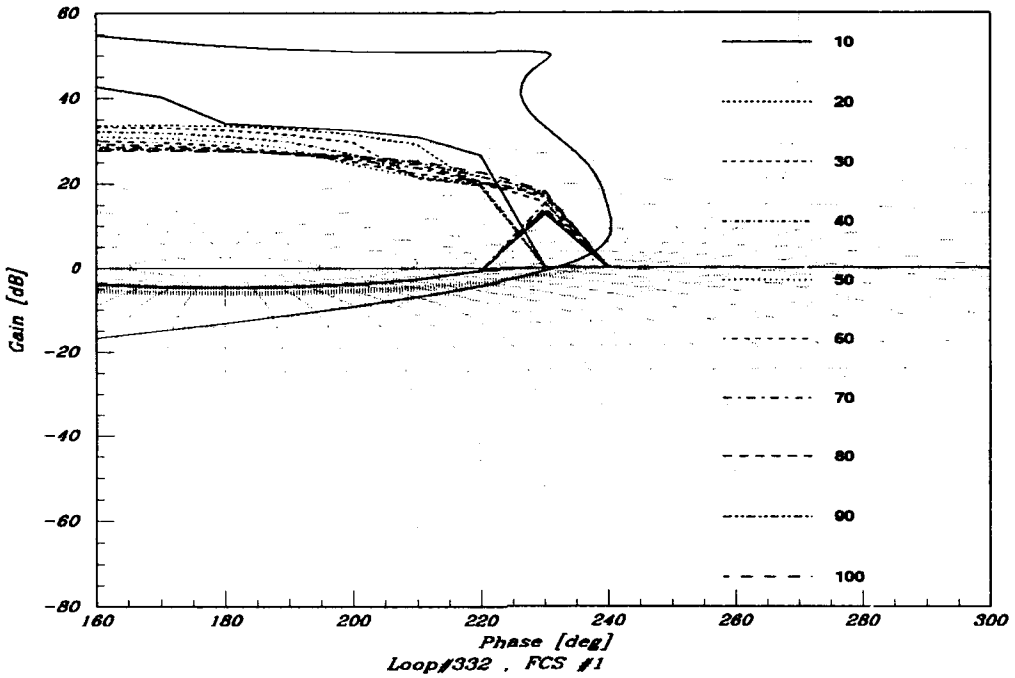

Figure 6.14. Loop Shape for FCS#1 $l_{3(2)}$ with Stability Boundaries

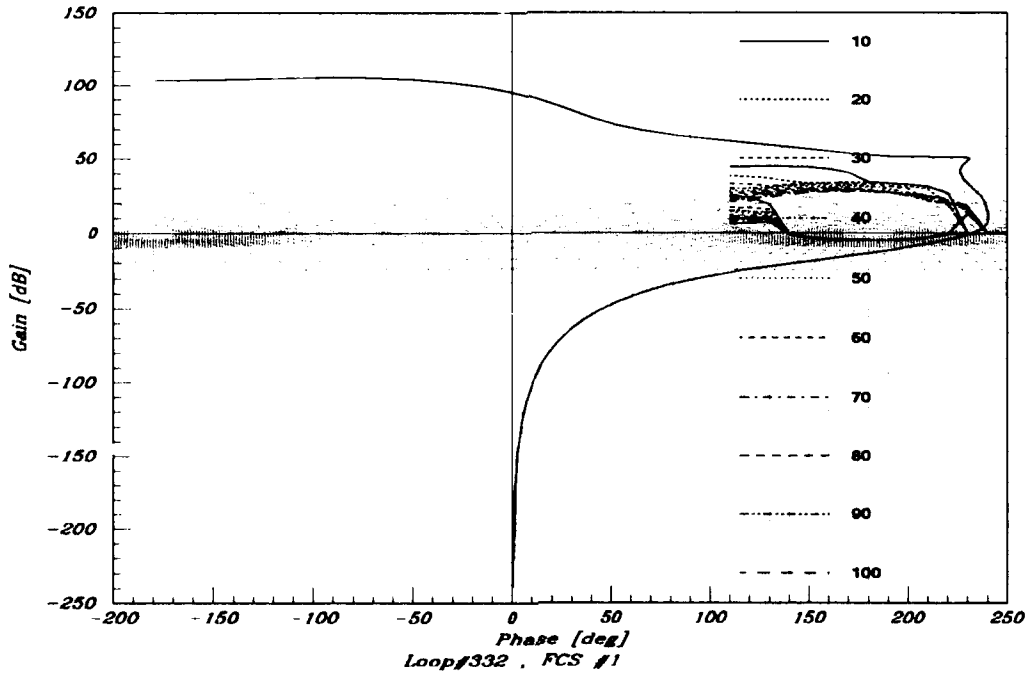

Figure 6.15. Loop Shape for FCS#1 $l_{3(2)}$ with Γ-Boundaries

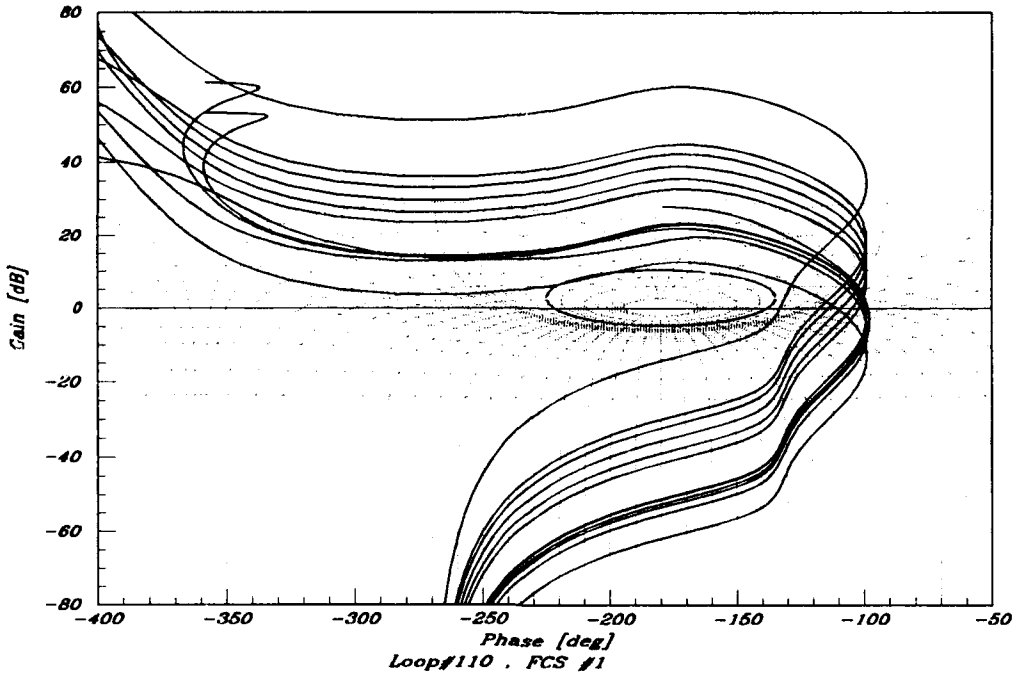

Figure 6.16. All FCS#1 $l_{1(0)}$s

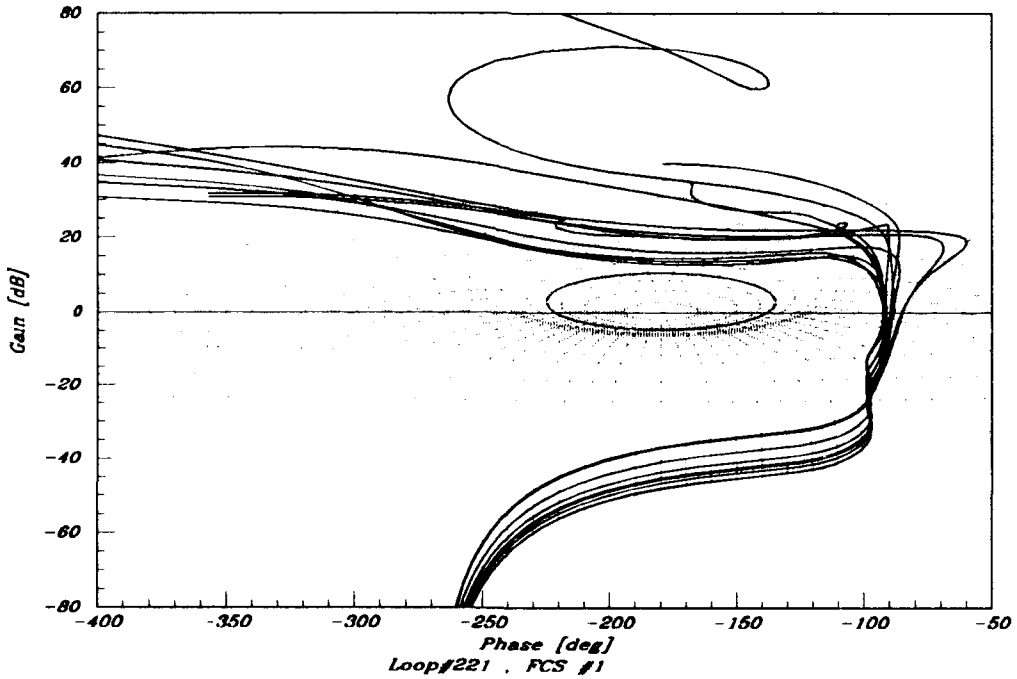

Figure 6.17. All FCS#1 $l_{2(1)}$s

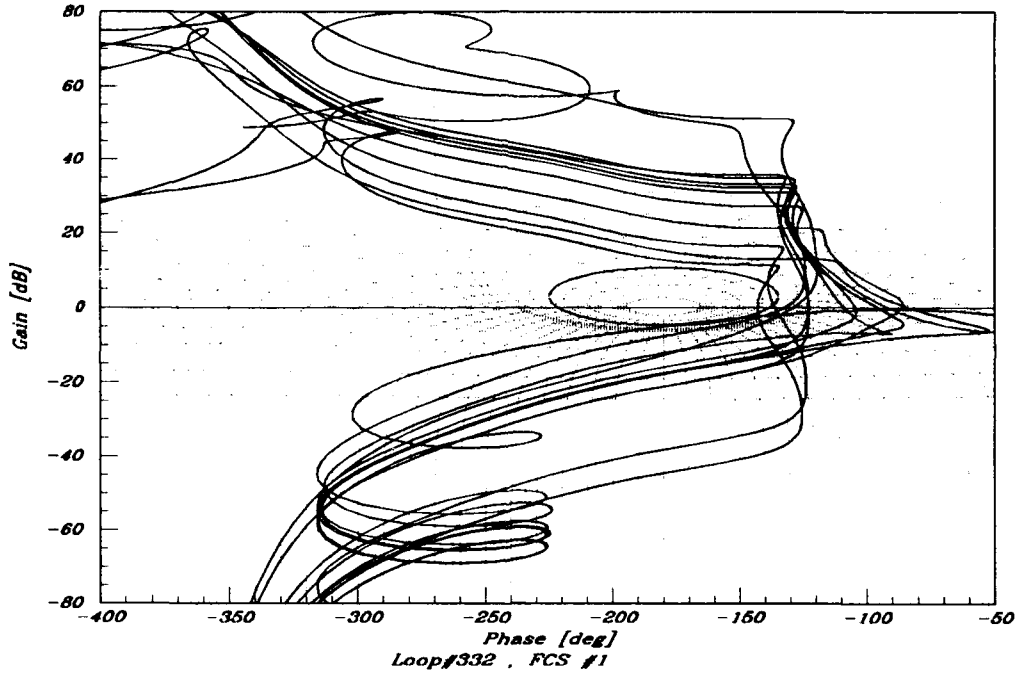

Figure 6.18. FCS#1 $l_{3(2)}$s, note: the $l_{3(2)}$s for 4 of the $q_{33(2)}$ are missing, see text

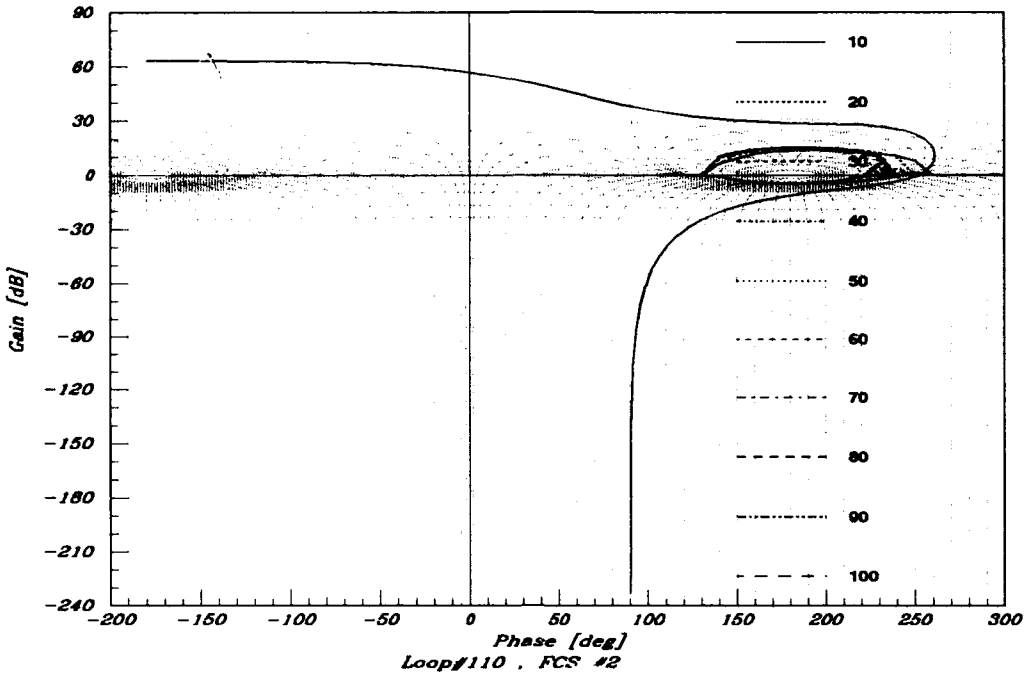

Figure 6.19. Loop Shape for FCS#2 $_{1(0)}$ with Stability Boundaries

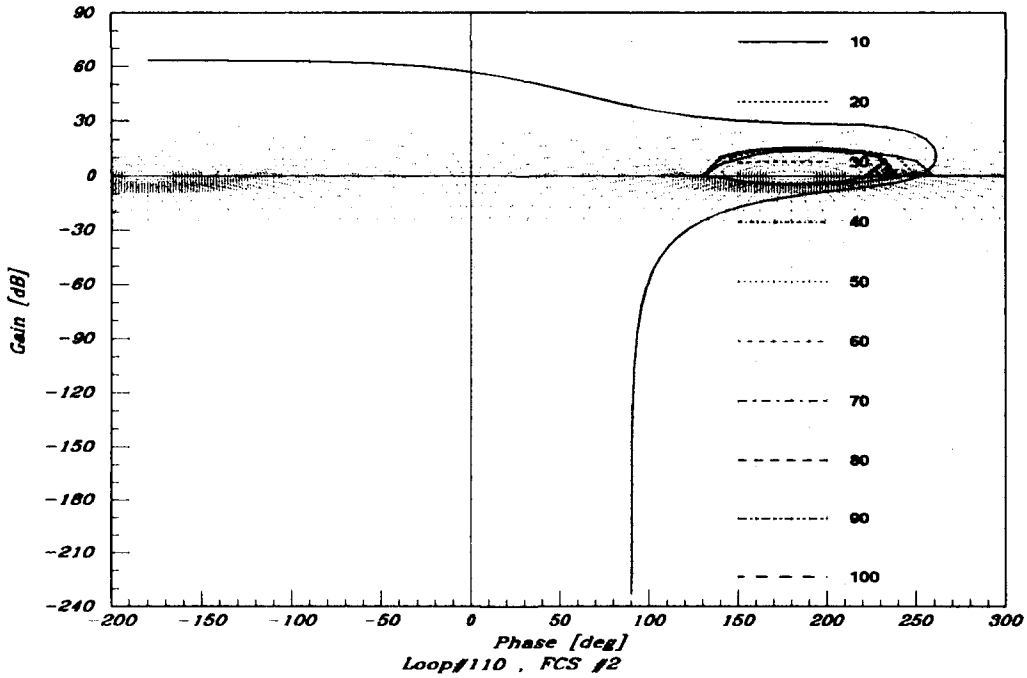

Figure 6.20. Loop Shape for FCS#2 $l_{1(0)}$ with Γ-Boundaries

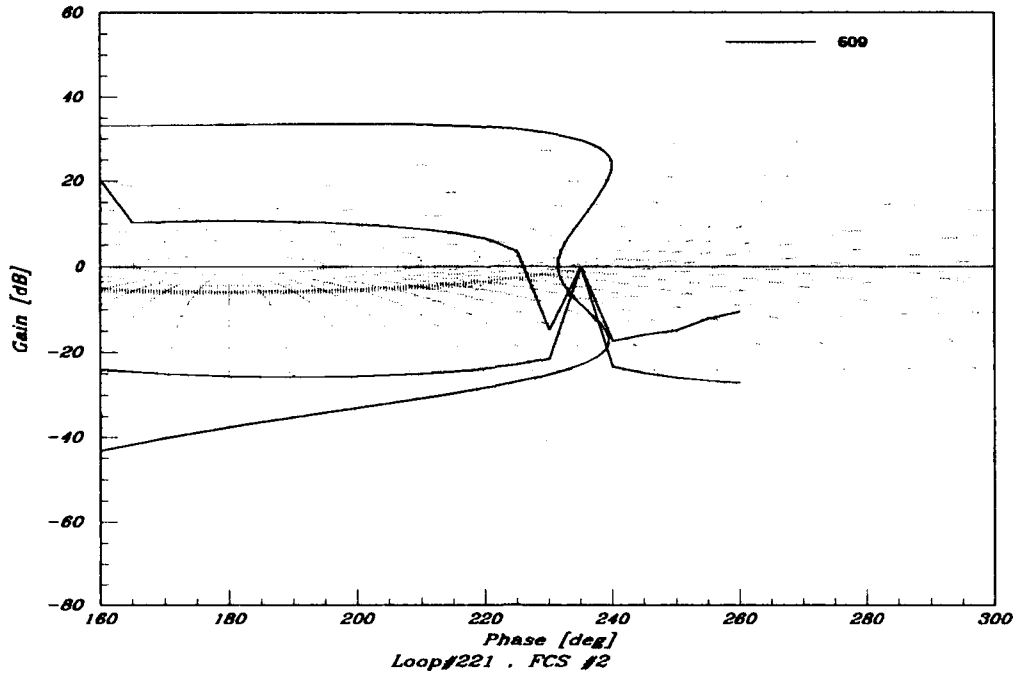

Figure 6.21. Loop Shape for FCS#2 $l_{2(1)}$ with Stability Boundaries

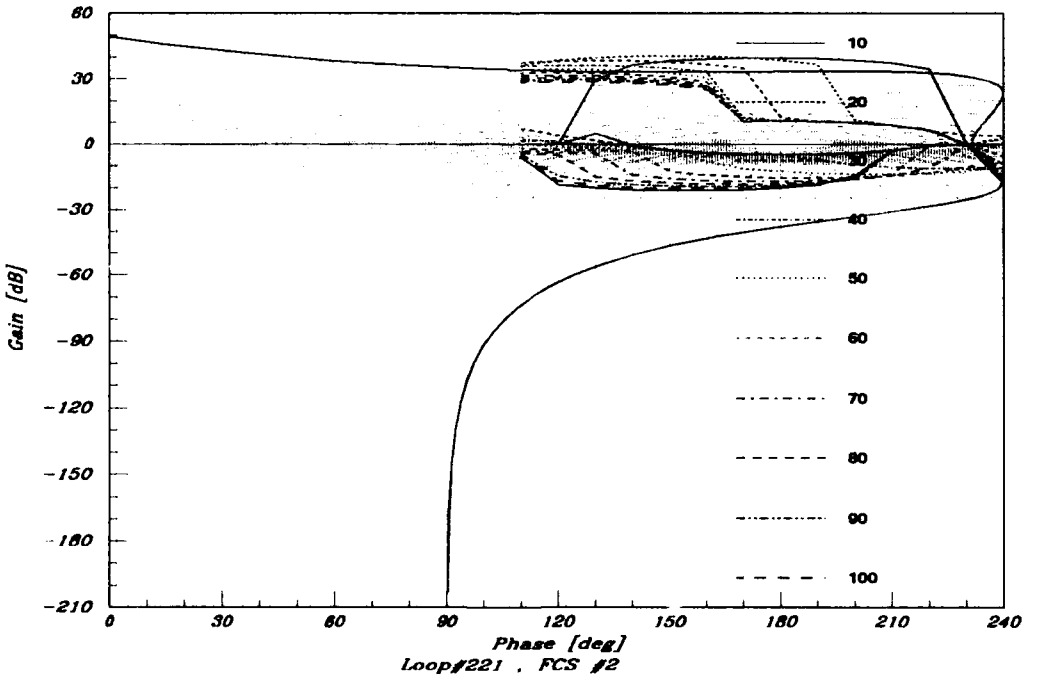

Figure 6.22. Loop Shape for FCS#2 $l_{2(1)}$ with Γ-Boundaries

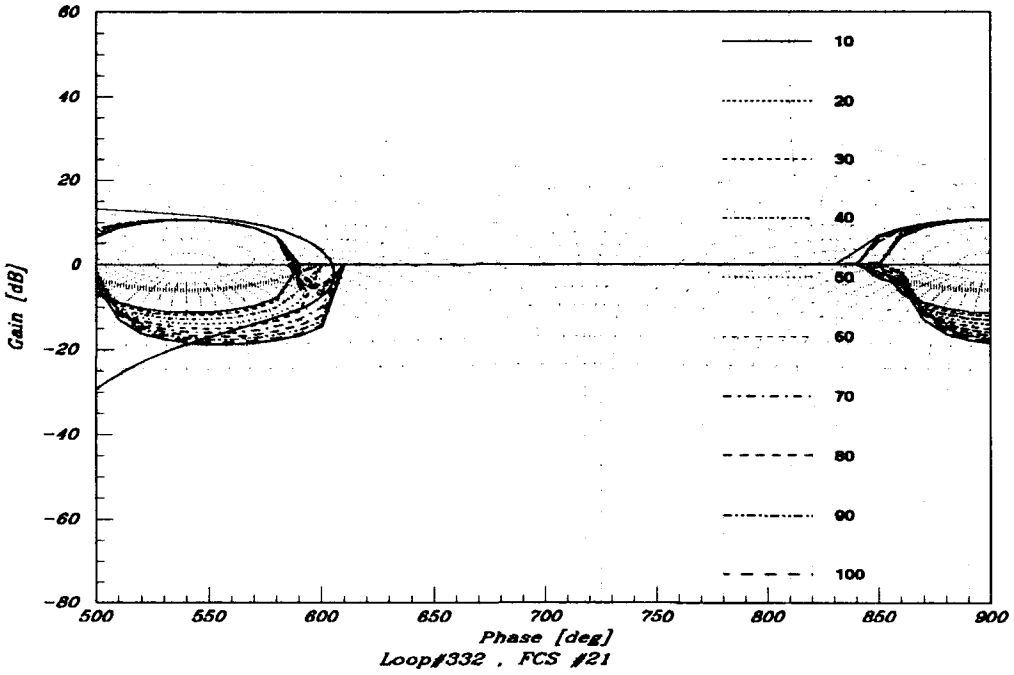

Figure 6.23. Loop Shape for FCS#21 $l_{3(2)}$ with Stability Boundaries

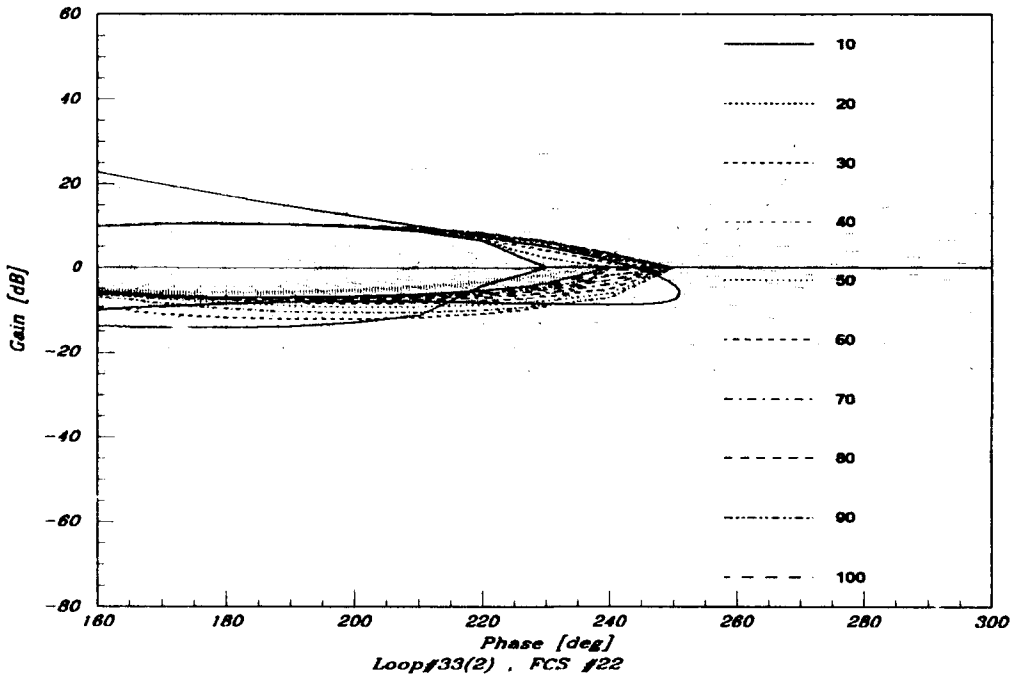

Figure 6.24. Loop Shape for FCS#22 $l_{3(2)}$ with Stability

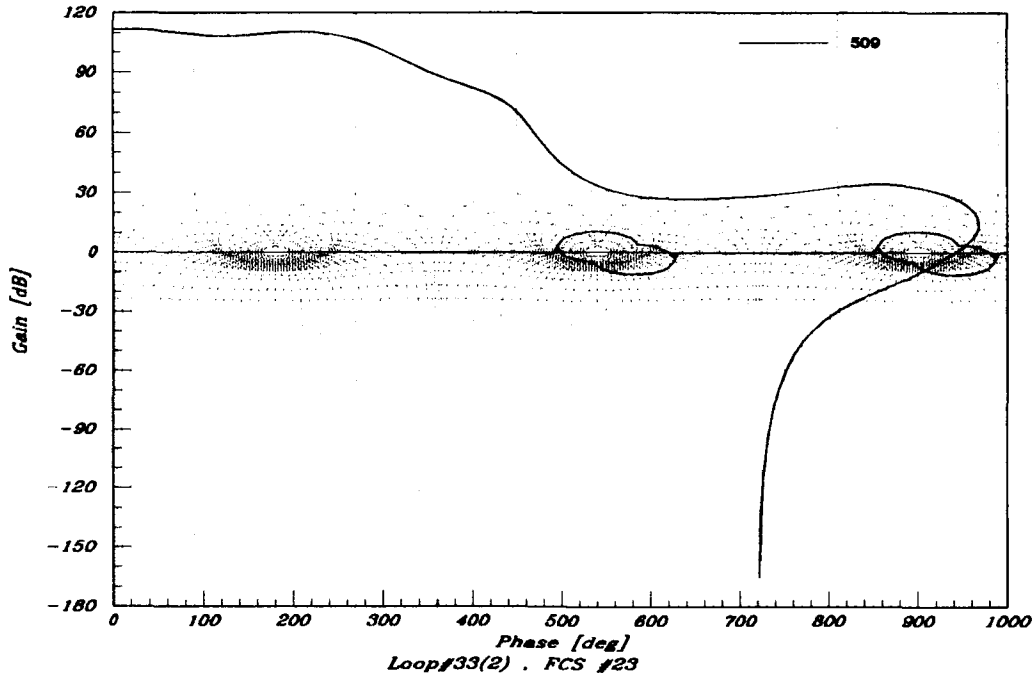

Figure 6.25. Loop Shape for FCS#23 $l_{3(2)}$ with Stability

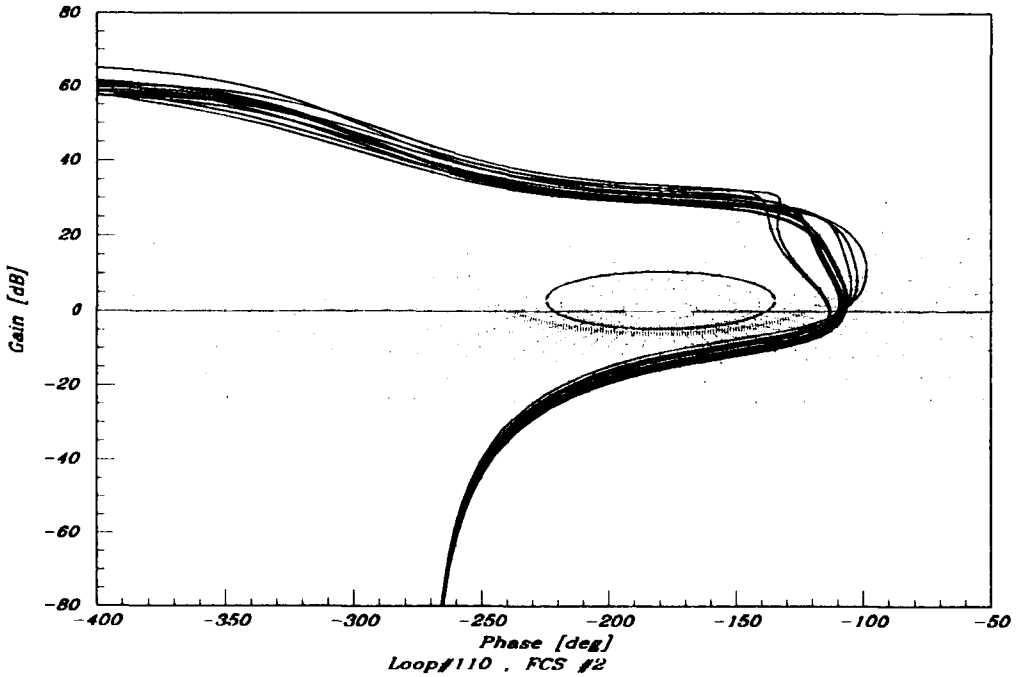

Figure 6.26. All FCS#2 $l_{1(0)}$s

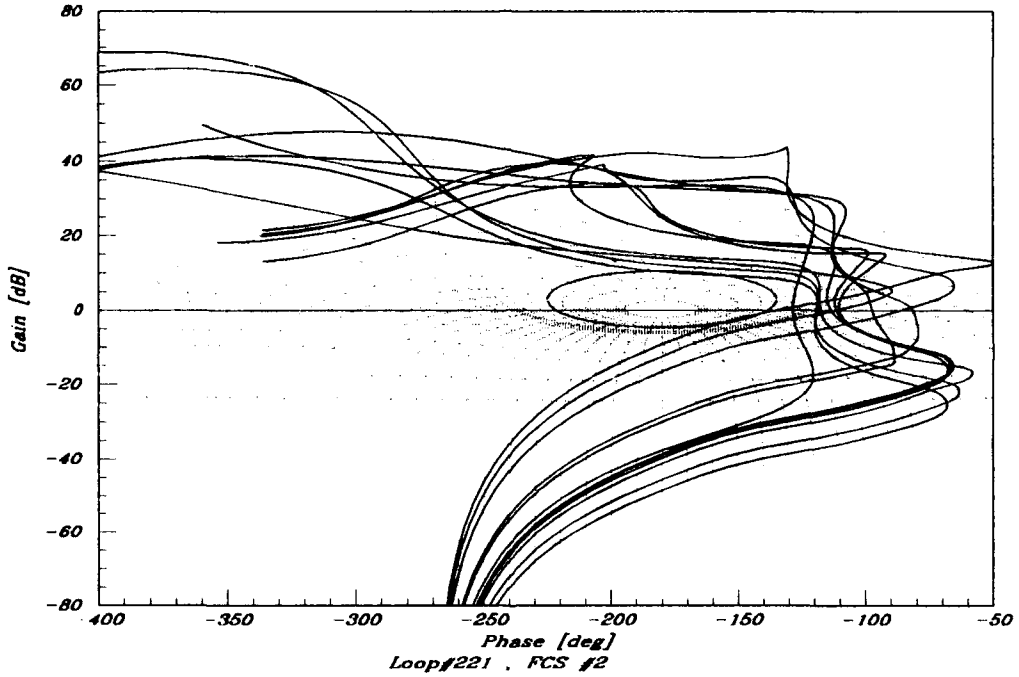

Figure 6.27. All FCS#2 $l_{2(1)}$s

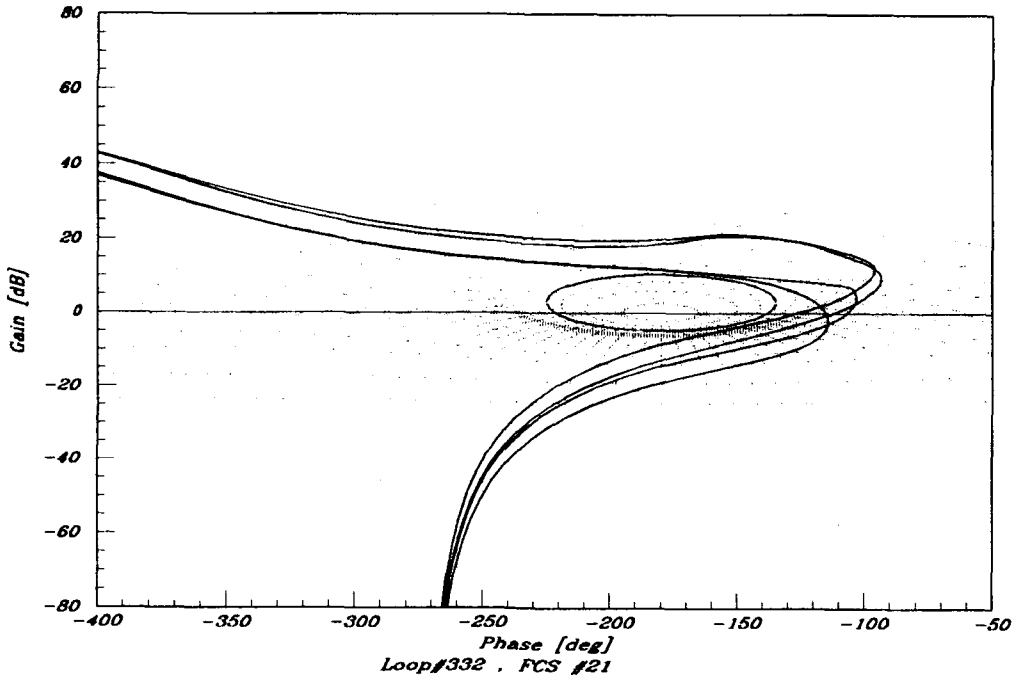

Figure 6.28. All FCS#21 $l_{3(2)}$s

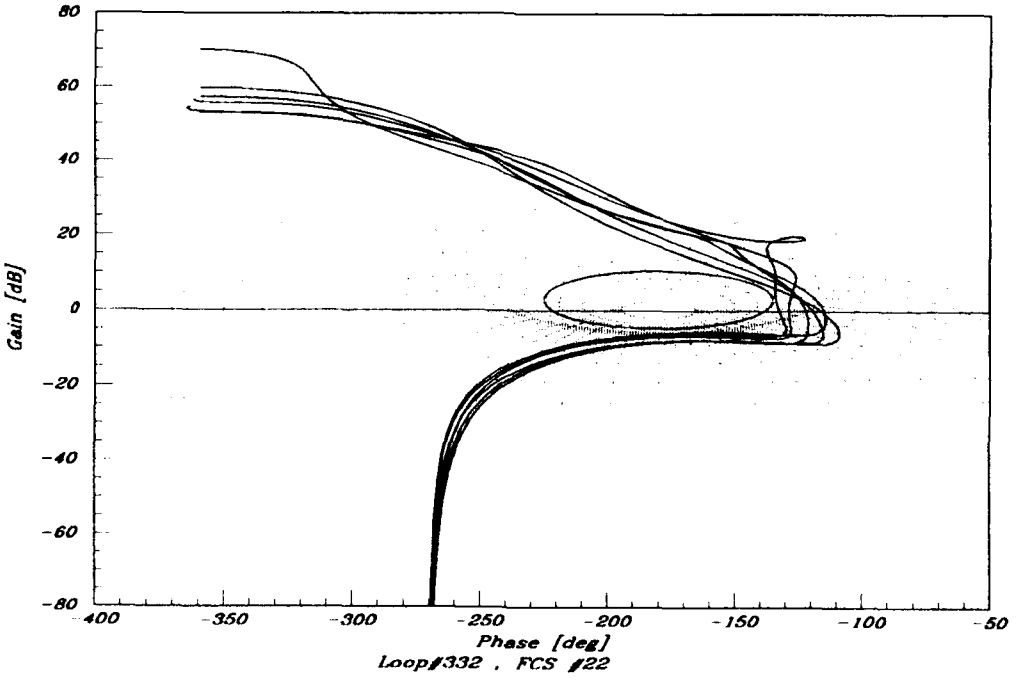

Figure 6.29. All FCS#22 $l_{3(2)}$s

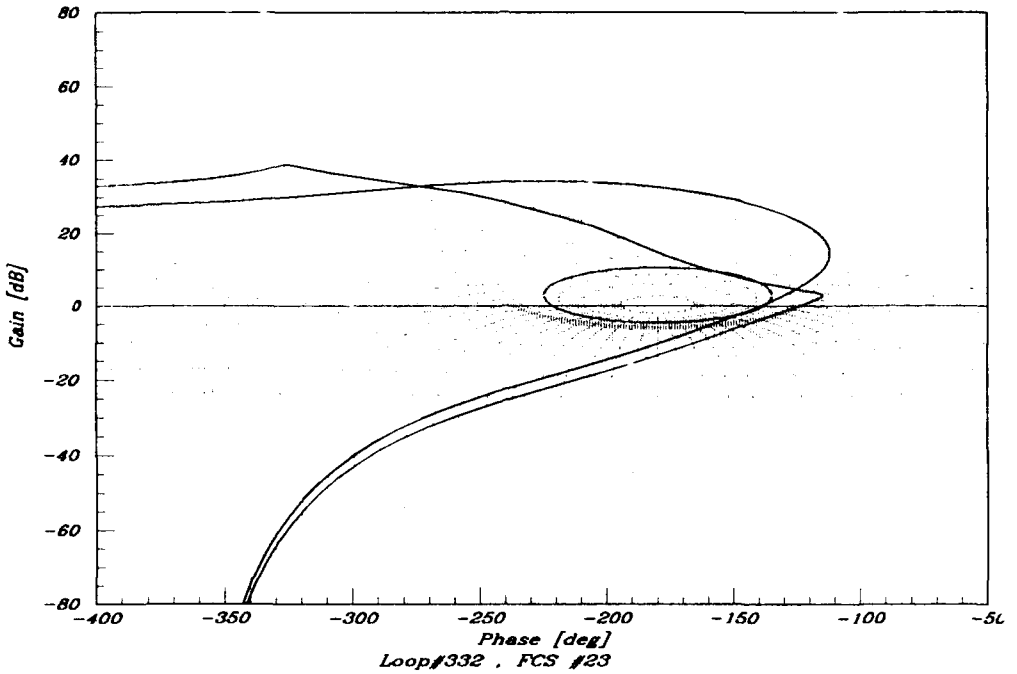

Figure 6.30. All FCS#22 $l_{3(2)}$s

6.6 ω_ϕ Specifications

Throughout the loop shaping process, it is difficult, and for many of the loops, impossible, to meet the 30 $\frac{rad}{\text{sec}}$ specification on ω_ϕ . The problem lies in the number of RHP poles involved in the loops. When there are RHP poles present in $q_{o_{ij(k)}}$ it is necessary to start shaping $l_{o_{i(k)}}$ with these poles. A RHP real pole causes a phase of $-180°$ at 0 $\frac{rad}{\text{sec}}$. This shifts $l_{o_{i(k)}}$ to the left. For example, with three RHP real poles present, $l_{o_{i(k)}}$ must translate at least 540° to the right on the NC before encircling the boundaries. This large translation causes the large ω_ϕ . For this thesis only 1 out of 8 loop designs met the specified ω_ϕ . All maximum ω_ϕ are shown in Table 6.1.

6.7 Prefilter Design

The method used to design the prefilters is the same as outlined in Chapter 2. First, B_U and B_L transfer functions are found that delineate the time response boundaries. The time response specifications are based on MIL-STD-1797A, 'Flying

Table 6.1. Maximum ω_ϕ on All FCS

FCS#	loop # (i)	Maximum ω_ϕ $\frac{rad}{sec}$
1	1	40
1	2	50
1	3	320
2	1	60
2	2	100
21	3	270
22	3	30
23	3	3000

Qualities of Piloted Aircraft'. [17] Next, the frequency response of $\mathcal{L}_{i(k)}$ is plotted on the same plot as B_U and B_L. Finally, F_i is designed so that $\mathcal{L}_{i(k)}$ is contained between B_U and B_L. At higher ω's, B_L can be shifted lower by adding high frequency poles, and therefore violations of B_L at high frequencies can be ignored. Because of limitations in using Matrix_x , some of the prefilters have to be approximated. Figures 6.31 through 6.38 show the Bode plots of the final designed CLTFs'. Some of the time responses can not be plotted due to the numerical limitations of Matrix_x and the high order of the $qij(k)$s. The time responses that can be plotted are shown in Figures 6.39 through 6.43. Appendix 5 contains all the F_1, F_2, and F_3 designed in this thesis.

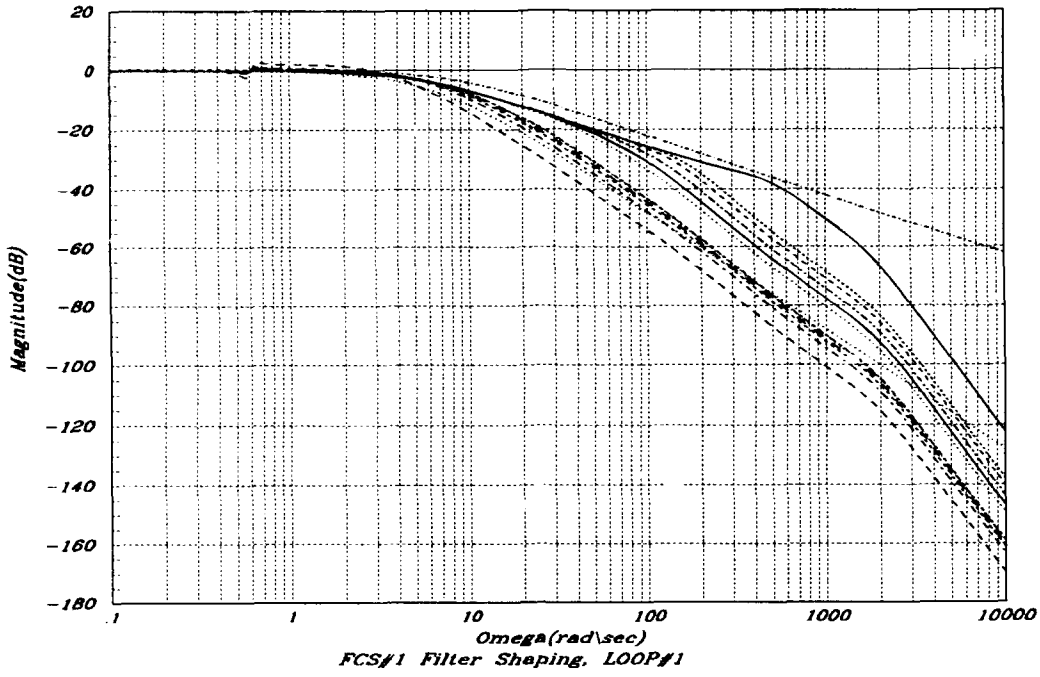

Figure 6.31. FCS#1 $l_{1(0)}$s Filter Shaping

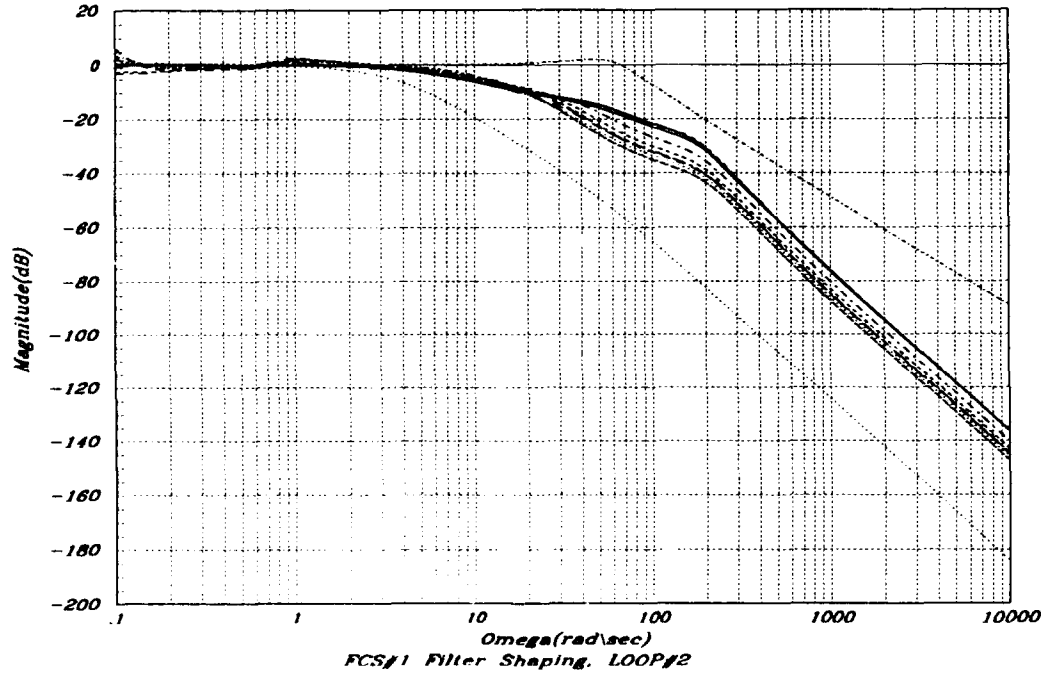

Figure 6.32. FCS#1 $l_{2(1)}$s Filter Shaping

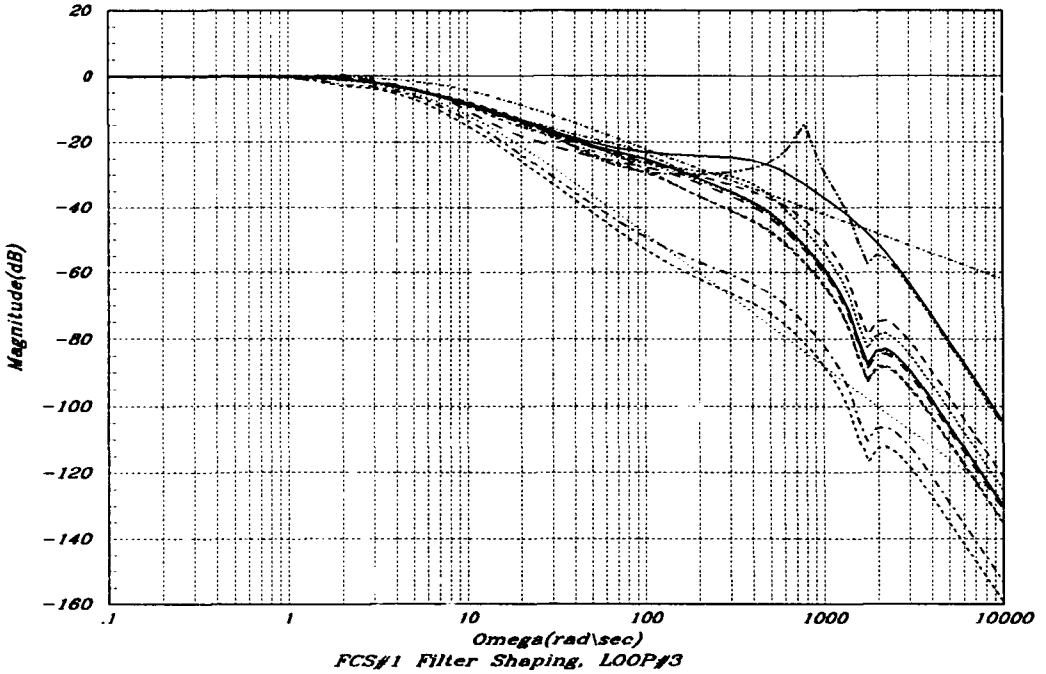

Figure 6.33. FCS#1 $l_{3(2)}$s Filter Shaping

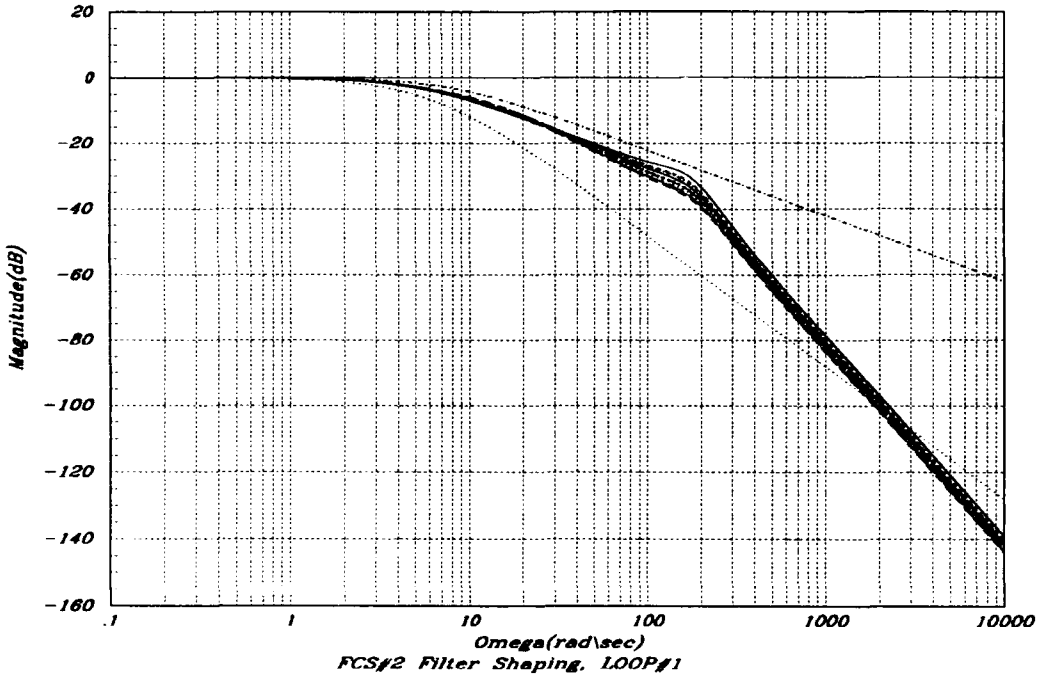

Figure 6.34. FCS#2 $l_{1(0)}$s Filter Shaping

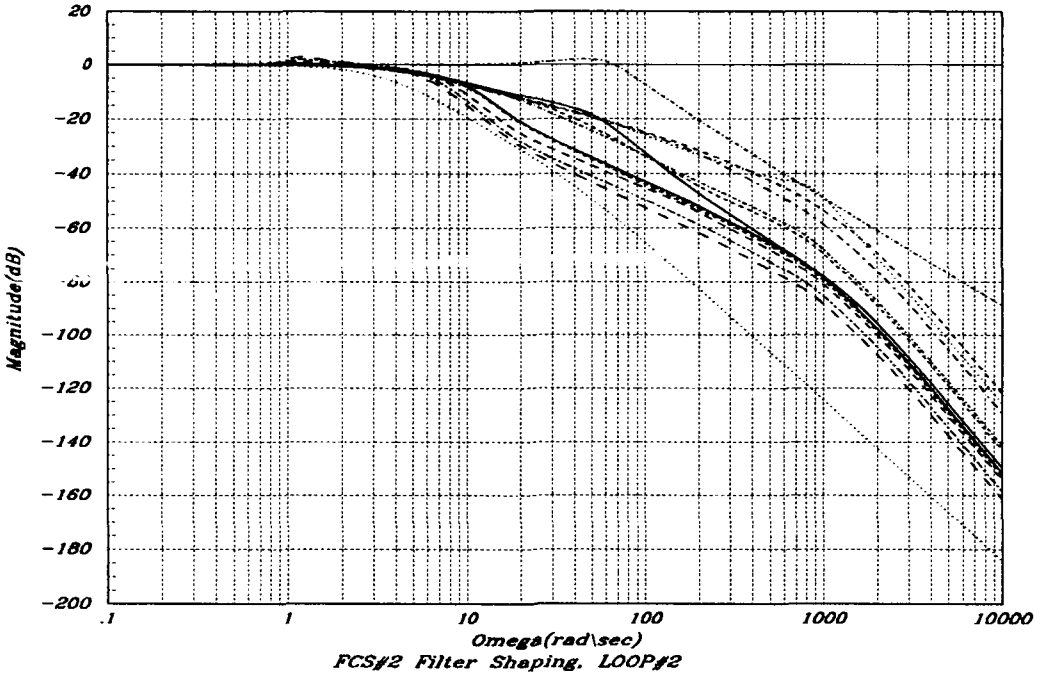

Figure 6.35. FCS#2 $l_{2(1)}$s Filter Shaping

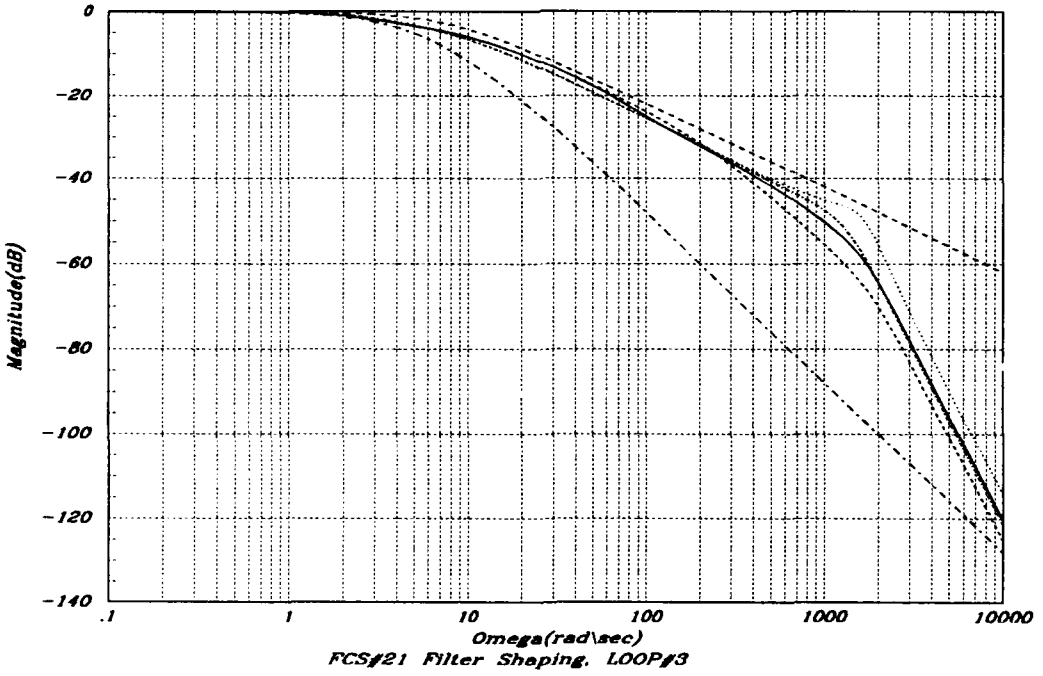

Figure 6.36. FCS#21 $l_{3(2)}$s Filter Shaping

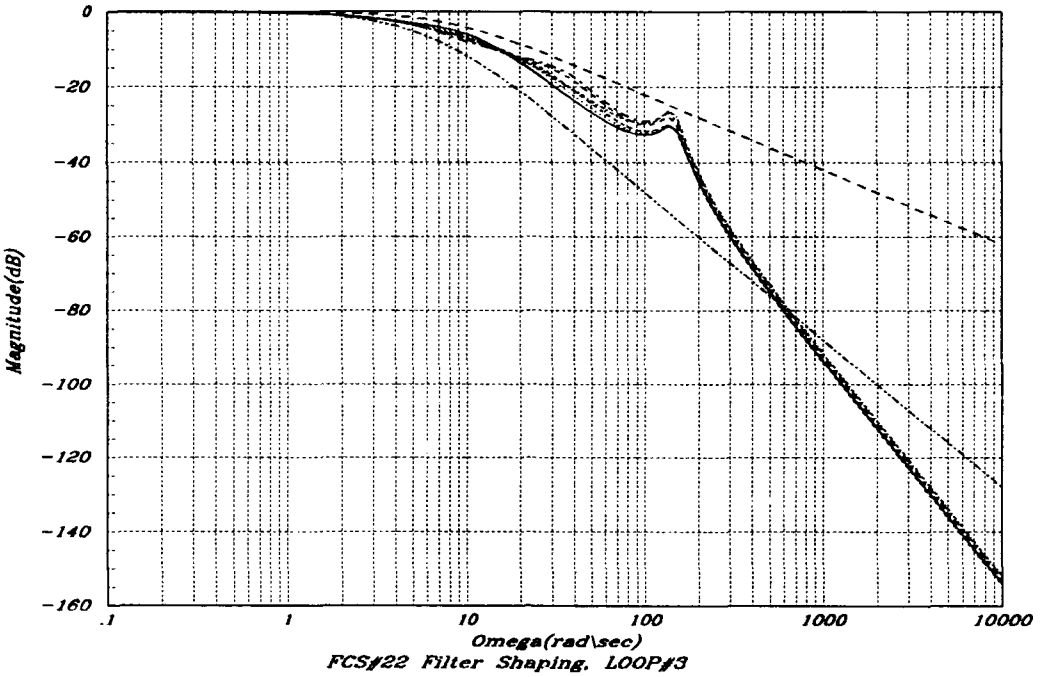

Figure 6.37. FCS#22 $l_{3(2)}$s Filter Shaping

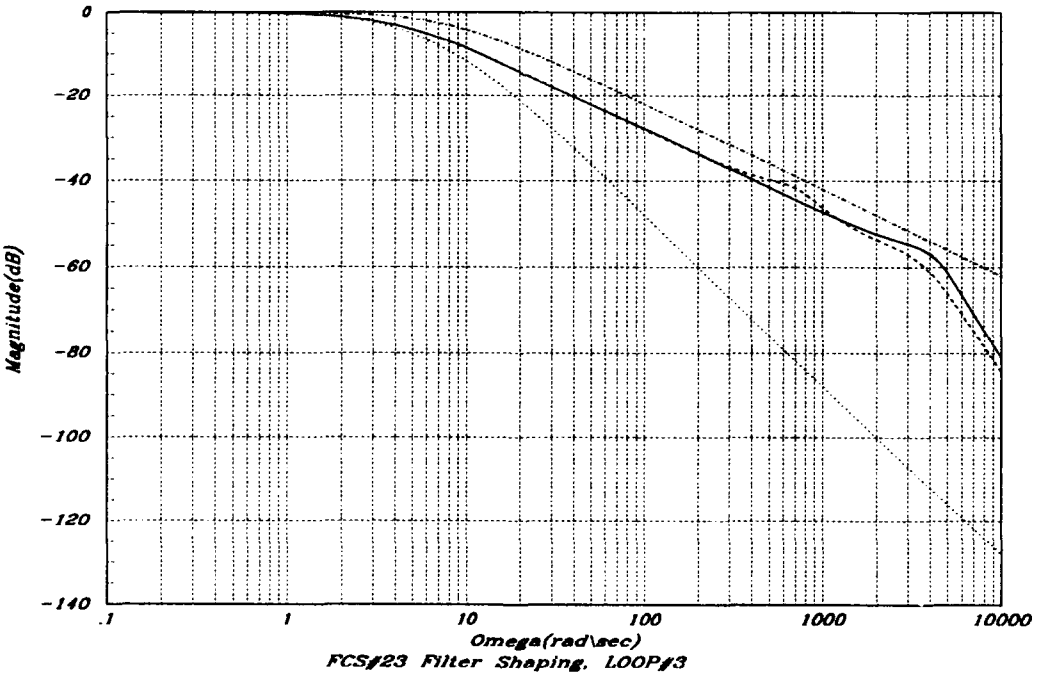

Figure 6.38. FCS#23 $l_{3(2)}$s Filter Shaping

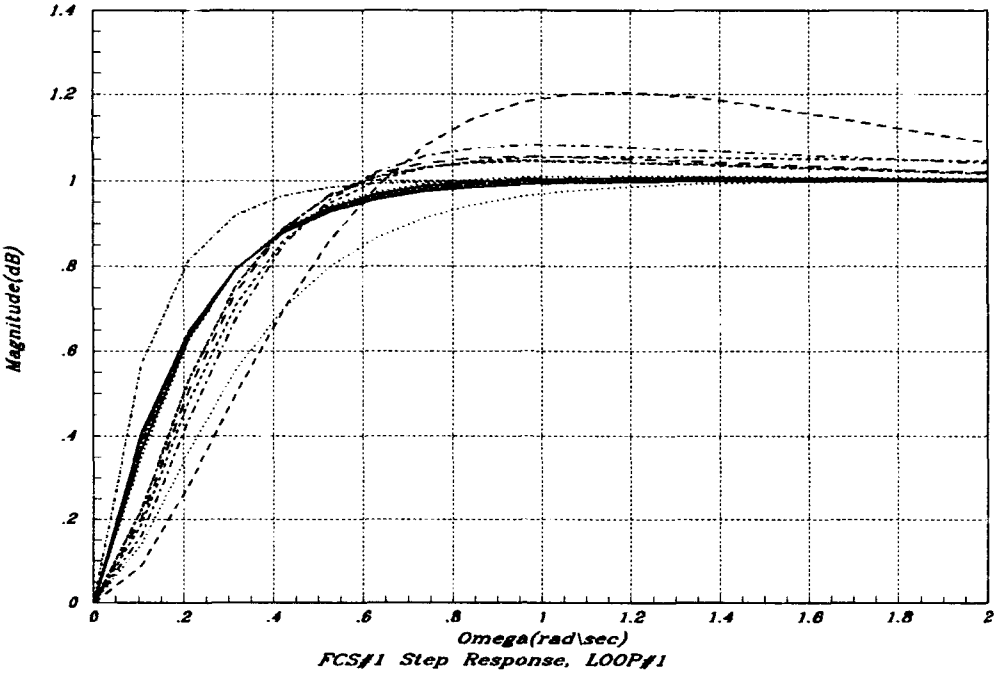

Figure 6.39. FCS#1 $l_{1(0)}$s Time Response

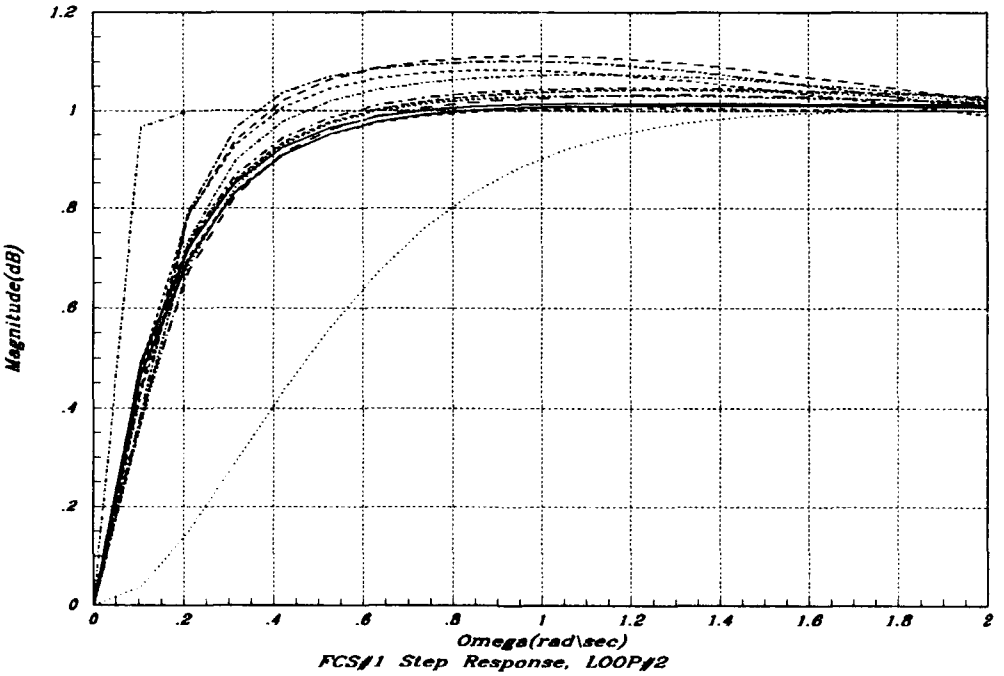

Figure 6.40. FCS#1 $l_{2(1)}$s Time Response

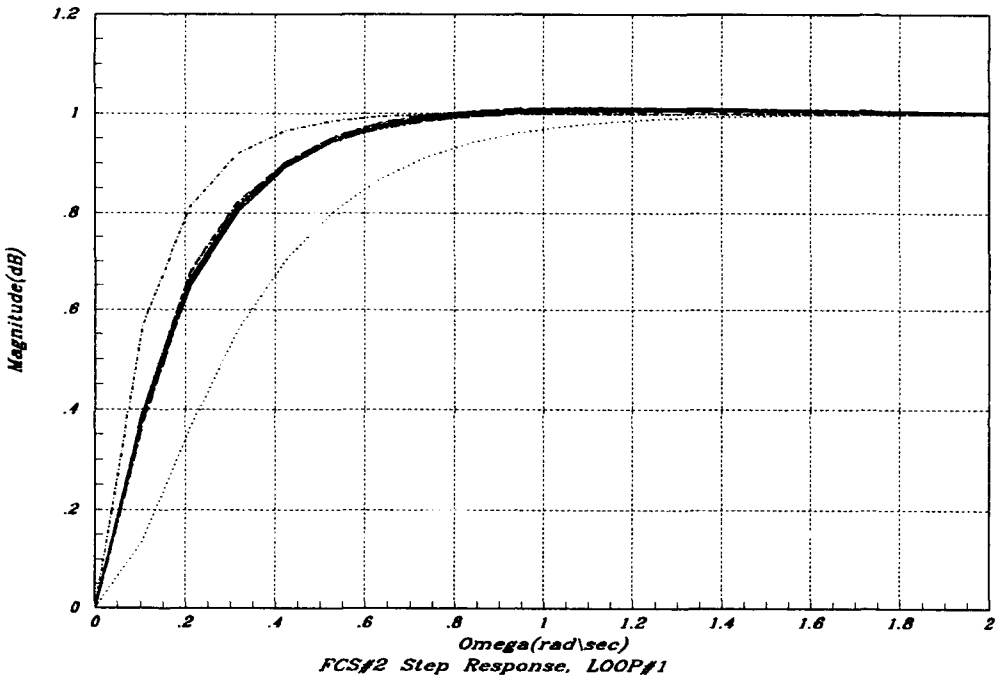

Figure 6.41. FCS#2 $l_{1(0)}$s Time Response

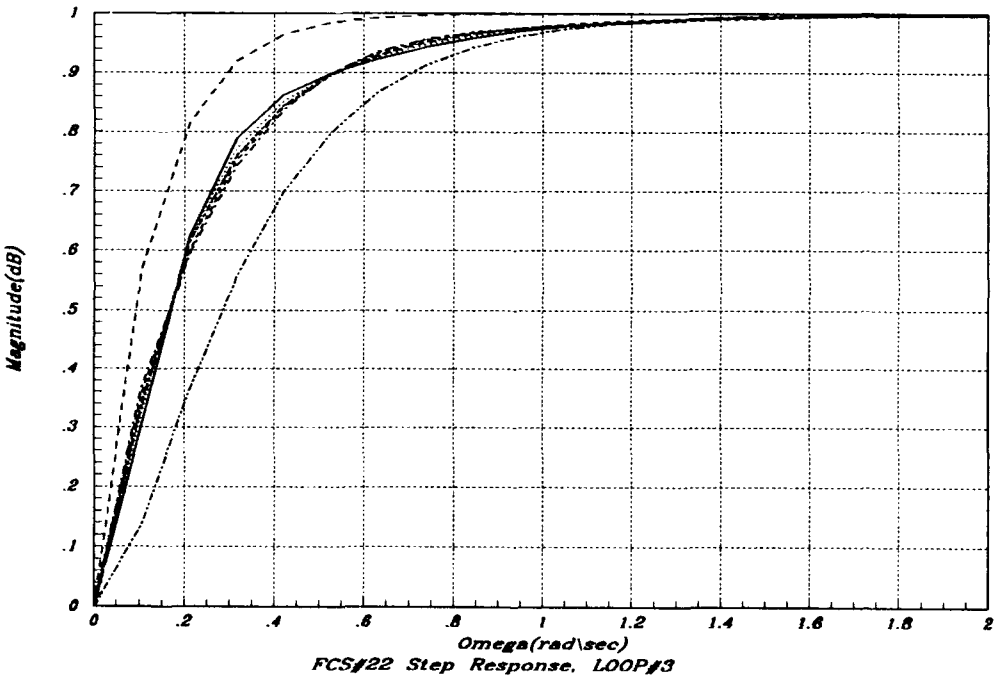

Figure 6.42. FCS#22 $l_{3(2)}$s Time Response

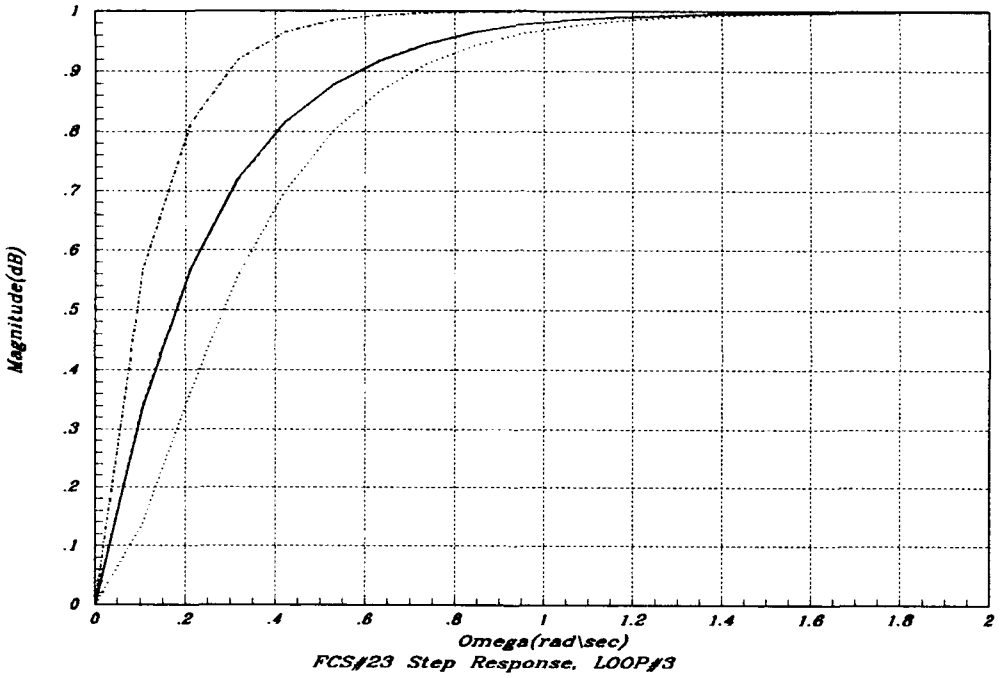

Figure 6.43. FCS#23 $l_{3(2)}$s Time Response

6.8 Conclusion

This chapter describes G and F development. First the reasons for scheduling are discussed. Next the shaping of individual loops is covered. During the loop shaping process, it is found that most of the loops violate the specified ω_ϕ because of constriants on the loops. Finally, the design of the prefilters is covered. When the CLTF's are simulated the results are generally good. Chapter 7 described the modeling problem that become evident during the nonlinear simulation, that prevent a successful simulation.

VII. Problems Encountered with Nonlinear Simulation

7.1 Introduction

In this chapter, problems encountered during the nonlinear simulation are described. The nonlinear simulation is based on Cord's six degree of freedom nonlinear YF-16 simulation program. [4] First, the need for a method of controller order reduction is outlined. Next, a problem in the modeling process is described. Finally, the simulation of a flawed pitch-up/pitch-down maneuver is described. Note: the pitch-up/velocity vector roll maneuvers are not simulated due to problems encountered with the nonlinear simulation program as explained at the end of the next section.

7.2 Reduced Order G_{ij}s

After programming the designed FCS into the YF-16 simulation program, it is found, through experimentation, that the highest order G that this program can accommodate is 8^{th}. Since the designed FCS G_{ij}s all are higher order than 8^{th}, then order reduction must be accomplished. The method used to reduced the order of the G_{ij}s is based upon obtaining a lower order approximation from the Bode plot of the designed G_{ij}. By plotting the Lm(G_{ij})s on a Bode plot, a straight line approximation $[G_{ij}]_m$ can be made. Using this approximation, $[\mathcal{L}_{i(k)}]_m = [G_{ii}]_m \mathcal{Q}_{ii(k)}$ is plotted on a Nichols chart. If there are violations of the 3 dB M-contour, $[G_{ii}]_m$ is modified and the modified $[\mathcal{L}_{i(k)}]_m$ is plotted. This method is repeated until a satisfactory lower order $[G_{ii}]_m$ is obtained. Plots of $[\mathcal{L}_{i(k)}]_m$ for all FCS's are shown in Figures 7.1 through 7.8. The lower order G_{ij}s are shown for FCS#1 in Equations (7.1) through (7.3). Those for FCS#2 are shown in Equations (7.4) and (7.5). The G_{ij}s for FCS#21, FCS#22, ans FCS#23 are shown in Equations (7.6), (7.7), (7.8), respectively. When these reduced order G_{ij}s are programmed in the YF-16 simulation program, only the pitch channel of FCS#1 results in satisfactory control of the simulated YF-16.

$$[G_{11}]_m = \frac{(3.0000D-03)S^4 + (3.1800D-03)S^3 + (2.3394D-03)S^2 + (1.1473D-03)S^1 + (3.8858D-04)}{S^7 + (2450)S^6 + (4120000)S^5 + (200000000)S^4} \tag{7.1}$$

$$[G_{22}]_m = \frac{(1.9200D+07)S^4 + (3.0720D+07)S^3 + (1.7280D+07)S^2 + (3.8400D+06)S^1 + (2.4000D+05)}{S^7 + (1630)S^6 + (688000)S^5 + (19200000)S^4} \tag{7.2}$$

$$[G_{33}]_m = \frac{(6.0000D-01)S^4 + (6.6000D-01)S^3 + (8.9550D-01)S^2 + (3.6390D-01)S^1 + (6.7035D-02)}{S^8 + (2.7400D+03)S^7 + (4.8280D+06)S^6 + (1.3888D+09)S^5 + (4.8000D+10)S^4} \tag{7.3}$$

$$[G_{11}]_m = \frac{(7.5610D+05)S^4 + (8.9376D+06)S^3 + (1.4956D+07)S^2 + (1.3950D+07)S^1 + (9.1100D+06)}{S^7 + (3.0000D+02)S^6 + (6.0002D+04)S^5 + (4.0002D+06)S^4} \tag{7.4}$$

$$[G_{22}]_m = \frac{(4.0386D+0)S^4 + (5.8964D+08)S^3 + (6.9424D+08)S^2 + (3.9572D+08)S^1 + (8.4375D+07)}{S^7 + (2625)S^6 + (2790000)S^5 + (506250000)S^4} \tag{7.5}$$

$$[G_{33}]_m = \frac{(1.8000D+10)S^4 + (5.4000D+10)S^3 + (5.8500D+10)S^2 + (2.7000D+10)S^1 + (4.5000D+09)}{S^7 + (6030)S^6 + (9180200)S^5 + (271200000)S^4 + (1800000000)S^3} \tag{7.6}$$

$$[G_{33}]_m = \frac{(1312500)S^4 + (31500000)S^3 + (240187500)S^2 + (603750000)S^1 + (393750000)}{S^7 + (350)S^6 + (45625)S^5 + (2625000)S^4 + (56250000)S^3} \tag{7.7}$$

$$[G_{33}]_m = \frac{(9.3750D+15)S^3 + (2.1562D+17)S^2 + (1.5000D+18)S^1 + (2.8125D+18)S^1}{S^7 + (3.0150D+04)S^6 + (3.0451D+08)S^5 + (1.0452D+12)S^4 + (1.5169D+14)S^3 + (5.6250D+15)S^2} \tag{7.8}$$

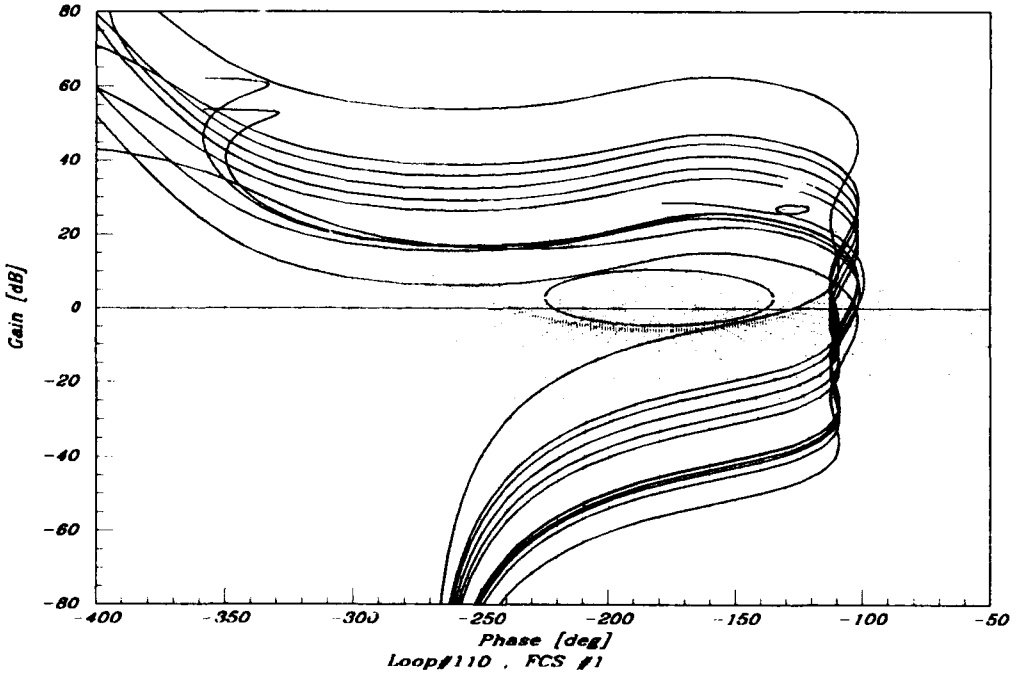

Figure 7.1. FCS#1 $[\mathcal{L}_{1(0)}]_m$

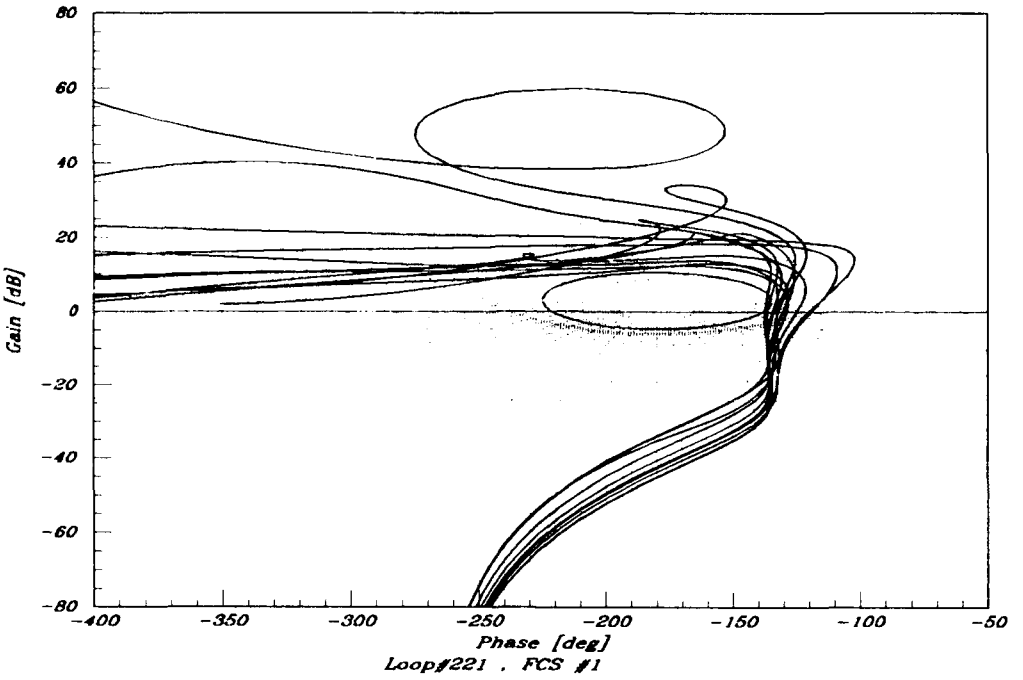

Figure 7.2. FCS#1 $[\mathcal{L}_{2(1)}]_m$

7.3 Modeling Problem

With the $[G_{ij}]_m$'s implemented in the simulation program, it is found that for the pitch-up/pitch-down maneuver, q output has an unwanted acceleration component. This can be seen in Figure 7.9, where after the first ramp-up/ramp-down of the response, the output should stay at zero until the ramp-down/ramp-up portion of the response is reached. The unwanted acceleration is very evident in Figure 7.10, where there is a zero input command. Instead of staying at zero there is an acceleration that causes the desired output to be displaced downward. The cause of this unwanted acceleration is traced back to the modeling process. As stated in Chapter 3, there is a step increase in the thrust at the start of the simulation that is not modeled. During system identification an assumption is made that the system under consideration is at steady state. This assumption is made to insure that all components of the output are due only to the declared input. In this case, since the step increase in thrust is not included as an input to the system, the plants that are identified have this input attributed to the q input. The thrust input is attributed

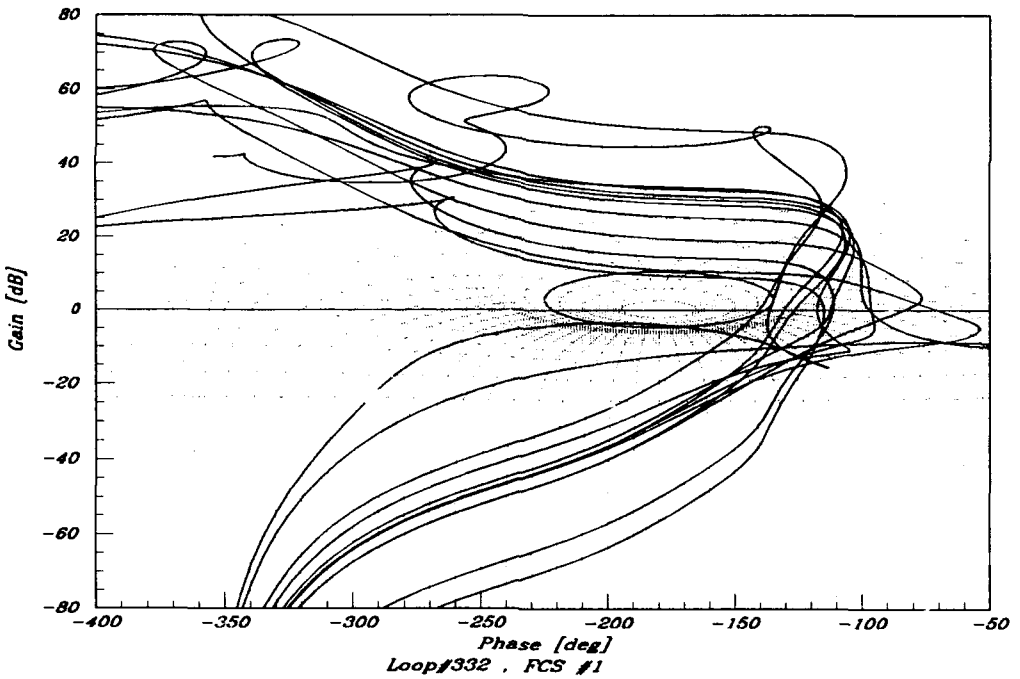

Figure 7.3. FCS#1 $[\mathcal{L}_{3(2)}]_m$

to the q input because it results in an output about the y-body axis (q-axis). Compounding this problem is the mechanism which computes the elevator trim angle, it does not account for the added control moment produced by the thrust vectoring. This has a very similar effect as a step increase in thrust. To model $\mathcal{V}_{ij(0)}$s directly, the $v_{ij(0)}$s are required to be equal order over equal order. This is true because Matrix_x will not accept an improper transfer function and the $v_{ij(0)}$s are to be inverted to find the $q_{ij(0)}$s. To ensure the $v_{ij(0)}$'s are equal order over equal order, an extra pole is inserted at -100 in each $v_{ij(0)}$. The assumption is that this pole is large enough in magnitude, to be insignificant in the $v_{ij(0)}$s and would be removed from the $q_{ij(0)}$s. As it turns out these poles are significant and can not be removed from the $q_{ij(0)}$s without altering the frequency response. It seems that the model requires at least an equal order over equal order which is an indication that there are other inputs that are not modeled. According to Horowitz, when there are inputs that are not modeled one would expect to see more zeros than poles. [9] In this case, the model is constrained to be equal order over equal order so there are not more zeros

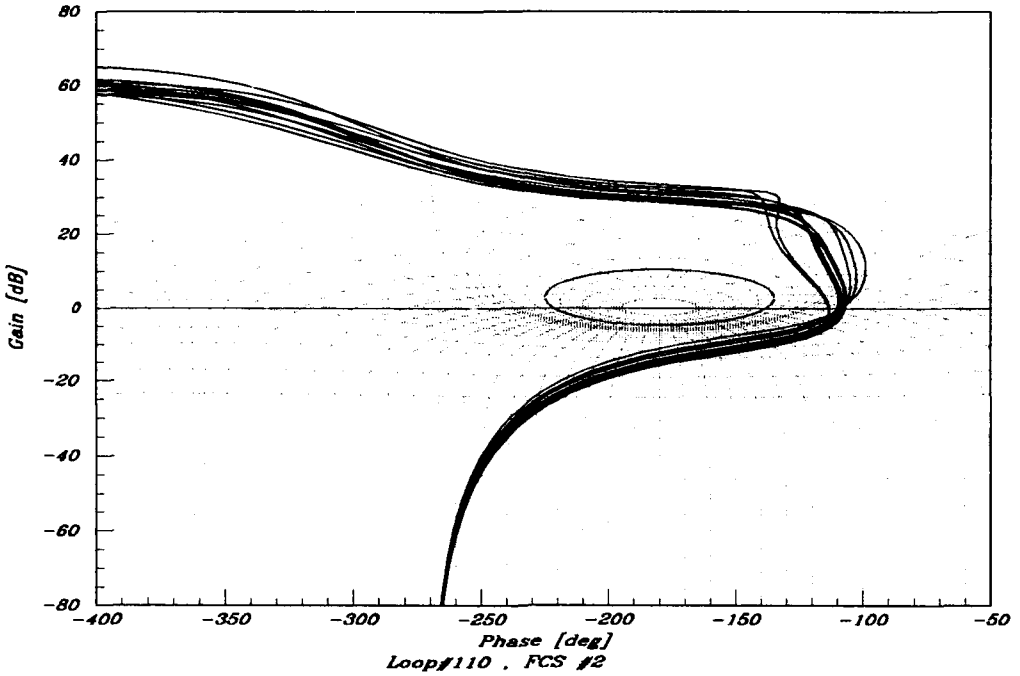

Figure 7.4. FCS#2 $[\mathcal{L}_{1(0)}]_m$

than poles. During the QFT design process, these plants with mismodeled transfer functions representing the pitch channel, cause the compensator to weight the contributions of the pitch input incorrectly and when the compensator is installed in the simulation program the unwanted acceleration is produced.

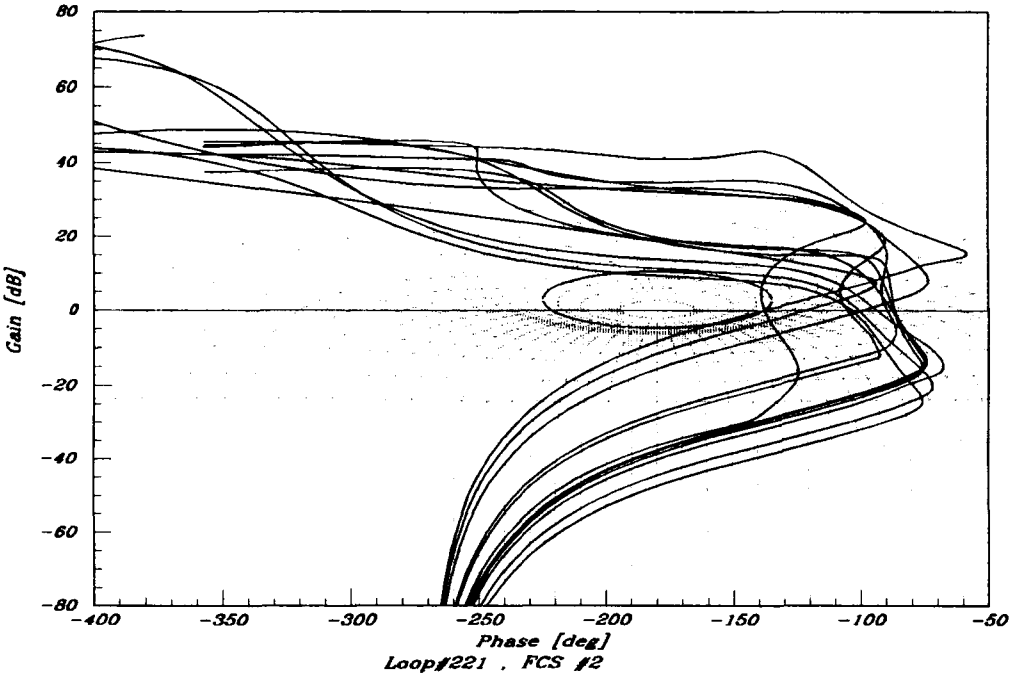

Figure 7.5. FCS#2 $[\mathcal{L}_{2(1)}]_m$

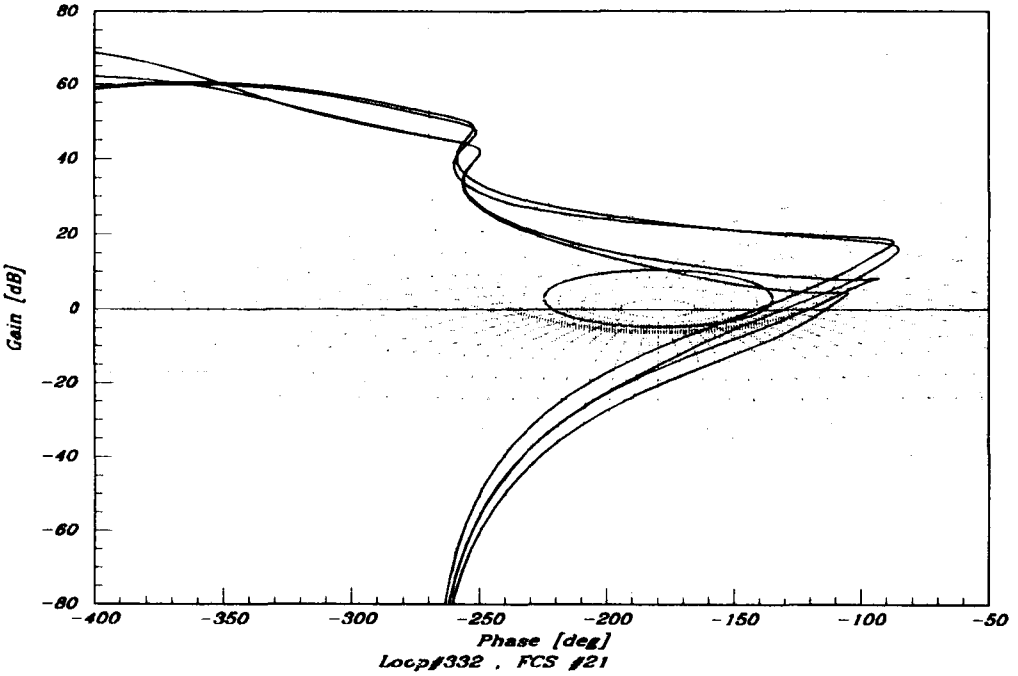

Figure 7.6. FCS#21 $[\mathcal{L}_{3(2)}]_m$

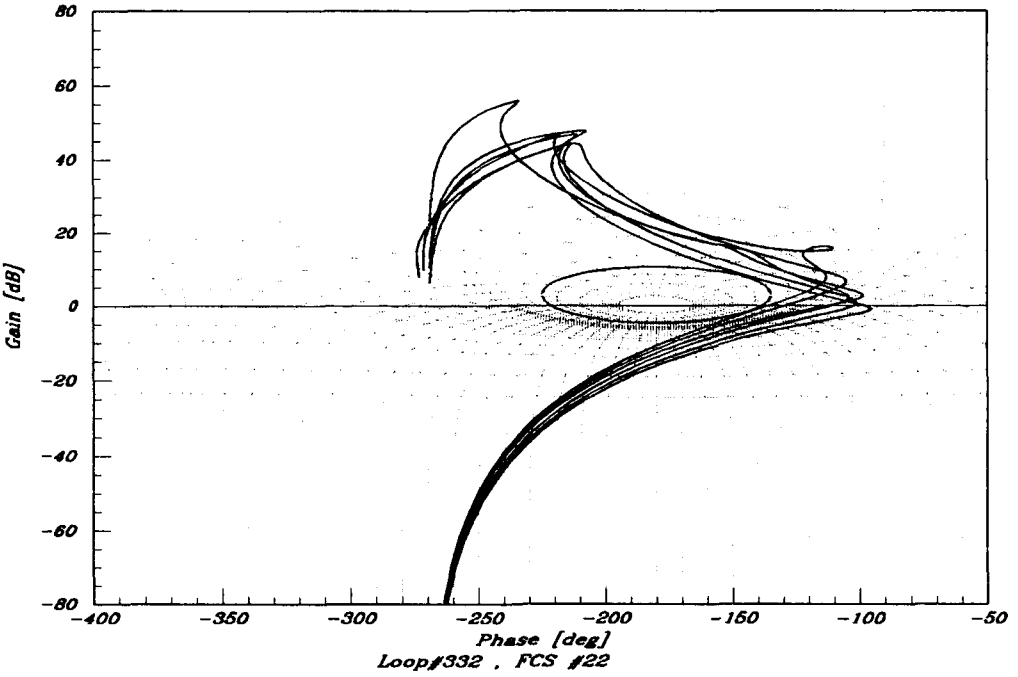

Figure 7.7. FCS#22 $[\mathcal{L}_{3(2)}]_m$

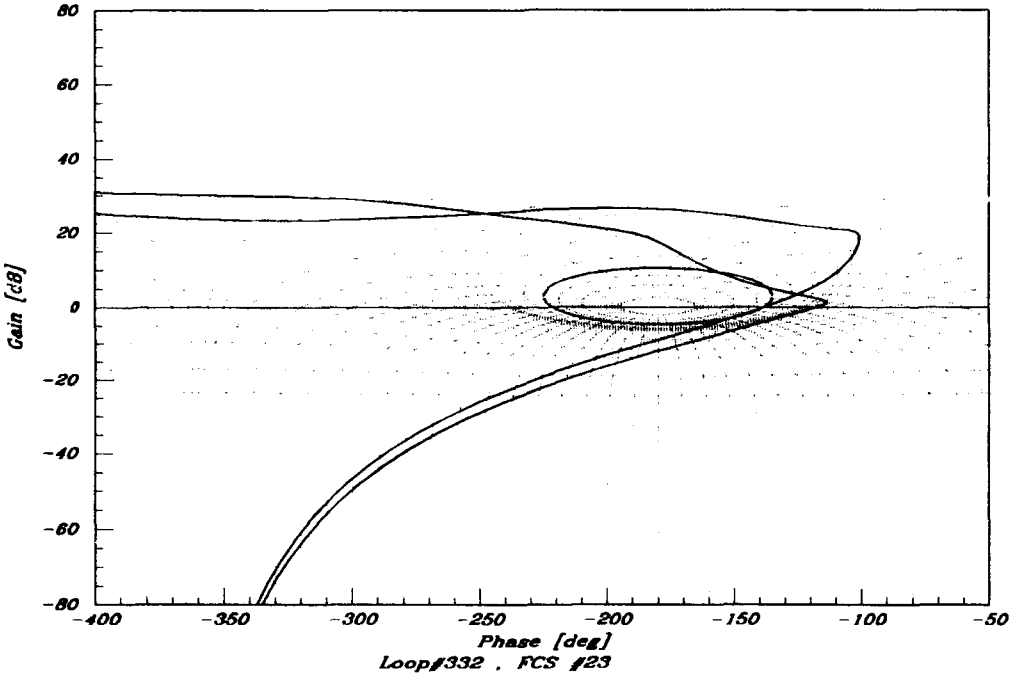

Figure 7.8. FCS#23 $[\mathcal{L}_{3(2)}]_m$

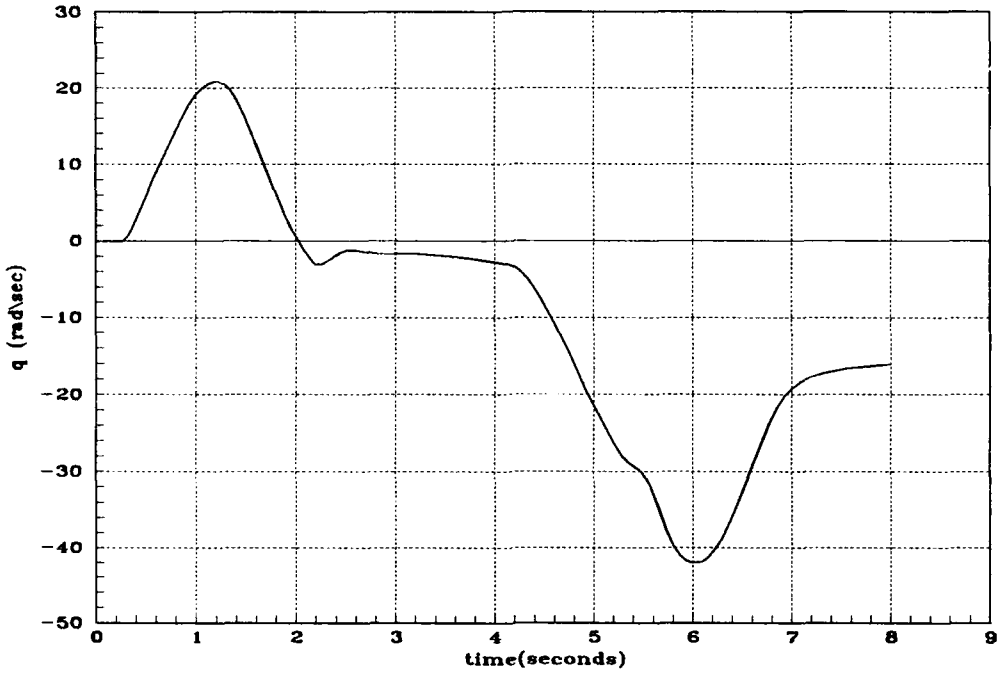

Figure 7.9. Nonlinear Simulation Showing Unwanted Acceleration

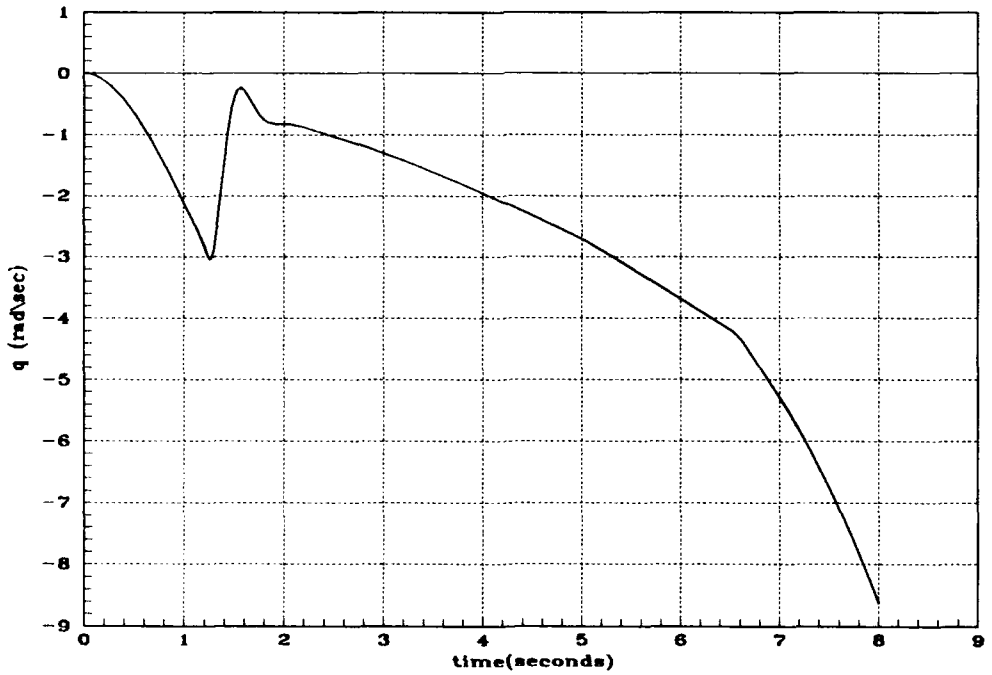

Figure 7.10. Nonlinear Simulation Showing Unwanted Acceleration with No Input

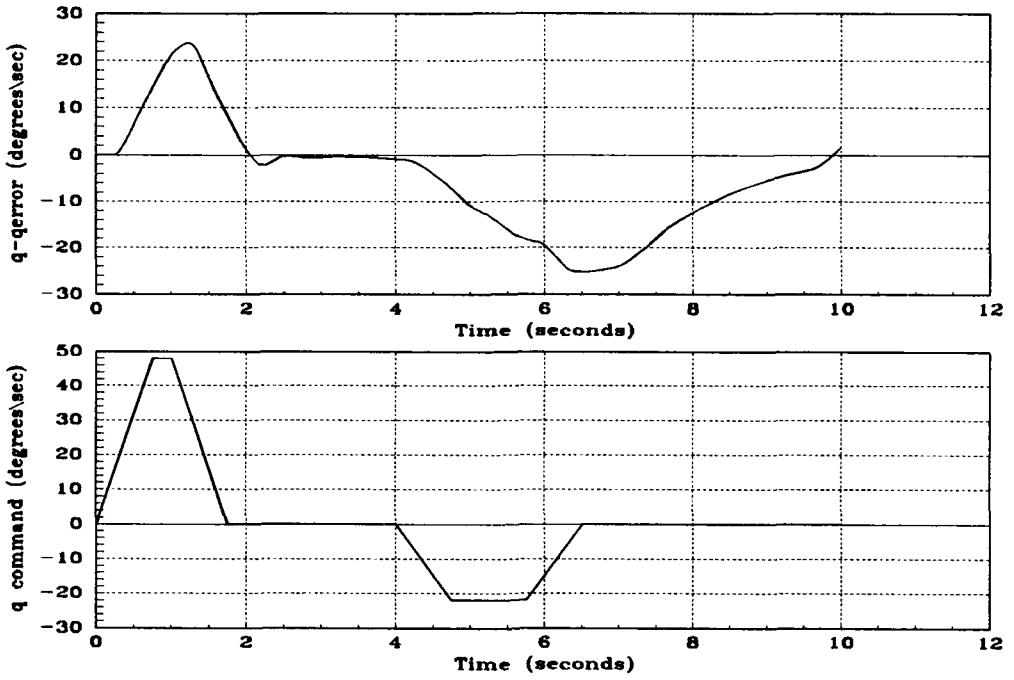

Figure 7.11. Nonlinear Simulation Showing Unwanted Acceleration with No Input

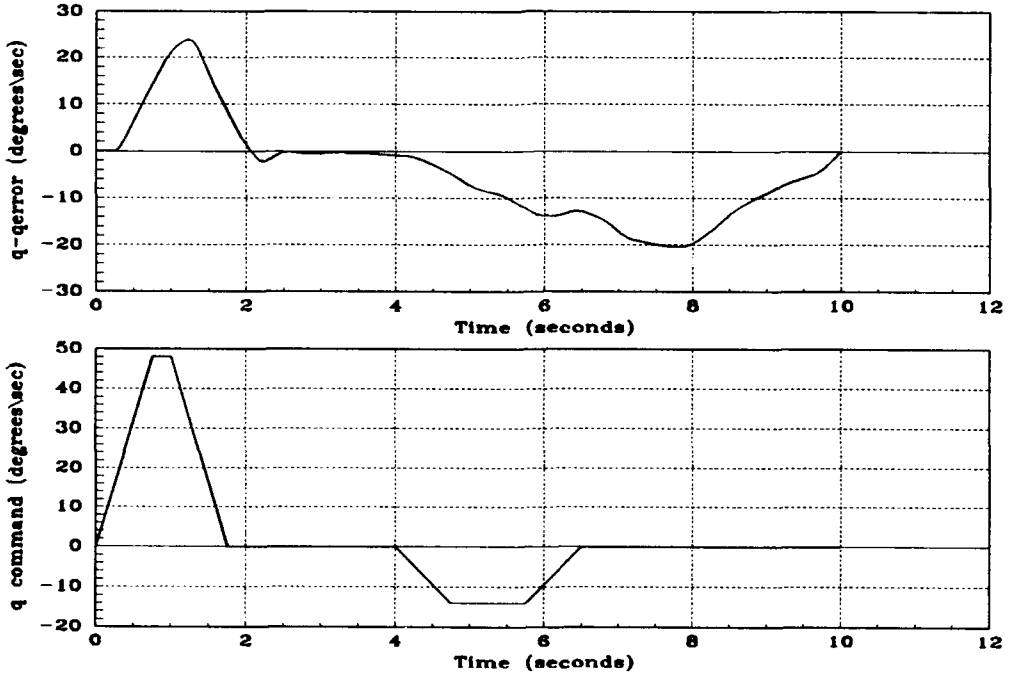

Figure 7.12. Nonlinear Simulation Showing Corrected Pitch-up/Pitch-down

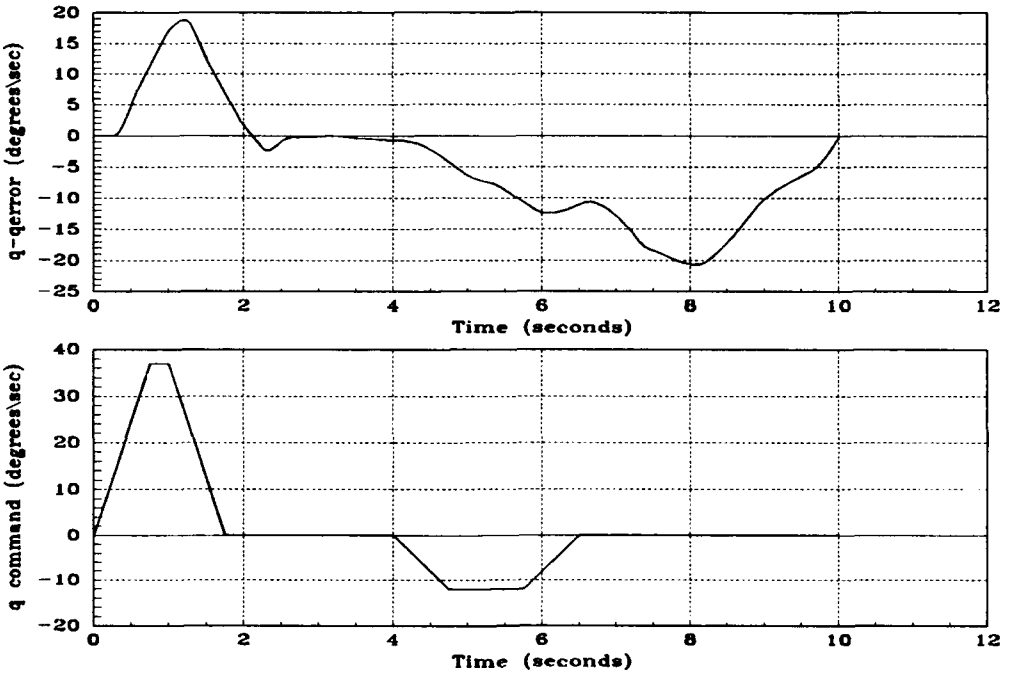

Figure 7.13. Nonlinear Simulation Showing Corrected Pitch-up/Pitch-down

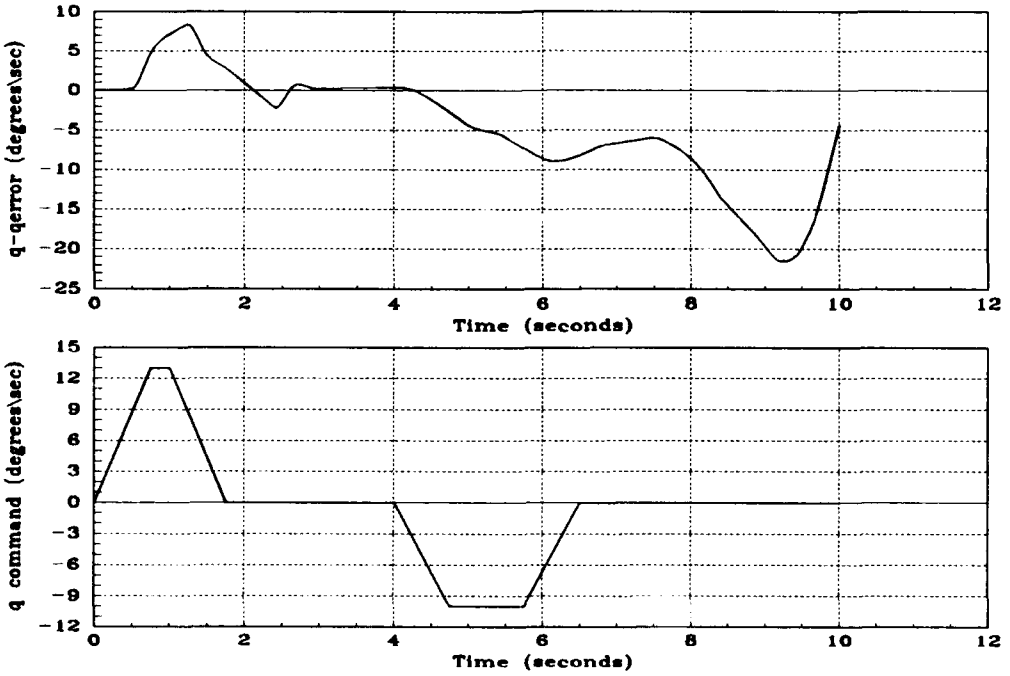

Figure 7.14. Nonlinear Simulation Showing Corrected Pitch-up/Pitch-down

7.4 Conclusion

This chapter describes the nonlinear simulations of the designed FCS. First the reasons for and the methods for G_{ij} order reduction are outlined. Then, the problem with modeling encountered during the nonlinear simulation of the manuevers is described.

VIII. Conclusion

8.1 Discussion

The purpose of this thesis is to advance the state of the art of FCS design by applying nonlinear QFT to the design of a FCS to control maneuvers of an agile aircraft. To do this, maneuvers are chosen that represent maneuvers that are desirable in within visual range combat. There are two maneuvers specified, a pitch-up/pitch-down maneuver and a pitch-up/velocity vector roll maneuver. By using a full six-degrees-of-freedom nonlinear YF-16 simulation, specifications for the maneuvers are developed. Once the specifications are developed, a set of maneuver simulations are flown that consists of enough members to adequately represent the specifications. Plant transfer functions are developed through the use of system identification, using the input/output time histories of the maneuvers. During the system identification process, the $q_{ij(0)}$ are found directly and are constrained to be minimum-phase. After identifying the plants, the cascaded MIMO QFT technique is used to design the FCS. Stability boundaries are generated through the use of a Matrix_x program. Because of limited algorithm robustness, it is found that many of the resulting models developed, have relatively high order. When the effective plants are first calculated, they contain RHP poles that make it impossible to achieve a viable design. To prevent the formation of these RHP poles, Γ-boundaries are developed. When the loops are reshaped using the Γ-boundries, many of the extra RHP poles disappear. Before shaping the loops it is found that FCS scheduling is needed because of large uncertainty in the magnitude and phase of the plants. During loop shaping it becomes evident that the design will not met the specified ω_ϕ because of multiple large RHP poles in the effective plants. Once all of the loops are shaped, prefilters are designed using a modified method that involves plotting all of the frequency response of the CLTF and comparing them with the desired frequency response model. The time response specifications are based on the military specifi-

cation, 'Flying Qualities of Piloted Aircraft', MIL-STD-1797A [17]. Because order of the designed FCS is too large for the YF-16 simulation program, an approximate FCS is developed through the use of straight line approximations on the Bode plot. After implementing the reduced order FCSs in the nonlinear simulation program, problems in the modeling process are encountered that prevent the simulation of the FCSs.

8.2 Conclusions

Maxlike The system identification algorithm, Maxlike, in Matrix_x is very useful for the problems encountered in nonlinear QFT. Because the model is defined by the user, maxlike is flexible enough to give transfer function plants directly, that are required for the nonlinear QFT design. For instance the inverse of the plant matrix is identified directly in this thesis.

Minimum-Phase Plants Using Maxlike, plants that appear to be NMP can be modeled as MP. The validity of the model is determined by the application and subsequent simulations. If the resulting MP transfer functions produce acceptable fits to the data then they can be used in the nonlinear QFT process.

Stability Boundaries Computer generated stability boundaries are very useful during the QFT design process. Using computer generated stability boundaries, the process of plotting and cutting out templates is avoided. By letting Matrix_x generate these boundaries, one can shape the loops on a Nichols chart with the boundaries superimposed. Care must be taken, when using these boundaries, to identify the actual boundaries of plant with large phase uncertainty.

Γ-Boundaries Boundaries can be developed that reduce the development of RHP in effective plants. As described in Chapter 4, many effective plants are developed that contain large RHP poles. Many of these poles are prevented by redsigning the controllers using Γ-boundaries.

Matrix$_x$ There is a limit to the robustness of the transfer function algorithms in Matrix$_x$. In Chapter 4 an experiment is described that shows that Matrix$_x$ algorithms are not robust enough to accommodate the manipulation of higher order transfer function.

Model All inputs to the system under consideration must be accounted for. In this case a step input of thrust was not properly modeled which caused an unwanted ramp in the output.

8.3 Recommendations

1. System identification methods tailored to QFT MIMO design need to be organised and/or developed. This is a big research area in which there is much in the literature. There are many CAD packages that contain system identification algorithms, two available at AFIT are Matrix$_x$ and Pro-Matlab [16] [15]. System Identification is one area of nonlinear QFT that needs to be developed. If system identification methods can be tailored to nonlinear QFT MIMO design, then the time required for a design can be shortened considerably.

2. The possibility, that plants, that are previously identified as NMP, be modeled with a system identification method that can constrain the model to be MP, should be investigated. In some cases a plant modeled as NMP may be adequately modeled as MP. This can be accomplished by using system identification with the constriant that the identified plants be MP. If the results of the system identification justify it, the plants can be modeled as MP.

3. A nonlinear QFT CAD package is needed that can overcome limitations that present packages have. A package such as Matrix$_x$ can be the core of a nonlinear QFT CAD package if robust algorithms can be developed that will accommodate high order transfer functions.

4. The application of nonlinear QFT to specific maneuvers seems to be an attractive method of FCS design because of the ability to rigorously model a

nonlinear plant. Another attraction of this method is the method of collecting data to form the model. The data can be collected from actual flight data

5. Thrust vectoring is a significant control in operating aircraft at high angle of attack. Research should be done that defines the boundaries an F-16 can operate in using thrust vectoring.

Appendix A. **Example Maneuvers**

This appendix contains four examples of the input/output time histories used to develop the maneuvers.

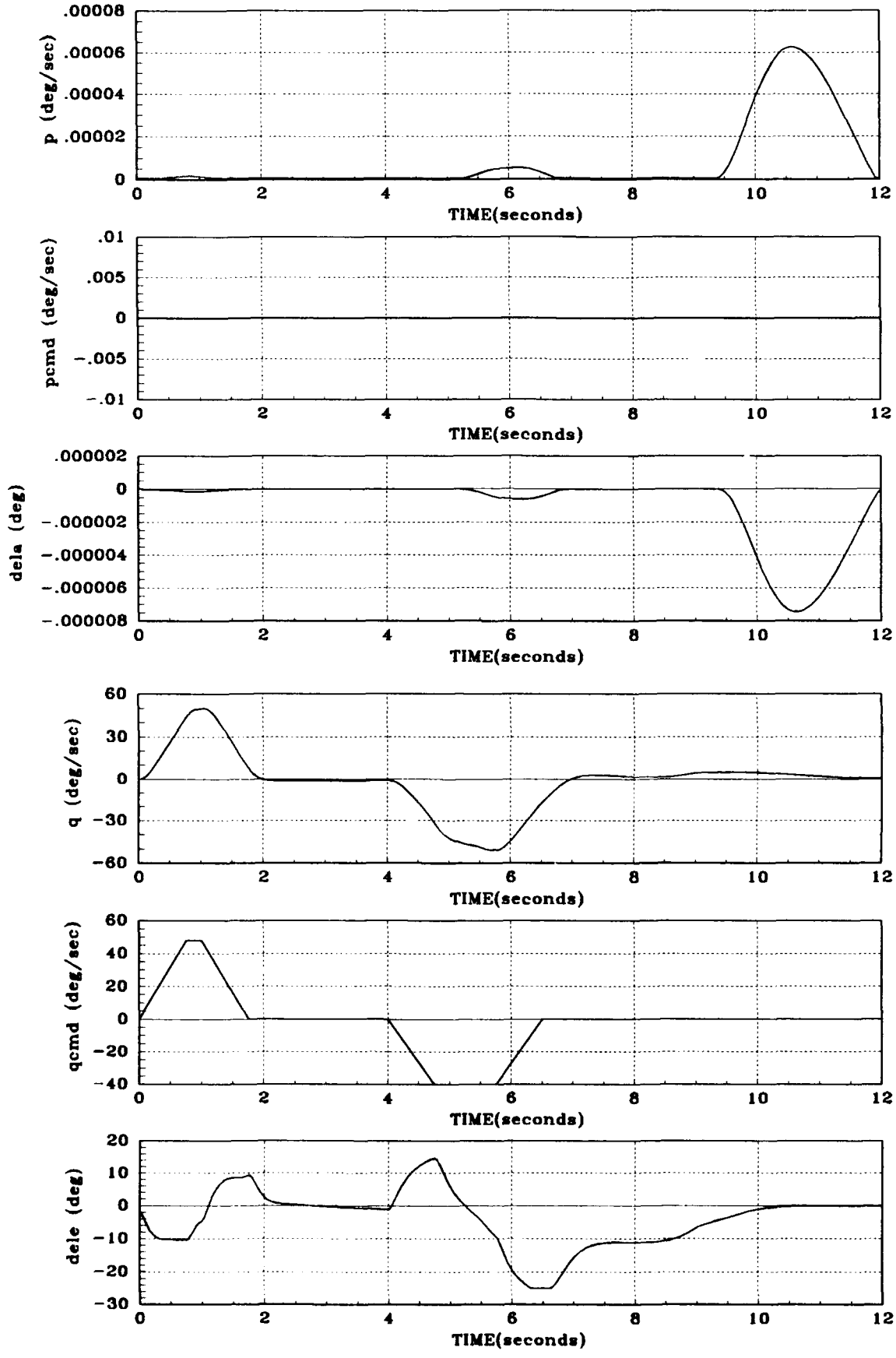

Figure A.1. Example Maneuver #111

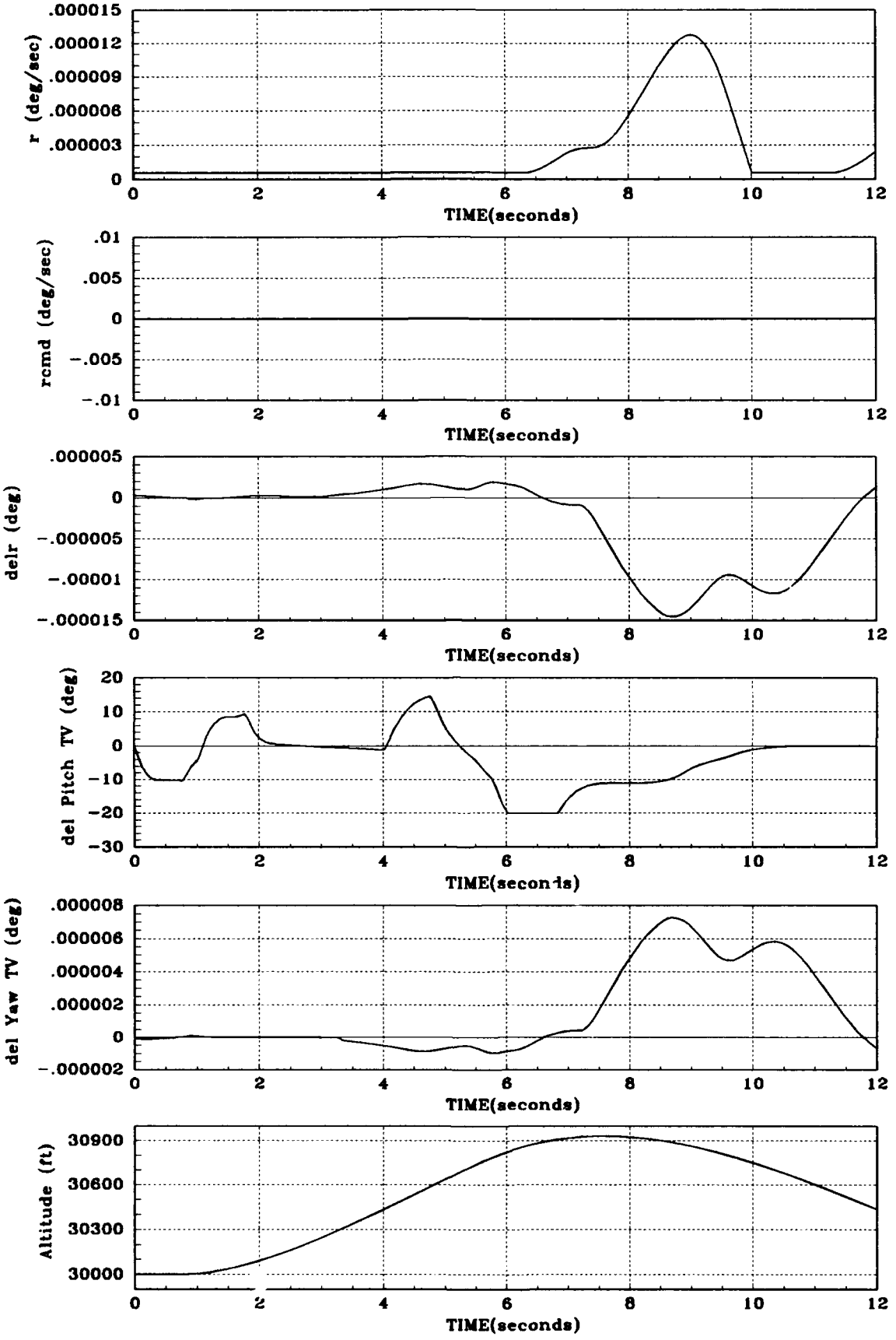

Figure A.2. Example Maneuver #111, cont'd

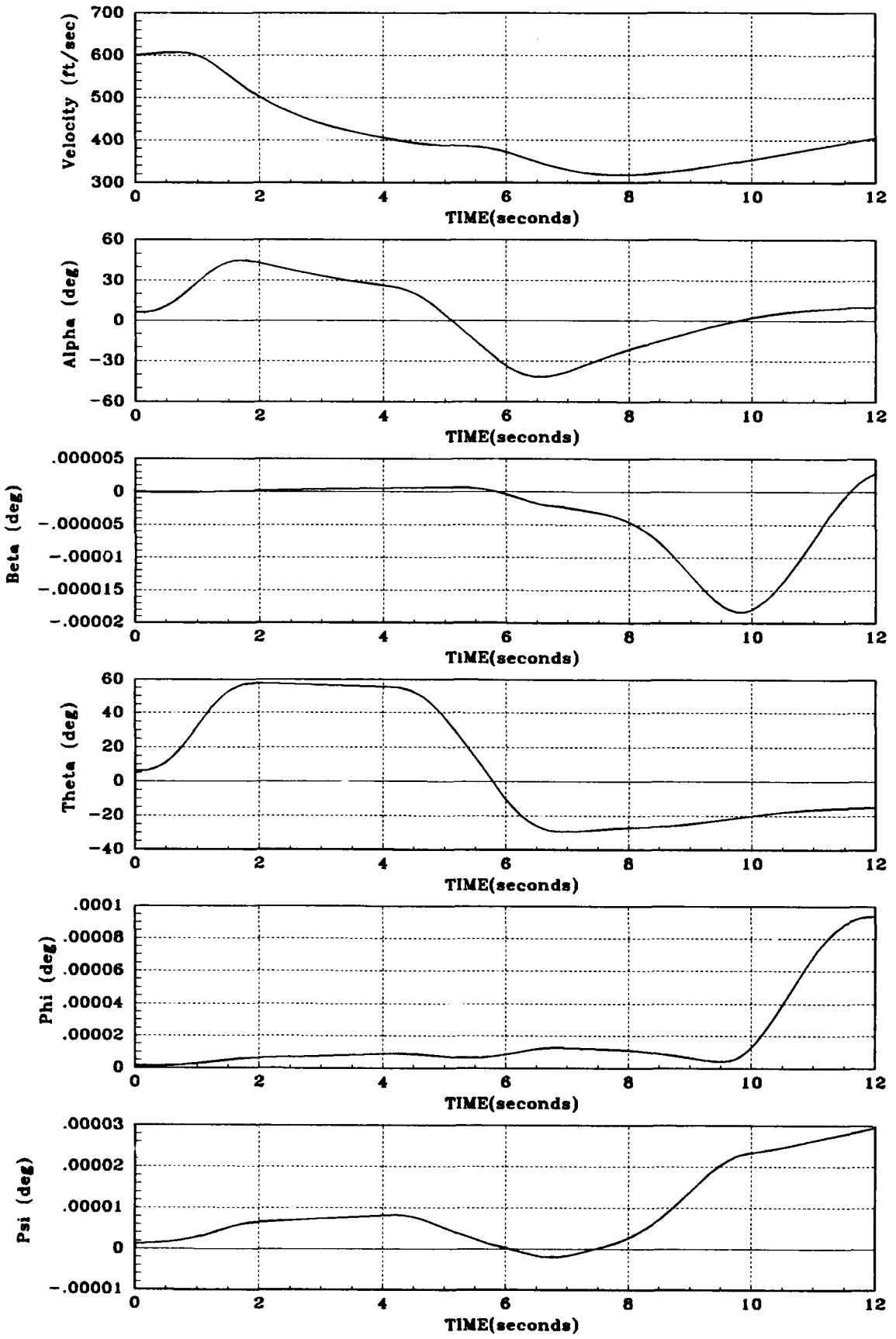

Figure A.3. Example Maneuver #111, cont'd

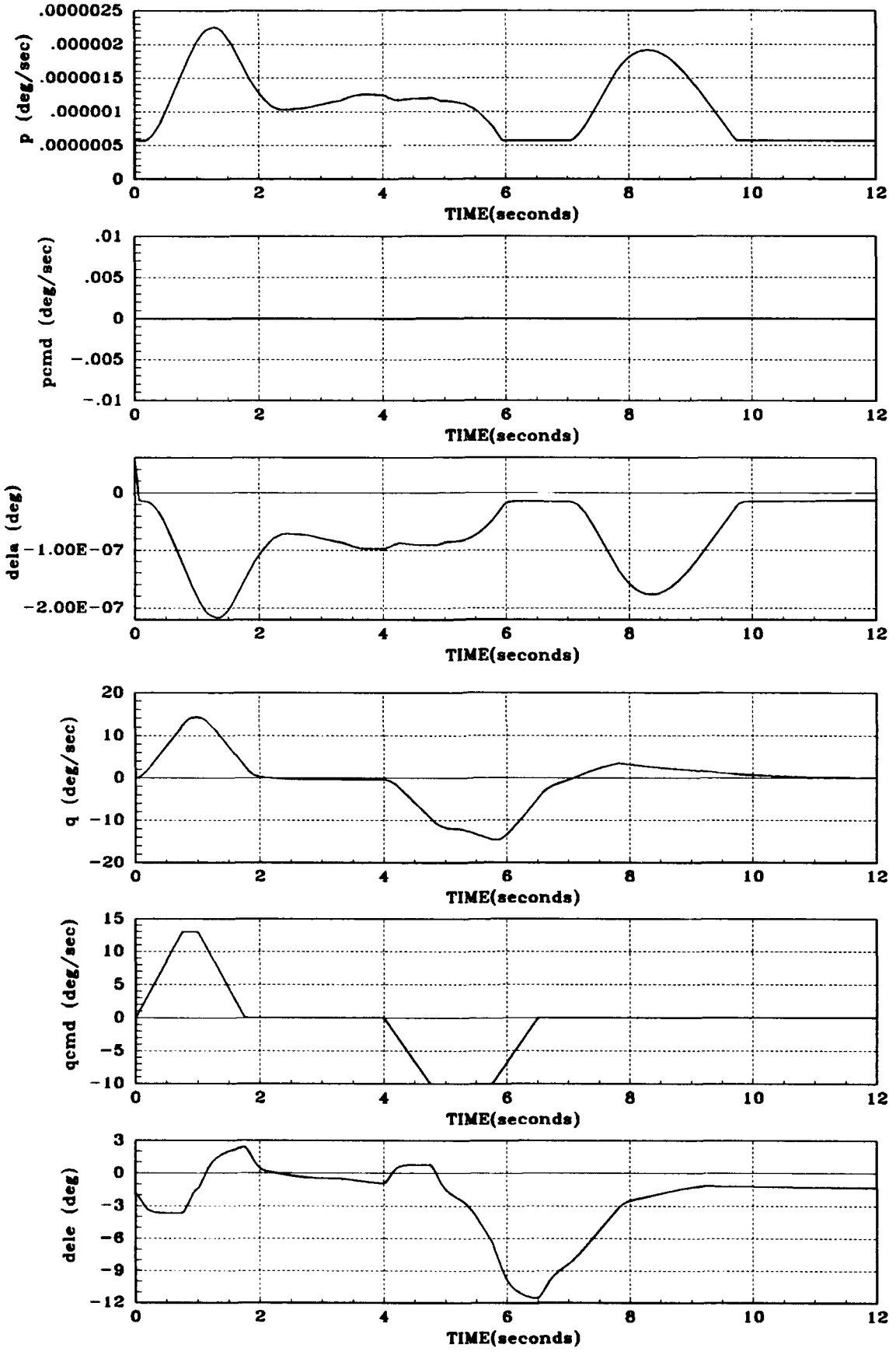

Figure A.4. Example Maneuver #144

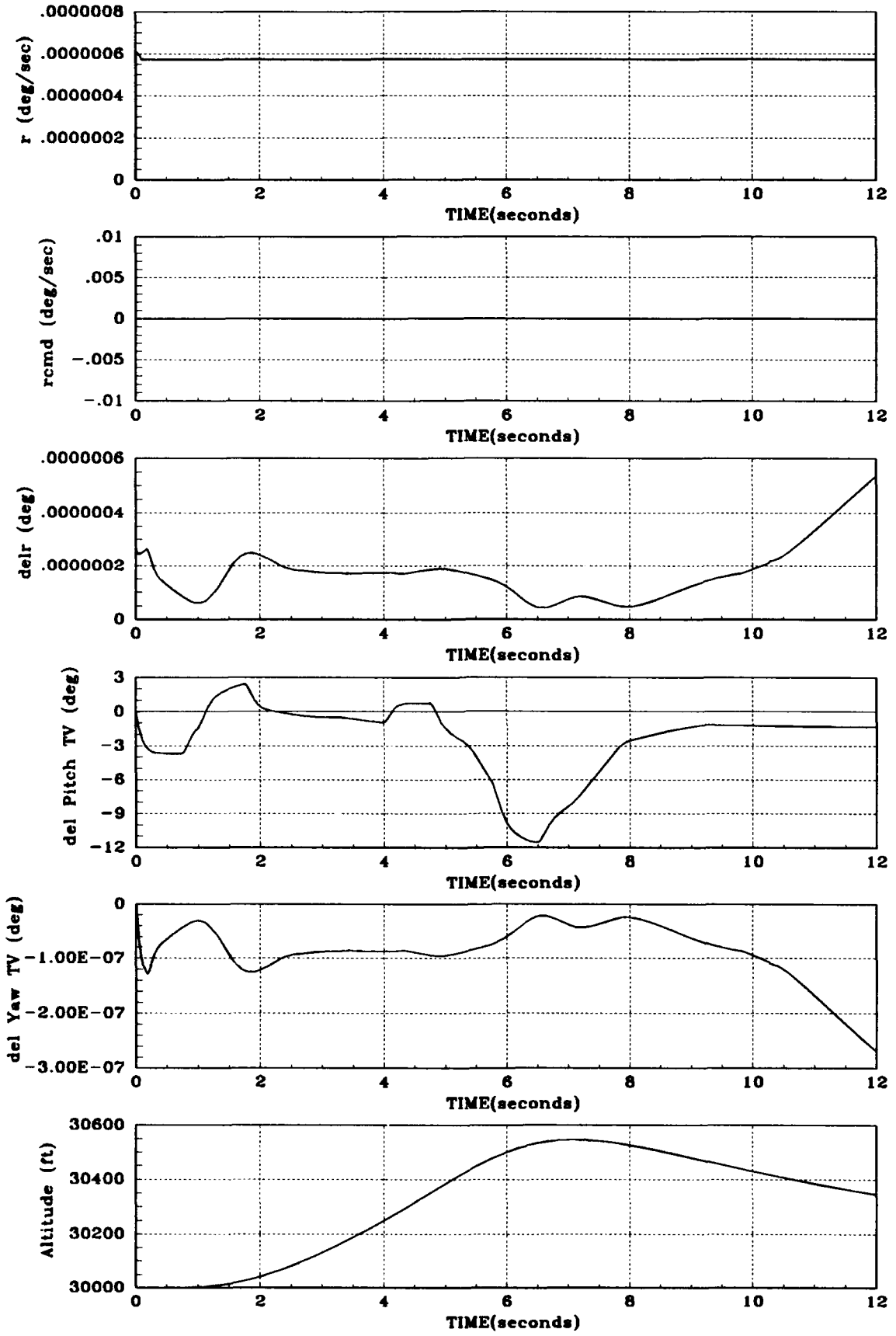

Figure A.5. Example Maneuver #144, cont'd

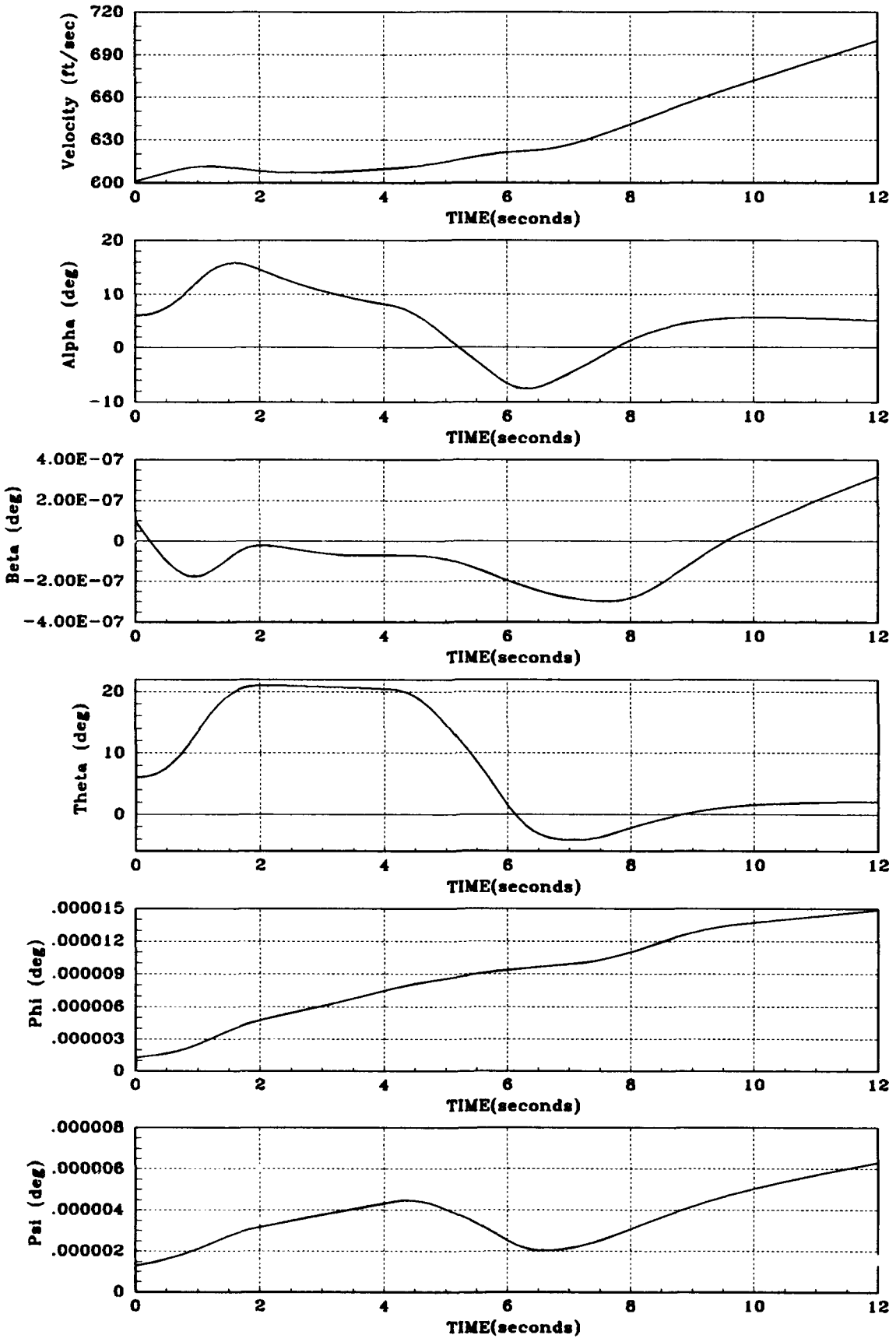

Figure A.6. Example Maneuver #144, cont'd

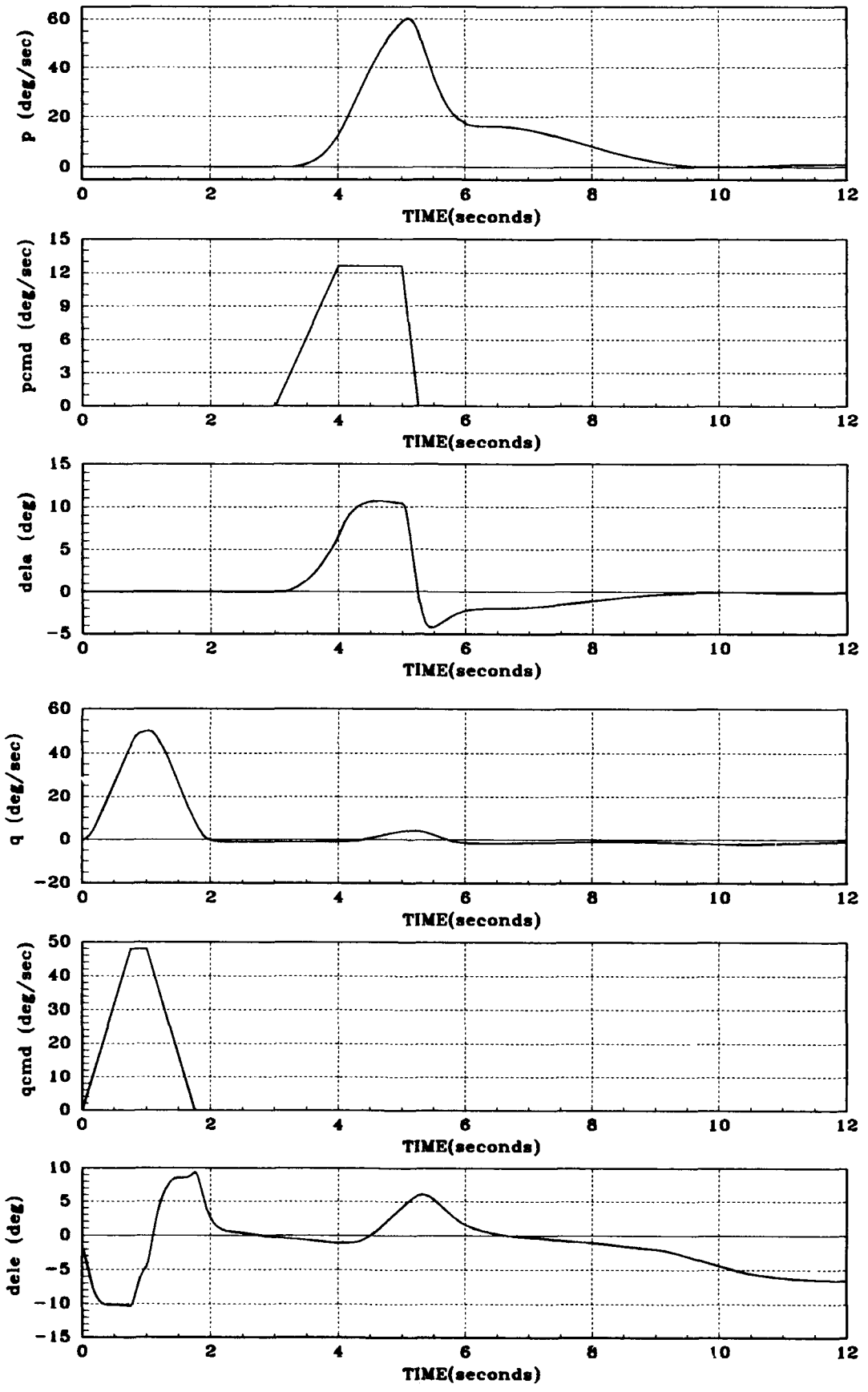

Figure A.7. Example Maneuver #211

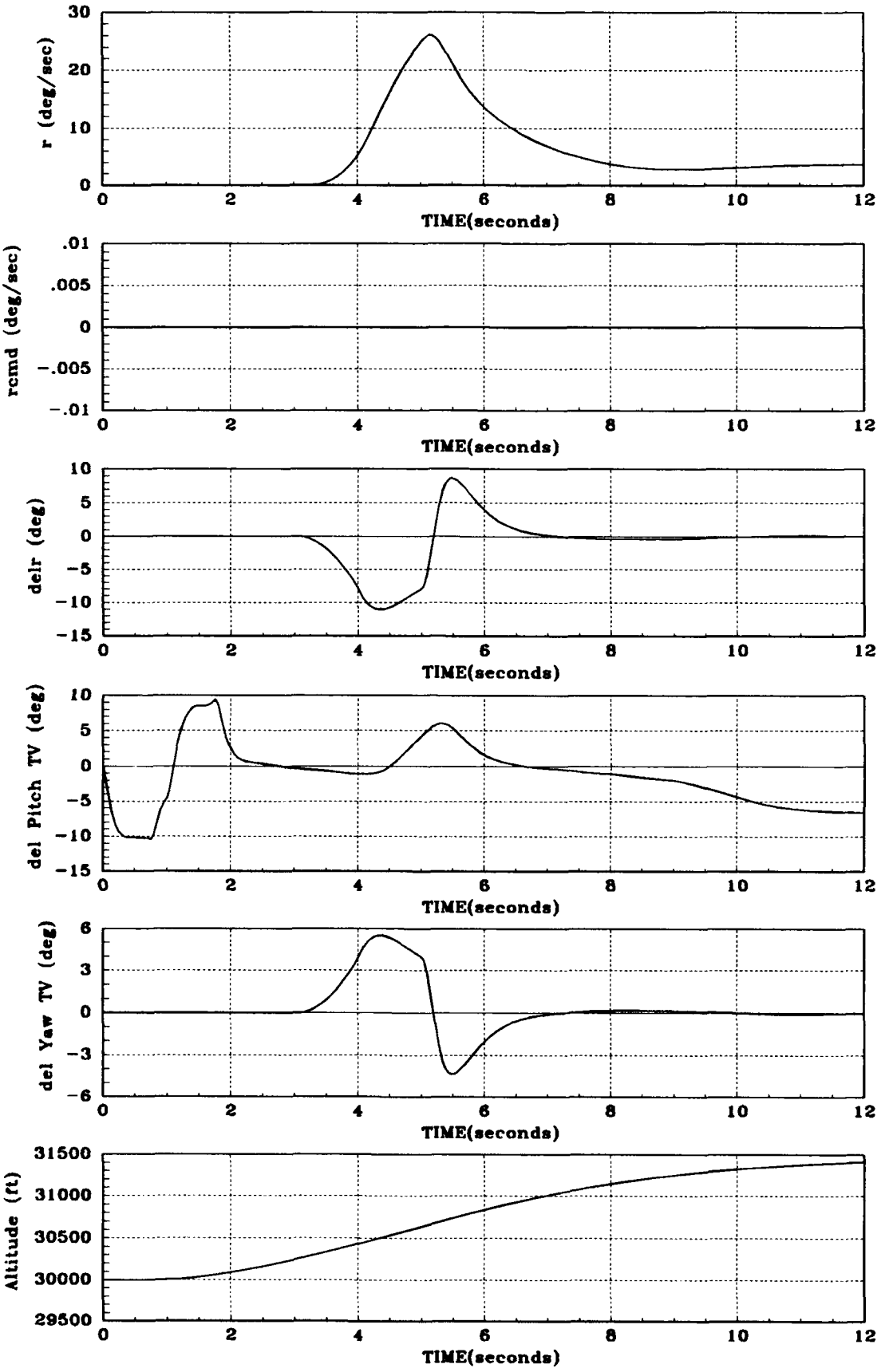

Figure A.8. Example Maneuver #211, cont'd

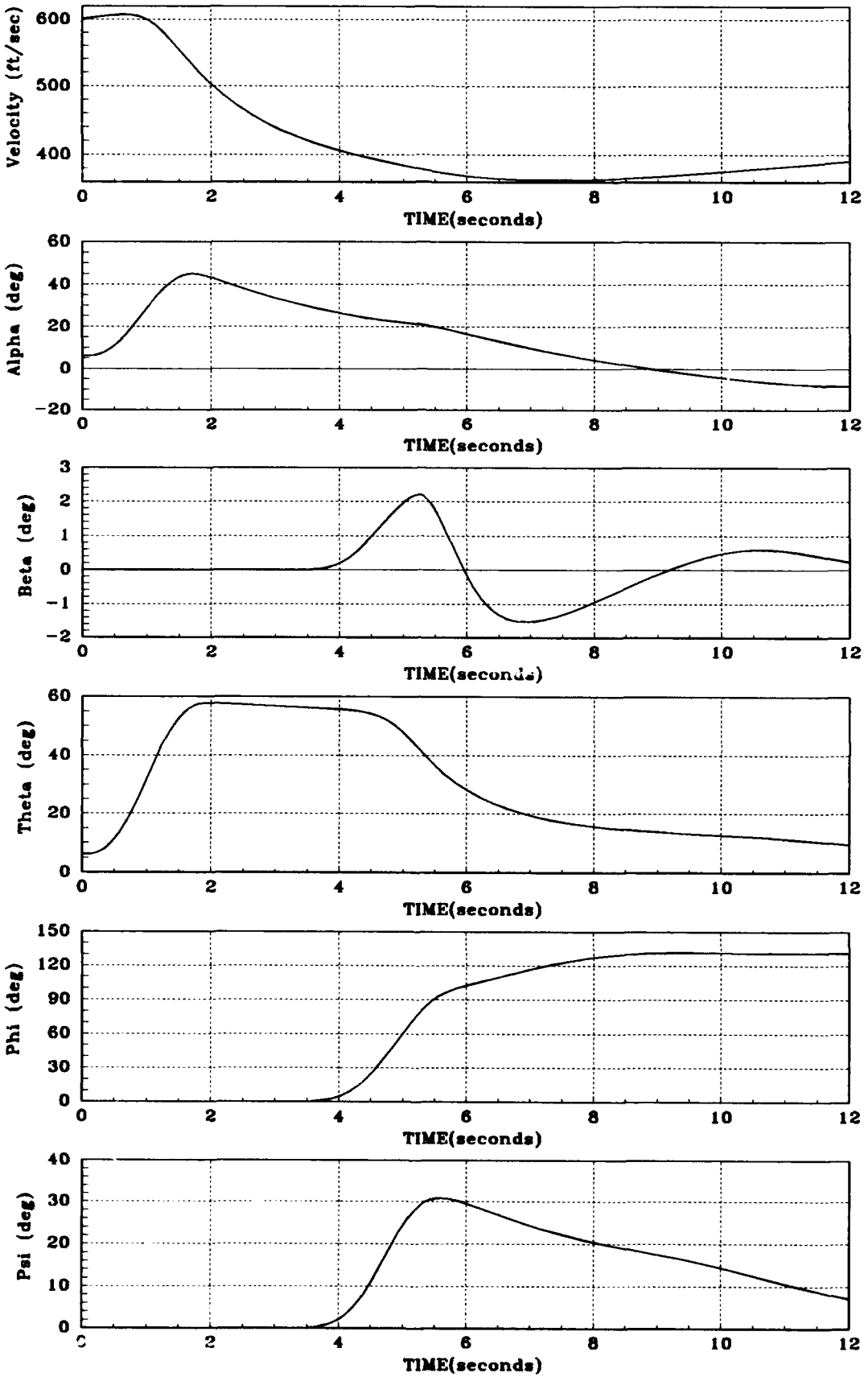

Figure A.9. Example Maneuver #211, cont'd

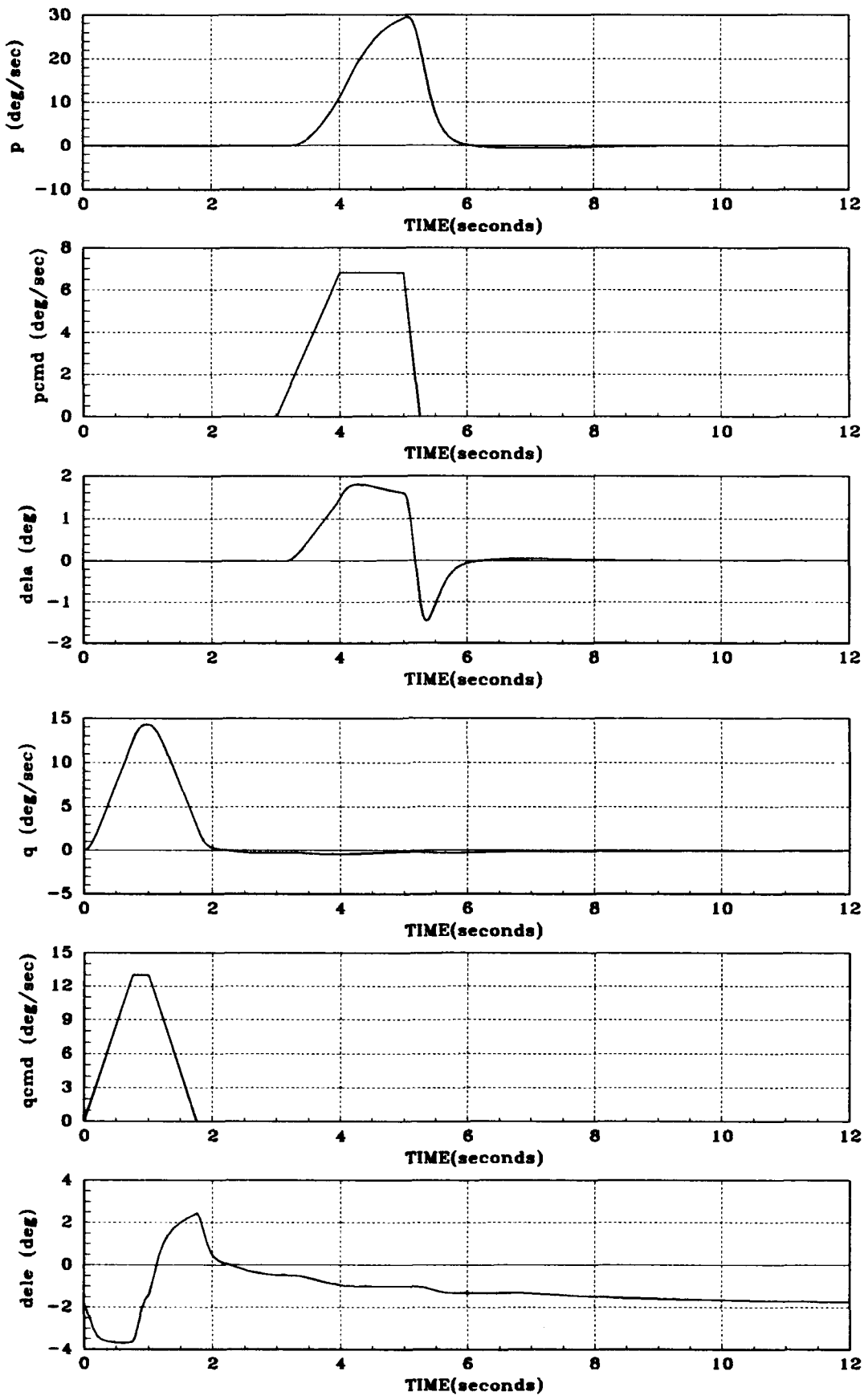

Figure A.10. Example Maneuver #243

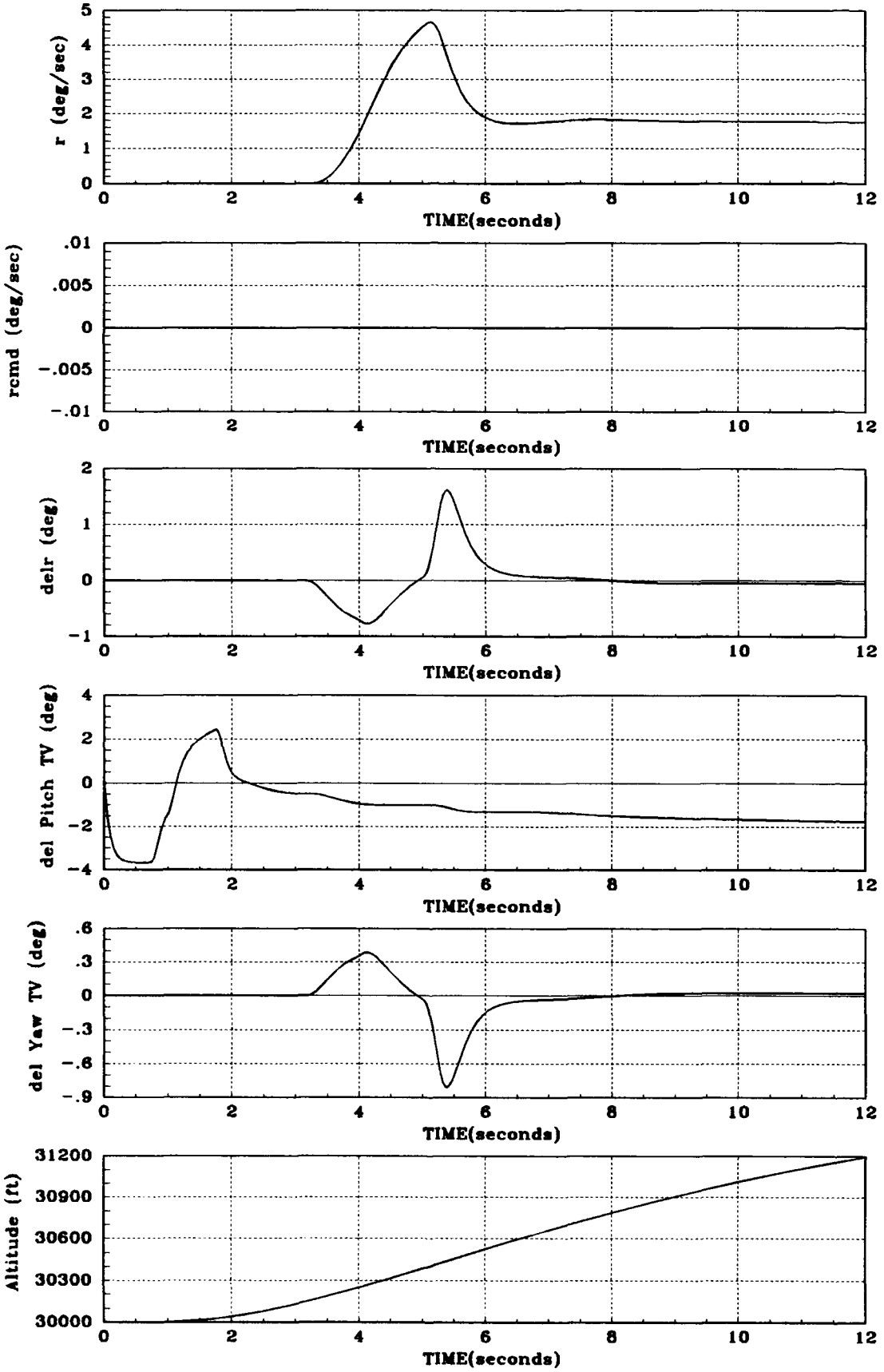

Figure A.11. Example Maneuver #243, cont'd

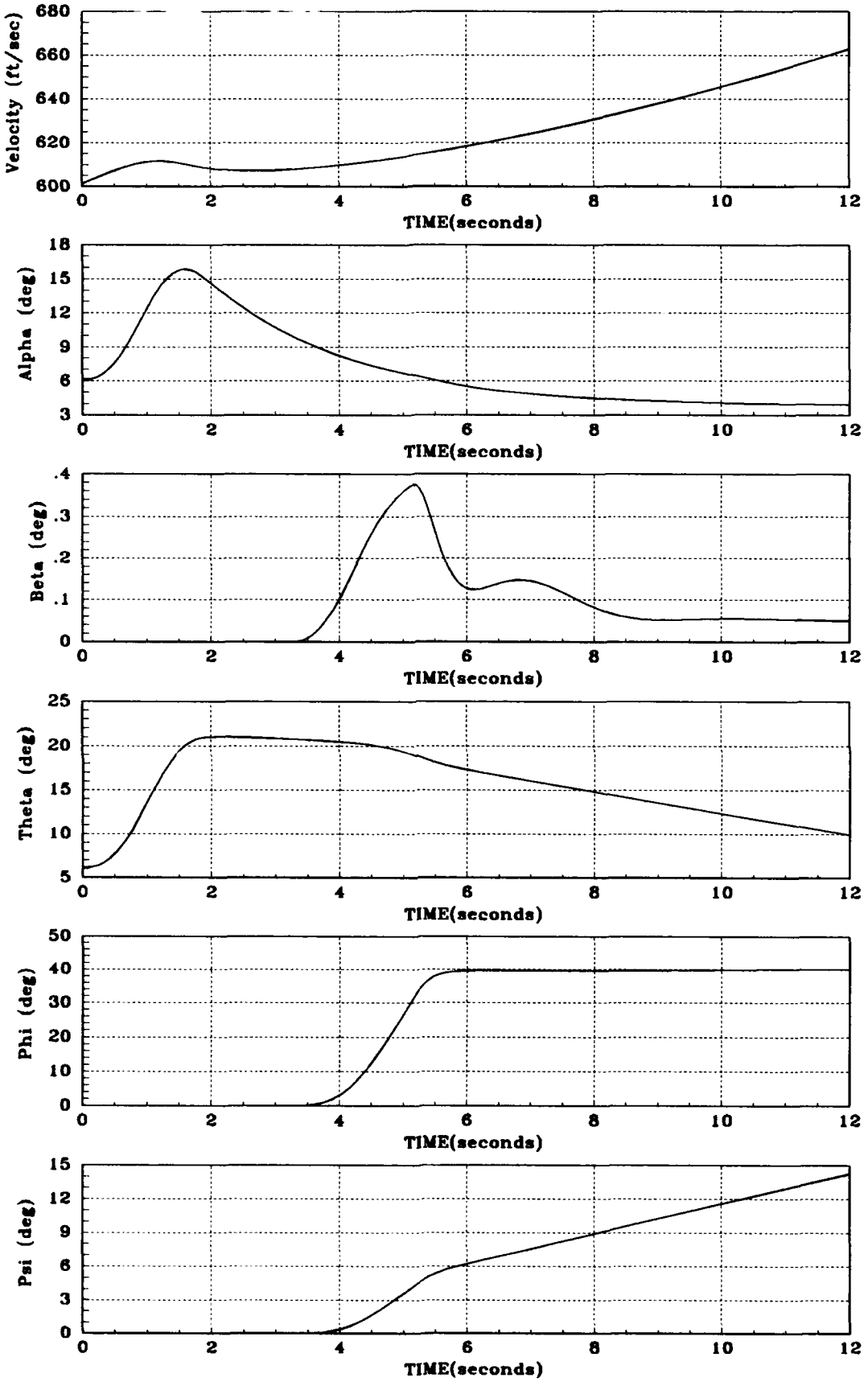

Figure A.12. Example Maneuver #243, cont'd

Appendix B. **System Identification Plots**

This appendix contains plots of all of the system identifications runs where y_{out} is the output, u is the input, and $\hat{u}$ is the input based on the identified transfer function. For these runs, the inverse of the plant, V, is the form of the transfer function to be identified.

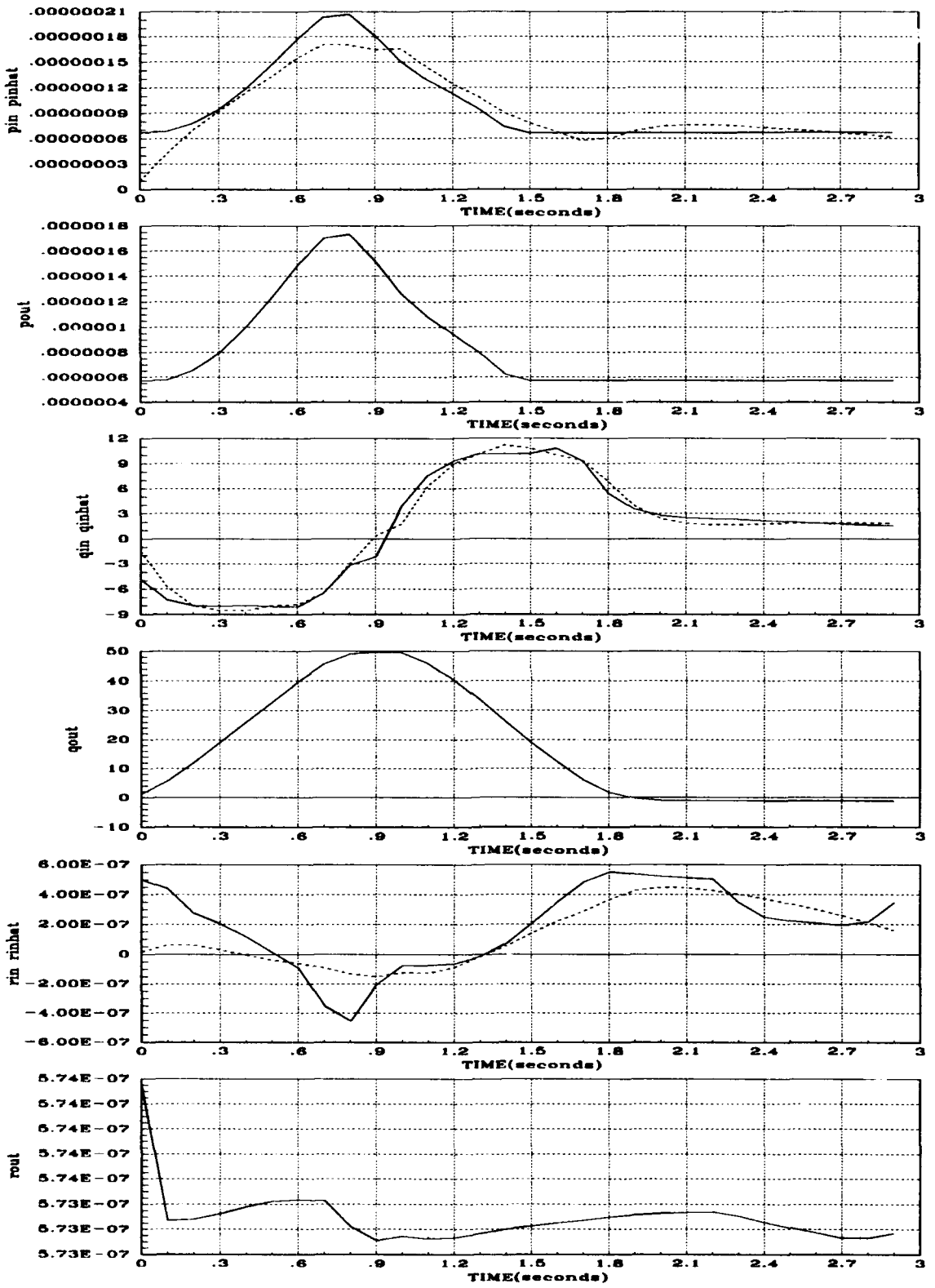

Figure B.1. u, $\hat{u}$, and y_{out} for Plant #1111

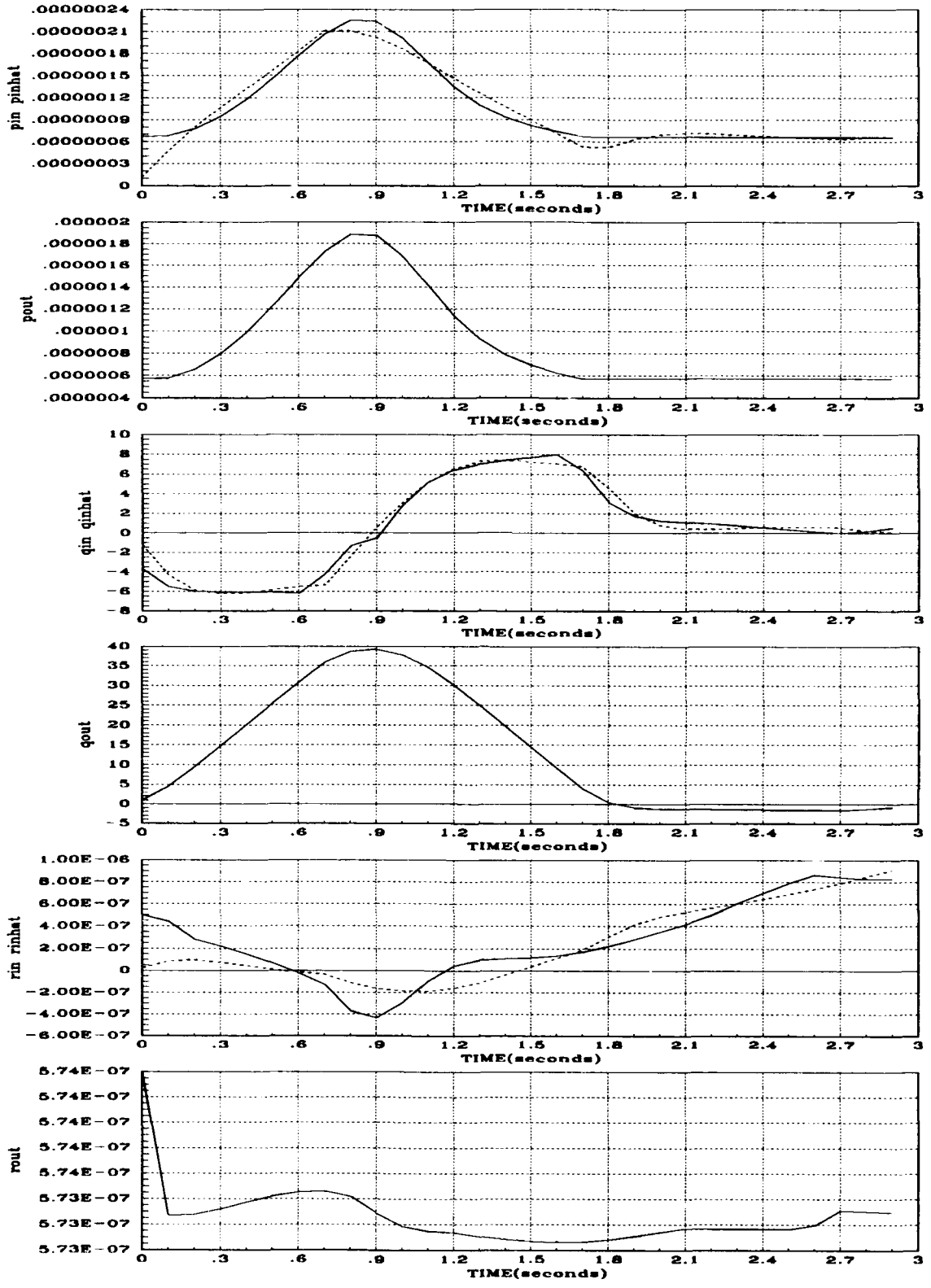

Figure B.2. u, $\hat{u}$, and y_{out} for Plant #1112

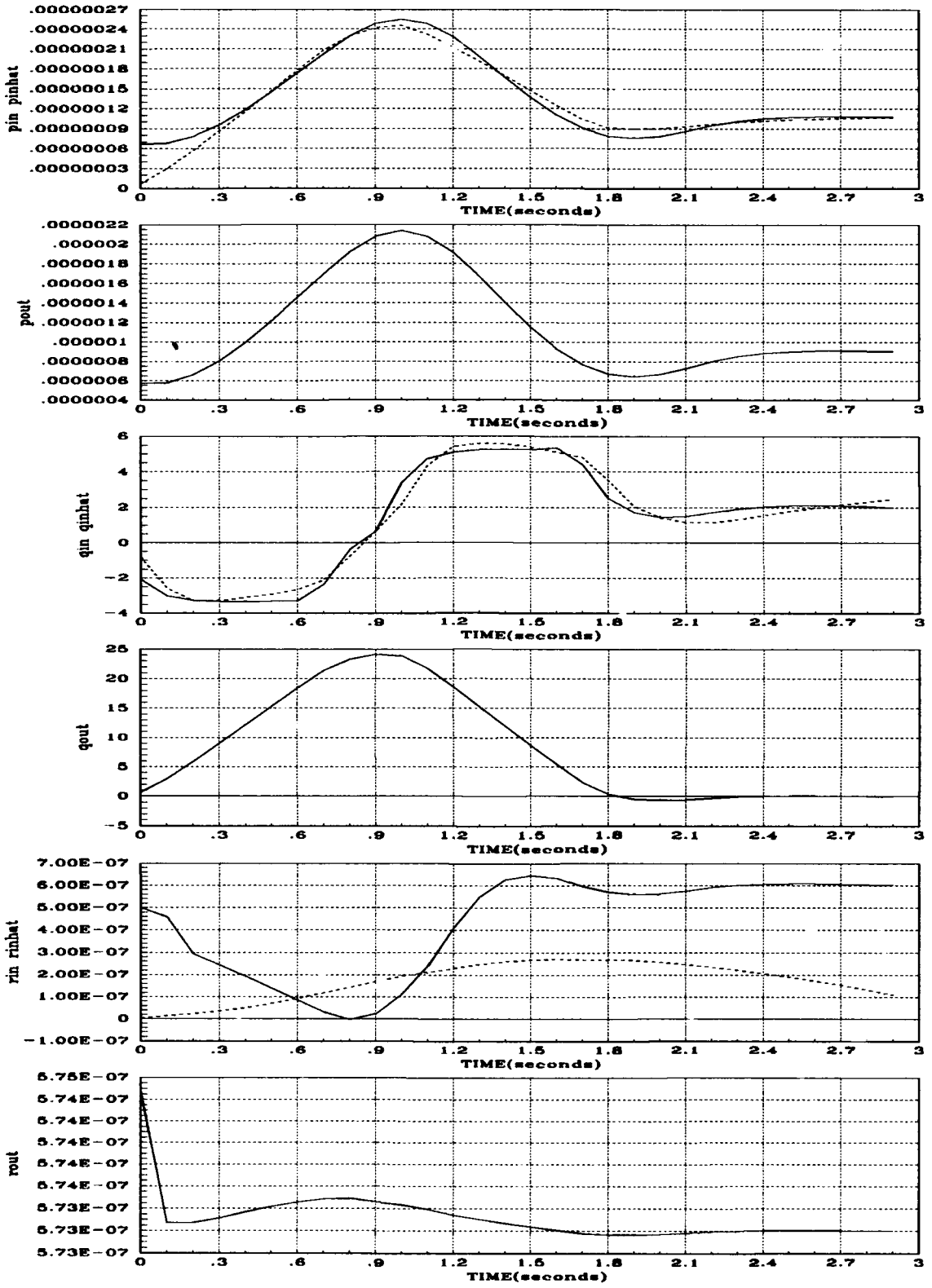

Figure B.3. u, $\hat{u}$, and y_{out} for Plant #1113

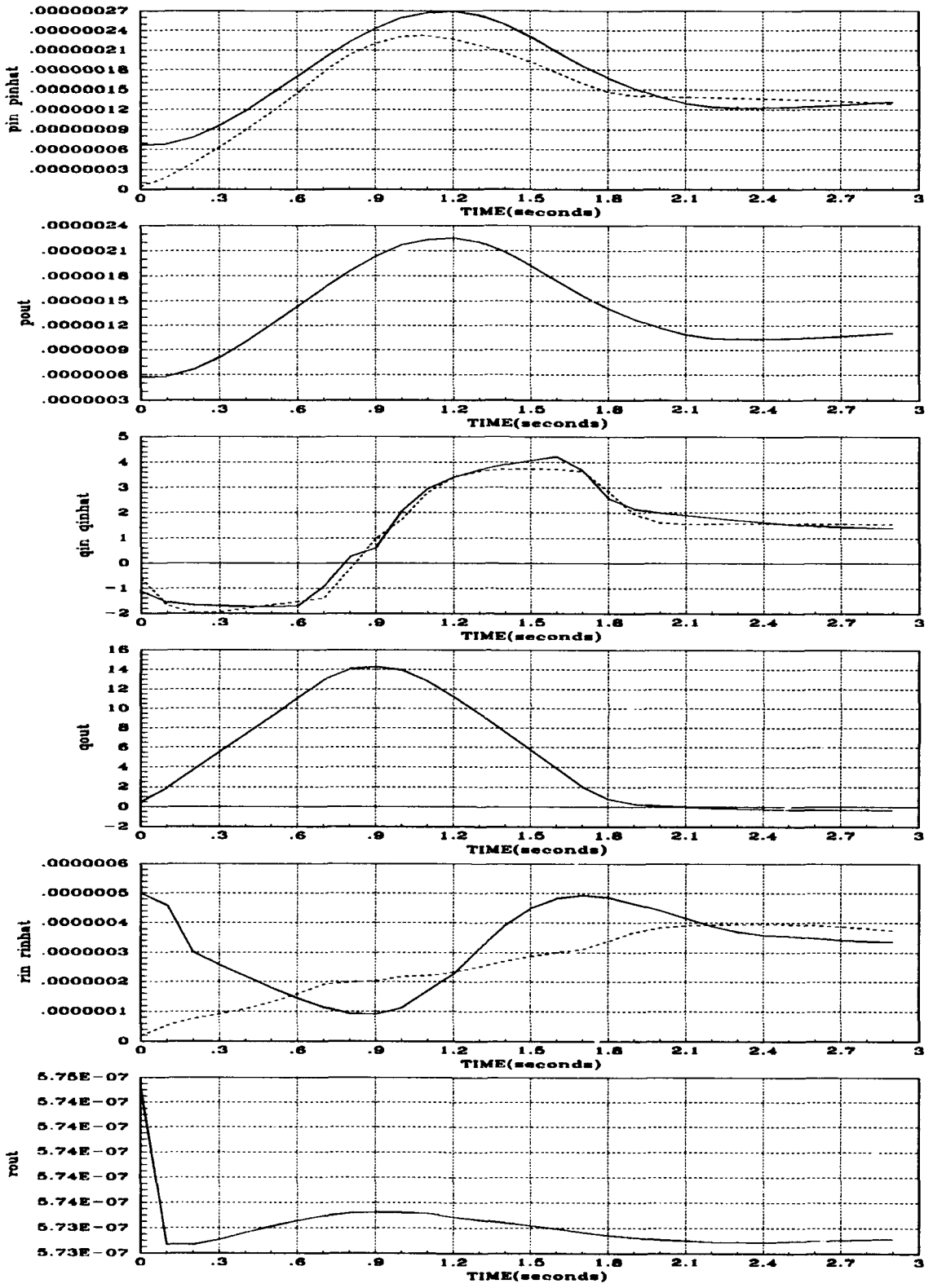

Figure B.4. u, $\hat{u}$, and y_{out} for Plant #1114

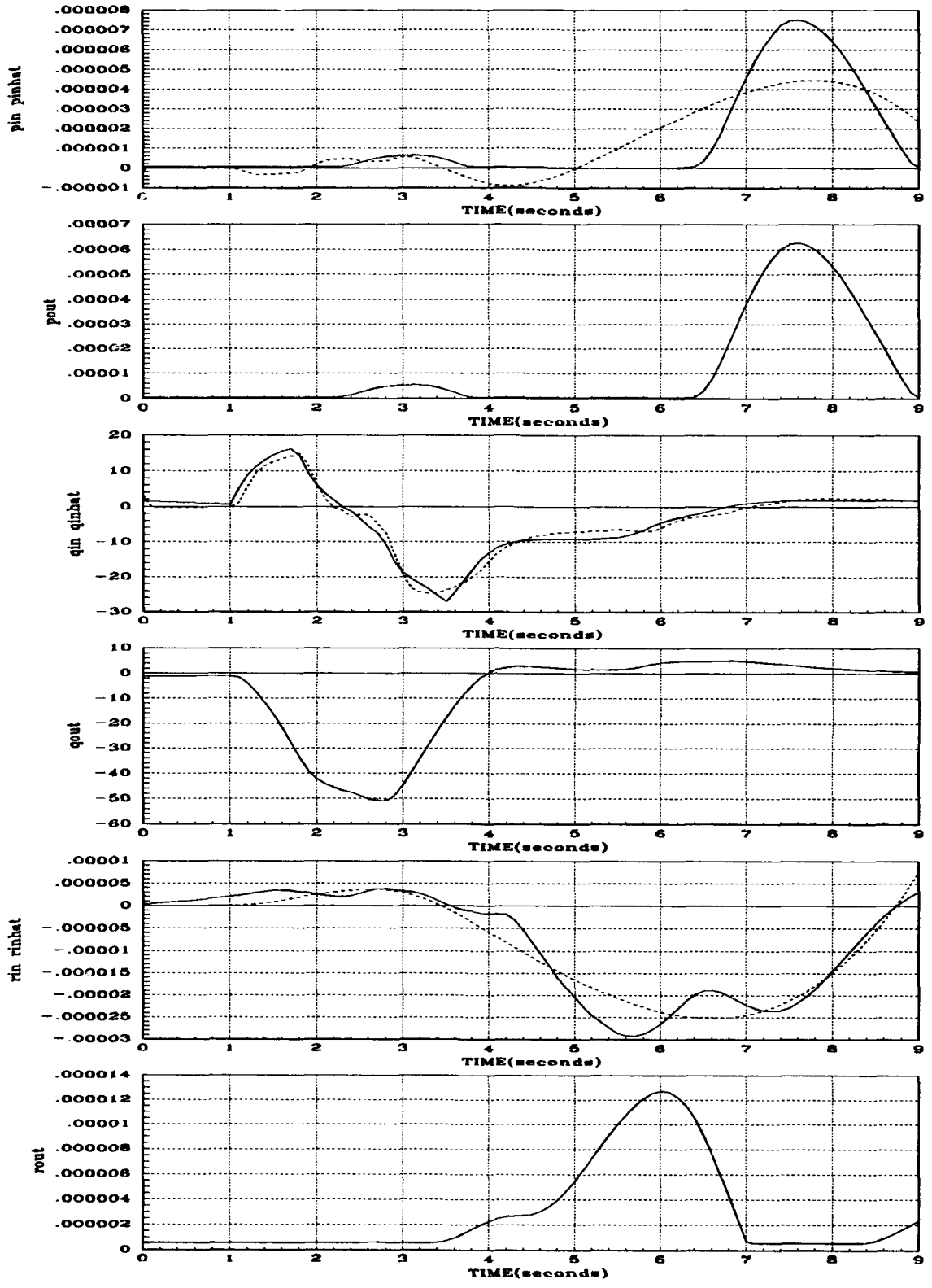

Figure B.5. u, $\hat{u}$, and y_{out} for Plant #2111

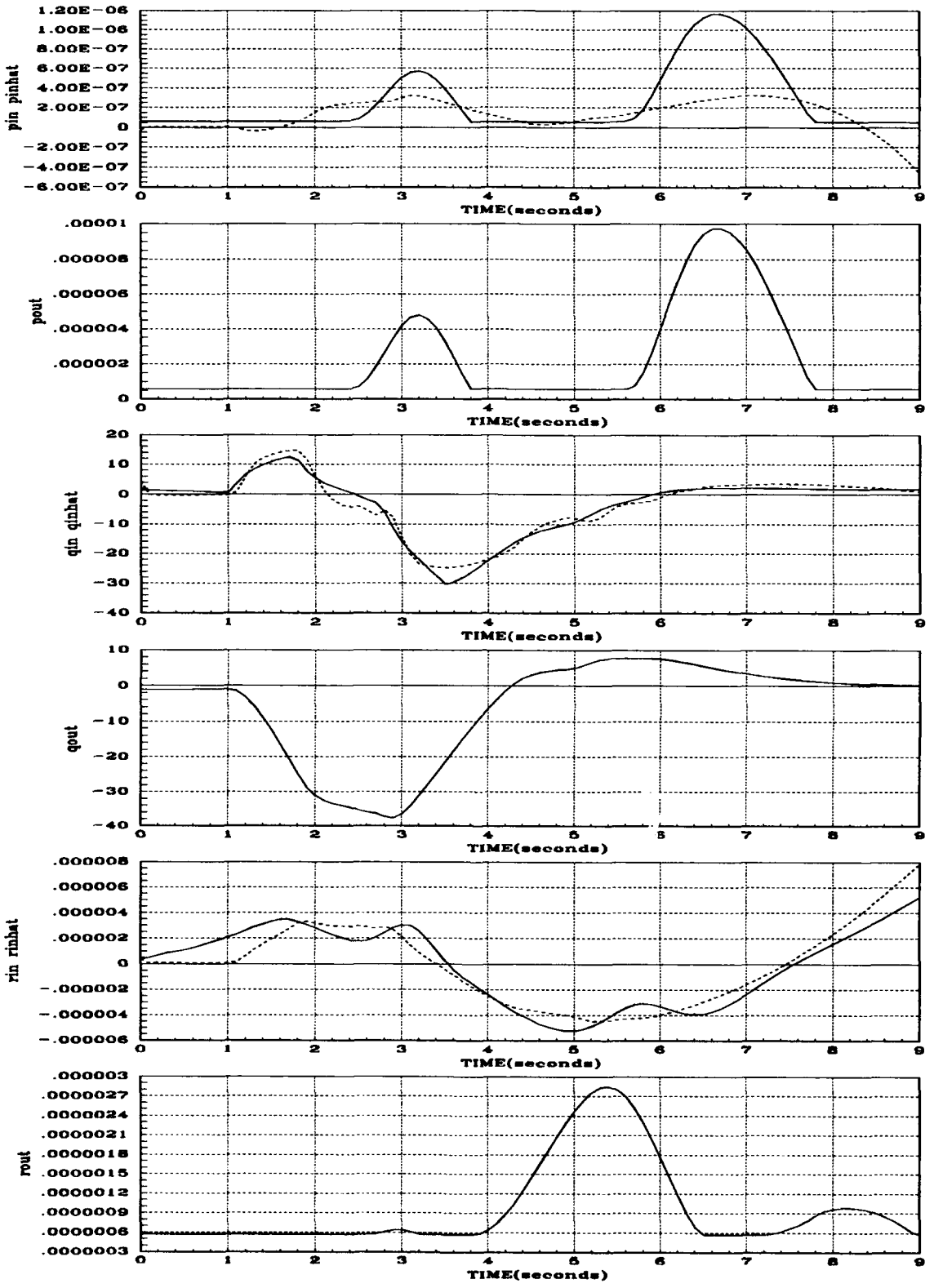

Figure B.6. u, $\hat{u}$, and y_{out} for Plant #2112

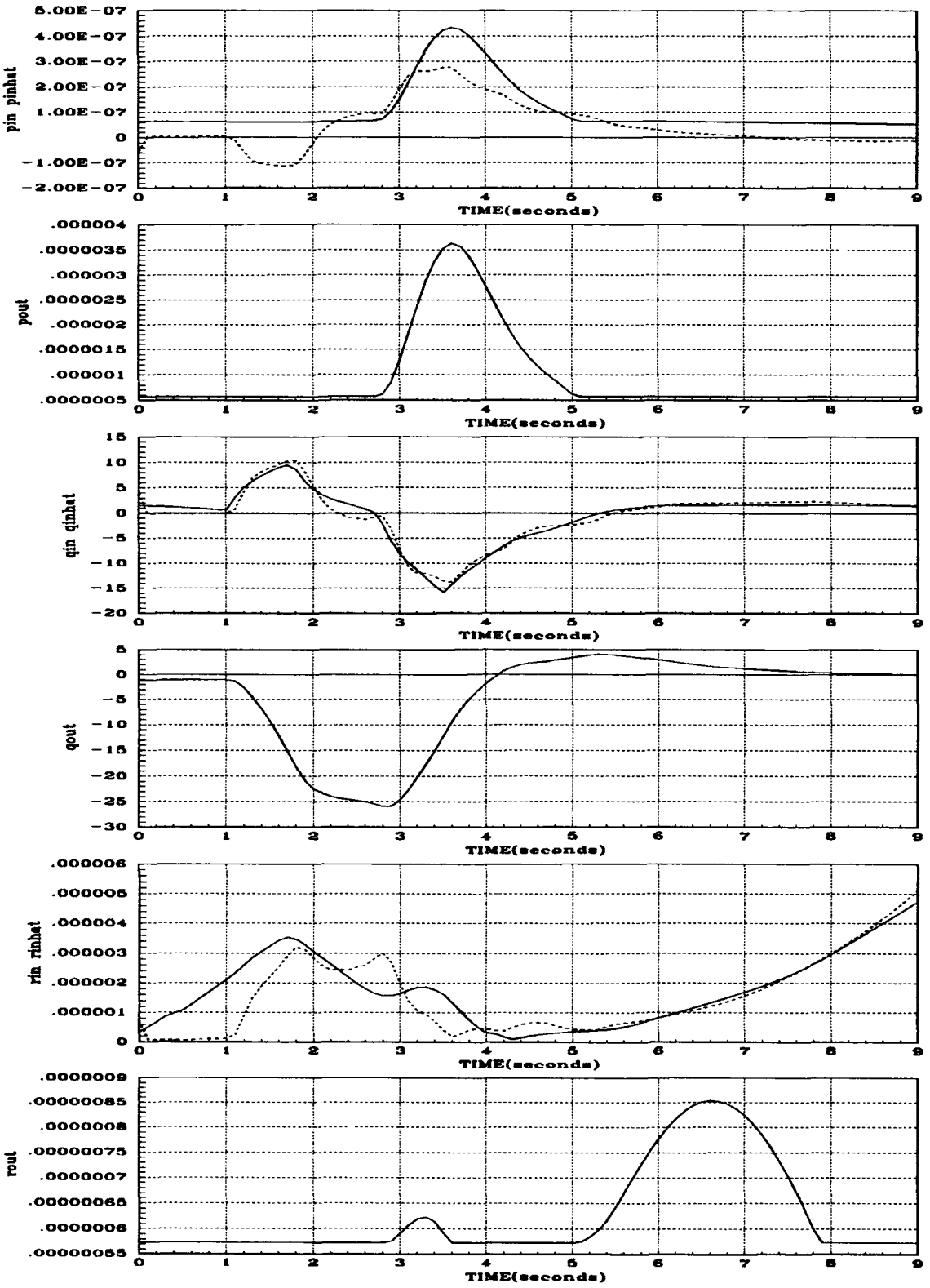

Figure B.7. u, $\hat{u}$, and y_{out} for Plant #2113

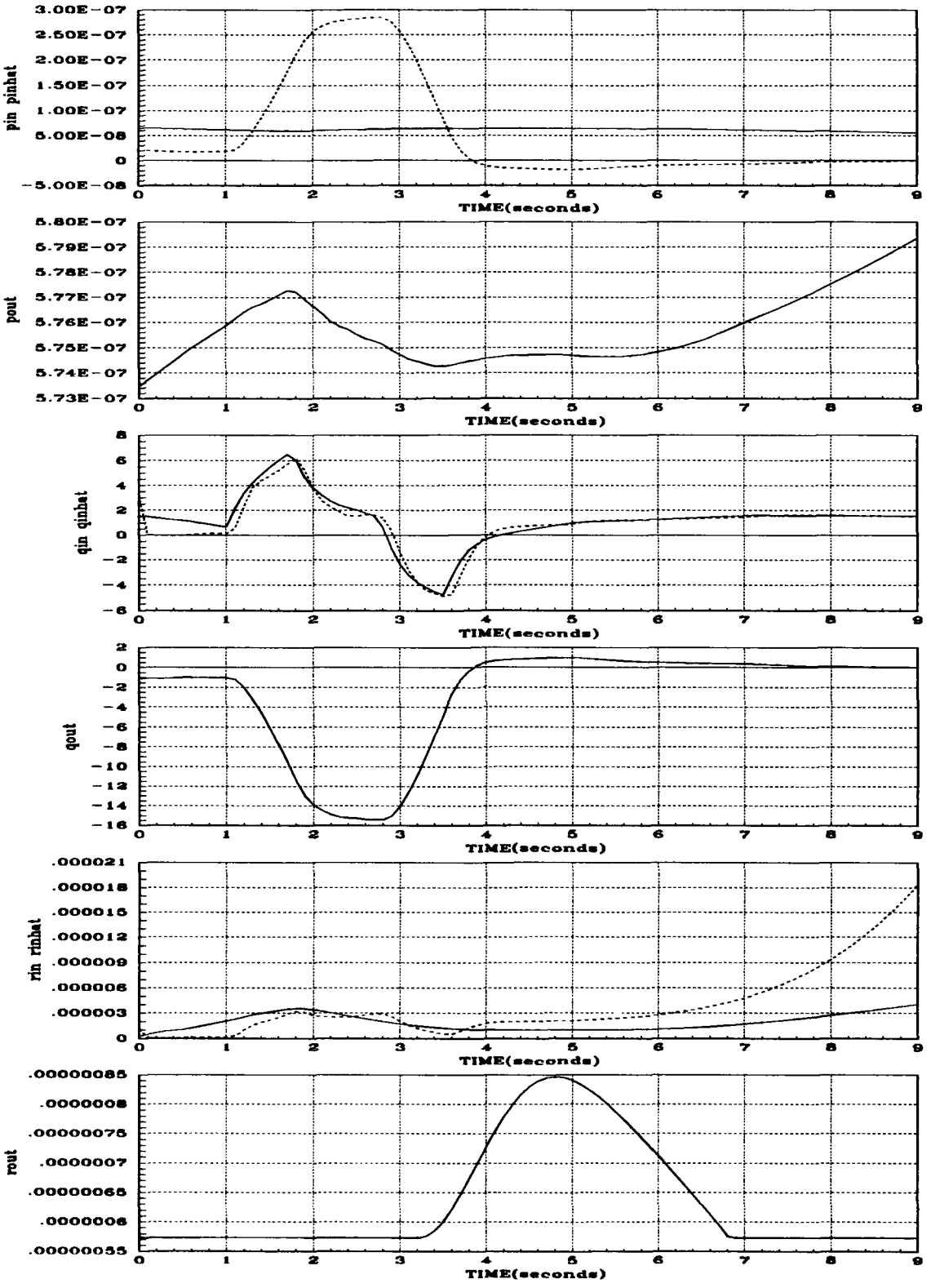

Figure B.8. u, $\hat{u}$, and y_{out} for Plant #2114

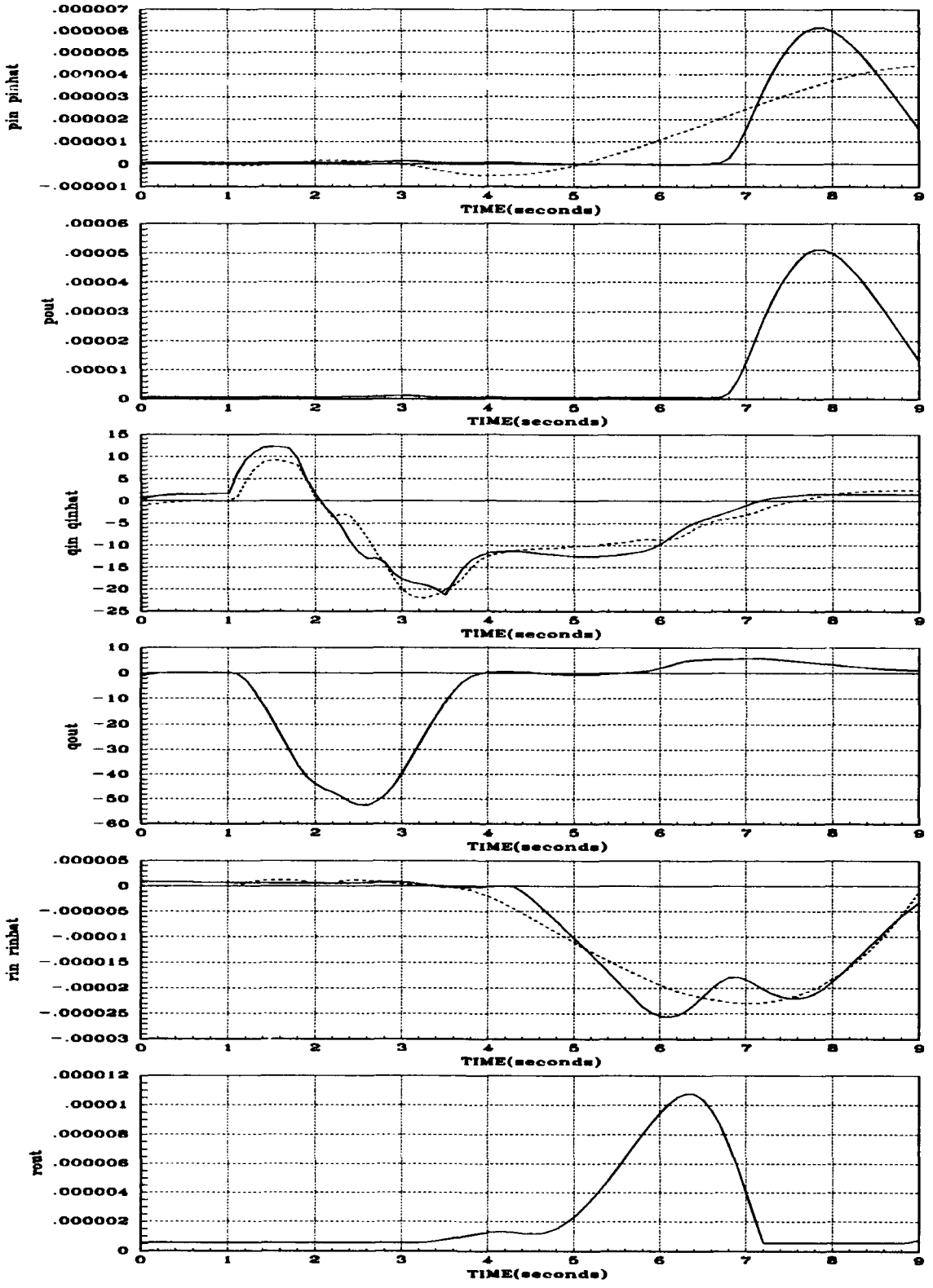

Figure B.9. u, $\hat{u}$, and y_{out} for Plant #2121

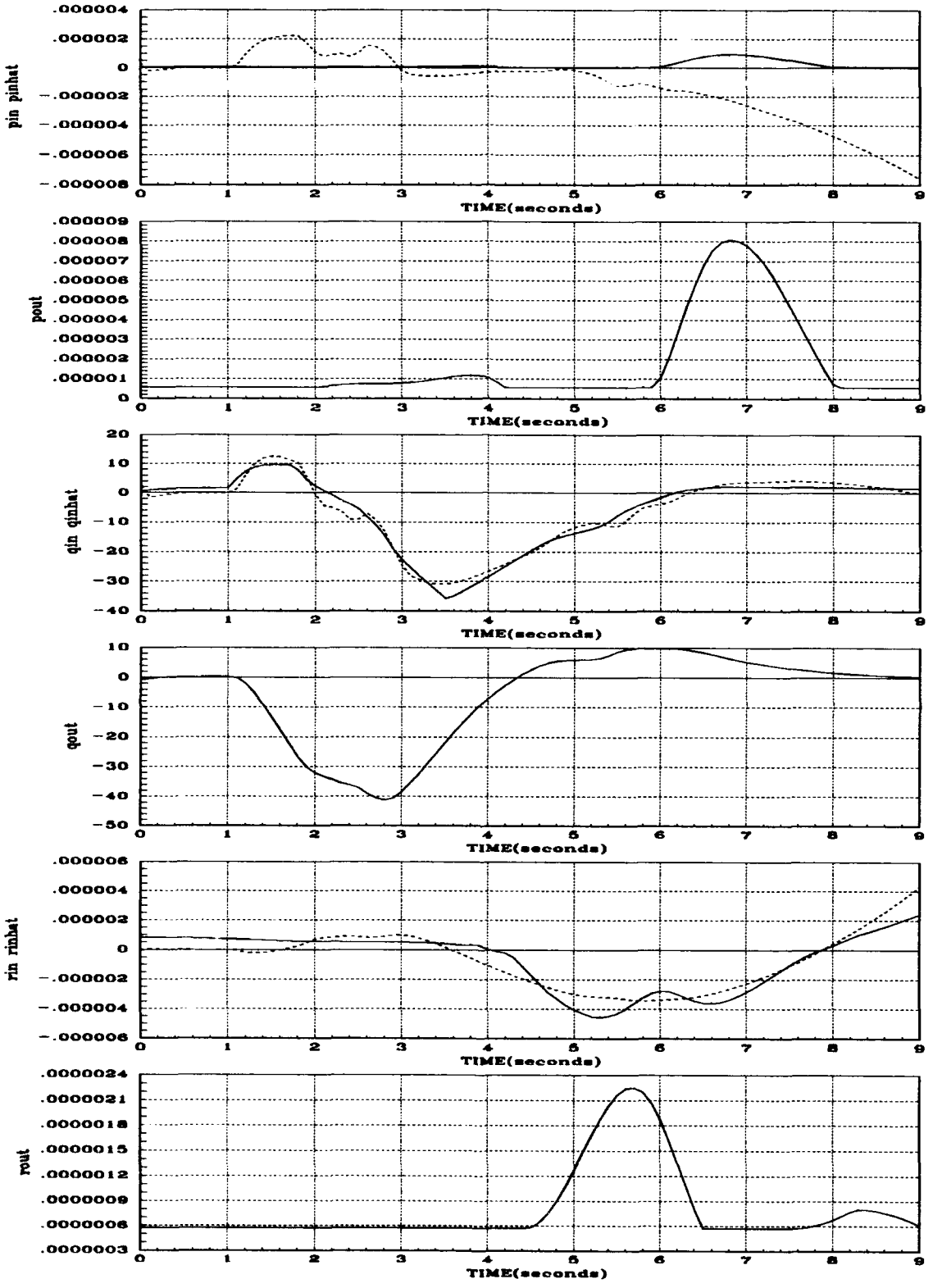

Figure B.10. u, $\hat{u}$, and y_{out} for Plant #2122

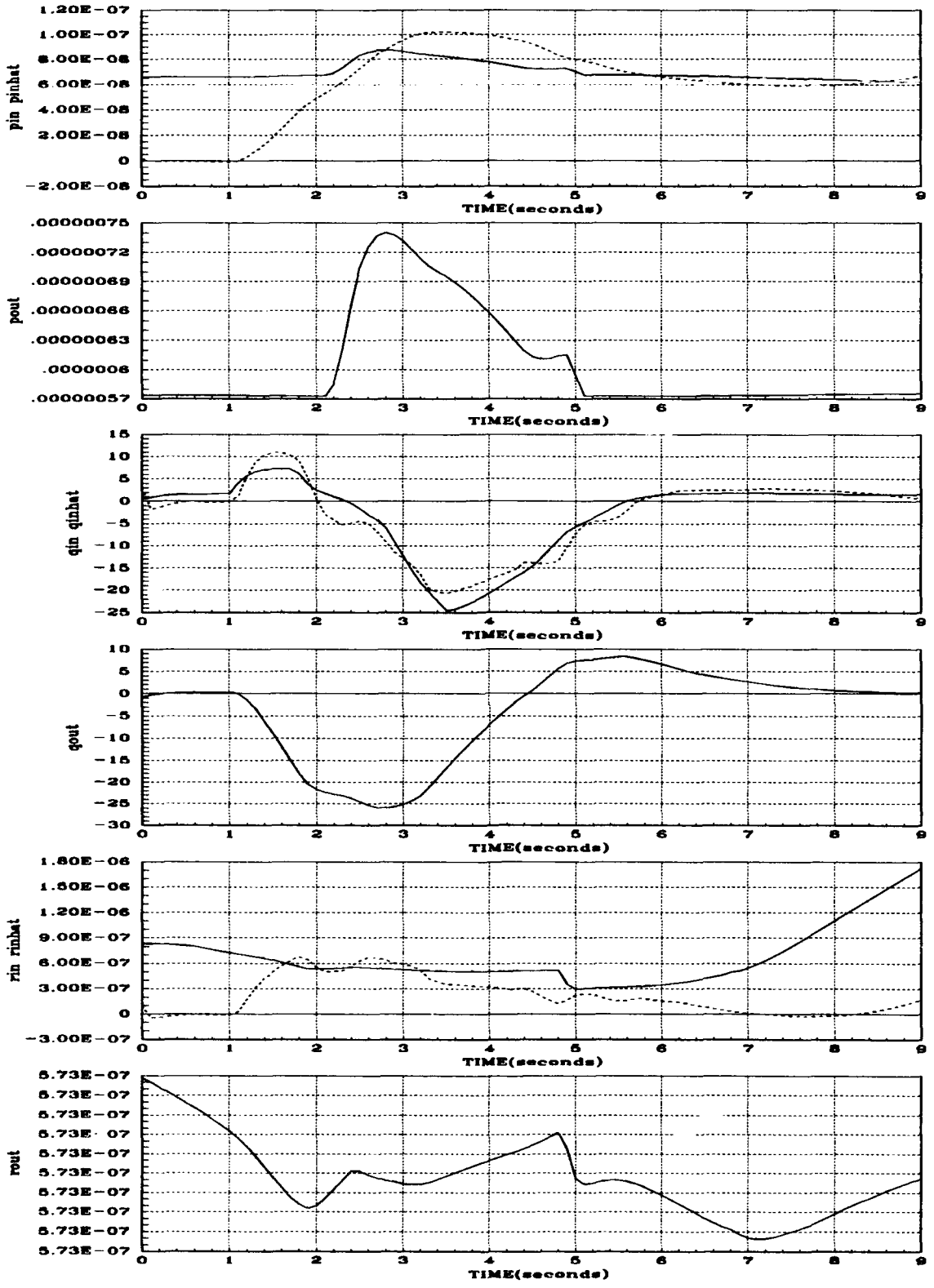

Figure B.11. u, $\hat{u}$. and y_{out} for Plant #2123

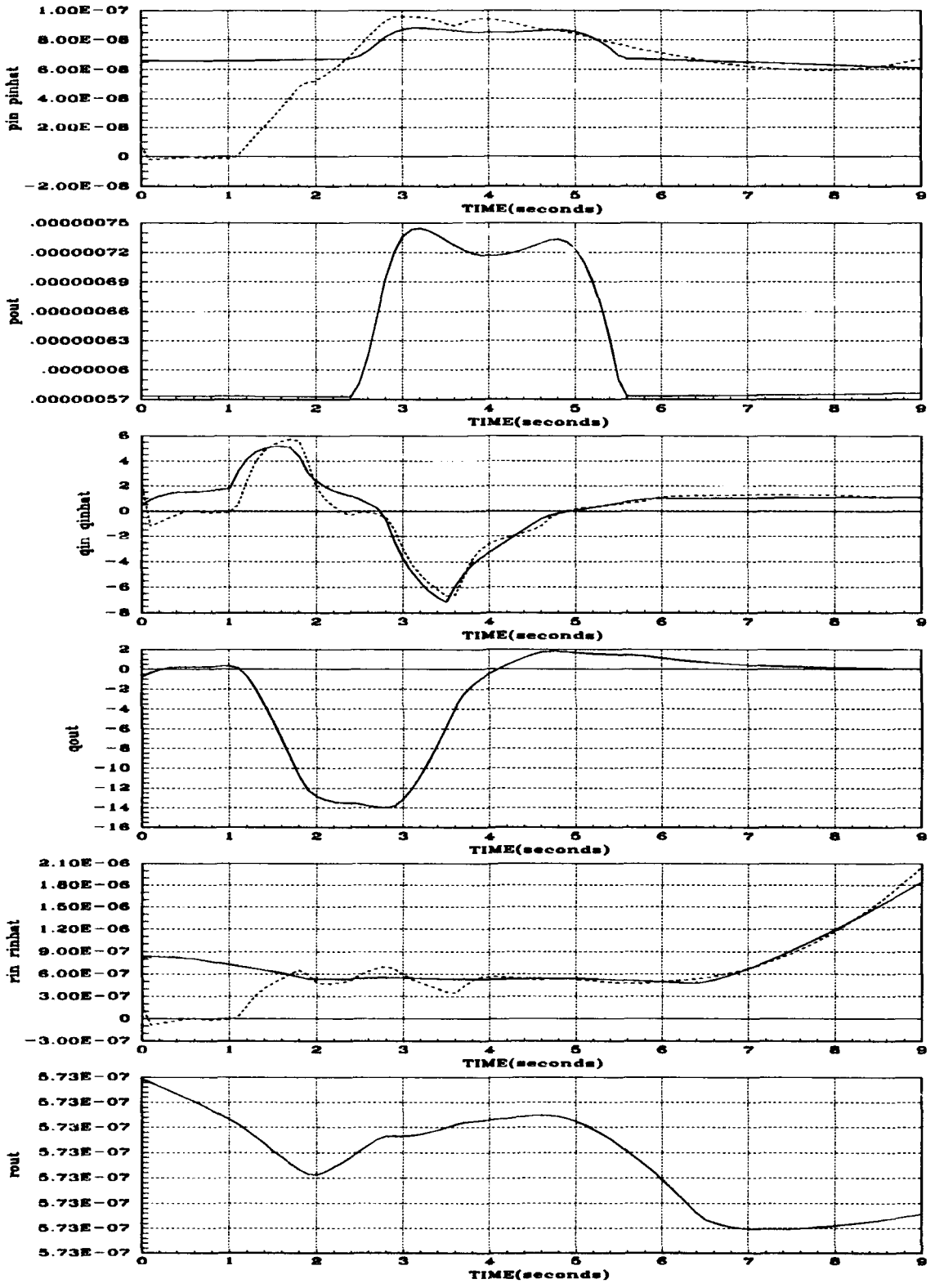

Figure B.12. u, $\hat{u}$, and y_{out} for Plant #2124

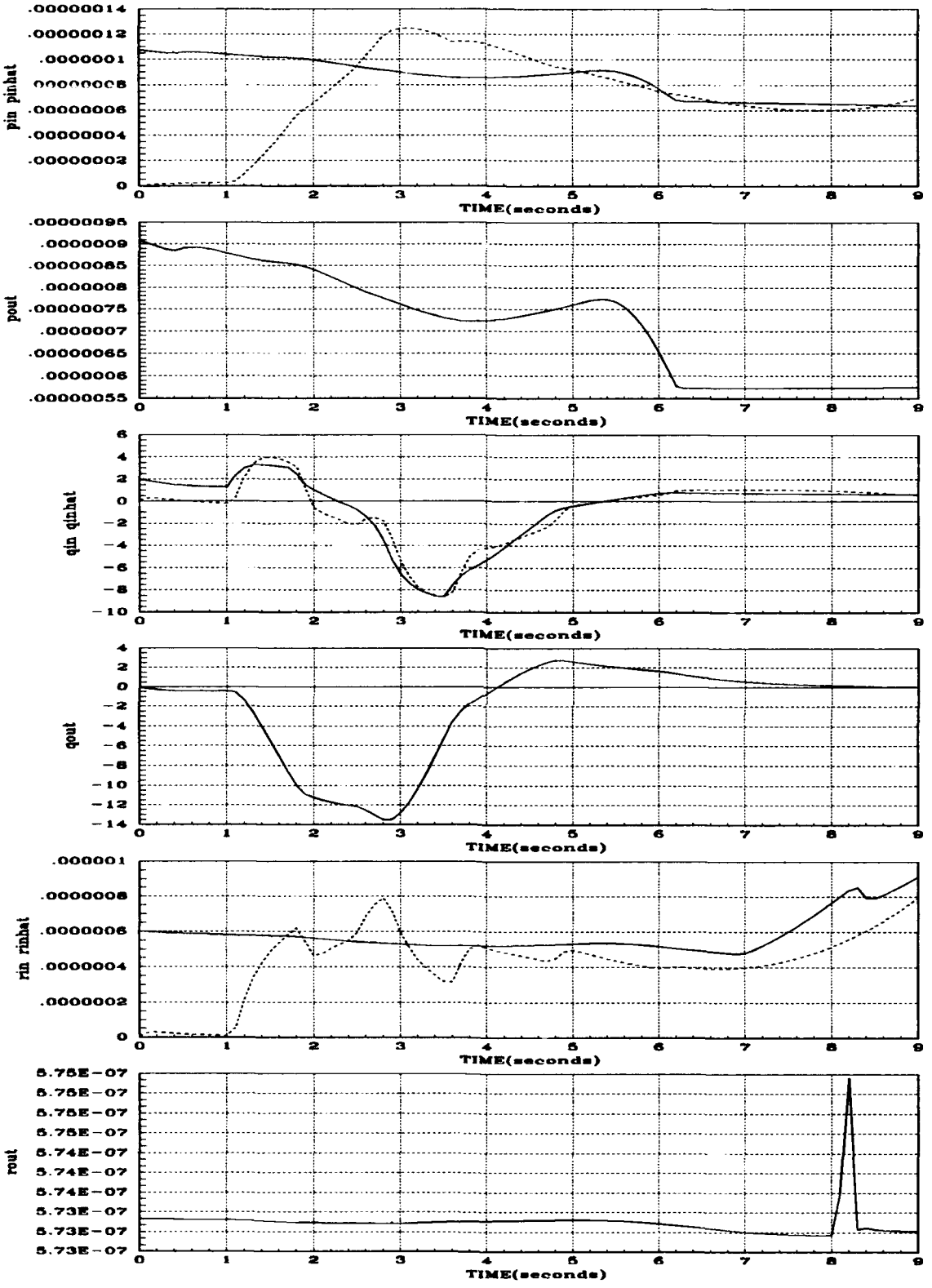

Figure B.13. u, $\hat{u}$, and y_{out} for Plant #2134

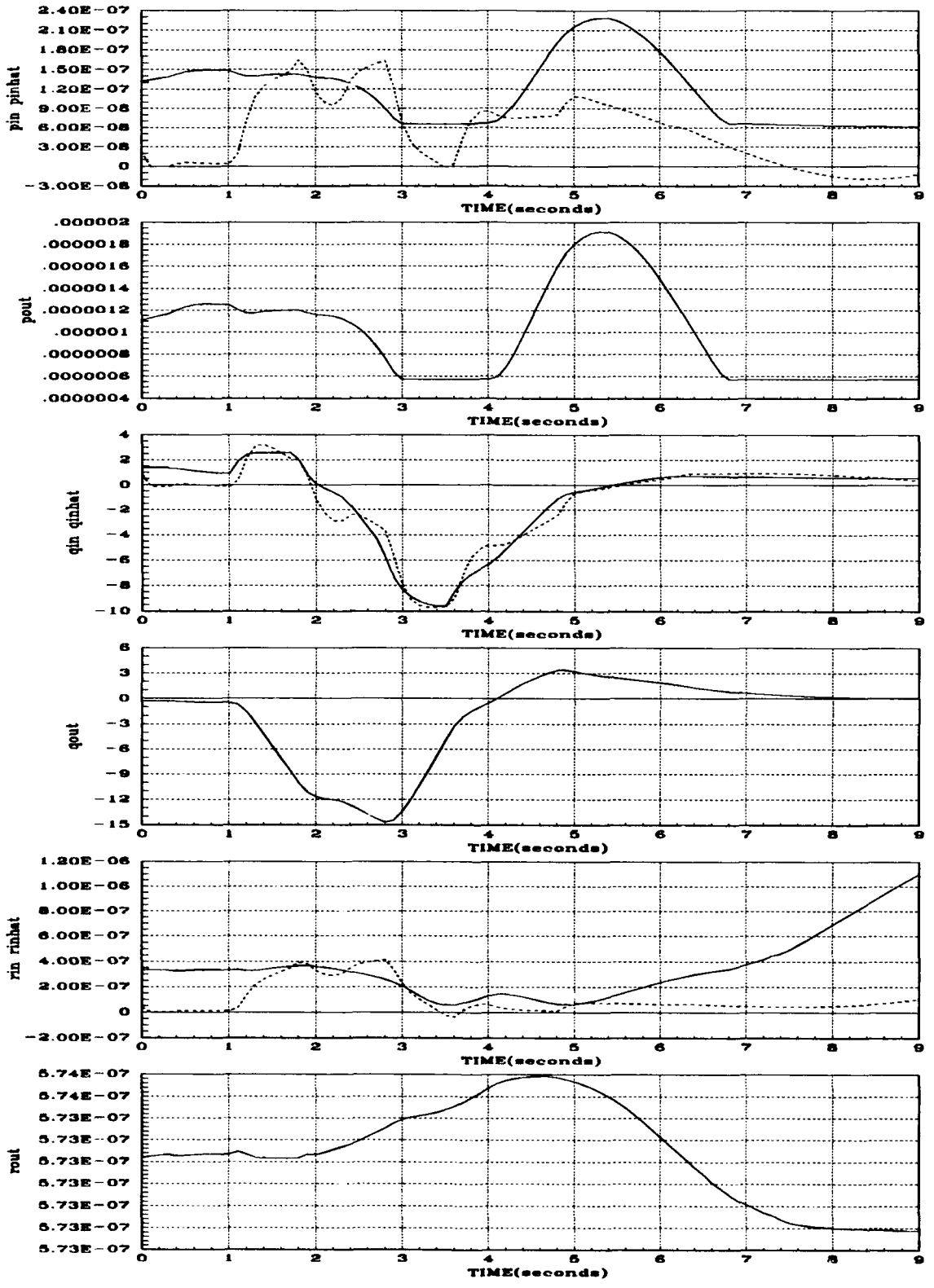

Figure B.14. u, $\hat{u}$, and y_{out} for Plant #2144

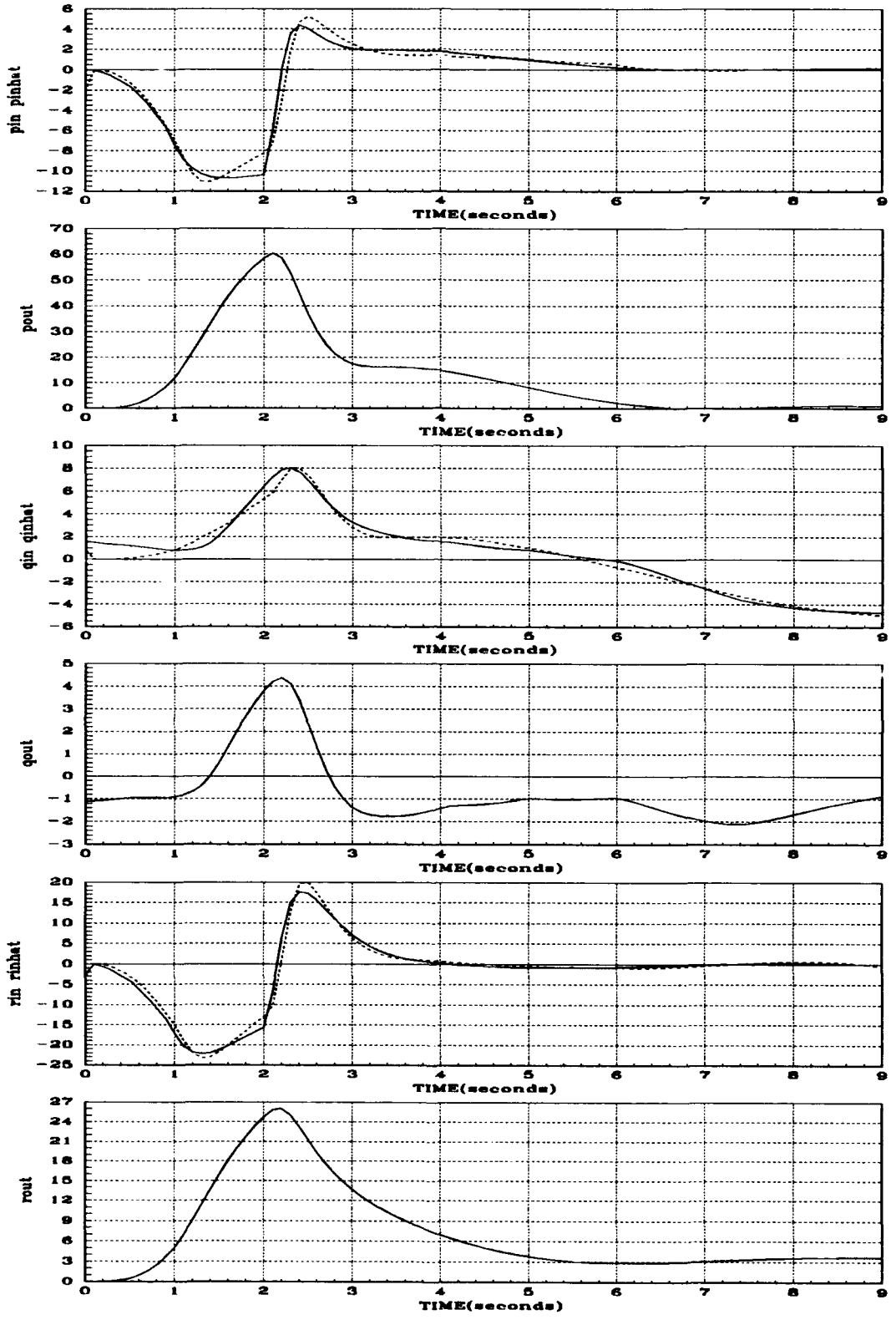

Figure B.15. u, $\hat{u}$, and y_{out} for Plant #2211

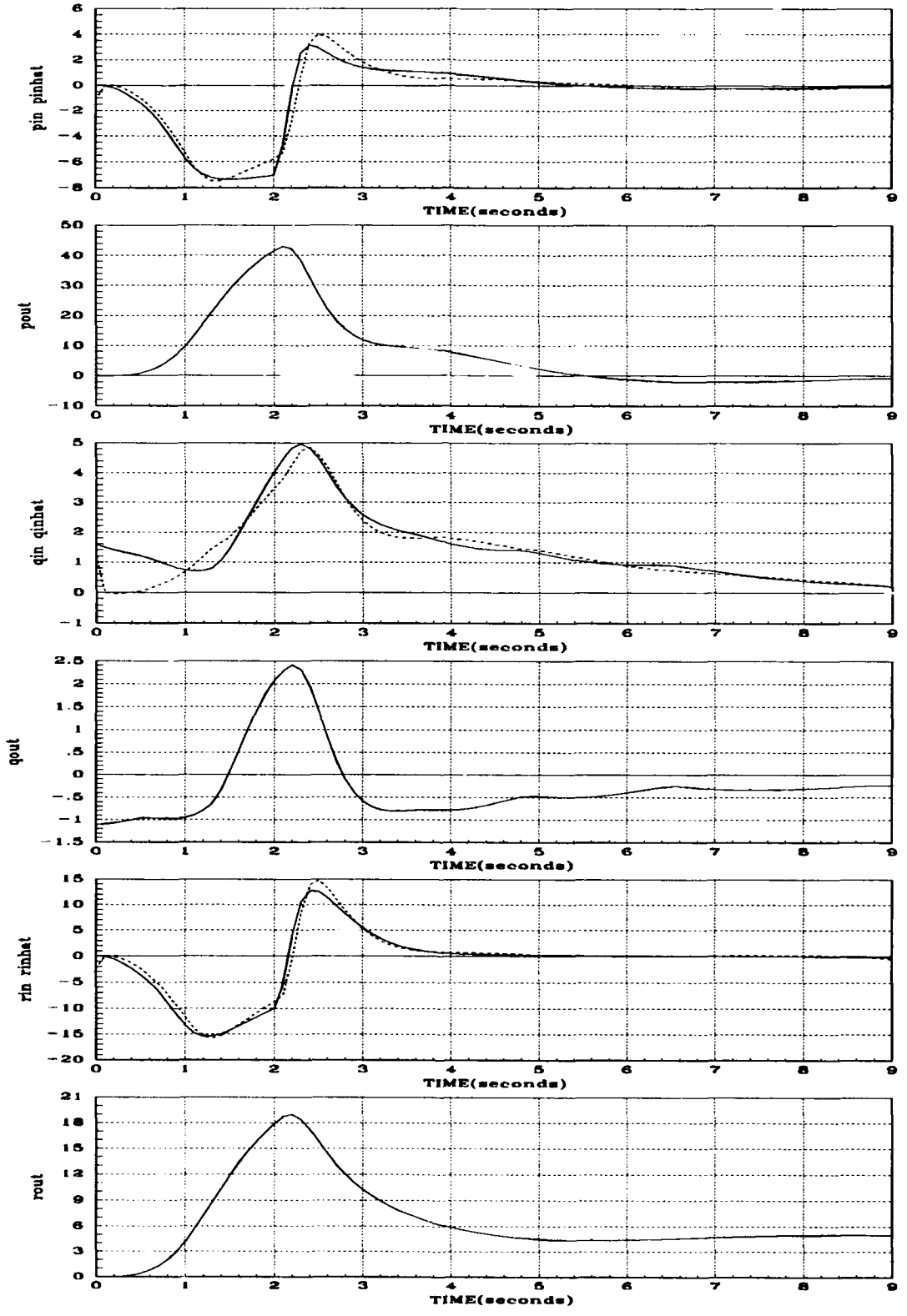

Figure B.16. u, $\hat{u}$, and y_{out} for Plant #2212

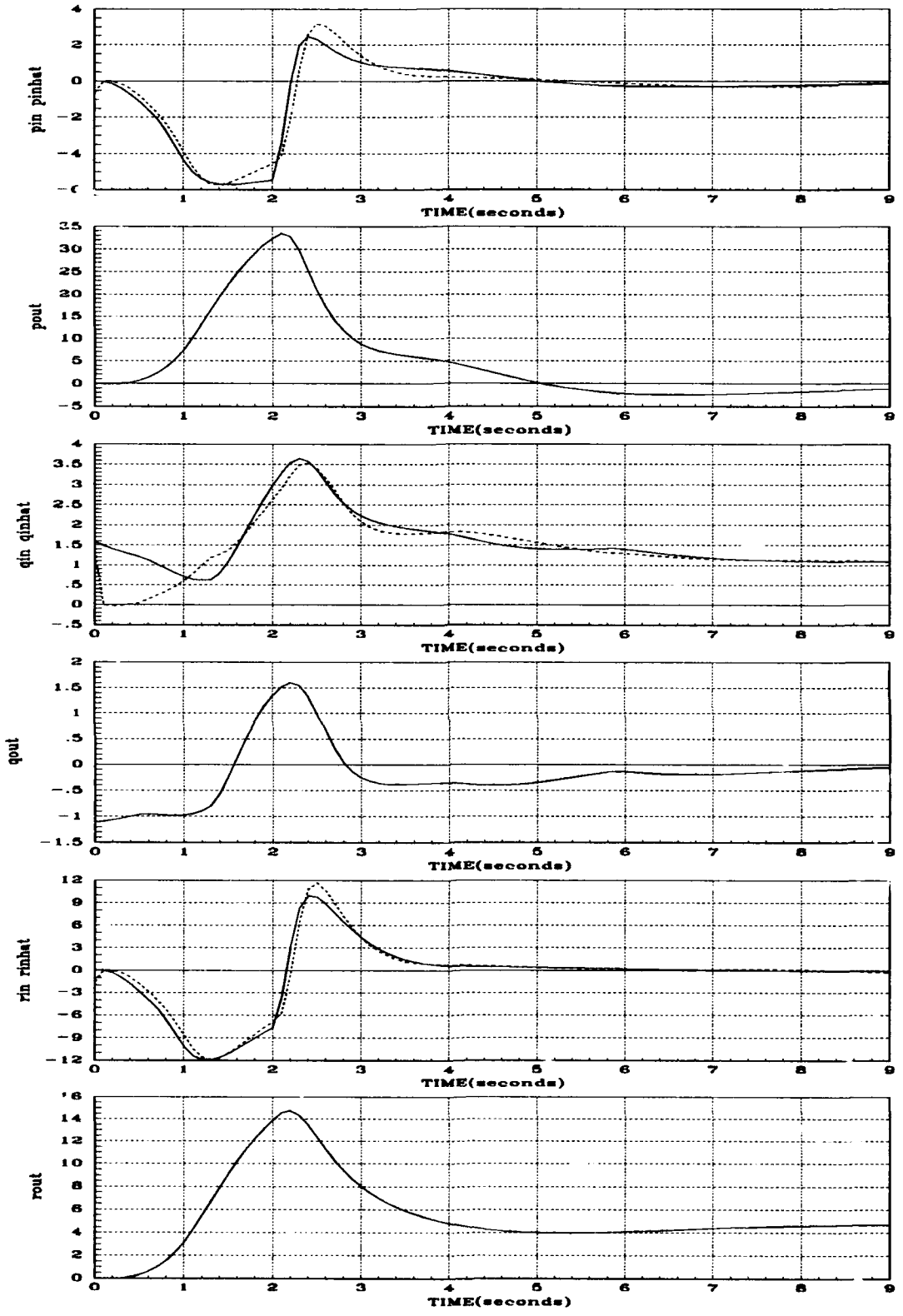

Figure B.17. u, $\hat{u}$, and y_{out} for Plant #2213

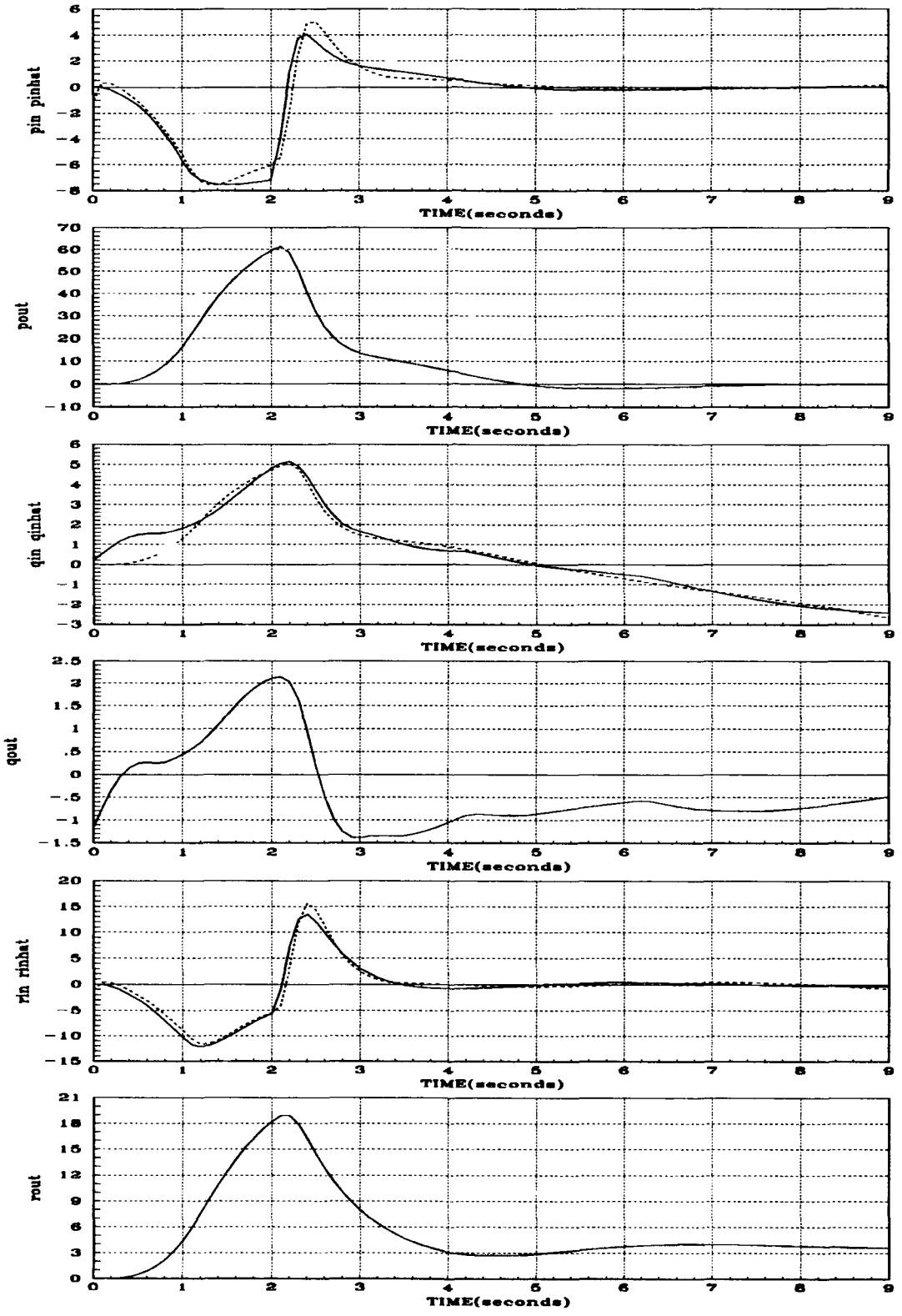

Figure B.18. u, $\hat{u}$, and y_{out} for Plant #2221

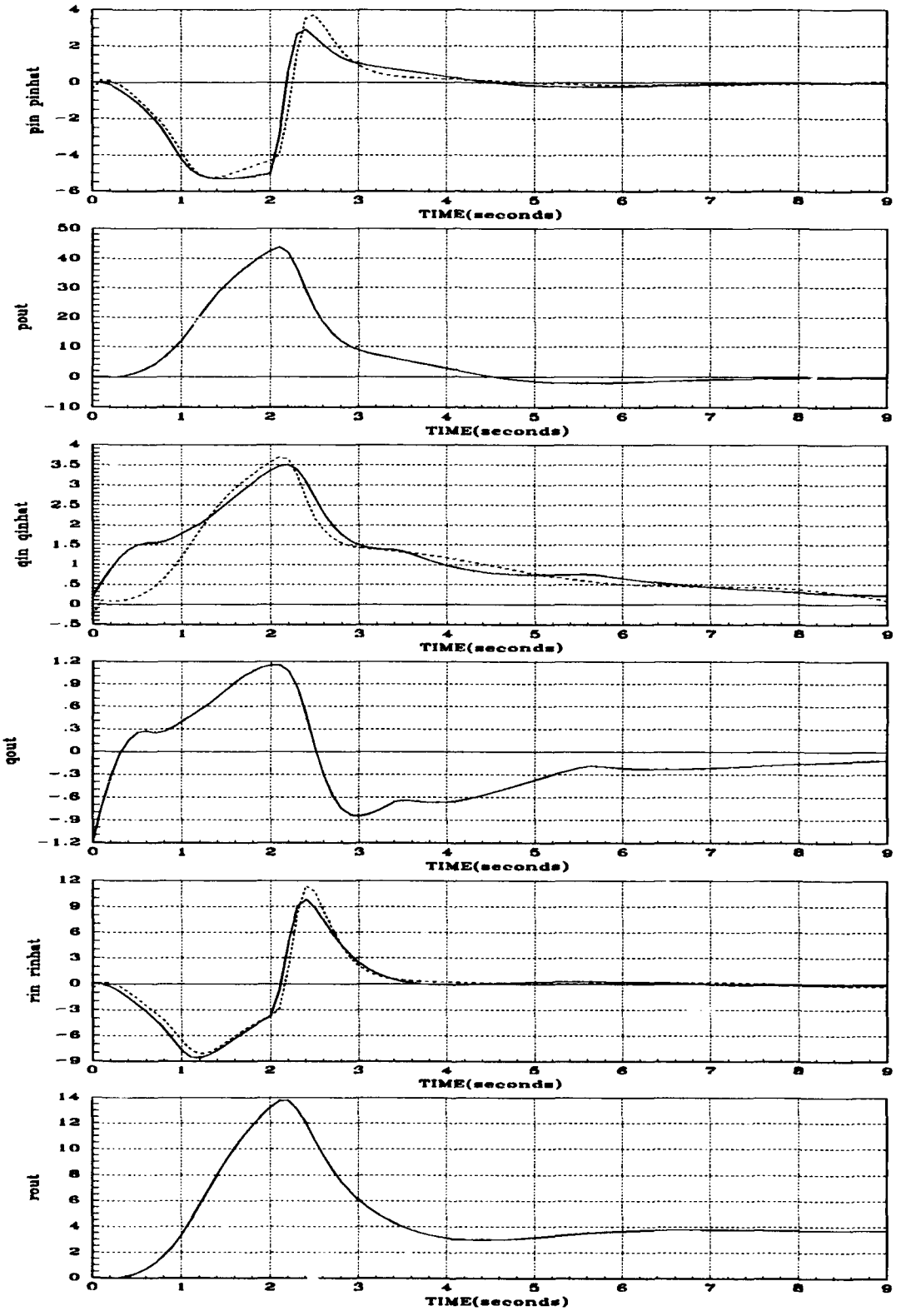

Figure B.19. u, $\hat{u}$, and y_{out} for Plant #2222

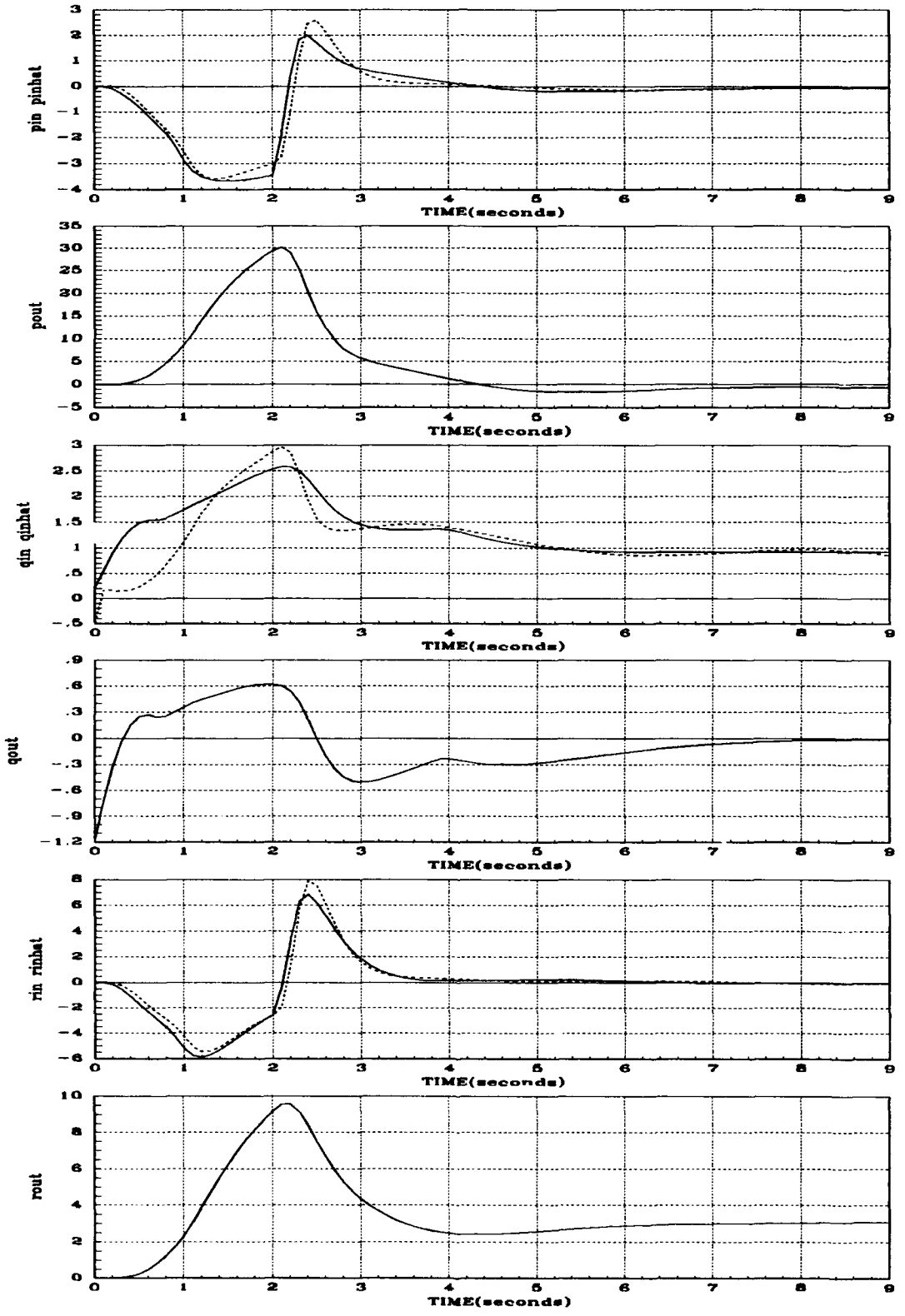

Figure B.20. u, $\hat{u}$, and y_{out} for Plant #2223

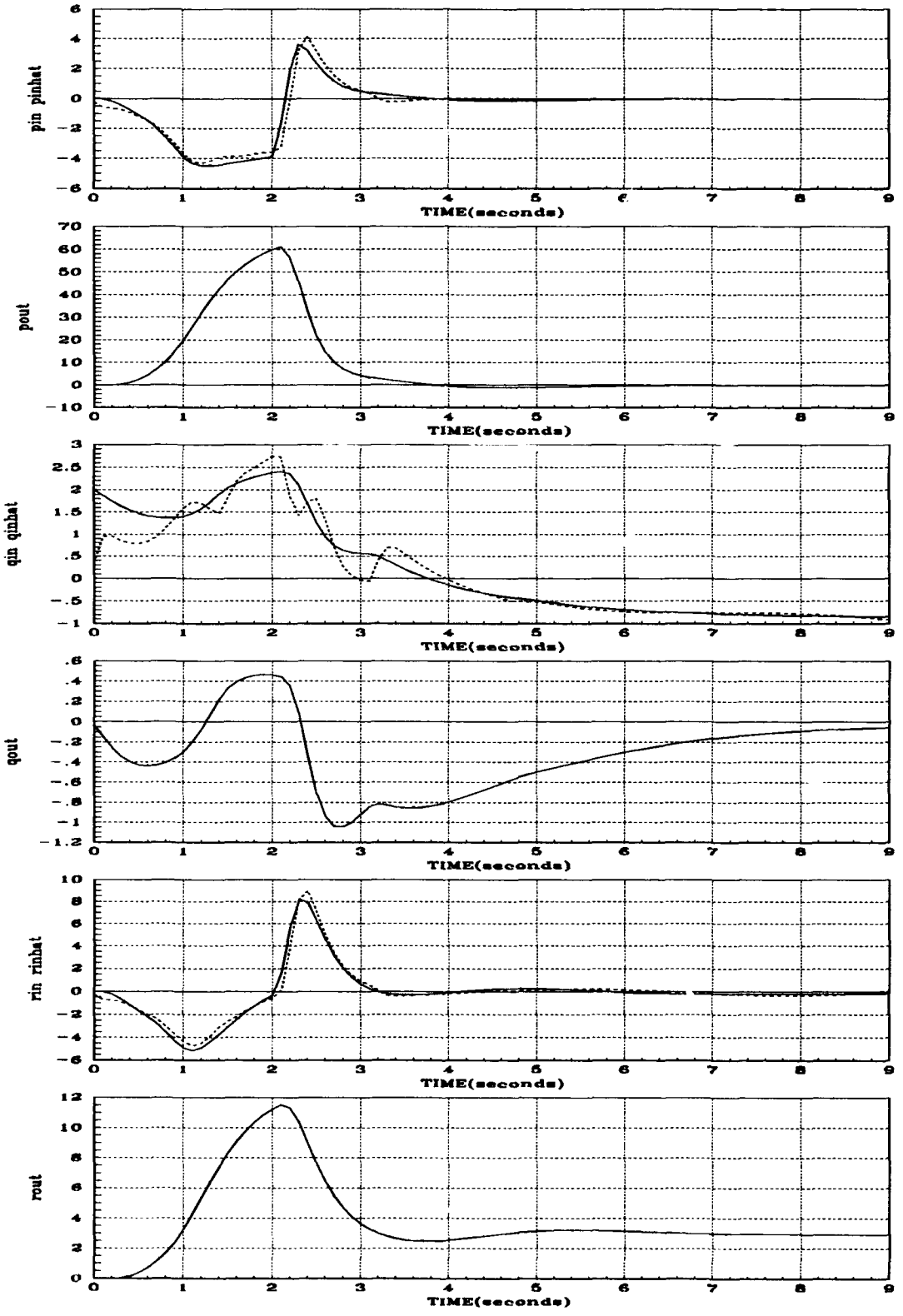

Figure B.21. u, $\hat{u}$, and y_{out} for Plant #2231

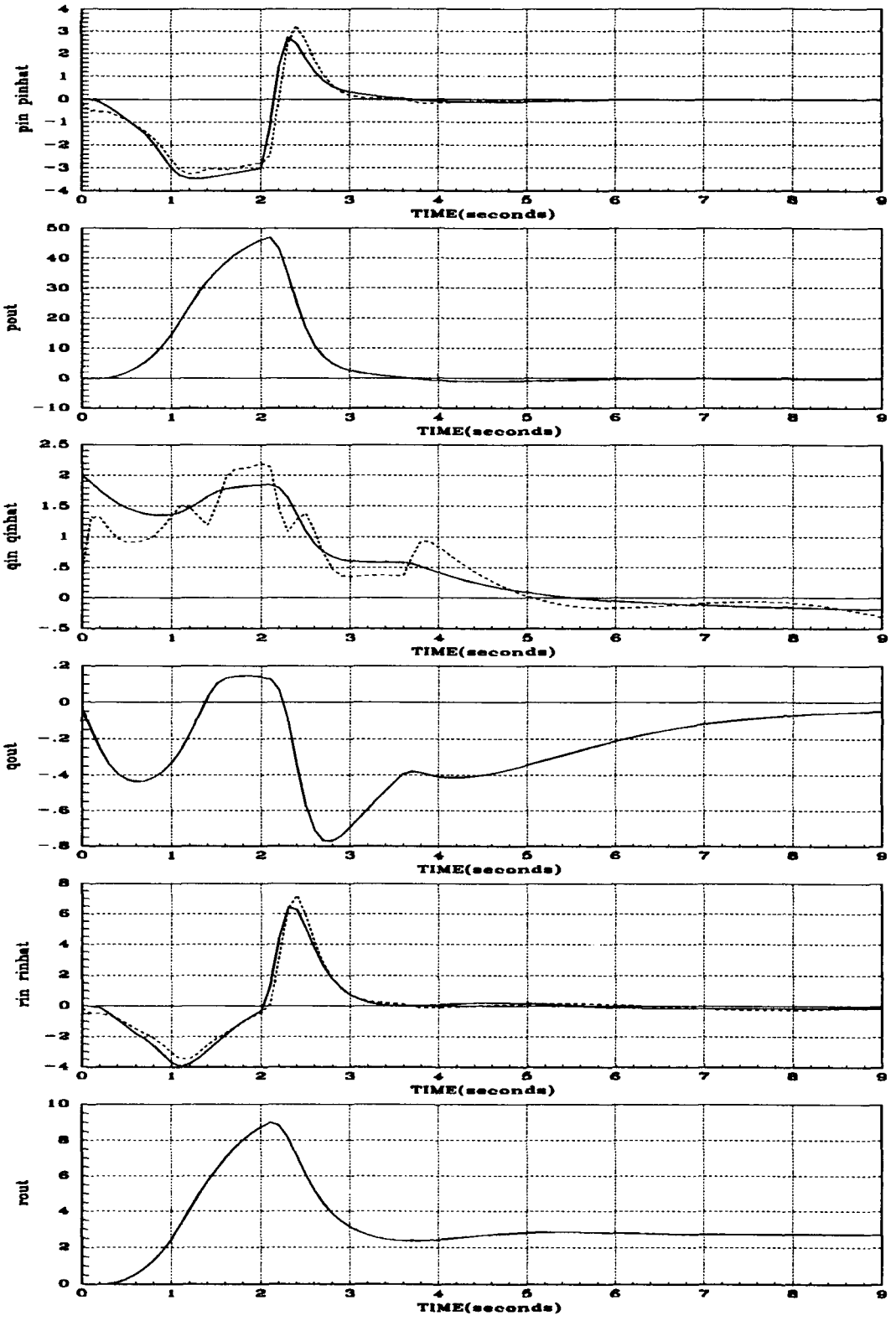

Figure B.22. u, $\hat{u}$, and y_{out} for Plant #2232

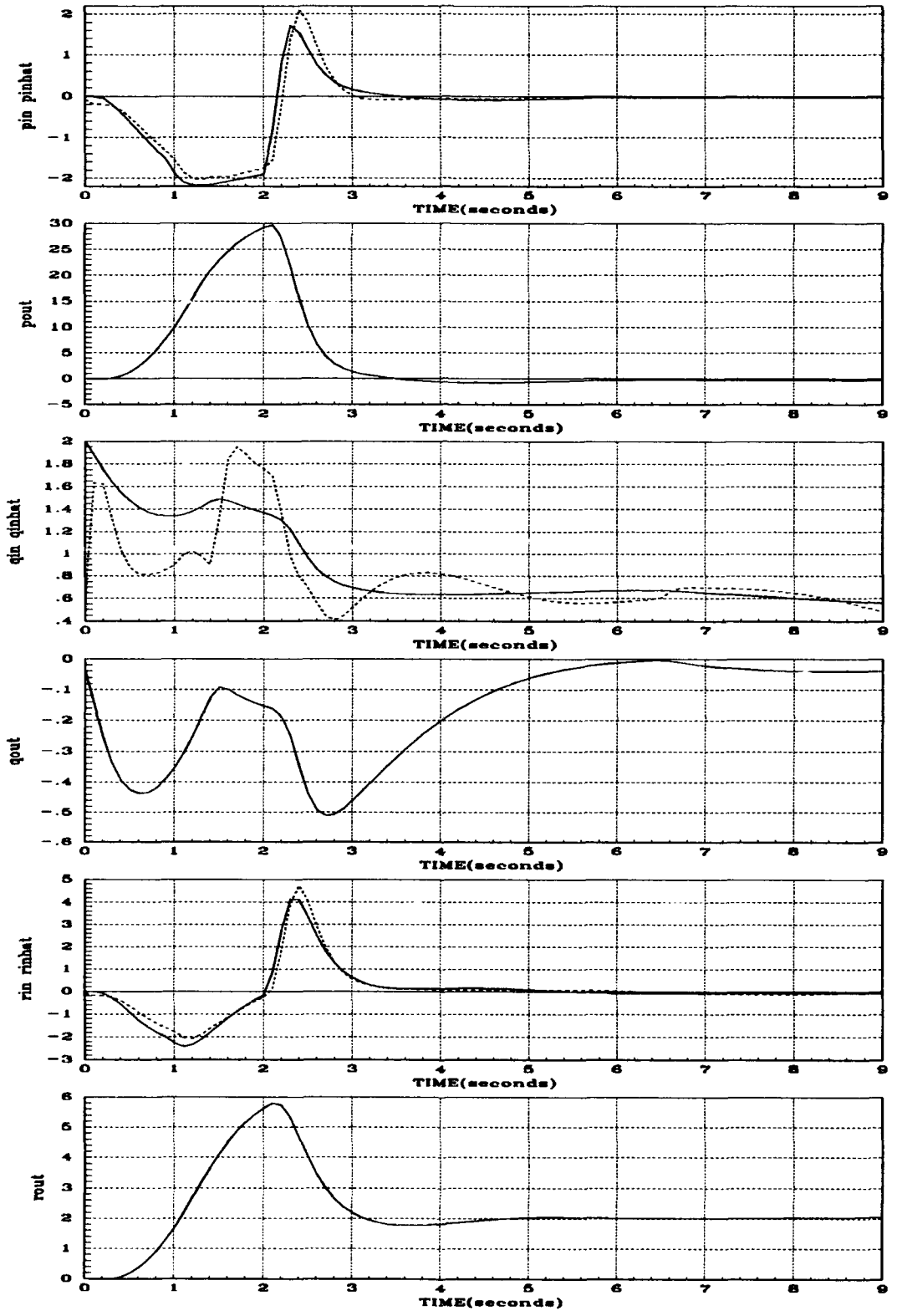

Figure B.23. u, $\hat{u}$, and y_{out} for Plant #2233

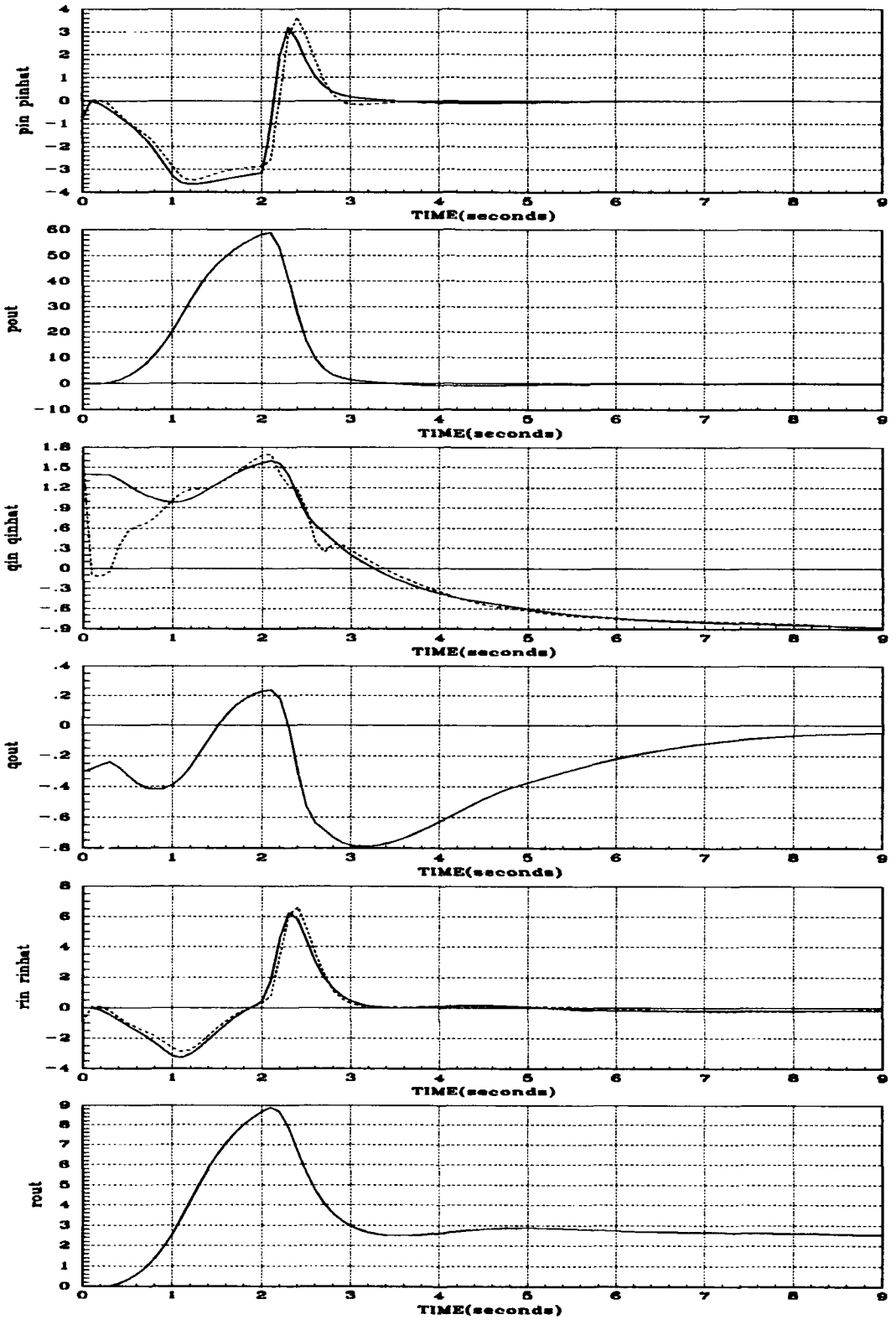

Figure B.24. u, $\hat{u}$, and y_{out} for Plant #2241

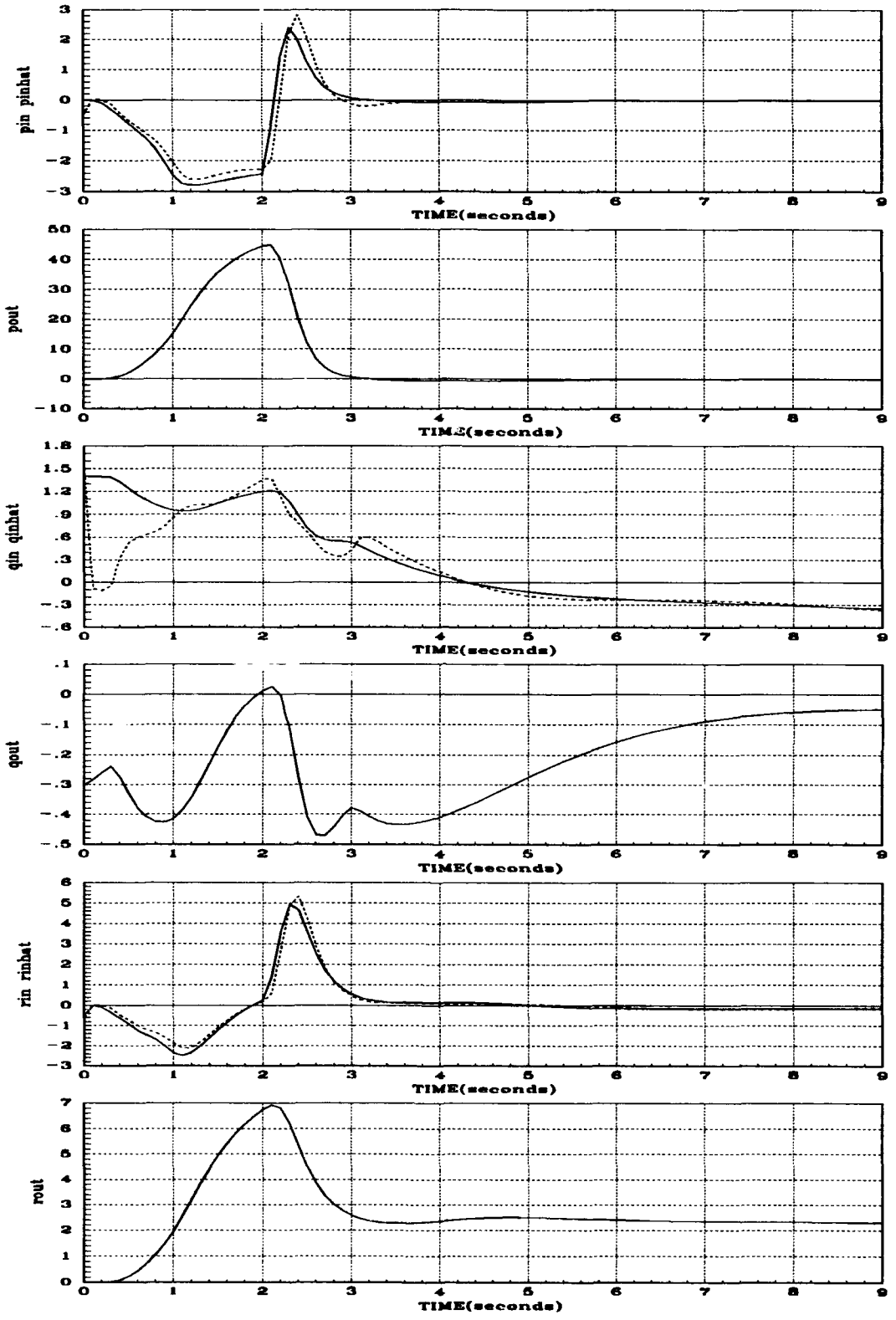

Figure B.25. u, $\hat{u}$, and y_{out} for Plant #2242

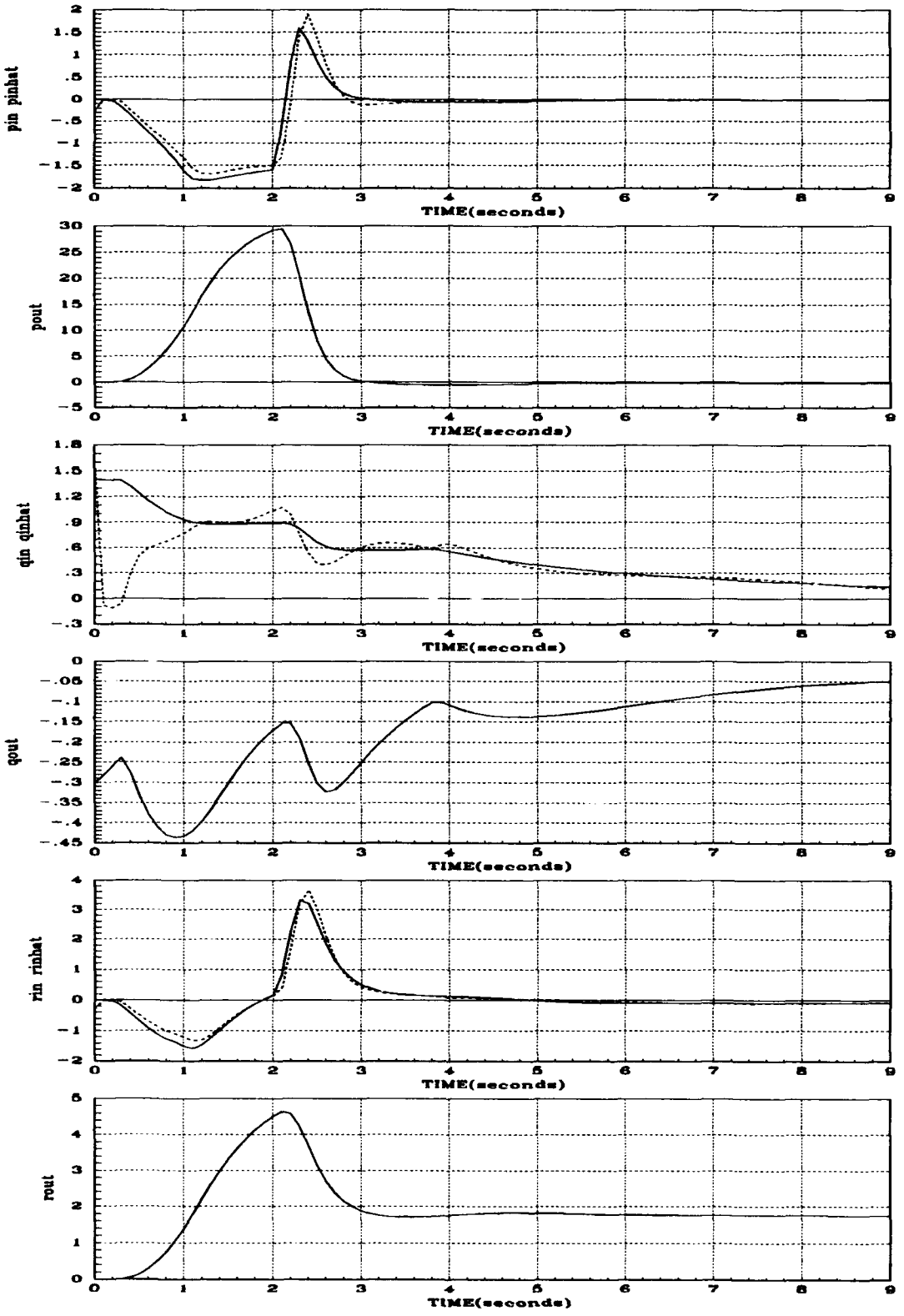

Figure B.26. u, $\hat{u}$, and y_{out} for Plant #2243

Appendix C. **Transfer Functions**

This appendix includes Plants for all Maneuvers developed through system identification in Chapter 4.

C.1 Plants for Maneuver #1111

$$q_{110} = \frac{1.1735D+12(s-100)s^4}{(s-1.8835D-01 \pm j1.2787D-01)(s+2.3350D-01)(s+6.6586D-02 \pm j2.3888D-01)}$$

$$q_{120} = \frac{1.1717D+08(s-100)s^4}{(s+4.4142D-01)(s-2\ 3887D-01 \pm j4.7240D-01)(s-5.7658D-01)(s-2.8668D+01)}$$

$$q_{130} = \frac{1.3116D+12(s-100)s^4}{(s-1.7042D-01 \pm j1.1753D-01)(s+2.0838D-01)(s+6.3821D-02 \pm j2.1147D-01)}$$

$$q_{210} = \frac{-8.2533D+04(s-100)s^4}{(s-4.1851D-01 \pm j1.2852D+00)(s+1.0945D+00 \pm j7.9371D-01)(s-1.3526D+00)}$$

$$q_{220} = \frac{-7.9189D-01(s-100)s^4}{(s+4.7364D-01)(s-6.8060D-01)(s-2.8766D-01 \pm j7.6561D-01)(s+2.2785D+00)}$$

$$q_{230} = \frac{-7.9651D+04(s-100)s^4}{(s+2.5942D-01 \pm j1.8083D-01)(s-3.1678D-01)(s-1.0129D-01 \pm j3.0312D-01)}$$

$$q_{310} = \frac{5.2911D+11(s-100)s^4}{(s-2.8715D-01 \pm j1.9166D-01)(s+3.7366D-01)(s+1.0269D-01 \pm j3.7021D-01)}$$

$$q_{320} = \frac{6.3525D+07(s-100)s^4}{(s-4.5998D-01 \pm j3.7614D-01)(s+1.0671D+00 \pm j3.8719D-01)(s+4.8065D+01)}$$

$$q_{330} = \frac{4.5118D+11(s-100)s^4}{(s-2.5022D-01 \pm j1.6915D-01)(s+3.2097D-01)(s+8.3650D-02 \pm j3.1166D-01)}$$

C.2 Plants for Maneuver #2111

$$q_{110} = \frac{1.3251D+10(s-100)s^4}{(s-5.1168D-01 \pm j3.2726D-01)(s-2.7356D-02 \pm j6.0847D-01)(s+6.7882D-01)}$$

$$q_{120} = \frac{1.0269D+07(s-100)s^4}{(s+5.4144D-01)(s+6.4370D-01 \pm j5.3935D-01)(s-2.3058D+00)(s+1.5615D+01)}$$

$$q_{130} = \frac{6.0629D+10(s-100)s^4}{(s-6.2334D-01 \pm j4.2673D-01)(s+8.5773D-01)(s+3.7169D-01 \pm j8.1324D-01)}$$

$$q_{210} = \frac{5.6347D+03(s-100)s^4}{(s+7.1662D-02 \pm j3.4765D-01)(s-2.9750D-01 \pm j2.1275D-01)(s+4.5381D-01)}$$

$$q_{220} = \frac{-3.6453D-01(s-100)s^4}{(s+3.0272D-01 \pm j2.1214D-01)(s-9.8071D-01 \pm j8.1370D-01)(s+2.5704D+00)}$$

$$q_{230} = \frac{-1.6215D+04(s-100)s^4}{(s-5.2214D-01)(s-2.0686D-01 \pm j4.9714D-01)(s+4.7265D-01 \pm j3.3941D-01)}$$

$$q_{310} = \frac{3.4369D+09(s-100)s^4}{(s-3.3572D-01 \pm j2.2375D-01)(s+6.5455D-02 \pm j4.3983D-01)(s+5.2153D-01)}$$

$$q_{320} = \frac{-1.3357D+07(s-100)s^4}{(s+5.3378D-01)(s-6.4942D-01)(s+7.8106D-01)(s-5.9569D+00)(s-3.0043D+01)}$$

$$q_{330} = \frac{-4.6058D+09(s-100)s^4}{(s-4.7544D-01)(s+4.0506D-01 \pm j2.7530D-01)(s-1.7544D-01 \pm j4.5905D-01)}$$

C.3 Plants for Maneuver #2112

$$q_{110} = \frac{1.6695D+10(s-100)s^4}{(s-2.9462D-01)(s+2.4582D-01 \pm j1.6603D-01)(s-1.0916D-01 \pm j2.9339D-01)}$$

$$q_{120} = \frac{4.8339D+07(s-100)s^4}{(s+4.7466D-01)(s+3.2845D-01 \pm j6.1091D-01)(s-1.7495D+00)(s+3.0655D+01)}$$

$$q_{130} = \frac{-3.0061D+11(s-100)s^4}{(s-2.9564D-01)(s-1.9735D-01 \pm j3.2196D-01)(s+3.2026D-01 \pm j2.2457D-01)}$$

$$q_{210} = \frac{6.2309D+03(s-100)s^4}{(s-4.1561D-01)(s-1.6075D-01 \pm j3.8974D-01)(s+3.8052D-01 \pm j2.6670D-01)}$$

$$q_{220} = \frac{-2.5008D-01(s-4.2732D-02)(s-4.2732D-02)(s-4.2732D-02)(s-4.2732D-02)(s-100)}{(s+2.4360D-01 \pm j2.0867D-01)(s-6.6886D-01)(s-1.6082D+00)(s+2.8867D+00)}$$

$$q_{230} = \frac{-3.5242D+04(s-100)s^4}{(s+4.7048D-01)(s+2.2655D-01 \pm j4.8535D-01)(s-4.3559D-01 \pm j3.1175D-01)}$$

$$q_{310} = \frac{1.1154D+12(s-100)s^4}{(s+8.7164D-01)(s-6.2117D-02 \pm j1.0553D+00)(s-8.9575D-01 \pm j6.4361D-01)}$$

$$q_{320} = \frac{-2.9600D+06(s-100)s^4}{(s-1.2809D-01)(s+4.3613D-01 \pm j2.3457D-01)(s-9.3616D-01)(s-2.4845D+01)}$$

$$q_{330} = \frac{9.8882D+10(s-100)s^4}{(s+5.3386D-01)(s-4.6382D-01 \pm j3.2645D-01)(s+1.8024D-01 \pm j5.7787D-01)}$$

C.4 Plants for Maneuver #2113

$$q_{110} = \frac{5.0933D+10(s-100)s^4}{(s+2.7955D-01)(s+9.9977D-02\pm j2.7605D-01)(s-2.4760D-01\pm j1.9164D-01)}$$

$$q_{120} = \frac{2.0279D+07(s-100)s^4}{(s+2.3850D-01\pm j1.7510D-01)(s-8.2430D-01\pm j1.4965D-01)(s+4.6893D+00)}$$

$$q_{130} = \frac{2.4692D+11(s-100)s^4}{(s+3.6370D-01)(s-3.2234D-01\pm j2.3317D-01)(s+1.3121D-01\pm j3.8847D-01)}$$

$$q_{210} = \frac{-2.9002D+04(s-100)s^4}{(s+1.3645D-01\pm j3.9027D-01)(s+4.4281D-01)(s-3.8500D-01\pm j3.0683D-01)}$$

$$q_{220} = \frac{-2.8103D-01(s-6.5700D-02)(s-6.5700D-02)(s-6.5700D-02)(s-6.5700D-02)(s-100)}{(s+2.6435D-01\pm j2.1108D-01)(s-5.2433D-01)(s+1.4069D+00)(s-2.1874D+00)}$$

$$q_{230} = \frac{-7.3474D+04(s-100)s^4}{(s-4.6061D-01\pm j3.3534D-01)(s+2.0008D-01\pm j5.4263D-01)(s+5.8344D-01)}$$

$$q_{310} = \frac{1.1691D+10(s-100)s^4}{(s+2.9010D-01)(s+1.2295D-01\pm j3.1325D-01)(s-2.8235D-01\pm j2.1559D-01)}$$

$$q_{320} = \frac{-1.5272D+06(s-100)s^4}{(s-2.4297D-01)(s+2.7085D-01\pm j2.7427D-01)(s-1.0468D+00)(s-9.3016D+00)}$$

$$q_{330} = \frac{3.6475D+10(s-100)s^4}{(s+3.2153D-01)(s-3.2165D-01\pm j2.3318D-01)(s+1.3820D-01\pm j4.0051D-01)}$$

C.5 Plants for Maneuver #2114

$$q_{110} = \frac{1.2987D+12(s-100)s^4}{(s+2.4479D-01)(s-3.3362D-01\pm j2.4190D-01)(s+1.2852D-01\pm j4.4252D-01)}$$

$$q_{120} = \frac{-5.4251D+07(s-100)s^4}{(s+1.4856D-01\pm j1.4623D-01)(s-5.2524D-01)(s-1.0916D+00)(s-9.9205D+00)}$$

$$q_{130} = \frac{1.2580D+12(s-100)s^4}{(s+2.6912D-01)(s-3.4806D-01\pm j2.5143D-01)(s+1.3591D-01\pm j4.5319D-01)}$$

$$q_{210} = \frac{-3.7872D+04(s-100)s^4}{(s+3.6930D-01\pm j8.1380D-02)(s-3.8916D-01)(s-1.2302D-01\pm j3.7438D-01)}$$

$$q_{220} = \frac{-3.4547D-01(s-1.5114D-04)(s-1.5114D-04)(s-1.5114D-04)(s-1.5114D-04)(s-100)}{(s+2.6520D-01)(s+1.0227D-01\pm j4.5158D-01)(s-1.3718D+00\pm j2.4439D-01)}$$

$$q_{230} = \frac{-3.8617D+04(s-100)s^4}{(s+3.8668D-01\pm j1.1734D-01)(s-4.0781D-01)(s-1.3216D-01\pm j3.9316D-01)}$$

$$q_{310} = \frac{-7.5715D + 10(s-100)s^4}{(s+4.7595D-01)(s-1.7723D-01 \pm j5.1192D-01)(s-5.4541D-01)(s+6.7049D-01)}$$

$$q_{320} = \frac{-9.5425D + 05(s-100)s^4}{(s-3.3190D-01)(s+2.4448D-01 \pm j2.4778D-01)(s-9.6939D-01)(s-9.9078D+00)}$$

$$q_{330} = \frac{-8.4457D + 10(s-100)s^4}{(s+5.3823D-01)(s-1.8924D-01 \pm j5.5047D-01)(s-5.8244D-01)(s+6.7985D-01)}$$

C.6 Plants for Maneuver #1121

$$q_{110} = \frac{1.4967D + 11(s-100)s^4}{(s-1.3462D-01 \pm j9.2905D-02)(s+1.6951D-01)(s+4.8278D-02 \pm j1.6635D-01)}$$

$$q_{120} = \frac{8.2255D + 07(s-100)s^4}{(s+3.7298D-01)(s-1.8845D-01 \pm j3.9281D-01)(s-4.6119D-01)(s-3.3663D+01)}$$

$$q_{130} = \frac{1.6768D + 11(s-100)s^4}{(s-1.2049D-01 \pm j8.4489D-02)(s+1.4804D-01)(s+4.5929D-02 \pm j1.4579D-01)}$$

$$q_{210} = \frac{-1.9360D + 04(s-100)s^4}{(s-1.0367D-01 \pm j6.3626D-02)(s+1.8576D-02 \pm j1.4237D-01)(s+1.6637D-01)}$$

$$q_{220} = \frac{-8.2440D-01(s-5.8696D-02)(s-5.8696D-02)(s-5.8696D-02)(s-5.8696D-02)(s-100)}{(s-9.7426D-02)(s-2.1409D-01)(s-1.9832D-02 \pm j5.2669D-01)(s+2.6699D+00)}$$

$$q_{230} = \frac{-1.5315D + 04(s-100)s^4}{(s-9.5920D-02 \pm j6.1540D-02)(s+2.2734D-02 \pm j1.2491D-01)(s+1.4253D-01)}$$

$$q_{310} = \frac{1.8669D + 11(s-100)s^4}{(s-2.5719D-01)(s-1.0268D-01 \pm j2.4691D-01)(s+2.3385D-01 \pm j2.0512D-01)}$$

$$q_{320} = \frac{3.7557D + 07(s-100)s^4}{(s-6.5234D-01)(s+2.1781D-02 \pm j7.0132D-01)(s+1.4590D+00)(s+2.9067D+01)}$$

$$q_{330} = \frac{4.3930D + 10(s-100)s^4}{(s-1.7860D-01)(s-6.7826D-02 \pm j1.7165D-01)(s+1.5600D-01 \pm j1.2606D-01)}$$

C.7 Plants for Maneuver #2121

$$q_{110} = \frac{1.0457D + 10(s-100)s^4}{(s-3.8048D-01 \pm j2.4671D-01)(s+2.3910D-02 \pm j4.8440D-01)(s+5.6082D-01)}$$

$$q_{120} = \frac{9.6582D + 07(s-100)s^4}{(s+4.1217D-01)(s+7.9362D-01 \pm j4.3930D-01)(s-3.7393D+00)(s+3.7669D+01)}$$

$$q_{130} = \frac{1.3278D + 11(s-100)s^4}{(s-6.0990D-01 \pm j4.1967D-01)(s+8.6477D-01)(s+3.7387D-01 \pm j8.3527D-01)}$$

$$q_{210} = \frac{4.8855D+03(s-100)s^4}{(s-3.0984D-01 \pm j2.0883D-01)(s+5.8771D-02 \pm j3.8353D-01)(s+4.8641D-01)}$$

$$q_{220} = \frac{-5.6243D-01(s-100)s^4}{(s+2.8094D-01 \pm j1.9574D-01)(s-8.5167D-01 \pm j9.9894D-01)(s+4.7258D+00)}$$

$$q_{230} = \frac{-1.5323D+04(s-100)s^4}{(s-5.4880D-01)(s-2.1775D-01 \pm j5.2094D-01)(s+4.9626D-01 \pm j3.5676D-01)}$$

$$q_{310} = \frac{4.9337D+09(s-100)s^4}{(s-2.5538D-01 \pm j1.6225D-01)(s+5.1558D-02 \pm j3.3548D-01)(s+4.0105D-01)}$$

$$q_{320} = \frac{-3.9581D+06(s-100)s^4}{(s+5.0865D-01)(s-9.8382D-01)(s+1.6700D+00 \pm j2.3878D-01)(s+1.2210D+01)}$$

$$q_{330} = \frac{-8.0893D+09(s-100)s^4}{(s+3.1565D-01 \pm j1.9473D-01)(s-3.7720D-01)(s-1.3841D-01 \pm j3.6805D-01)}$$

C.8 Plants for Maneuver #2122

$$q_{110} = \frac{4.9833D+09(s-100)s^4}{(s-1.2290D-01 \pm j8.5042D-02)(s+3.3480D-02 \pm j1.5659D-01)(s+1.7599D-01)}$$

$$q_{120} = \frac{-2.0187D+06(s-100)s^4}{(s+5.3494D-02 \pm j4.6898D-01)(s+5.7028D-01)(s+5.0125D-01 \pm j2.6525D+00)}$$

$$q_{130} = \frac{-3.0669D+10(s-100)s^4}{(s-2.7437D-01)(s-9.3901D-02 \pm j2.6477D-01)(s+2.2985D-01 \pm j1.6644D-01)}$$

$$q_{210} = \frac{1.1910D+04(s-100)s^4}{(s-4.5773D-01)(s-1.7627D-01 \pm j4.3156D-01)(s+4.1912D-01 \pm j2.7956D-01)}$$

$$q_{220} = \frac{-3.0259D-01(s-3.5025D-02)(s-3.5025D-02)(s-3.5025D-02)(s-3.5025D-02)(s-100)}{(s+7.4266D-01 \pm j2.0961D-01)(s-7.7948D-01)(s-1.4887D+00)(s+5.1650D+00)}$$

$$q_{230} = \frac{-5.0323D+04(s-100)s^4}{(s+7.8654D-01)(s-6.5125D-01 \pm j4.7236D-01)(s+2.9557D-01 \pm j7.7300D-01)}$$

$$q_{310} = \frac{-1.6100D+11(s-100)s^4}{(s-2.5813D-01 \pm j5.7440D-01)(s-6.3431D-01)(s+6.0260D-01 \pm j4.1533D-01)}$$

$$q_{320} = \frac{1.1678D+07(s-100)s^4}{(s-1.5055D-01)(s+5.6659D-01 \pm j1.4565D-01)(s-1.6793D+00)(s+2.9420D+01)}$$

$$q_{330} = \frac{-3.8532D+11(s-100)s^4}{(s-6.9427D-01)(s+6.0581D-01 \pm j3.7260D-01)(s-2.5319D-01 \pm j6.6831D-01)}$$

C.9 Plants for Maneuver #2123

$$q_{110} = \frac{1.0127D+11(s-100)s^4}{(s-1.8705D-01)(s-7.7698D-02\pm j1.8049D-01)(s+1.6965D-01\pm j1.4972D-01)}$$

$$q_{120} = \frac{-3.9092D+08(s-100)s^4}{(s+1.8317D-01\pm j1.7932D-01)(s-7.1004D-01\pm j3.8582D-01)(s-6.0134D+01)}$$

$$q_{130} = \frac{1.0475D+11(s-100)s^4}{(s-1.8723D-01)(s-7.8462D-02\pm j1.8074D-01)(s+1.7049D-01\pm j1.5106D-01)}$$

$$q_{210} = \frac{-2.1273D+05(s-100)s^4}{(s+6.8540D-01)(s-6.5060D-01\pm j4.9194D-01)(s+3.4984D-01\pm j8.0054D-01)}$$

$$q_{220} = \frac{-2.4343D-01(s-3.4094D-02)(s-3.4094D-02)(s-3.4094D-02)(s-3.4094D-02)(s-100)}{(s+2.1599D-01\pm j1.9200D-01)(s-4.6222D-01)(s-1.3968D+00)(s+4.5796D+00)}$$

$$q_{230} = \frac{-8.2463D+04(s-100)s^4}{(s+4.9404D-01)(s-4.9444D-01\pm j3.6849D-01)(s+2.7093D-01\pm j5.7567D-01)}$$

$$q_{310} = \frac{5.0013D+10(s-100)s^4}{(s-1.7591D-01)(s-1.1141D-01\pm j1.8284D-01)(s+1.9067D-01\pm j2.1025D-01)}$$

$$q_{320} = \frac{-7.2974D+06(s-100)s^4}{(s+3.0679D-01\pm j2.1726D-01)(s-4.2258D-01\pm j8.4324D-01)(s-1.1712D+01)}$$

$$q_{330} = \frac{5.0195D+10(s-100)s^4}{(s-1.6789D-01)(s-1.1431D-01\pm j1.7836D-01)(s+1.8960D-01\pm j2.1103D-01)}$$

C.10 Plants for Maneuver #2124

$$q_{110} = \frac{1.4580D+10(s-100)s^4}{(s-1.8730D-02)(s-1.0577D-01\pm j1.0159D-01)(s+1.1353D-01\pm j1.2783D-01)}$$

$$q_{120} = \frac{-1.0390D+08(s-100)s^4}{(s+2.0274D-01\pm j1.8702D-01)(s-7.0940D-01)(s-1.4348D+00)(s-2.2077D+01)}$$

$$q_{130} = \frac{1.5862D+10(s-100)s^4}{(s-3.7456D-02)(s-1.0089D-01\pm j1.0242D-01)(s+1.1791D-01\pm j1.3010D-01)}$$

$$q_{210} = \frac{-1.7328D+04(s-100)s^4}{(s+1.4567D-01\pm j4.4275D-01)(s-3.9898D-01\pm j2.8861D-01)(s+6.4283D-01)}$$

$$q_{220} = \frac{-3.3587D-01(s-1.3644D-01)(s-1.3644D-01)(s-1.3644D-01)(s-1.3644D-01)(s-100)}{(s+2.5185D-01\pm j1.2745D-01)(s-3.5860D-01)(s+9.1940D-01)(s-3.0459D+00)}$$

$$q_{230} = \frac{-1.7813D+04(s-100)s^4}{(s+1.4221D-01\pm j4.3835D-01)(s-3.9181D-01\pm j2.8206D-01)(s+6.4563D-01)}$$

$$q_{310} = \frac{7.1611D+09(s-100)s^4}{(s-3.2760D-02)(s-1.4603D-01\pm j1.3766D-01)(s+1.5355D-01\pm j1.9692D-01)}$$

$$q_{320} = \frac{-4.2072D+06(s-100)s^4}{(s+3.0922D-01\pm j2.9632D-01)(s-6.6991D-01)(s-3.0152D+00\pm j2.1593D+00)}$$

$$q_{330} = \frac{7.1559D+09(s-100)s^4}{(s-3.1979D-02)(s-1.4481D-01\pm j1.3512D-01)(s+1.5208D-01\pm j1.9660D-01)}$$

C.11 Plants for Maneuver #1131

$$q_{110} = \frac{6.9176D+10(s-100)s^4}{(s-1.3778D-01)(s-4.3416D-02\pm j1.3077D-01)(s+1.0966D-01\pm j9.1966D-02)}$$

$$q_{120} = \frac{9.2104D+07(s-100)s^4}{(s+1.0691D-01\pm j1.8877D-01)(s-3.1679D-01\pm j2.1725D-01)(s-7.6254D+01)}$$

$$q_{130} = \frac{9.5546D+10(s-100)s^4}{(s-1.2543D-01)(s-4.5232D-02\pm j1.1805D-01)(s+1.0678D-01\pm j9.4032D-02)}$$

$$q_{210} = \frac{-7.1332D+04(s-100)s^4}{(s+1.2209D-01)(s-3.2863D-01)(s-6.8061D-02\pm j3.4784D-01)(s+3.7690D-01)}$$

$$q_{220} = \frac{-8.5349D-01(s-3.8906D-02)(s-3.8906D-02)(s-3.8906D-02)(s-3.8906D-02)(s-100)}{(s-1.2964D-01)(s-4.2736D-01)(s+8.1542D-02\pm j7.6122D-01)(s+5.6592D+00)}$$

$$q_{230} = \frac{-3.9110D+04(s-100)s^4}{(s+3.3024D-01\pm j2.2082D-01)(s-4.1274D-01)(s-1.2529D-01\pm j3.9441D-01)}$$

$$q_{310} = \frac{1.2138D+11(s-100)s^4}{(s-2.6774D-01\pm j1.8095D-01)(s+3.2546D-01)(s+9.6848D-02\pm j3.5097D-01)}$$

$$q_{320} = \frac{1.7441D+08(s-100)s^4}{(s-3.0282D-01\pm j5.7234D-01)(s+6.9995D-01)(s-1.0075D+01\pm j1.1525D+01)}$$

$$q_{330} = \frac{6.3922D+10(s-100)s^4}{(s+2.4250D-01)(s-2.0216D-01\pm j1.4028D-01)(s+7.6068D-02\pm j2.4608D-01)}$$

C.12 Plants for Maneuver #2134

$$q_{110} = \frac{8.6624D+09(s-100)s^4}{(s-1.5740D-01)(s-6.6605D-02\pm j1.5118D-01)(s+1.4330D-01\pm j1.3204D-01)}$$

$$q_{120} = \frac{-1.3972D+08(s-100)s^4}{(s+2.1103D-01\pm j1.8624D-01)(s-7.8434D-01\pm j4.8328D-01)(s-5.0168D+01)}$$

$$q_{130} = \frac{1.1021D+10(s-100)s^4}{(s-1.4740D-01)(s-6.3321D-02\pm j1.4198D-01)(s+1.3537D-01\pm j1.2430D-01)}$$

$$q_{210} = \frac{9.8434D+03(s-100)s^4}{(s+3.6872D-01 \pm j3.0014D-01)(s-5.1884D-01)(s-1.5757D-01 \pm j5.0230D-01)}$$

$$q_{220} = \frac{-3.3909D-01(s-5.3926D-02)(s-5.3926D-02)(s-5.3926D-02)(s-5.3926D-02)(s-100)}{(s-2.2842D-01)(s+1.8474D-01 \pm j1.7786D-01)(s-1.9767D+00)(s+3.7740D+00)}$$

$$q_{230} = \frac{1.4643D+04(s-100)s^4}{(s+3.9070D-01 \pm j3.1725D-01)(s-5.3602D-01)(s-1.6671D-01 \pm j5.1710D-01)}$$

$$q_{310} = \frac{5.4599D+09(s-100)s^4}{(s-1.0967D-01)(s-1.1005D-01 \pm j1.3887D-01)(s+1.5777D-01 \pm j1.8459D-01)}$$

$$q_{320} = \frac{-4.1037D+06(s-100)s^4}{(s+2.4687D-01 \pm j2.2977D-01)(s-9.8941D-01 \pm j2.3693D-01)(s-7.2636D+00)}$$

$$q_{330} = \frac{8.4543D+09(s-100)s^4}{(s-8.7034D-03)(s-1.4456D-01 \pm j1.2889D-01)(s+1.4180D-01 \pm j1.8648D-01)}$$

C.13 Plants for Maneuver #1141

$$q_{110} = \frac{1.9415D+11(s-100)s^4}{(s-2.4266D-01 \pm j1.6285D-01)(s+2.9371D-01)(s+7.5519D-02 \pm j3.2063D-01)}$$

$$q_{120} = \frac{1.1435D+08(s-100)s^4}{(s+4.0762D-01)(s-2.4808D-01 \pm j4.9739D-01)(s-6.0617D-01)(s-1.3176D+02)}$$

$$q_{130} = \frac{3.8613D+11(s-100)s^4}{(s+2.6047D-01)(s-2.3558D-01 \pm j1.6108D-01)(s+9.1054D-02 \pm j3.0329D-01)}$$

$$q_{210} = \frac{-1.1686D+05(s-100)s^4}{(s-3.6304D-03)(s-8.9804D-01 \pm j7.3518D-01)(s+9.7001D-01 \pm j1.6560D+00)}$$

$$q_{220} = \frac{-8.4623D-01(s-100)s^4}{(s+4.0368D-01)(s-3.5426D-01 \pm j5.9990D-01)(s-7.6596D-01)(s+5.6342D+00)}$$

$$q_{230} = \frac{-1.2895D+05(s-100)s^4}{(s-3.6414D-01)(s+3.4713D-01 \pm j1.4006D-01)(s-1.3580D-01 \pm j3.5770D-01)}$$

$$q_{310} = \frac{7.2517D+10(s-100)s^4}{(s-2.7972D-01 \pm j1.8797D-01)(s+3.4702D-01)(s+9.3666D-02 \pm j3.6775D-01)}$$

$$q_{320} = \frac{2.7367D+07(s-100)s^4}{(s+5.3956D-01)(s-5.0012D-01 \pm j4.5010D-01)(s-4.4285D+00 \pm j5.6548D+00)}$$

$$q_{330} = \frac{7.9537D+10(s-100)s^4}{(s+2.8597D-01)(s-2.4047D-01 \pm j1.6513D-01)(s+9.0345D-02 \pm j2.9768D-01)}$$

C.14 Plants for Maneuver #2144

$$q_{110} = \frac{1.7056D+10(s-100)s^4}{(s-3.6149D-01)(s-1.1919D-01\pm j3.4635D-01)(s+2.9122D-01\pm j2.3130D-01)}$$

$$q_{120} = \frac{-1.3479D+07(s-100)s^4}{(s+2.9166D-01\pm j1.9896D-01)(s-3.1455D-01\pm j1.0596D+00)(s-7.5903D+00)}$$

$$q_{130} = \frac{4.2426D+10(s-100)s^4}{(s-3.7480D-01)(s-1.1982D-01\pm j3.5607D-01)(s+2.9917D-01\pm j2.4227D-01)}$$

$$q_{210} = \frac{8.5798D+03(s-100)s^4}{(s+4.2718D-01\pm j3.0871D-01)(s-5.7767D-01)(s-2.0096D-01\pm j5.6228D-01)}$$

$$q_{220} = \frac{-3.8187D-01(s-3.6384D-02)(s-3.6384D-02)(s-3.6384D-02)(s-3.6384D-02)(s-100)}{(s-1.7575D-01)(s+1.7196D-01\pm j1.7090D-01)(s-1.7507D+00)(s+6.1784D+00)}$$

$$q_{230} = \frac{4.9964D+04(s-100)s^4}{(s+4.9475D-01\pm j3.9365D-01)(s-7.2197D-01)(s-2.4607D-01\pm j6.9460D-01)}$$

$$q_{310} = \frac{1.0782D+10(s-100)s^4}{(s+1.7219D-01)(s-2.0682D-01\pm j1.5389D-01)(s+1.1134D-01\pm j2.4605D-01)}$$

$$q_{320} = \frac{-7.2518D+06(s-100)s^4}{(s+2.7400D-01\pm j1.9853D-01)(s-2.4595D-01\pm j6.3777D-01)(s-1.6295D+01)}$$

$$q_{330} = \frac{1.8414D+10(s-100)s^4}{(s+1.5304D-01)(s-1.9141D-01\pm j1.4520D-01)(s+1.0656D-01\pm j2.2413D-01)}$$

C.15 Plants for Maneuver #2211

$$q_{110} = \frac{-2.9501D+00(s-100)s^4}{(s+2.9358D-01)(s+1.5480D-01\pm j3.2042D-01)(s-1.2027D+00)(s-1.0018D+01)}$$

$$q_{120} = \frac{5.4786D-01(s-100)s^4}{(s+5.3125D-01)(s-5.1484D-01\pm j2.8692D-01)(s+3.0772D-01\pm j6.3867D-01)}$$

$$q_{130} = \frac{-2.7284D-01(s-100)s^4}{(s+3.1932D-01)(s+2.0343D-01\pm j3.2116D-01)(s-7.2340D-01\pm j5.5154D-01)}$$

$$q_{210} = \frac{-1.6251D+00(s-100)s^4}{(s+1.3075D-01)(s+3.0966D-01)(s-4.9152D-01\pm j1.7110D-01)(s+9.7227D+00)}$$

$$q_{220} = \frac{-1.4213D+00(s-100)s^4}{(s-2.4812D-02)(s-4.3214D-01\pm j1.6076D-01)(s+6.9982D-01\pm j5.8600D-01)}$$

$$q_{230} = \frac{5.9419D-01(s-100)s^4}{(s+3.4379D-01\pm j2.8974D-01)(s-8.0989D-01\pm j1.4731D-01)(s-8.3791D-01)}$$

$$q_{310} = \frac{-8.9112D-01(s-100)s^4}{(s+3.7669D-01 \pm j2.2868D-01)(s-1.0231D+00)(s+9.4073D-01 \pm j1.5585D+00)}$$

$$q_{320} = \frac{3.9907D-01(s-100)s^4}{(s-6.1337D-01)(s+4.4891D-01 \pm j4.3733D-01)(s-3.0287D-01 \pm j6.5823D-01)}$$

$$q_{330} = \frac{-1.2938D-01(s-100)s^4}{(s+3.4651D-01 \pm j2.2268D-01)(s-7.1375D-01)(s+6.4840D-02 \pm j7.1752D-01)}$$

C.16 Plants for Maneuver #2212

$$q_{110} = \frac{-2.5899D+00(s-100)s^4}{(s+1.5166D-01)(s+2.4715D-01 \pm j3.4495D-01)(s-1.3312D+00)(s-8.4688D+00)}$$

$$q_{120} = \frac{9.8973D-01(s-100)s^4}{(s+4.1611D-01)(s-5.5316D-01 \pm j2.5372D-01)(s+2.7090D-01 \pm j8.1237D-01)}$$

$$q_{130} = \frac{-3.1298D-01(s-100)s^4}{(s+1.3388D-01 \pm j4.5181D-01)(s+5.0277D-01)(s-8.3874D-01 \pm j5.7037D-01)}$$

$$q_{210} = \frac{-3.3921D+00(s-100)s^4}{(s-2.6976D-01)(s+2.7623D-01 \pm j3.1898D-01)(s-8.3517D-01)(s+1.9205D+01)}$$

$$q_{220} = \frac{-9.2455D-01(s-100)s^4}{(s+3.9286D-01)(s-6.0145D-01 \pm j3.4276D-01)(s+2.6365D-01 \pm j7.3212D-01)}$$

$$q_{230} = \frac{1.1253D+00(s-100)s^4}{(s-3.3283D-02 \pm j5.8464D-01)(s+6.2088D-01)(s-1.3179D+00)(s-2.3133D+00)}$$

$$q_{310} = \frac{-7.2723D-01(s-100)s^4}{(s+4.0604D-01 \pm j3.9317D-01)(s-6.3725D-01)(s+5.3457D-01 \pm j1.4046D+00)}$$

$$q_{320} = \frac{4.7806D-01(s-100)s^4}{(s+1.7766D-01)(s+1.3684D-01 \pm j5.3055D-01)(s-5.6541D-01 \pm j3.3676D-01)}$$

$$q_{330} = \frac{-1.5160D-01(s-100)s^4}{(s-3.6869D-01 \pm j2.6408D-01)(s+5.5957D-01)(s+4.9157D-02 \pm j6.6485D-01)}$$

C.17 Plants for Maneuver #2213

$$q_{110} = \frac{-2.4836D+00(s-100)s^4}{(s+1.2980D-01)(s+2.4176D-01 \pm j3.4535D-01)(s-1.4052D+00)(s-7.4094D+00)}$$

$$q_{120} = \frac{1.8237D+00(s-100)s^4}{(s+2.8421D-01)(s-6.0401D-01 \pm j1.4894D-01)(s+5.7848D-02 \pm j9.9416D-01)}$$

$$q_{130} = \frac{-3.3050D-01(s-100)s^4}{(s+1.1351D-01 \pm j4.5473D-01)(s+5.0086D-01)(s-8.3174D-01 \pm j5.6753D-01)}$$

$$q_{210} = \frac{-4.0889D+00(s-100)s^4}{(s+2.7891D-01 \pm j3.3279D-01)(s-4.5009D-01)(s-8.0759D-01)(s+2.0496D+01)}$$

$$q_{220} = \frac{-8.1639D-01(s-100)s^4}{(s+2.2160D-01)(s-6.1207D-01 \pm j2.8582D-01)(s+1.3478D-01 \pm j6.6846D-01)}$$

$$q_{230} = \frac{1.1498D+00(s-100)s^4}{(s+6.2583D-01)(s-8.8051D-02 \pm j6.2744D-01)(s-1.6361D+00 \pm j3.3446D-01)}$$

$$q_{310} = \frac{-6.9867D-01(s-100)s^4}{(s-5.6096D-01)(s+5.0085D-01 \pm j5.2446D-01)(s+4.2774D-01 \pm j1.3615D+00)}$$

$$q_{320} = \frac{7.2019D-01(s-100)s^4}{(s+2.3748D-01)(s+1.9002D-02 \pm j6.2491D-01)(s-8.3132D-01 \pm j1.8606D-01)}$$

$$q_{330} = \frac{-1.6282D-01(s-100)s^4}{(s+6.6606D-01)(s-5.0197D-01 \pm j4.4413D-01)(s+9.6755D-02 \pm j7.1600D-01)}$$

C.18 Plants for Maneuver #2221

$$q_{110} = \frac{-1.9429D+00(s-100)s^4}{(s+4.8464D-01)(s+6.5580D-02 \pm j4.8102D-01)(s-1.0495D+00)(s-6.8396D+00)}$$

$$q_{120} = \frac{1.1889D+00(s-100)s^4}{(s-8.7530D-02 \pm j5.1270D-01)(s+5.4148D-01 \pm j5.2092D-01)(s-7.8964D-01)}$$

$$q_{130} = \frac{-4.9646D-01(s-1.9606D-04)(s-1.9606D-04)(s-1.9606D-04)(s-1.9606D-04)(s-100)}{(s-5.2071D-01 \pm j3.9405D-01)(s+5.1564D-01 \pm j4.3131D-01)(s-1.5883D+00)}$$

$$q_{210} = \frac{-7.4804D+00(s-100)s^4}{(s+1.7820D-02 \pm j3.8243D-01)(s+4.1368D-01)(s-9.8501D-01)(s+3.7775D+01)}$$

$$q_{220} = \frac{-2.7257D+01(s-100)s^4}{(s-1.2744D-01 \pm j2.2370D-01)(s-1.2106D+00)(s+1.4476D+00)(s+4.1752D+00)}$$

$$q_{230} = \frac{1.0665D+00(s-2.3429D-04)(s-2.3429D-04)(s-2.3429D-04)(s-2.3429D-04)(s-100)}{(s+4.6983D-01 \pm j3.9925D-01)(s-6.3426D-01 \pm j2.5682D-01)(s-2.6675D+00)}$$

$$q_{310} = \frac{-8.6710D-01(s-5.7000D-04)(s-5.7000D-04)(s-5.7000D-04)(s-5.7000D-04)(s-100)}{(s-4.5966D-01)(s+3.9878D-01 \pm j7.7992D-01)(s+1.8366D+00 \pm j5.4867D-01)}$$

$$q_{320} = \frac{1.0004D+00(s-8.2390D-04)(s-8.2390D-04)(s-8.2390D-04)(s-8.2390D-04)(s-100)}{(s+7.5609D-01)(s+1.6870D-01 \pm j8.3113D-01)(s-1.0968D+00 \pm j5.3846D-01)}$$

$$q_{330} = \frac{-2.8313D-01(s-6.0021D-04)(s-6.0021D-04)(s-6.0021D-04)(s-6.0021D-04)(s-100)}{(s-5.9992D-01 \pm j5.9995D-01)(s+9.8471D-01)(s+2.9751D-01 \pm j1.1501D+00)}$$

C.19 Plants for Maneuver #2222

$$q_{110} = \frac{-1.8153D+00(s-100)s^4}{(s+5.4143D-01)(s+5.7060D-02\pm j5.5880D-01)(s-9.5234D-01)(s-7.1895D+00)}$$

$$q_{120} = \frac{3.0840D+00(s-100)s^4}{(s+6.7089D-03\pm j4.7012D-01)(s-8.7928D-01)(s+6.6129D-01\pm j8.1758D-01)}$$

$$q_{130} = \frac{-5.9350D-01(s-100)s^4}{(s+5.7275D-01\pm j4.8794D-01)(s-5.5126D-01\pm j5.1732D-01)(s-2.0234D+00)}$$

$$q_{210} = \frac{-1.1314D+01(s-1.6440D-04)(s-1.6440D-04)(s-1.6440D-04)(s-1.6440D-04)(s-100)}{(s+2.9263D-01)(s+8.8330D-02\pm j3.5541D-01)(s-1.3611D+00)(s+4.8439D+01)}$$

$$q_{220} = \frac{4.6105D+00(s-100)s^4}{(s+3.3577D-01)(s-6.9475D-01)(s-4.6729D-01\pm j9.2394D-01)(s+1.5515D+00)}$$

$$q_{230} = \frac{9.7390D-01(s-8.3346D-04)(s-8.3346D-04)(s-8.3346D-04)(s-8.3346D-04)(s-100)}{(s-5.9821D-02)(s+2.7710D-01\pm j2.1951D-01)(s-1.1653D+00)(s-2.1161D+00)}$$

$$q_{310} = \frac{-8.7081D-01(s-8.1004D-04)(s-8.1004D-04)(s-8.1004D-04)(s-8.1004D-04)(s-100)}{(s-4.5359D-01)(s+3.7490D-01\pm j8.6870D-01)(s+1.6623D+00)(s+1.9444D+00)}$$

$$q_{320} = \frac{2.4924D+00(s-3.0869D-04)(s-3.0869D-04)(s-3.0869D-04)(s-3.0869D-04)(s-100)}{(s+5.6202D-01)(s+2.4557D-01\pm j9.0280D-01)(s-1.2320D+00\pm j4.6016D-01)}$$

$$q_{330} = \frac{-3.0220D-01(s-8.5464D-04)(s-8.5464D-04)(s-8.5464D-04)(s-8.5464D-04)(s-100)}{(s-6.8546D-01\pm j6.6713D-01)(s+9.6862D-01)(s+2.1744D-01\pm j1.0850D+00)}$$

C.20 Plants for Maneuver #2223

$$q_{110} = \frac{-1.7234D+00(s-100)s^4}{(s+5.2838D-01)(s+5.3049D-02\pm j5.5240D-01)(s-9.2115D-01)(s-7.0739D+00)}$$

$$q_{120} = \frac{9.8879D+00(s-100)s^4}{(s-4.8765D-02\pm j4.8385D-01)(s-9.0839D-01)(s+1.4761D+00\pm j1.0698D+00)}$$

$$q_{130} = \frac{-6.6338D-01(s-1.6962D-04)(s-1.6962D-04)(s-1.6962D-04)(s-1.6962D-04)(s-100)}{(s+5.6377D-01\pm j4.9117D-01)(s-5.5530D-01\pm j5.3013D-01)(s-2.0673D+00)}$$

$$q_{210} = \frac{-6.6391D+00(s-100)s^4}{(s-1.8123D-01)(s+2.8650D-01\pm j3.5880D-01)(s-2.1744D+00)(s+2.2337D+01)}$$

$$q_{220} = \frac{2.4116D+00(s-7.8559D-04)(s-7.8559D-04)(s-7.8559D-04)(s-7.8559D-04)(s-100)}{(s+2.9987D-01)(s-3.5740D-01\pm j7.0765D-01)(s-8.4512D-01)(s+1.9090D+00)}$$

$$q_{230} = \frac{5.6123D-01(s-100)s^4}{(s-3.5992D-02\pm j6.8443D-01)(s+6.9204D-01)(s-1.0879D+00\pm j8.1422D-01)}$$

$$q_{310} = \frac{-8.4949D-01(s-1.9314D-03)(s-1.9314D-03)(s-1.9314D-03)(s-1.9314D-03)(s-100)}{(s-4.3908D-01)(s+3.6764D-01\pm j9.1963D-01)(s+1.5038D+00\pm j4.8878D-01)}$$

$$q_{320} = \frac{3.8943D+01(s-1.9607D-04)(s-1.9607D-04)(s-1.9607D-04)(s-1.9607D-04)(s-100)}{(s+4.3615D-01)(s-6.8584D-01\pm j6.5499D-01)(s+4.7205D+00\pm j8.1603D-01)}$$

$$q_{330} = \frac{-3.3028D-01(s-2.0247D-03)(s-2.0247D-03)(s-2.0247D-03)(s-2.0247D-03)(s-100)}{(s+9.3895D-01)(s-7.1954D-01\pm j6.7683D-01)(s+1.7859D-01\pm j1.0206D+00)}$$

C.21 Plants for Maneuver #2231

$$q_{110} = \frac{-1.6659D+00(s-100)s^4}{(s+5.5673D-01)(s+6.3690D-02\pm j5.6408D-01)(s-2.1193D+00\pm j8.1130D-01)}$$

$$q_{120} = \frac{1.8277D-01(s-100)s^4}{(s+3.2424D-01\pm j3.1969D-01)(s-1.4649D-01\pm j5.4278D-01)(s-5.8115D-01)}$$

$$q_{130} = \frac{-2.0241D+00(s-100)s^4}{(s-5.5387D-01\pm j5.0423D-01)(s+5.6086D-01\pm j5.1703D-01)(s-9.1929D+00)}$$

$$q_{210} = \frac{4.1793D+00(s-100)s^4}{(s+9.3083D-02\pm j4.3554D-01)(s+4.8704D-01)(s-2.7577D+00\pm j3.2948D+00)}$$

$$q_{220} = \frac{-1.1283D-01(s-100)s^4}{(s-8.4966D-02)(s+2.2962D-01)(s+1.4893D-02\pm j3.0901D-01)(s-3.2371D-01)}$$

$$q_{230} = \frac{1.4181D+00(s-100)s^4}{(s+5.9598D-01\pm j5.1336D-01)(s-8.3126D-01)(s-9.6849D-01\pm j1.0950D+00)}$$

$$q_{310} = \frac{-1.7054D+00(s-100)s^4}{(s+4.7591D-01\pm j3.6567D-01)(s+5.5503D-03\pm j6.8670D-01)(s+1.0620D+01)}$$

$$q_{320} = \frac{1.5536D-01(s-100)s^4}{(s+3.0814D-01)(s-3.8032D-01\pm j1.2136D-01)(s+4.5767D-02\pm j4.8103D-01)}$$

$$q_{330} = \frac{-3.6350D-01(s-100)s^4}{(s+5.6846D-01\pm j4.8479D-01)(s-7.9908D-01)(s-6.2478D-01\pm j9.7950D-01)}$$

C.22 Plants for Maneuver #2232

$$q_{110} = \frac{-1.7635D+00(s-100)s^4}{(s+5.4482D-01)(s+8.3398D-02\pm j5.3869D-01)(s-2.1819D+00\pm j1.3429D+00)}$$

$$q_{120} = \frac{2.0800D-01(s-100)s^4}{(s+2.4733D-01\pm j3.1411D-01)(s-1.3113D-01\pm j4.9923D-01)(s-5.2576D-01)}$$

$$q_{130} = \frac{-2.1482D+00(s-100)s^4}{(s+5.5586D-01\pm j5.2153D-01)(s-5.9416D-01\pm j5.1535D-01)(s-8.1645D+00)}$$

$$q_{210} = \frac{6.4792D+00(s-100)s^4}{(s+8.5057D-02 \pm j5.1043D-01)(s+5.5657D-01)(s+3.1834D+00 \pm j5.1336D+00)}$$

$$q_{220} = \frac{-8.1208D-02(s-100)s^4}{(s+2.5513D-01)(s-2.4239D-01 \pm j1.1628D-01)(s+1.5070D-02 \pm j3.2493D-01)}$$

$$q_{230} = \frac{5.0114D-01(s-100)s^4}{(s-7.2056D-01)(s+6.2954D-01 \pm j5.3310D-01)(s-4.1589D-01 \pm j1.1313D+00)}$$

$$q_{310} = \frac{-1.9567D+00(s-100)s^4}{(s+4.9735D-01 \pm j4.1525D-01)(s-4.9046D-02 \pm j7.4676D-01)(s+1.0925D+01)}$$

$$q_{320} = \frac{2.3449D-01(s-100)s^4}{(s+1.3332D-01 \pm j1.8243D-01)(s-1.7893D-01 \pm j5.0203D-01)(s-5.9489D-01)}$$

$$q_{330} = \frac{-3.7080D-01(s-100)s^4}{(s+6.3141D-01 \pm j5.3781D-01)(s-9.4434D-01)(s-6.0229D-01 \pm j9.9720D-01)}$$

C.23 Plants for Maneuver #2233

$$q_{110} = \frac{-2.0445D+00(s-100)s^4}{(s+4.0216D-01)(s+7.4807D-02 \pm j4.0424D-01)(s-1.3154D+00)(s-5.1161D+00)}$$

$$q_{120} = \frac{5.5022D-01(s-100)s^4}{(s+1.4265D-01)(s-3.2580D-01 \pm j1.4363D-01)(s-1.4795D-02 \pm j5.5365D-01)}$$

$$q_{130} = \frac{-2.3115D+00(s-100)s^4}{(s+4.7614D-01 \pm j4.4189D-01)(s-5.2085D-01 \pm j4.2885D-01)(s-4.6728D+00)}$$

$$q_{210} = \frac{-1.6518D+01(s-100)s^4}{(s+3.8575D-01)(s+7.1754D-02 \pm j4.3190D-01)(s+2.6261D+00)(s-3.9335D+01)}$$

$$q_{220} = \frac{-6.5733D-02(s-100)s^4}{(s+2.9407D-01)(s+9.9098D-02 \pm j3.9090D-01)(s-3.4419D-01 \pm j2.4331D-01)}$$

$$q_{230} = \frac{2.5835D-01(s-100)s^4}{(s-4.6617D-01)(s+4.2696D-01 \pm j3.5597D-01)(s-3.9106D-01 \pm j7.3085D-01)}$$

$$q_{310} = \frac{-2.0162D+00(s-100)s^4}{(s+3.8203D-01 \pm j2.9765D-01)(s-7.0477D-02 \pm j7.3070D-01)(s+6.9898D+00)}$$

$$q_{320} = \frac{6.0994D-01(s-100)s^4}{(s+3.0264D-01)(s-2.4402D-02 \pm j5.2853D-01)(s-7.1405D-01 \pm j2.8199D-01)}$$

$$q_{330} = \frac{-4.7134D-01(s-100)s^4}{(s-6.3307D-01)(s+5.1576D-01 \pm j4.1246D-01)(s-4.2714D-01 \pm j7.4643D-01)}$$

C.24 Plants for Maneuver #2241

$$q_{110} = \frac{-2.2838D+00(s-100)s^4}{(s+5.4240D-01)(s+8.4502D-02\pm j5.4508D-01)(s-1.2484D+00)(s-5.5330D+00)}$$

$$q_{120} = \frac{4.1359D-01(s-100)s^4}{(s+2.5247D-01\pm j3.5781D-01)(s-3.6976D-01\pm j6.7396D-01)(s-8.6179D-01)}$$

$$q_{130} = \frac{-1.1434D+01(s-100)s^4}{(s-5.3552D-01\pm j5.1478D-01)(s+5.5859D-01\pm j5.2841D-01)(s-5.5250D+01)}$$

$$q_{210} = \frac{1.5339D+01(s-100)s^4}{(s+9.3075D-02\pm j4.8177D-01)(s+5.6289D-01)(s-2.3069D+00)(s-2.0711D+01)}$$

$$q_{220} = \frac{-1.8749D-01(s-100)s^4}{(s+2.3289D-01\pm j2.4899D-01)(s-2.0736D-01\pm j4.6028D-01)(s-6.1100D-01)}$$

$$q_{230} = \frac{1.4223D+00(s-100)s^4}{(s+7.1731D-01\pm j5.8610D-01)(s-6.9190D-01\pm j9.1213D-01)(s-1.4384D+00)}$$

$$q_{310} = \frac{-3.3945D+00(s-100)s^4}{(s+5.2628D-01\pm j4.5915D-01)(s-1.9237D-01\pm j7.9848D-01)(s+1.4214D+01)}$$

$$q_{320} = \frac{3.3419D-01(s-100)s^4}{(s+2.8686D-01\pm j3.4867D-01)(s-3.1628D-01\pm j6.5375D-01)(s-9.6510D-01)}$$

$$q_{330} = \frac{-4.1208D-01(s-100)s^4}{(s+7.1871D-01\pm j6.0533D-01)(s-6.2985D-01\pm j9.7036D-01)(s-1.4006D+00)}$$

C.25 Plants for Maneu #2242

$$q_{110} = \frac{-2.0808D+00(s-100)s^4}{(s+5.2832D-01)(s+9.2051D-02\pm j5.2770D-01)(s-1.1824D+00)(s-5.9138D+00)}$$

$$q_{120} = \frac{6.2113D-01(s-100)s^4}{(s+1.8884D-01\pm j3.3203D-01)(s-4.5737D-01\pm j4.3776D-01)(s-1.9648D+00)}$$

$$q_{130} = \frac{1.8547D+00(s-100)s^4}{(s-5.3147D-01\pm j4.9299D-01)(s+5.4766D-01\pm j5.4127D-01)(s+8.7612D+00)}$$

$$q_{210} = \frac{3.0695D+01(s-100)s^4}{(s+7.3981D-02\pm j6.1777D-01)(s+6.8875D-01)(s-3.4002D+00\pm j1.0688D+01)}$$

$$q_{220} = \frac{-1.9126D-01(s-100)s^4}{(s+2.3500D-01\pm j2.7232D-01)(s-3.3875D-01\pm j4.6851D-01)(s-9.7473D-01)}$$

$$q_{230} = \frac{8.3405D-01(s-100)s^4}{(s+7.7683D-01\pm j6.5046D-01)(s-7.1994D-01\pm j1.0439D+00)(s-1.4920D+00)}$$

$$q_{310} = \frac{-3.0455D + 00(s - 100)s^4}{(s + 5.2659D - 01 \pm j4.8198D - 01)(s - 2.8582D - 01 \pm j8.7598D - 01)(s + 1.0278D + 01)}$$

$$q_{320} = \frac{5.3681D - 01(s - 100)s^4}{(s + 2.5098D - 01 \pm j3.4695D - 01)(s - 4.7938D - 01 \pm j5.5161D - 01)(s - 1.7541D + 00)}$$

$$q_{330} = \frac{-5.4511D - 01(s - 100)s^4}{(s + 7.3979D - 01 \pm j6.3399D - 01)(s - 6.9379D - 01 \pm j9.3224D - 01)(s - 1.7872D + 00)}$$

C.26 Plants for Maneuver #2243

$$q_{110} = \frac{-2.0490D + 00(s - 100)s^4}{(s + 4.4250D - 01)(s + 8.4514D - 02 \pm j4.4206D - 01)(s - 1.0527D + 00)(s - 6.6044D + 00)}$$

$$q_{120} = \frac{1.1573D + 00(s - 100)s^4}{(s + 8.0794D - 02 \pm j2.9236D - 01)(s - 3.6507D - 01 \pm j3.0765D - 01)(s - 2.8841D + 00)}$$

$$q_{130} = \frac{1.3447D + 00(s - 100)s^4}{(s - 5.1752D - 01 \pm j4.5259D - 01)(s + 5.1816D - 01 \pm j5.4443D - 01)(s + 3.6340D + 00)}$$

$$q_{210} = \frac{-1.1037D + 01(s - 100)s^4}{(s + 2.0853D - 02 \pm j5.5109D - 01)(s + 5.8328D - 01)(s + 3.4445D + 00)(s - 1.4437D + 01)}$$

$$q_{220} = \frac{-1.8376D - 01(s - 100)s^4}{(s + 1.5931D - 01 \pm j2.4509D - 01)(s - 3.1062D - 01 \pm j2.9209D - 01)(s - 1.2132D + 00)}$$

$$q_{230} = \frac{3.6486D - 01(s - 100)s^4}{(s + 6.6048D - 01 \pm j5.3166D - 01)(s - 9.5007D - 01)(s - 4.2695D - 01 \pm j8.9941D - 01)}$$

$$q_{310} = \frac{-2.9339D + 00(s - 100)s^4}{(s + 4.6804D - 01 \pm j4.3771D - 01)(s - 4.0220D - 01 \pm j8.3156D - 01)(s + 7.2709D + 00)}$$

$$q_{320} = \frac{1.0281D + 00(s - 100)s^4}{(s + 1.9814D - 01 \pm j3.3401D - 01)(s - 4.3570D - 01 \pm j3.8085D - 01)(s - 2.9013D + 00)}$$

$$q_{330} = \frac{-6.5987D - 01(s - 100)s^4}{(s + 7.4399D - 01 \pm j6.1021D - 01)(s - 5.5780D - 01 \pm j9.5914D - 01)(s - 1.3582D + 00)}$$

Appendix D. **Full Order G's**

This appendix includes full order G's developed in Chapter 6 for all FCS's

G's for FCS#1

$$g_{11(0)} = \left(\frac{1.2787D-03(s-5.1168D-01 \pm j-3.2726D-01)(s-2.7356D-02 \pm j6.0847D-01)}{s^4}\right)$$

$$\left(\frac{(s-1.5000D+00)(s-5.0000D+02)}{(s-1.0000D+00)(s-1.0000D+02)(s-1.8000D+02)(s-1.2000D+03 \pm j1.6000D+03)}\right)$$

$$\left(\frac{1}{(s-1.2000D+03 \pm j-1.6000D+03)}\right)$$

$$g_{22(1)} = \left(\frac{-1.3037D+10(s+4.7364D-01)(s-6.8060D-01)(s-2.8766D-01 \pm j-7.6561D-01)}{s^4}\right)$$

$$\left(\frac{(s+2.2818D+00)(s-5)(s-3.0821D+02 \pm j4.3257D+02)}{(s+8.1580D-01)(s-7.0000D+00)(s-1.0000D+02)(s-2.8207D+02 \pm j4.0795D+02)}\right)$$

$$\left(\frac{(s-9.7937D+02 \pm j-1.4039D+03)}{(s-2.8207D+02 \pm j-4.0795D+02)(s-1.0071D+03 \pm j-1.4252D+03)}\right)$$

$$\left(\frac{1}{(s-4.0000D+03 \pm j9.1652D+03)}\right)$$

$$g_{33(2)} = \left(\frac{6.4216D-01(s-5.4229D-02 \pm j2.9825D-02)(s-2.5359D-01 \pm j1.8071D-01)}{s^4}\right)$$

$$\left(\frac{(s-3.0000D-01 \pm j9.5394D-01)(s-6.0000D-01 \pm j-1.9079D+00)}{(s-6.2273D-02 \pm j9.4181D-02)(s-1.0000D+00)(s-2.2500D+00 \pm j-1.0897D+00)}\right)$$

$$\left(\frac{(s-1.5000D+01)(s-9.0000D+01)(s-6.2909D+02)(s-8.5720D+01 \pm j1.6993D+03)}{(s-2.2500D+00 \pm j1.0897D+00)(s-5.5000D+01)(s-1.0000D+02)}\right)$$

$$\left(\frac{(s-8.5720D+01 \pm j-1.6993D+03)(s-1.7780D+03)}{(s-3.0821D+02 \pm j-4.3257D+02)(s-9.0001D+02)(s-1.0072D+03 \pm j1.4252D+03)}\right)$$

$$\left(\frac{1}{(s-1.2000D+03 \pm j-1.6000D+03)}\right)$$

G's for FCS#2

$$g_{11(0)} = \left(\frac{-7.5610D+05(s-3.0000D-01 \pm j9.5394D-01)(s-1.2027D+00)(s-1.0018D+01)}{s^4}\right)$$

$$\left(\frac{1}{(s-1.0000D+02)(s-1.0000D+02 \pm j-1.7321D+02)}\right)$$

$$g_{22(1)} = \left(\frac{-2.6539D+08(s-2.4966D-02)(s-4.3214D-01 \pm j1.6076D-01)(s-3.0000D-01 \pm j9.5394D-01)}{s^4}\right)$$

$$\left(\frac{(s-3.0000D-01 \pm j-9.5394D-01)(s-1.1859D+00)(s-1.5000D+01)}{(s-5.0000D-01)(s-1.2027D+00)(s-1.0003D+01)(s-1.0015D+01)}\right)$$

$$\left(\frac{(s-1.2946D+01 \pm j-1.3229D+01)(s-4.8346D+02 \pm j-8.5657D+02)}{(s-3.5000D+01)(s-2.2375D+02)(s-3.8752D+02 \pm j8.2171D+02)}\right)$$

$$\left(\frac{1}{(s-1.2000D+03 \pm j-9.0000D+02)}\right)$$

G for FCS#21

$$g_{33(2)} = \left(\frac{3.9150D+09(s-5.0197D-01 \pm j-4.4413D-01)(s-9.0000D-01 \pm j-4.3589D-01)}{s^4}\right)$$

$$\left(\frac{(s-4.5000D+00 \pm j2.1794D+00)(s-7.3239D+00)(s-1.1168D+02 \pm j-4.1343D+01)}{(s-1.0000D+00)(s-1.0833D+01)(s-5.6392D+01)(s-8.3320D+01 \pm j-5.3314D+01)}\right)$$

$$\left(\frac{(s-1.1168D+02 \pm j4.1343D+01)(s-1.2154D+02 \pm j1.9180D+02)}{(s-8.3320D+01 \pm j5.3314D+01)(s-1.0000D+02)(s-7.8557D+01 \pm j-1.6310D+02)}\right)$$

$$\left(\frac{1}{(s-1.2000D+03 \pm j1.6000D+03)}\right)$$

G for FCS#22

$$g_{33(2)} = \left(\frac{-1.0978D+06(s-9.2200D-01 \pm j-1.0618D-01)(s-5.4238D-01 \pm j1.0705D+00)}{s^4}\right)$$

$$\left(\frac{(s-4.5000D+00 \pm j2.1795D+00)(s-1.4598D+01)(s-2.2094D+01 \pm j-3.2387D+00)}{(s-1.0000D+00)(s-1.1922D+00)(s-1.8758D+01 \pm j-4.3555D+00)}\right)$$

$$\left(\frac{(s-2.2094D+01 \pm j3.2387D+00)(s-3.4106D+01)}{(s-2.2848D+01)(s-2.3644D+01)(s-1.0170D+02)(s-3.0000D+01 \pm j1.4697D+02)}\right)$$

$$\left(\frac{1}{(s-3.0000D+01 \pm j-1.4677D+02)}\right)$$

G for FCS#23

$$g_{33(2)} = \left(\frac{-1.6589D+16(s-2.2036D-02)(s-7.1634D-01)(s-3.0000D-01\pm j-9.5394D-01)}{s^4}\right)$$

$$\left(\frac{(s-7.4901D+00)(s-3.0000D+00\pm j-9.5394D+00)(s-2.0000D+01)}{(s-2.5324D-02)(s-1.0000D+00)(s-1.0018D+01)(s-2.7825D+01\pm j-4.5541D+01)}\right)$$

$$\left(\frac{(s-3.0000D+01)(s-9.0749D+01\pm j1.6102D+02)}{(s-2.7825D+01\pm j4.5541D+01)(s-7.1143D+01)(s-6.3827D+01\pm j1.6311D+02)}\right)$$

$$\left(\frac{1}{(s-5.0000D+03)(s-1.0200D+04\pm j-1.3600D+04)}\right)$$

Appendix E. **Prefilters**

This appendix includes all of the prefilters used in this thesis.

F's for FCS#1

$$f_{11(0)} = \frac{0.01(s+400)}{(s+4)}$$

$$f_{22(1)} = \frac{0.1(s+50)}{(s+5)}$$

$$f_{33(2)} = \frac{(0.05(s+80)}{(s+4)}$$

F's for FCS#2

$$f_{11(0)} = \frac{0.05(s+100)}{(s+5)}$$

$$f_{22(1)} = \frac{5}{(s+5)}$$

F for FCS#21

$$f_{33(2)} = \frac{5}{(s+5)}$$

F for FCS#22

$$f_{33(2)} = \frac{0.04(s+100)}{(s+4)}$$

F for FCS#23

$$f_{33(2)} = \frac{4}{(s+4)}$$

Bibliography

1. Anderson, Capt Joseph A. "Agile Fighter Aircraft Simulation." *AIAA 27th Aerospace Sciences Meeting*. January 1989.

2. Barfield, Finley, A., "Head Contol Engineer AFTI/F-16. Personal Interviews. ." Flight Dynamics Directorate, Wright Labs, Wright-Patterson AFB, OH, April 1991 through October 1991.

3. Capone, Francis J. and Mason, Mary L. *Multiaxis Aircraft Control Power from Thrust Vectoring at High Angles of Attack*. Technical Report NASA-TM-87741, NASA, June 1986.

4. Cord, Thomas, "Personal Interviews. ." Flight Dynamics Directorate, Wright Labs, Wright-Patterson AFB, OH, April 1991 through August 1991.

5. D'Azzo, John J. and Constantine H. Houpis. *Linear Control System Analysis & Design —Conventional and Modern* (Third Edition). McGraw-Hill, 1988.

6. Hodgkinson, J. et al. "Relationships Between Flying Qualities, Transient Agility, and Operational Effectiveness of fighter Aircraft." *AAIA Atmospheric Flifgt Mechanics Conference*. August 1988.

7. Horowitz, Isaac. "Improved Design Technique For Uncertain Multiple-Input-Multiple-Output Feedback Systems," *International Journal of Control, Vol. 36*(No. 6):pp 977-988 (1982).

8. Horowitz, Isaac. and Yaniv, Oded. "Quantitative Cascaded Multiple-Input Multiple-Output Synthesis by an Improved Method," *International Journal of Control, Vol. 42*(No. 2):pp 305-331 (1985).

9. Horowitz, Isaac M., "Personal Conversation and Correspondance." Distinguished Visiting Professor of Electrical Engineering, Air Force Institute of Technology, Wright-Patterson AFB, OH, May 1991 through December 1991.

10. Houpis, Constantine H., "Personal Conversation, Correspondance and Class Notes." Professor of Electrical Engineering, Air Force Institute of Technology, Wright-Patterson AFB, OH, May 1990 through December 1991.

11. Houpis, Constantine H. *Quantitative Feedback Theory (QFT)—Technique for Designing Multivariable Control Systems*. Technical Report AFWAL-TR-86-3107, Wright-Patterson AFB, OH: Flight Dynamics Laboratory, January 1987.

12. Kobylarz, Lt Thomas J. *Flight Controller Design with Nonlinear Aerodynamics, Large Parameter Uncertainty, and Pilot Compensation*. MS thesis, Air Force Institute of Technology, Wright-Patterson AFB, OH, December 1988.

13. Lacey, Capt Donald J. *A Robust Digital Flight Control System for an Unmanned Research Vehicle Using Discrete Quantitative Feedback Theory.* MS thesis, Air Force Institute of Technology, Wright-Patterson AFB, OH, December 1991.

14. Ljung, Lennart and Söderström, Torsten. *Theory and Practice of Recursive Identification.* The MIT Press, 1983.

15. Pro-Matlab User's Guide, The Math Works Inc., South Natick, MA, 01760.

16. Matrix_x CAD/CAE Program, Integrated Systems Inc., Santa Clara, CA, 95054-1215.

17. Military Specification—Flying Qualities of Piloted Aircraft. MIL-STD-1797A. 30 January 1990.

18. Miller, Lt Russel B. *Multi-Input Multi-Output Flight Control System Design for the YF-16 using Nonlinear QFT and Pilot Compensation.* MS thesis, Air Force Institute of Technology, Wright-Patterson AFB, OH, December 1990.

19. Nguyen, Luat T and William P Gilbert. "Impact of Emerging Technologies on Future Combat Aircraft Agility." *AAIA/SFTE/DGLR/SETP Fifth Biannual Flight Test Conference.* May 1990.

20. Sating, Richard R, "Student. Personal Interviews. ." Air Force Institute of Technology, Wright-Patterson AFB, OH, June 1991.

21. Tamrat, B. F. "Fighter Aircraft Agility Assessment Concepts and Their Implication on Future Agile Fighter Design." *AIAA/AHS/ASEE Aircraft Design, Systems and Operations Meeting.* September 1988.